The Wolfson School of Mechanical, Electrical
and Manufacturing Engineering

A Novel Active Control of Trolleybus Current Collection System (ACTCCS)

(ACTCCS Research Thesis)

PhD Student: Min Chen

Supervisors: Dr Christopher Ward
Dr Ella–Mae Hubbard
Dr Peter Hubbard

February 2020

Abstract

The trolleybus has been a popular public transport vehicle for more than a hundred years across the world. However, the typical features of double passive pantograph-booms with two-wire overhead line often creates complicated catenary webs (particularly at crossroads) and can result in easily de-wiring and arcing issues. In this thesis, a novel concept of Active Control of Trolleybus Current Collection System (ACTCCS) is introduced with actuator-controlled solo-pantograph and single overhead line (catenary formed by two wires fitted on a frame with enough electric clearance and creep) as well as electric (traction)-electric (battery or supercapacitor backup) hybrid (E-E hybrid) propulsion.

Dynamic models of both passive and active catenary-pantograph systems are developed with half-trolleybus, pre-load, self-generation static force, non-linear and linearized, bouncing and finally hybrid non-linear models as well as complex catenary webs (particularly at crossroads and switch etc.). The simulations are carried out to explore and fully explain the phenomenon of contact loss, electrical arcing, de-wirement etc. in such catenary-pantograph systems.

Phase advance (PA) and phase advance-integrator (PA-I) control systems are introduced into an active catenary-pantograph system in order to reduce electrical arcing and facilitate planned de-wirement and re-wirement. The PA and PA-I control system simulations are carried out using contact force and position as the feedback control mechanism. Typical requirements of the actuator used to achieve the active control are also estimated in this work.

From a theoretical and demonstration perspective, the models presented in this work make a significant contribution to a dynamic theory of conventional and novel models in catenary-pantograph systems. In addition to trolleybus systems, this work could also be used for the analysis and explanation of railway catenary-pantograph systems.

Acknowledgements

It is impossible that the research of ACTCCS (Active Control Trolleybus Current Collection System) would have been fulfilled without the excellent guidance and support from my supervisors Dr Christopher Ward, Dr Ella-Mae Hubbard and Dr Peter Hubbard. Their excellent teaching, supervision and guidance with rich knowledge always inspired me throughout this study.

I am grateful to Professor Roger Dixon and Professor TX Mei, who, as examiners, gave me professional and helpful advice and comments that helped guide me to correct the original version of the thesis.

I would like to thank Dr Tony Allen (my ex-supervisor at Nottingham Trent University) for his ongoing professional advice and for proof-reading the various drafts of this thesis. He did a similar, excellent job for me whilst I was studying for a Master of Science Degree with distinction at Nottingham Trent University.

I would also like to thank Professor Roger Dixon, the Research Dean of Wolfson Engineering School of Loughborough University, for his professional encouragement and advice in his examination of my first and second years as well as for providing an excellent research environment in the school.

Thanks are also due to Mr Roy Horne, who gave me professional advice and comments on the single overhead line concept, during the development of the original idea of A Novel Active Control of Trolleybus Current Collection System (ACTCCS).

I would especially like to thank my wife, Dr Shaoyi Zhang for her love as well as everything she has done for me. We have been together for over a quarter of a century and I dedicate this work to my wife and our only baby girl Jing-Ar Chenzhang - a wonderful gift.

I also wish to make a special present of this thesis to my parents, Mr. Hanmian Chen and Mrs. Zhongxin Ma-Chen, for their loves and for giving me the life. They both passed away last November, and I am very proud of the education and knowledge they gave me. Their charitable words and expectations are always with me throughout my whole life and encouraged me to achieve this PhD study. I never forget the early education from my maternal grandmother Jingxiu Xu-Ma.

I would also say thanks to my only younger sister and her husband, Mrs. Zheng Chen-Hou and Mr. Jiangpin Hou. I never forget the help and support they have given to their older brother (me). As a special gift, I would like to dedicate this work to my lovely and clever nephew Boya Hou.

I would also like to thank all my colleagues in Loughborough University. They are: Dr Nike Wright, Mrs Hasma Antong, Mrs Emma Ebinger, Mr Sam Bemment, Ms Priya Parthasarathy, Mrs Mitixa Jani, Ms Sharon Henson, Mrs Sharon Want, Nabilah Farhat and Dived Brock. Their patient assistance helped me gain further knowledge in English and computer skills.

I would like to say many thanks to my relatives and friends for their long time helps and supports. They are as follows:

Mrs. Zhonglian Ma-Zhang, Mr. Shaonan Zhang, Mr. Zhongren Ma, Mrs. Zhongzhi Ma-Zhang, Mr. Hang Gao, Mr. Gan Chen, Mr. Yongsheg Zhang, Mrs Su Zhang-Shi, Mr. Yukuan Ma, Mr. Jiarong Zhang-Chen, Mr. Shuhua He, Mr. Shenwu Song, Mrs. Yiannan Zhang-Song, Mr. Xiaodong Liu, Mr Ming Liu, Mr Yong Pan, Mr Guangzhong Meng, Mr Rongbing Xia, Mr. Sijin Liu; Mr. Roy Horne; Dr Hans Bleijs, Mr. Robert Goodwin, Mr. Andy Moore, Mr. Steve Glenn, Mr. David Woolhouse, Mr. Martin Gunn, Mrs. Ping Peng-Liao, Mr. David Liao, Mr. Huihuan Zhang. You all have motivated and helped me to reach this far and I am really blessed to have you all in my life.

Finally, there is a person who should never be forgotten in my life and who deserves especially be thanked:

Mr. Zhongliang Ma is my closest and most honest friend; we have known each other for more than four decades. He always stood by me through my difficult times and has shared in my sadness as well as in my happiness.

List of Contents

List of Tables

List of Figures

List of Appendix Simulink Configuration Diagrams

Chapter 1

Background of trolleybus active pantograph control

1.1 Introduction

The interactions between transportation and society are paradoxical in nature since transportation conveys substantial socioeconomic benefits but, at the same time impacts significantly on environmental systems. The most important impacts are as follows [1]:

- Climate change
- Air quality
- Noise
- Water quality
- Soil quality
- Biodiversity
- Land take

As an electric transportation system help moderate the first three of impacts means of urban public transport, trams have now been successfully re-introduced (or, re-invented as light rail) in the UK [2, p2] and European continent. However, the huge installation cost and time overruns [2] are still a big barrier to new tram systems being implemented. Consequently, a re-invented trolleybus could be an alternative solution for urban public transport in the future. Like the trams, modern trolleybuses are powered by electricity. However, unlike trams, trolleybuses use rubber tyres, like normal buses, without rail tracks. Compared to tram and underground systems, new trolleybus systems require smaller investment and shorter implementation times due to being use able to existing road networks. The trolleybus is also more advantageous from the aspect of life expectancy of vehicle fleet operation compared to conventional bus systems [3] as it has a reduced number of high maintenance systems such as reciprocating engines etc. What advantage does trolleybus have over metal electric bus? However, the lack of an ‘earthed’ rail tracks means that the trolleybus system requires two overhead lines – live and neuter. This two overhead line system is the major disadvantage of the trolleybus system. In many countries, there is a mix of persistent original trolleybus systems and new generation ones, as new systems are created. There are 363 trolleybus systems with more than 40,000 vehicles in use in public transport system around the World [4]. In Western Europe, trolleybuses have been introduced (or re-introduced) in recent times [4, p3]. Leeds’ NGT (New Generation Transport) [5] project was the first trolleybus system to be considered in the UK since they disappeared in the 1960s. Though the NGT was not

implemented, a re-invented trolleybus may provide a “bridge” towards fully electric public transport systems between 2020 and 2050 [6, 7].

The trolleybus concept has also been extended into the commercial freight system. In order to meet the requirements of reducing emission, minimising disruption and lowering cost of installation, operation, and maintenance, Siemens have recently launched the advanced eHighway project, which has been now under the test in California, Sweden and German since 2012 [9]. This system uses a conventional twin-line overhead pantograph system.

In this work is introduced that a novel new concept that Active Control of Trolleybus Current Collection System (ACTCCS) uses a solo pantograph with single overhead line for current collection. It keeps all the advantages of a conventional trolleybus but can automatically de-wire and re-wire the pantograph, reducing the required amount of fixed infrastructure; and, removing the need for complicated overhead line webs at crossroads and junctions. During wireless operation, the trolleybus would need to be powered by a stored energy source, such as batteries or super-capacitors.

1.2 Trolleybus status and main issues

The key technologies for trolleybuses were invented over one hundred years ago. Today’s advanced technology, such as high-power semiconductors, carbon-fibre (for pantographs) and programmable controls etc., have been widely applied on rail vehicles and trams, and are now being adopted on modern trolleybuses. However, in principle the basic design of the passive twin-rod pantograph with double overhead lines system, shown in Figure1.2.1 [10], [11] has not changed greatly.

Figure 1.2.1-*Oldest and most modern trolleybuses* [10], [11]
both with twin-rod pantograph remains

Even the recent 'New Bus for London' all-electric vehicles planned to help meet London's 2025 CO^2 emissions plan[12], the issue still remains of double overhead lines and complicated overhead line webs at crossroads and junctions. To illustrate this, the latest design of London's prototype new generation trolleybus [9] is shown in Figure1.2.2 [13], the larger trolley-trucks in mining are shown in Figure1.2.3 [8] the eHighway project test of Siemens in Gävle, Sweden is shown in Figure1.2.4 [14]

Figure 1.2.2-*Impression of London's prototype new generation trolleybus outside Ealing Town Hall* [13]

Figure 1.2.3-*left, Unit Rig M100 100-ton trolley-truck* [8 1970-1977-Quebec Cartier Mine, Canada]***; right, Haulpak (now Komatsu) 685E 190 tons trolley-truck in Barrick Goldstrike mine, Nevada*** [8 1994-2001-Barrick Goldstrike, Nevada]

Figure 1.2.4-*left, eHighway Innovative electric road freight transport* [9]***; right, eHighway, Gävle, Sweden*** [14]

The main issues [15], such as non-flexible operation and ungainly ‘spider’s webs’ overhead wire system, (shown in Figure1.2.5 [16] [17]) have been widely recognised. These ‘webs’ can cause problems for existing trolleybus’ passive pantograph, particularly at crossroads, section insulators and isolator switches [18]. Arcing between the catenary hardware at these features and the carbon sliders of pantograph-head can be created. As well as this, the problem of unplanned de-wiring (with subsequent manual re-wiring) has been taxing operators, causing severe congestion and chaos at peak times since trolleybuses inception. Novel ideas of active and automatic de-wiring and re-wirement are in various stages of research, and some have been patented [16-23] these will be described further in Section 2.3.

Figure 1.2.5 C*omplicated trolleybus overhead line webs at crossroads* [16] [17]

1.3 Concept of ACTCCS Trolleybus

The concept of ACTCCS is a fully active system using advanced technologies such as: multi-channel control actuation system; real time location system (RTLS); and electric (traction)-electric (battery or supercapacitor backup) hybrid (E-E hybrid) propulsion. It will be capable of automatically de-wiring and re-wiring the pantograph, as well as allowing the E-E hybrid

trolleybus to run by battery or super-capacitors while de-wired through ‘wire-free’ sections. The ACTCCS will have a solo pantograph and be in contact with the single overhead line (OHL) made of two contact wires, along with being optionally mounted on top of the trolleybus on the centre line or eccentrically for specific application requirement.

Overcoming the issues of arcing and unplanned de-wirement (an inherent quality of the passive pantograph) is one of the keys aims of introducing the ACTCCS. Therefore, a fundamental modelling of passive and active pantograph of trolleybus have been completed (see chapter 3, 4 and 5).

With the newly proposed system, there will not be any unsightly complicated wire networks above crossroads, junctions, sharp bends or depots. Drivers will be able to go through crossroads or any emergency de-wirement operation (such as switching lanes to move around a vehicle break down) with no need to think about de-wiring or re-wiring in a similar fashion to the operation of a diesel-powered bus. As an E-E hybrid type trolleybus, the battery or super-capacitors will automatically be switched on during de-wired operation. As a possible extension, the ACTCCS could be applicable to future hybrid lorries running on the “eHighway” [24]. Figure1.3.1 is a pictorial description of ACTCCS trolleybus and the solo-boom pantograph with single overhead line where the positive and negative wires are closely coupled in the same structure.

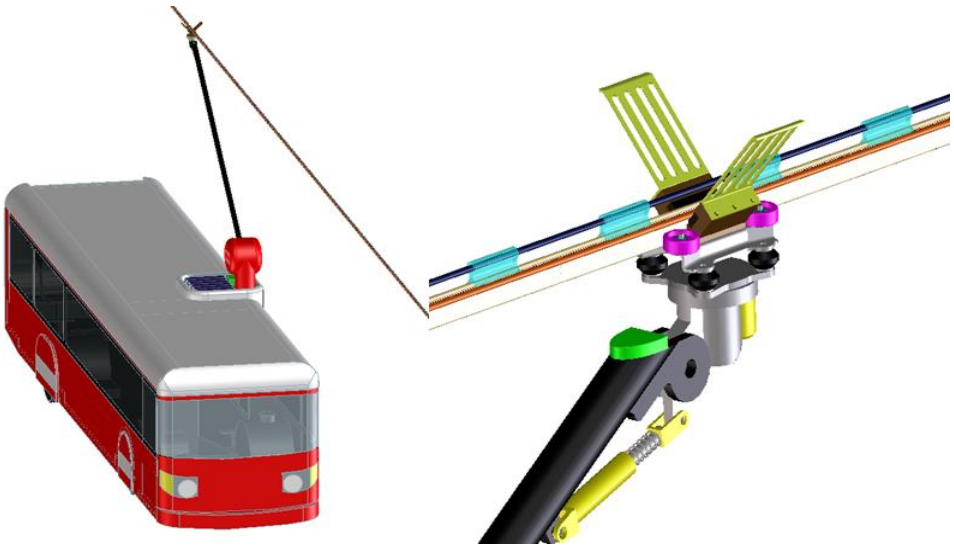

Figure 1.3.1- ***Novel ACTCCS trolleybus (left) and pantograph head with single overhead line (right)***

Figure 1.3.2 is pictorial description of hybrid lorry running on the E-motorway using the idea of ACTCCS.

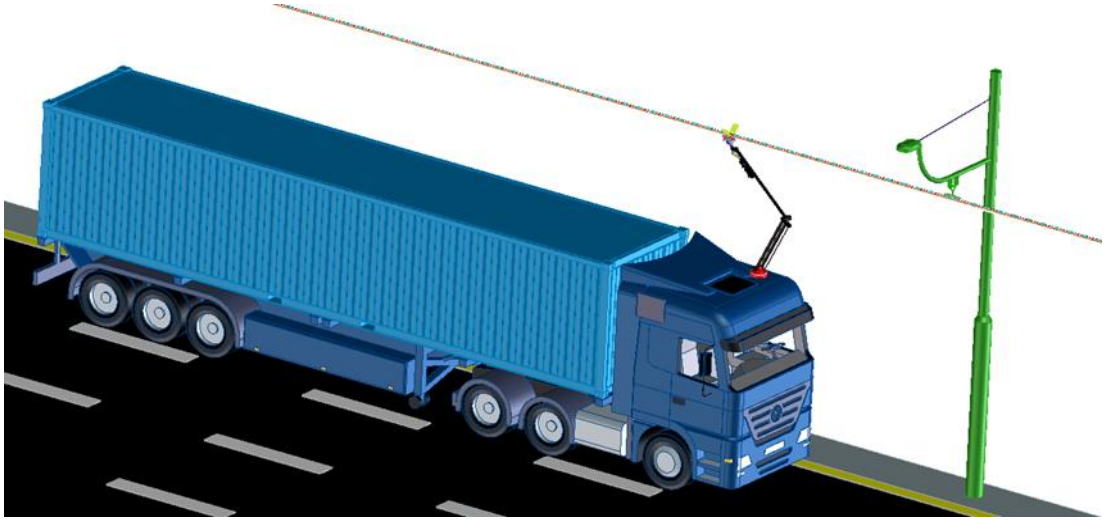

Figure 1.3.2-*Hybrid lorry fitted with ACTCCS running on the E-motorway*

1.4 Research contribution

In this thesis, a novel new concept of Active Control of Trolleybus Current Collection System (ACTCCS) is introduced with solo-pantograph and single overhead line (catenary) for current collection as well as electric (traction)-electric (battery or supercapacitor backup) hybrid (E-E hybrid) propulsion. As fundamental requirement of this concept, the dynamics of catenary-pantograph, active control methods and the comparison are investigated throughout the whole study. The key contributions of this study are as follows:

- Dynamic model of half passive trolleybus with a passive catenary-pantograph system
- Self-generation static force is introduced for modelling of catenary-pantograph system
- Dynamic model and identified the worst situation of trolleybus with a passive catenary-pantograph system (at 20m/s) applied on different road disturbances
- Dynamic bouncing and hybrid non-linear models of passive catenary-pantograph system
- Complex catenary definition and models such as at crossover and switches
- Use dynamic bouncing and complex trolleybus webs' models to build risk rank of unexpected de-wirement and electrical arcing
- Control method (PA-I) of active pantograph of trolleybus for catenary-pantograph system in st operation by contact force
- Control method (PA-I) of active pantograph of trolleybus for planned de-wirement and re-wirement operation by pantograph-head position

Chapter 2

Literature review

2.1 Aim, scope and sources of the reviews

The aim of this section is to review the relevant literature applicable to the current collection system of trolleybuses in order to identify the issues affecting existing and advanced trolleybus current collection system. The experience and technology of other kind pantographs such as trams and trains are also considered, for reference and comparison.
To date, no research employing full active control of current collection system for trolleybuses has been identified; although there have been a large number of studies of similar technologies for high-speed railway systems such as [25], [26] and [27] etc. This literature review initially concentrated on trolleybus pantographs. The scope then broadens to focus on the contact modelling of the catenary (including pantograph) and active pantograph system dynamics as well as the partial component of the system in both trolleybus and train/tram systems. Human factors and ergonomics were also considered when evaluating and considering how the drivers' behaviour is affected by the performance and control design of ACTCCS. This will be briefly reviewed in this chapter, however no further study of this is considered in this thesis.

2.2 The benefits of the ACTCCS research for potential market

The trolleybus is an old form of public transport that used to be very popular in the EU and the UK [28]; in the 1930s there were more than 2300 trolleybuses in London [29]. But from the late 1950s, diesel buses gradually replaced trolleybuses (as well as trams) due to lower costs and higher flexibility of operations. Environmental considerations described in "Transport, Energy and Environment, The Geography of Transport Systems" [1] and "Market Research Summary Report" [2] etc., at the beginning of the 1980s led to renewed interest in electric propulsion systems like those on light rail systems and modern trams. Compared to a tram system, a trolleybus network such as NGT could deliver many of the benefits of trams but at around half the cost [30]. In Quito, Ecuador, the 11.2km long trolleybus project cost just £57.6M to construct [31]. As mentioned in Chapter 1, there are now 363 trolleybus systems with more than 40,000 vehicles in use around the world; and this number is predicted to expand in the coming decades [4]. Thus, this research into ACTCCS is valuable, timely and marketable for developing the next generation trolleybus system that could be used to replace or upgrade existing systems. This work could help provide greener, cheaper and more efficient options in urban public transport markets as well as reducing the visual impact due to the use of single overhead wire and solo boom. Some cities have shown interest in

trolleybus system for upgrading their new public transport system (i.e. Leeds in the UK and the Malatya in central Turkey [32]), though the former city decided not to take up this option.

2.3 The existing technology and research of trolleybus

In general, there are few articles focussing on technologies for trolleybuses. Most articles in the trolleybuses area are related to new technology application of trolleybuses as well as new technologies for hybrid propulsion [33, 34], electronics, information and traction systems such as GPS, AC hub driving motors and low floors [15]. A paper has been identified that investigated the application of air-suspension to a trolleybus [35] in which the disturbance model was used for simulation study.

2.3.1 Active pantograph concepts

As ACTCCS is the main subject of this thesis, the current collection system is the key focal area. In [36] and [37] a concise overview of the terminology and essential parametric data of the trolleybus in respect of the current collection system of trolleybuses is presented. Articles of Analysis and Design of Tbus Overhead [38] and Tension and strain on overheated trains [39] both describe the effects of wire sag and tension as well as the phenomenon of trolleybus pantograph de-wirement. Although few articles have been found in the trolleybus area, some interesting points of single pantograph architecture and automatic re-wirement function are raised in two articles: [40] shown in Figure 2.3.1; and [41] shown in Figure 2.3.2. These two figures provide a pictorial description of the two systems. Both show the use of two overhead lines and collectors, as per conventional trolleybus system. The ACTCCS single overhead wire and collector presented in this thesis is fundamentally different in operation.

In “Retraction Systems” (Figure 2.3.1 left) [41], there are a few words of description in respect of “the major potential for the future of a new single pantograph-boom collector for technical and aesthetic improvements” [42] gained with a fork configuration of pantograph. Apparently, it is not an active pantograph. In qualitative terms, it is highly likely that there is an in-balance between the two contact points which would lead to contact loss or de-wirement with even a small perturbation of the road surface. The fixed distance between the two collectors will also cause de-wirement during passage of any catenary misalignment or sudden vehicle manoeuvre.

In “DIaLOGIKa” [43], the trolleybus automatically reconnects with the overhead line (Figure 2.3.1 right). The big issues with this method are the impracticality due to the lack of lateral actuation travel by the cable driven method during lane changes and when running through sharp bends.

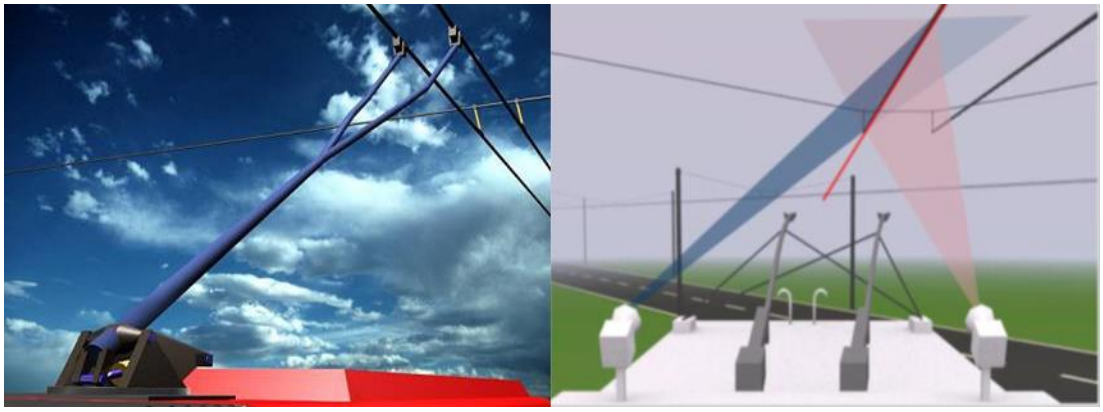

Figure 2.3.1-*Retraction Systems (left)* [40]***; DIaLOGIKa’s solution(right)*** [41]

2.3.2 Patent search

A global patent search was carried out as part of the initial research to further identify the latest trends in trolleybus’ pantograph development and relevant technology.

Patent Seekers Ltd were contracted to independently search patents in trolleybus technology in the WO (World Intellectual Property Organization), US (United States Patent and Trademark Office), EPO (European Patent Office), GB (British Intellectual Property Office), DE (German Patent and Trade Mark Office), CN (China Patent & Trademark Office), JP (Japan Patent Office), KR (Korean Intellectual Property Office) counties and the rest of the world. Coverage is not complete for ‘rest of the world’ countries and assessment were based on machine translations of titles, abstracts and picking up of any family members e.g. through the patent cooperation treaty (PCT) process. The coverage was further restricted to English language titles and abstracts. The relevant patents were identified using the following search definition:

“This search relates to an electric trolleybus with a single pantograph pole for collecting power from a single overhead cable featuring two wires separated by an insulator, whereby the pantograph pole position is actively adjusted for optimum electrical contact by an actuator and may be de-wired and re-wired at junctions by means of a butterfly collector and a real-time guidance system” [44].

The search yielded approximately 1800 patent items relevant to trolleybus, of which about 450 abstracts and whole relevant drawings (some have no drawings) have been read and compared. After identifying and comparing, the relevant patents were shortlisted and compared as shown in Table 2.1.1:

Table 2.1.1 Patents search result

Patent number	Difference between searched patents and ACTCCS concept	Similarities
US20130245876	No active control; Double overhead line and pantograph-booms with ropes actuation	Function of automatic de-wiring and rewiring (by imagines sensing system)
US20130018766 **EP0026147** **US20140097054** **EP0030906**	No active control; Double overhead line and pantograph-booms.	Function of automatic de-wiring and passive rewiring; US20130018766 with the partial solo lower boom; Solo pantograph-boom is an alternative choice of EP0026147
CN1486889 **US4357501** **EP0043763** **WO1988007952** **EP0046562**	Double overhead lines; No active control Note: WO1988007952A1 with partial solo lower pantograph-boom	Solo or partial solo pantograph-boom
DE102012002749	Double overhead lines and pantograph-booms; No active control	Funnel channel for automatic overhead line parallel aligning the current collector (to ACTCCS' current collector butterfly plate)

EP1150858	Double overhead lines and pantograph-booms; No real active control	Automatic preventing de-wirment and pantograph-boom over position
EP0989015	Double overhead lines and pantograph-booms; No function of automatic de-wiring and rewiring	Keeping contact force stable by sensitive sensor
EP1226997	Despite being called single overhead, this is a three overhead lines system in which two conventional overhead wires remained as the DC suppler lines.	None
CN104149631A	Double overhead lines, no active control	Solo or partial solo pantograph-boom; Battery and charging during running

The identified relevant patents are as follows [43]:

CN104149631A, US4357501A, US2013245876A, CN204279119U, CN104385929A, GB190103036A, CN204279120U, RU140654U, US3547237A, JP7336802A

CN104149631A is most relevant document found as the subject matter appears to disclose a hybrid-power single-braid trolley bus system which includes a single-braid trolley pole which is monitored using a camera system. The single pantograph boom can be electronically controlled such that it may lift and freely revolve so that the upper duplex could break away from a power wire in sections of road without a power line such as at large crossroads [44]. However, the key difference is that is not an actively controlled system, and no reference is made to a single overhead line catenary solution. No further academic research could be found in the area.

2.4 Review of associated research in trolleybus and catenary-pantograph systems

As few specific papers could be found detailing research in the area of trolleybus' catenary-pantograph systems, the following four broader areas involved in trolleybus were searched. These are: Catenary-pantograph dynamics, Active catenary-pantograph with control, vehicle/road suspension dynamics and Human factors.

2.4.1 Catenary-Pantograph Dynamics

The catenary-pantograph dynamics of railway systems are relevant to the academic research of ACTCCS, due to the similarities of the fundamental problem. In [52] there is a general linking of the catenary-pantograph system of railways, trams and trolleybuses.
For urban transport at low speeds, the light rail (tram) is similar to the trolleybus in both speed and function. When modelling the electrical contact between the wire and the pantograph, 'pure' contact with the wire (i.e. there is no loss of contact during operation) is popular when creating simulation without the messenger wire, as shown towards the left of Figure 2.4.1 [52]. Meanwhile the vertical pre-displacement (e.g. 0-249 mm depending on position from pole, span between poles and around temperature) [40] and stiffness of catenary are also defined for application (e.g. 1117 – 2716 N/m) [25].

Many components and specifications of trolleybus overhead line system are the same as, or similar to, as those found in light railway systems [25, 54]. The trolleybus wire solutions are also well utilised for light rail systems where low speed and low power capacity is required [55].

In simple catenary, the contact wire is suspended from the messenger wire by droppers. The static sag and stiffness of the contact wire are smaller than those for the single wire.

In compound catenary, there is an auxiliary messenger wire between the messenger and contact wires that is parallel with the contact wire. The compound catenary has a smaller static stiffness variation in comparison with the simple catenary which allows a higher train speed [56] due to a reduction in the possibility of standing waves being established.

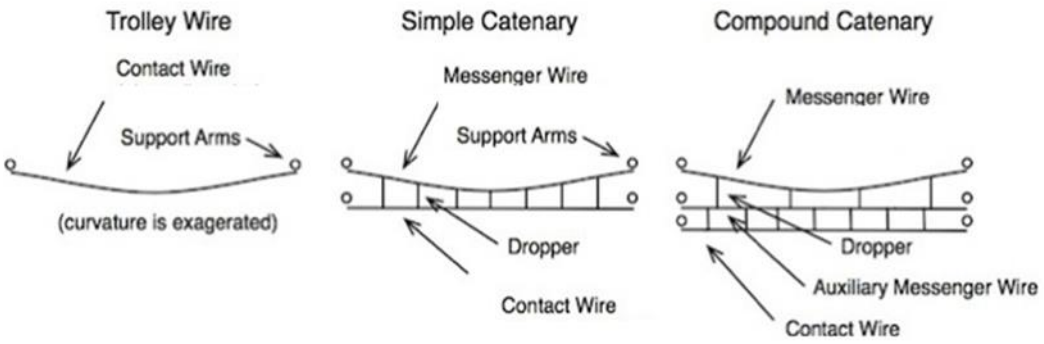

Figure 2.4.1-*Different configurations of overhead lines* [52]

The different fixed configuration types of overhead line are shown in Figure 2.4.2. As the current collector of the pantograph are different for trolleybus and electrified railway system, including light rail (e.g. trams) and heavy rail (e.g. high-speed trains), the fixing methods to stanchions also varies. In a trolleybus application there are normally no steady arms and messenger wires, compared to light and heavy rail.

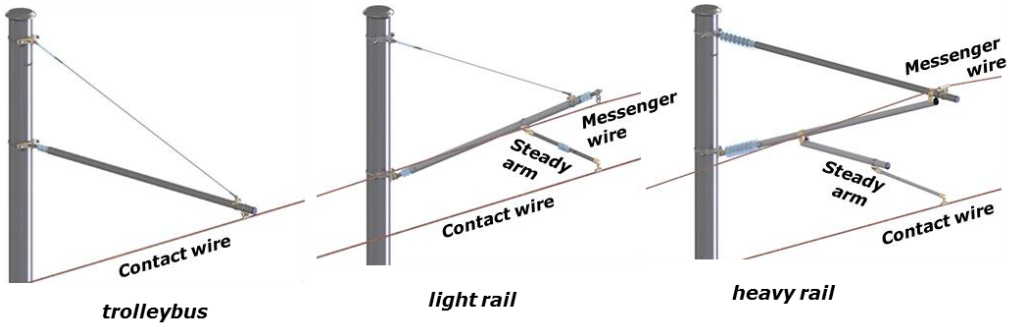

Figure 2.4.2-*Different fix configuration of overhead line* [55]

Most of the articles in this category investigate the catenary-pantograph interaction of high-speed rail vehicles. These frame the catenary-pantograph dynamic models as follows:

Model of contact wire e.g. [57]: There are two basic models of contact wire dynamics; the pure contact wire type and the catenary type with messenger cables and droppers. Many of the articles such as [58] involve wave propagation velocity and frequency, as well as two further articles involve string vibration and standing wave dynamics [59, 60]. At least one article [61] shows an analysis with constant bending stiffness and constant tension which would be particularly useful for modelling of the ACTCCS' single overhead line.

Modelling of a two-node Euler-Bernoulli-Timoshenko beam has been citied in most papers modelling the catenary, but basic data such as mass, spring damping rate and stiffness are

referenced from experiments described in [57]. Few of them adopt the data from specific tests.

Model of pantograph [62]: There are different degrees of freedom pantograph models which range from one to three mass models with linear force laws, to models which include joint friction and bump stops with four and more masses [56]. In this thesis the vertical model of ACTCCS, uses a two degree of freedom model [26].

Models comparison [56]: The speed of trolleybus is much lower than high speed trains, therefore after comparison the models of simple pure catenary wire and basic two degree of freedom pantograph, the latter have been used for research of ACTCCS. The geometric model of the pure catenary is a curve described by a uniform, flexible wire hanging under the influence of gravity [63]. The illustration of this and equations are shown in Figure 2.4.3, E1.4.1 and E1.4.2.

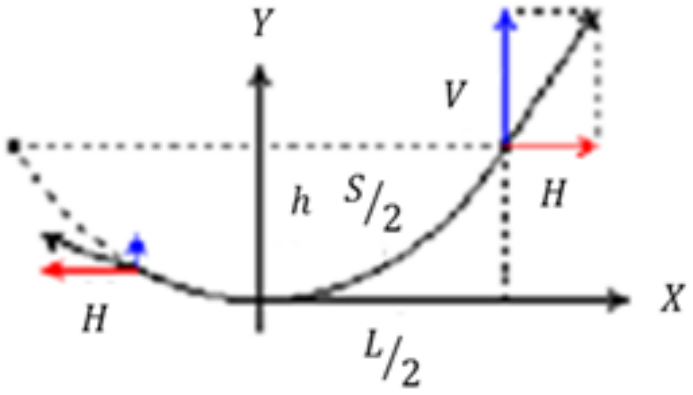

Figure 2.4.3-*Geometric model of the pure catenary* [63]

Where:

S: total length of the catenary
L: total length of the span
h: sag
w: weight per unit length
T = tension in catenary
H = Horizontal component of tension (constant)

$$\boldsymbol{H = \frac{w}{8h}(S^2 - 4h^2)} \qquad \text{E2.4.1}$$

$$T^2 = H^2 + \left(\frac{wS}{2}\right)^2 \qquad \text{E2.4.2}$$

The modelling and simulation process of a catenary-pantograph interaction is given in [47] for a trolley-truck system. Despite the pantograph of the trolley-truck (used in the mining industry) in this paper being closer related to rail application rather than a trolleybus.

In terms of bouncing models and simulation in application of hybrid non-linear catenary-pantograph, no articles were found. However, some articles were still useful for modelling and simulation as follows:

The simple ball bouncing on a rigid surface and dynamic model (without energy loss) was introduced by MathWork in [64] and this concept has been applied to the catenary-pantograph. In a formal application for catenary-pantograph dynamics, it is an important to take the horizontal velocity (trolleybus vehicle) of the pantograph into account as described in [64, 65].

A single mass-spring-damper ball impact phase with ground deformation and restitution occurring can be found in [66]. This is particularly useful when building a model of a catenary (flexible)-pantograph (bouncing) hybrid model. The impact between catenary and pantograph and its natural frequency of oscillation is given in [64, 67, 68].

The mathematics [69] and cable profile of a small suspension bridge [70] as well as simplified approximate triangles [71] are used to form the bi-separated sub-catenary; which in combination with an approximate energy conservation to correct the deviation of single mass-spring-damper ball is used in the application of catenary-pantograph.

2.4.2 Active catenary-pantograph with control

The performance of the control system in Active light rail pantographs have been evaluated on the basis of variations of displacement and acceleration between the pantograph and contact wire. An active control algorithm was developed by means of a linear quadratic regulation design to find a stabilizing algorithm for the pantograph system with respect to the dynamic contact force between the pantograph shoe and catenary [25]. Some of the methods are considered in this paper have been adopted in modelling of ACTCCS. These include: optimal, robust, adaptive, fuzzy, model predictive control (mpc) as described in [72, p6]. The Bode and Nichols (shown in Figure 2.4.4) diagram are recognized as effective analysis methods of control system [72, p7, p9].

Proportional-Integral-Derivative (PID) control is the most popular method in industrial applications. This can be attributed partly to their robust performance in a wide range of operating conditions and partly to their functional simplicity, which allows operating them to be tuned in a simple, straightforward manner [73]. Therefore, the PID is also in application of active pantograph control of high-speed trains [74].

Phase Advance (PA) can be thought of as a more practically applicable version of the PD (Proportional-Derivative is a simplified of PID) due the practical shortcoming of a pure derivative term amplifying high frequency noise [72]. It is often used in electric drive system [75].

The PA-I is a combination of PA and PI (Proportional- Integral, PID). This is usually used to reduce the steady state error of a system (PI), and that can be also used to improve stability (PD and PA).

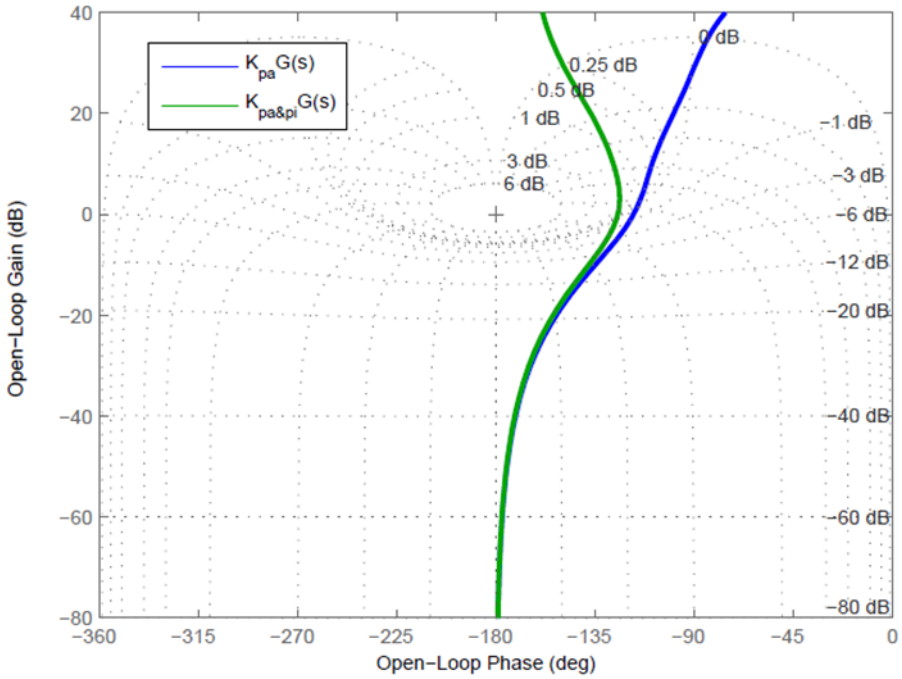

Figure 2.4.4- ***Nichols diagram for analysis of PA and PA-I control*** [72]

More advance model-based control algorithms, such as proportion LQG (Linear–quadratic–Gaussian) and LQR, are introduced in [72, 76, 77]. The linear quadratic regulator (LQR) design (in [76, 78, and 79]) is the key algorithm for a stabilizing control pantograph system with the time-varying contact force between the pantograph shoe and catenary. The LQR control principle diagram is shown in Figure 2.4.5.

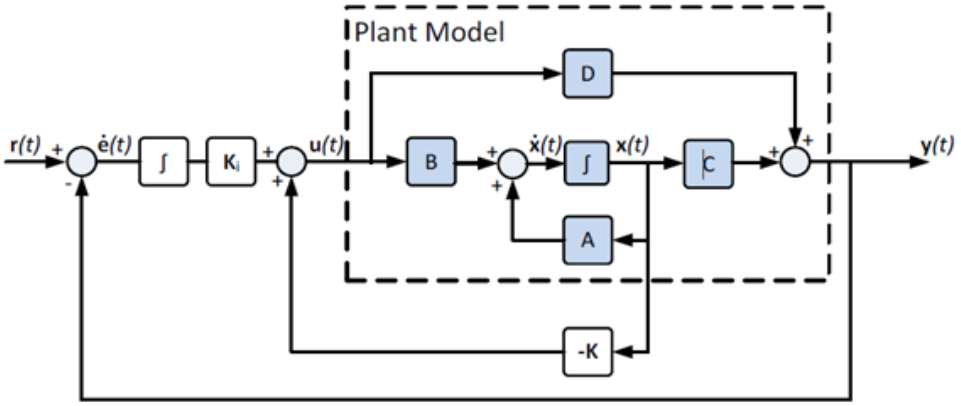

Figure 2.4.5- ***LQR control principle diagram*** [77]

The control analysis tools of Bode plot and Nichols chart as well as step response diagram are applicable to identify the issues and adjustment of control system design [72].

In [80], the performance of the control system is evaluated on the basis of variations of displacement and acceleration between the pantograph and contact wire with basic feedback control.

As application condition and status are not always linear, the hybrid equations would be considered for the theoretical study of nonlinear dynamic simulation and control design of ACTCCS [81].

2.4.3 Vehicle-road suspension dynamics

The trolleybus is a rubber tyre vehicle with electrical power traction, thus some papers [45, 46] investigating vehicle/road passive suspension system were reviewed and referenced in respect of modelling of basic quarter and half vertical vehicle/road passive suspension system. Two disturbance models of road, which are KTH [47] and SKODA [48] types, were found to be applicable in relation to trolleybus for comparison and application. The articles and papers [47, 49, 50, 51] also provide practical specification for simulation.

Figure 2.4.6- ***The SKODA 21 Tr low-floor trolleybus*** [48]

2.4.4 Human factors

Human factors include environmental, organisational and job factors as well as the human and individual characteristics which influence behaviour and quality at work as well as impact on health and safety considerations [82].

The control design of the trolleybus active pantographs can strongly impact on drivers' behaviour and performance quality particularly while turning, going through the crossroads and switches. De-wirement of a trolleybus is a typical example of the impact of drivers' behaviour, which was clearly shown in an email from a trolleybus expert of Vosshol [83] in Germany. The dynamic decision of the driver should be to follow the recognised trajectory and its (approximate) curvature in front of the vehicle and tries [84] in order to keep the pantograph in contact with the wires and the vehicle on the proper lane. Although the ACTCCS will be autonomous, the manoeuvring of the trolleybus will be still regulated by the standard method [37]. A number of extracted articles including papers on autonomous vehicles [85], transition curve [86] and Motivational Influences on Response Inhibition Measures [87] in psychology have also been reviewed. The knowledge will be useful to training the divers and designing the specific signs such as ready de-wiring, road crossing and switching. The concept of three steps in a transition curve and stop-signal reaction time (SSRT) would be taken into account for analysing and designing the algorithms, sensitive methods of control system for ACTCCS with self-decision function. Meanwhile identifying, picking up and managing effectively the information for sensing of control system of

ACTCCS have been reviewed from a book reviewed [88]. The various types of trolleybus overhead line crossing and switching equipment [89] are also investigated for estimating the behaviour of drivers during the switching and crossing.

2.5 Identification of gaps between the state of the art and ACTCCS

There are three key points that can be clearly recognised between the existing technology of trolleybus and ACTCCS. They are as follows:

Although there are many academic articles in the transport systems area only a few of these are directly involved with trolleybuses. However, there is no article considering catenary-pantograph dynamic research for trolleybus systems. Most of them are only in professional engineering publications, and in the project planning phase [4, 16, 19, 31, 35, and 38].

The twin rods pantograph with double overhead wires power system has not changed since trolleybus was introduced for public transport although there are some other ideas created [21, 42].

No academic articles have been found that investigate the active control of pantograph for trolleybus systems. Even papers that consider fundamental topics lack deeper study such as de-wirement and re-wirement etc. A single paper of light rail vehicle (tram) paper does provide some specifications that are useful for research. In addition, a few patents were identified that dealt with automatic de-wirement and re-wirement. However, as shown in Table 2.1 most of the patents deal with ideas of mechanical architectures or electrical connection rather than academic study.

2.6 Chapter Summary

Numerous articles in relevant areas of research have been reviewed, across a wide range of academic papers, books and articles in engineering publications. There were no specific articles found that considered catenary-pantograph dynamic research of trolleybus systems.

A significant academic map of ACTCCS research has thus been formed. Consequent to this, an implementable approach has been developed and conscious study strategies to achieve the objectives of this research have been defined.

Chapter 3

Passive catenary-pantograph modelling and analysis

3.1 Brief overview of passive trolleybus catenary-pantograph modelling

3.1.1 Introduction of trolleybus and catenary-pantograph modelling

As mentioned in the previous chapter, the "Active Control of Trolleybus Current Collection System" (ACTCCS) is a new concept for electrical power collection for trolleybuses, with a solo rod pantograph and specially designed single overhead line. The basic electrical power collection principle and the system dynamics of catenary-pantograph interaction are similar to that found on heavy and light rail systems. The only difference between the overhead power system on a train (or trams) and a road electric vehicle (including trolleybus) is the fact that the return current is sent through the steel wheels into the train or tram rail, whereas for a road vehicle (including trolleybus) this is not possible due to the isolating rubber tyres. Instead a second parallel overhead contact wire is introduced to allow the current to flow back to the feeder station [47]. Additionally, the dynamics of the trolleybus (i.e. rubber tyres and standard suspension) are similar to those of a diesel-powered bus. Figure 3.1.1 shows a side profile half trolleybus schematic with a passive catenary-pantograph (note this only considers the vertical contact of the catenary-pantograph interaction and does not include any lateral movement relative to the trolleybus that would be caused by wires stagger).

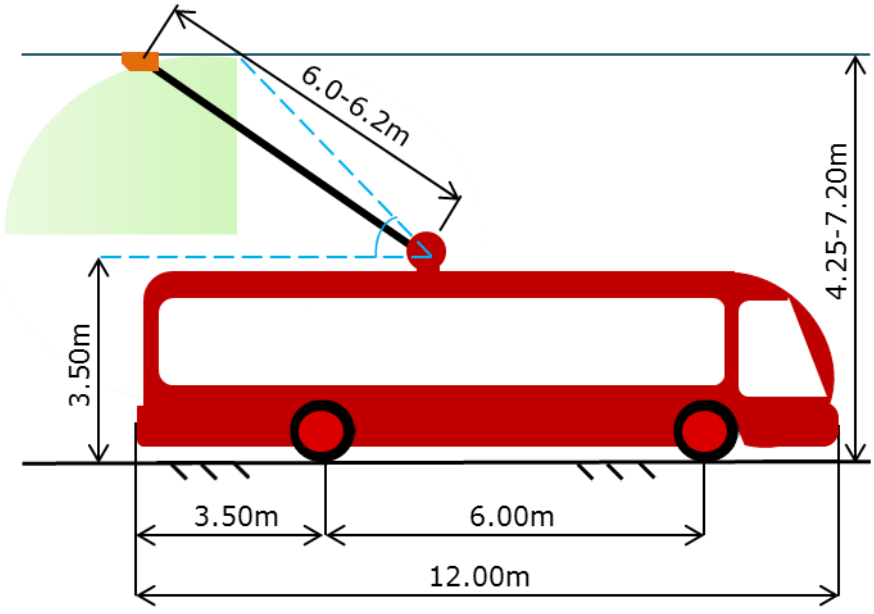

Figure 3.1.1-*Side view schematic of a trolleybus with catenary and passive pantograph*

This chapter is focused on developing a benchmark model for a passive current collection system that can be used to analyse contemporary performance and provide a comparison for the benefits of ACTCCS. This is a unique concept of single pantograph boom with single overhead wire (including two electrical wires with small clearance met minimum clearances) [155] for which no similar research in the trolleybus field has been identified.

In order to develop a single passive catenary-pantograph in the vertical dimension with half trolleybus side view system as a whole trolleybus model, there are three phases that need to be modelled and simulated. The three phases are as follows:

- Develop an integrated vertical passive single catenary-pantograph (after called “catenary-pantograph”) model for trolleybus (called “catenary-pantograph” hereafter)
- Develop a half trolleybus side view passive suspension system model (called “half trolleybus” hereafter)
- Integrate the two models to produce a comprehensive model of vertical passive single catenary-pantograph with half trolleybus side view passive suspension system (called “catenary-pantograph with half trolleybus” hereafter)

A schematic of the modelling stages mentioned above and their relationship is shown in Figure 3.1.2

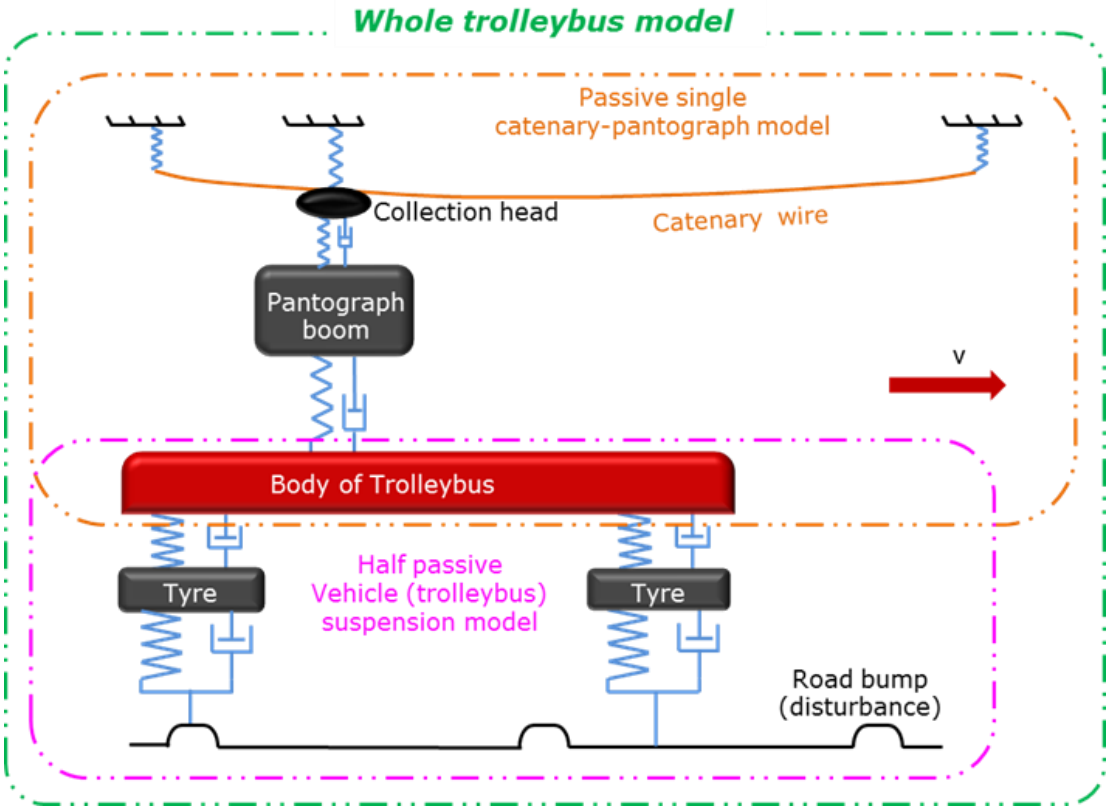

Figure 3.1.2-*Comprehansive trolleybus model combining catenary-pantograph with half trolleybus side view passive suspension system*

3.2 Modelling and simulation of catenary-pantograph for trolleybus

In reality, the catenary-pantograph system is an interactive system, therefore this study needed to create and integrate separate models of the catenary wire, initial pantograph position and self-generation static force to create a whole model of catenary-pantograph of the trolleybus.

3.2.1 Model of single catenary wire

Figure 3.2.1 shows the vertical displacement of single catenary (called “catenary” hereafter) wire with nominal stiffness for trolleybus’ pantograph. This is based on the pure contact wire without messenger cable, as described in Section 2.4

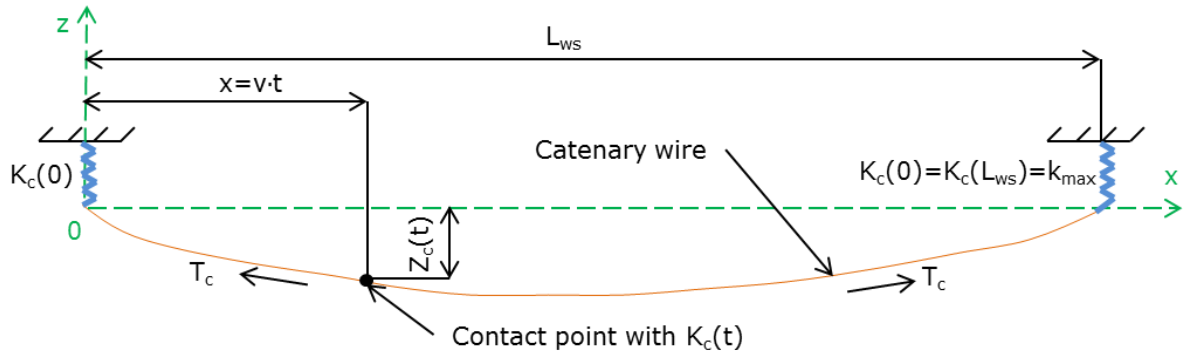

Figure 3.2.1 C*atenary wire model of trolleybus*

The vertical displacement and stiffness of the catenary wire are defined to be $Z_c(t)$ (modified from reference to [63]) and $K_c(t)$ [56]. The expressions are shown below:

$$\boldsymbol{Z_c(t) = \frac{g\cdot\rho}{2T_c}\left(v\cdot t - \frac{L_{ws}}{2}\right)^2 - \frac{g\cdot\rho}{8T_c}(L_{ws})^2 = \frac{g\cdot\rho}{2T_c}[(v\cdot t)^2 - (v\cdot t)\cdot L_{ws}]} \qquad \text{E3.2.1}$$

$$\boldsymbol{K_c(t) = k_{mean}\left(1 - a\cos\frac{2\pi}{L_{ws}}v\cdot t\right)} \qquad \text{E3.2.2}$$

$$\boldsymbol{Where:\ k_{mean} = \frac{k_{max}+k_{min}}{2},\ a = \frac{k_{max}-k_{min}}{k_{max}+k_{min}}}$$

Where:

$Z_c(t)$: pre-vertical displacement of catenary wire

$K_c(t)$: catenary wire nominal stiffness at contact point (N/m)

$K_c(0) = K_c(L_{ws}) = k_{max}$: catenary contact wire maximum stiffness (N/m)

k_{min}: catenary minimum stiffness (N/m) (not showing in Figure 3.2.1)

k_{mean}: catenary average stiffness (N/m)

α: Stiffness variation coefficient

L_{ws}: catenary wire span between two poles (m)

T_c: tension of catenary wire (N)

g: gravitation acceleration ($9.8 m/s^2$)

ρ: catenary wire linear mass per unit length (kg/m)

x: contact position distance from 0 of x-axis (x=v·t) (m)

v: trolleybus speed (m/s)

Note: $Z_c(t)$ is always zero or negative and $K_c(t)$ is always positive. Further it can be simply assumed that $Z_c(t)$ is the balanced position between gravity (g·ρ) and the tension of the catenary wire.

3.2.2 Initial position of pantograph under the preload

In the absence of a downward force from the wire, the pantograph could reach its maximum position under the preload pantograph spring mounted on the base of the pantograph. Comparing the size of pantograph-head to pantograph-boom, the size of pantograph-head can be ignored in calculation of position of the pantograph. There is also no contribution to the preload lift force from pantograph-head spring. In reality, the initial position of the pantograph would be at the balance point (rising angle) of gravity and preload lift force by pantograph-boom spring. Figure 3.2.2 is a schematic diagram showing the pantograph at its maximum and initial positions. The physical constraint positioned to limit for securely preventing the pantograph not accidently beyond the set highest position (virtual) which might never reach. Therefore, the support force from hard constraint will be not taken into account of the forthcoming models.

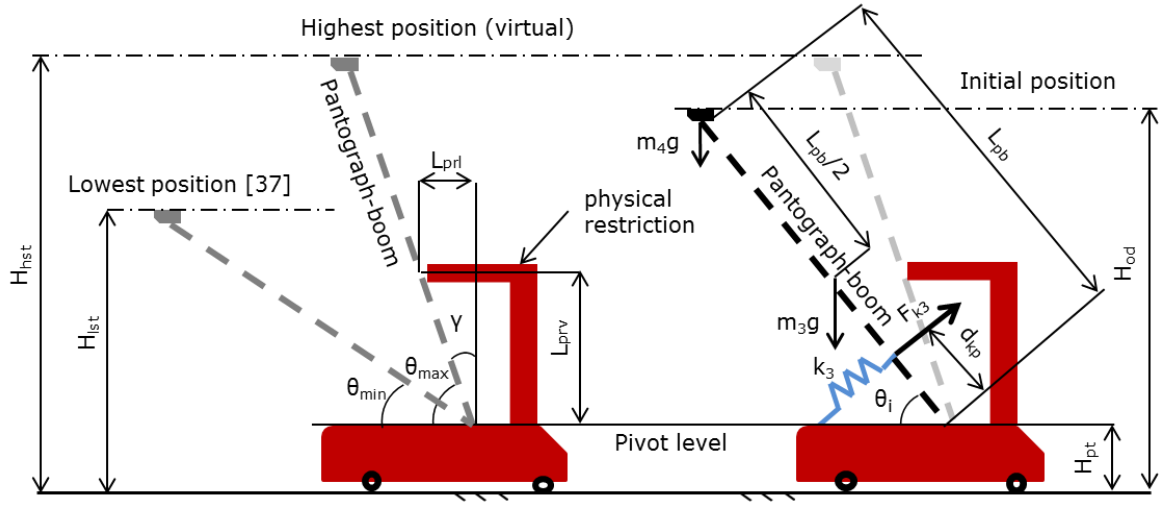

Figure 3.2.2-*Schematic diagram of trolleybus pantograph at highest virtual and initial positions*

Where:

H_{hst}: highest position of pantograph-head from ground (m)

H_{lst}: lowest preferred position of pantograph-head from ground (4.7 m) [37]

H_{od}: initial position of pantograph-head from ground (m)

H_{pt}: pivot position of pantograph from ground (3.50 m)

θ_{max}: pantograph highest lifting angle (degrees)

θ_{min}: pantograph preferred lowest lifting angle (degrees)

θ_i: pantograph initial lifting angle (degrees)

γ: pantograph angle between pantograph and vertical line (degrees)

L_{pb}: length of pantograph-boom (6.0 m)

m_3: pantograph-boom mass

k_3: pantograph-boom spring nominal stiffness (N/m)

F_{k3}: preload lift force provided by k_3 (N)

d_{kp}: distance from spring (k_3) fitting point to pantograph pivot point (m)

m_4: pantograph-head mass (4kg)

L_{prl}: effective level limitation of physical restriction (0.125 m)

L_{prv}: effective vertical limitation of physical restriction (0.40 m)

g: gravitation acceleration (9.8m/s^2)

In Figure 3.2.2, the sizes physical restriction was measured on a real pantograph of a trolleybus [102] and assume that the pantograph at highest position while the spring (k_3) fully relaxed under an adjustment [102]. For the maximum position and initial positions of the pantograph, the expressions and derivation are shown below:

Referring to left hand side of Figure 3.2.2

$$\tan\gamma = \frac{L_{prl}}{Lprv} = \frac{0.125}{0.40} \approx 0.286 \qquad \text{E3.2.3}$$

$$\therefore \gamma \approx 17.4^o; \ \ \therefore \ \theta_{max} \approx 90^o - 17.4^o = 72.6^o$$

$$H_{hst} = L_{pb} \cdot \cos\gamma + H_{pt} = 6 * \cos 18.4^o + 3.5 \approx 9.2m \qquad \text{E3.2.4}$$

It is also easy to get the pantograph preferred lowest lifting angle θ_{min} as a verification of pantograph initial lifting angle θi got and pantograph lifting angle θ during operation which means they both must be between θ_{min} and θ_{max} under any condition.

$$\theta_{min} = \sin^{-1}\frac{H_{lst} - H_{pt}}{L_{pb}} = \frac{4.7 - 3.5}{6} \approx 11.5^o$$

Referring to right hand side of Figure 3.2.2, the preload lift force (provide by k_3) and gravity of pantograph (including boom and head) in balance on torque equations are shown in E3.2.5 and E3.2.6 as well as the solution of them is shown in E3.2.7

$$F_{k3} \cdot d_{kp} = m_4 \cdot g \cdot L_{pb}\cos\theta_i + m_3 \cdot g \cdot \frac{L_{pb}}{2}\cos\theta_i \qquad \text{E3.2.5}$$

$$F_{k3} = k_3 \cdot d_{kp} \cdot tan\,\theta_i \qquad \text{E3.2.6}$$

$$\therefore sin\,\theta_i = \frac{-3k_3 \cdot {d_{kp}}^2 + \sqrt{\left(3k_3 \cdot {d_{kp}}^2\right)^2 + 16(m_4+m_3)^2 \cdot g^2 \cdot {L_{pb}}^2}}{4(m_4+m_3)g \cdot L_{pb}} \qquad \text{E3.2.7}$$

3.2.3 Model of catenary-pantograph of the trolleybus

The models of catenary and initial position of pantograph under equilibrium have been determined in Figure 3.2.2. During operation, it can be assumed that the pantograph of trolleybus can be modelled as movement around a lifting angle θ by a constrained angular movement Δθ, as shown in Figure 3.2.3.

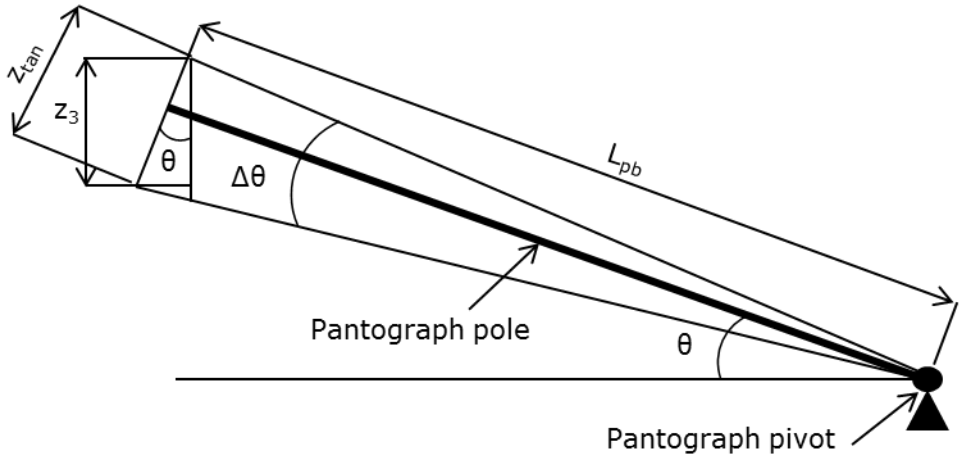

Figure 3.2.3-*Pantograph of trolleybus is around lifting angle θ with a constrained angular movement Δθ*

Where:

θ: pantograph lifting angle during operation (degrees)

Δθ: constrained angular movement Δθ (degrees)

L_{pb}: length of pantograph-boom (6.0 m)

z_3: pantograph boom vertical displacement (m)

Z_{tan}: pantograph boom vertical displacement (m)

Integrating all these models and assumptions, the full model of a trolleybus catenary-pantograph could be developed as shown in Figure 3.2.4

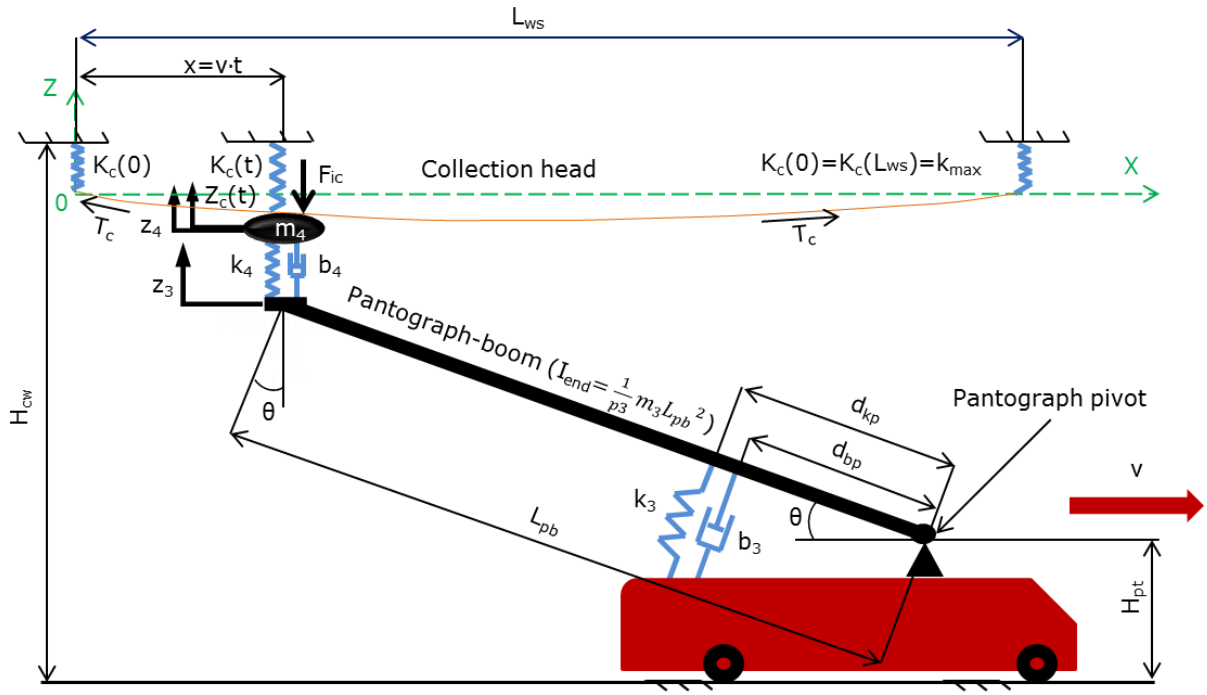

Figure 3.2.4-C*atenary-pantograph model of trolleybus*

Where:

$K_c(t)$: catenary contact wire nominal stiffness (N/m)

$K_c(0) = K_c(L_{ws}) = k_{max}$: catenary contact wire maximum stiffness (N/m)

k_{min}: catenary minimum stiffness (N/m) (not showing in Figure 3.2.1)

k_{mean}: catenary average stiffness (N/m)

L_{ws}: catenary contact wire span between two poles (m)

T_c: tensile force of catenary contact wire (N)

$Z_c(t)$: pre-catenary vertical displacement (m)

F_{ic}: integrated contact force between catenary and pantograph-head (N) [109]

H_{cw}: installation height of the catenary wire (normally from ground to fixed point on poles). It is determined the BSI British Standards in trolleybus (m) [37]

H_{pt}: pivot height of pantograph from ground (3.50 m)

z_3: pantograph boom vertical displacement (m)

m_3: pantograph-boom mass (kg)

b_3: pantograph-boom absorbers damping rate (Ns/m)

k_3: pantograph-boom spring nominal stiffness (N/m)

d_{bp}: distance from damper fitting point to pantograph pivot point (m)

d_{kp}: distance from spring fitting point to pantograph pivot point (m)

z_4: pantograph-head vertical displacement (trajectory) (m)

m_4: pantograph-head mass (kg)

b_4: collection head absorbers damping rate (Ns/m)

k_4: pantograph-head spring stiffness (N/m)

I_{end}: pantograph-boom moment of inertia to ($kg \cdot m^2$)

θ: pantograph-boom dynamic lifting angle (degrees)

L_{pb}: length of pantograph-boom (m)

g: gravitation acceleration ($9.8 m/s^2$)

ρ: catenary wire linear mass density (kg/m)

x: contact position distance from 0 of x-axis ($x=v \cdot t$) (m)

v: trolleybus speed (m/s)

Note: As a trolleybus is an urban transport system with an operational speed that is less than 70 % of the catenary wave propagation speed [99, p20], the wave propagation speed is not taken into account in the modelling of the catenary-pantograph system in the thesis. However, for higher speed applications, such as E-motorway mentioned in Section 1.3, Chapter 1, this would be necessary.

From Figure 3.2.3 and Figure 3.2.4 with Newton's second law in linear and rotational motions the dynamic model of the catenary-pantograph system can be derived as follows:

$$\boldsymbol{I_{end} \cdot \ddot{\Delta\theta} = -b_3 \cdot \dot{z}_3 \cdot \frac{d_{bp}}{L_{pb}} \cdot cos\,\theta \cdot d_{bp} - k_3 \cdot z_3 \cdot \frac{d_{kp}}{L_{pb}} \cdot \cos\theta \cdot d_{kp} + b_4 \cdot (\dot{z}_4 - \dot{z}_3) \cdot cos\,\theta \cdot L_{pb} + k_4 \cdot (z_4 - z_3) \cdot cos\,\theta \cdot L_{pb}} \quad \text{E3.2.8}$$

$$\boldsymbol{m_4 \ddot{z}_4 = -b_4(\dot{z}_4 - \dot{z}_3) - k_4(z_4 - z_3) - F_{ic}} \text{ [109]} \quad \text{E3.2.9}$$

$$\boldsymbol{where:\ I_{end} = \frac{1}{3} \cdot m_3 \cdot L_{pb}{}^2} \quad \text{E3.2.10}$$

The derivation of E3.2.8 is shown Appendix. S_{cd} E3.2.8. In E3.2.9, the integrated contact force between catenary wire and pantograph-head (F_{ic}) can be thought of as a combination of two kinds of forces: self-generation static force (F_{sg}) and dynamic contact force (F_{dc}). The derivation of $F_{sg\ and}$ F_{dc} will be carried out next.

As the dynamic displacement of pantograph is less than 70mm [145, 161], therefore the pantograph dynamic angular movement with 6.0 m length of pantograph-boom (L_{pb}) is definitely smaller than ($\Delta\theta \leqslant 15^o$). The following approximation is smaller than 1% in sine

and 2% in tangent from the measure of the angle [156]. The linearization could be made and derived as follows:

$$\Delta\boldsymbol{\theta} = \frac{\boldsymbol{Z_{tan}}}{\boldsymbol{L_{pb}}} = \frac{\boldsymbol{z_3}}{\boldsymbol{L_{pb}}\cdot\boldsymbol{\cos\theta}};\ \boldsymbol{where}\ \boldsymbol{z_3} = \boldsymbol{Z_{tan}}\cdot\boldsymbol{\cos\theta} \qquad \text{E3.2.11}$$

$$\Delta\ddot{\boldsymbol{\theta}} = \frac{\ddot{\boldsymbol{z}}_{\boldsymbol{tan}}}{\boldsymbol{L_{pb}}} = \frac{\ddot{\boldsymbol{z}}_{\boldsymbol{3}}}{\boldsymbol{L_{pb}}\cos\boldsymbol{\theta}} \qquad \text{E3.2.12}$$

Putting E3.2.10 into E3.2.8 produces E3.2.8A

$$\frac{\boldsymbol{1}}{\boldsymbol{3}}\cdot\boldsymbol{m_3}\cdot\boldsymbol{L_{pb}}^{\boldsymbol{2}}\cdot\frac{\ddot{\boldsymbol{z}}_{\boldsymbol{3}}}{\boldsymbol{L_{pb}}\cos\boldsymbol{\theta}} = -\boldsymbol{b_3}\cdot\dot{\boldsymbol{z}}_{\boldsymbol{3}}\cdot\frac{\boldsymbol{d_{bp}}}{\boldsymbol{L_{pb}}}\cdot\boldsymbol{cos\,\theta}\cdot\boldsymbol{d_{bp}} - \boldsymbol{k_3}\cdot\boldsymbol{z_3}\cdot\frac{\boldsymbol{d_{kp}}}{\boldsymbol{L_{pb}}}\cdot\boldsymbol{\cos\theta}\cdot\boldsymbol{d_{kp}} + \boldsymbol{b_4}\cdot$$
$$(\dot{\boldsymbol{z}}_{\boldsymbol{4}} - \dot{\boldsymbol{z}}_{\boldsymbol{3}})\cdot\boldsymbol{cos\,\theta}\cdot\boldsymbol{L_{pb}} + \boldsymbol{k_4}\cdot(\boldsymbol{z_4} - \boldsymbol{z_3})\cdot\boldsymbol{cos\,\theta}\cdot\boldsymbol{L_{pb}} \qquad \text{E3.2.8A}$$

For simplification of the mathematical expression, E3.2.8A and E3.2.9 can be re-written or re-ordered as E3.2.13, E3.2.11and E3.2.14 as follows:

$$\boldsymbol{m_3}\ddot{\boldsymbol{z}}_{\boldsymbol{3}} = -\boldsymbol{b_{3eq}}\cdot\dot{\boldsymbol{z}}_{\boldsymbol{3}}\cdot\boldsymbol{con^2\theta} - \boldsymbol{k_{3eq}}\cdot\boldsymbol{z_3}\cdot\boldsymbol{cos^2\theta} + \boldsymbol{3b_4}(\dot{\boldsymbol{z}}_{\boldsymbol{4}} - \dot{\boldsymbol{z}}_{\boldsymbol{3}})\cdot\boldsymbol{cos^2\theta} +$$
$$\boldsymbol{3k_4}(\boldsymbol{z_4} - \boldsymbol{z_3})\cdot\boldsymbol{cos^2\theta} \qquad \text{E3.2.13}$$

$$\boldsymbol{where}:\ \boldsymbol{b_{3eq}} = \boldsymbol{3b_3}\cdot\frac{\boldsymbol{d_{bp}}^{\boldsymbol{2}}}{\boldsymbol{L_{pb}}^{\boldsymbol{2}}};\ \boldsymbol{k_{3eq}} = \boldsymbol{3k_3}\cdot\frac{\boldsymbol{d_{kp}}^{\boldsymbol{2}}}{\boldsymbol{L_{pb}}^{\boldsymbol{2}}} \qquad \text{E3.2.14}$$

The self-generation static force (F_{sg}) between the catenary wire and pantograph-head is generated by the compressed pantograph-head (with stiffness k_4) and pantograph-boom (with stiffness k_3). This is due to the pantograph-head being forcedly pushed down by the catenary wire (the catenary wire installation level is much lower than initial position of pantograph-head). It remains as long as the pantograph engaged with the catenary wire. This applies to all kinds of electrified transport system such as trolleybus, light railways and trains and is the essential contact force that reduces variation in the dynamic contact force.

F_{sg} is a complex dynamic force that relates the displacement ($Z_c(t)$) and stiffness $K_c(t)$ of the catenary wire and the model of self-generation static force (F_{sg}) is shown in Figure 3.2.5. As the self-generation static force can be thought of as the pantograph lifting force acting on the catenary wire as it moves up or down with different displacements. Among all the possible displacements that the deflection of catenary may follow, called virtual displacements [105], the self-generation static force can be assumed and treated as a non-conservative force [106] as shown in equation E3.2.15.

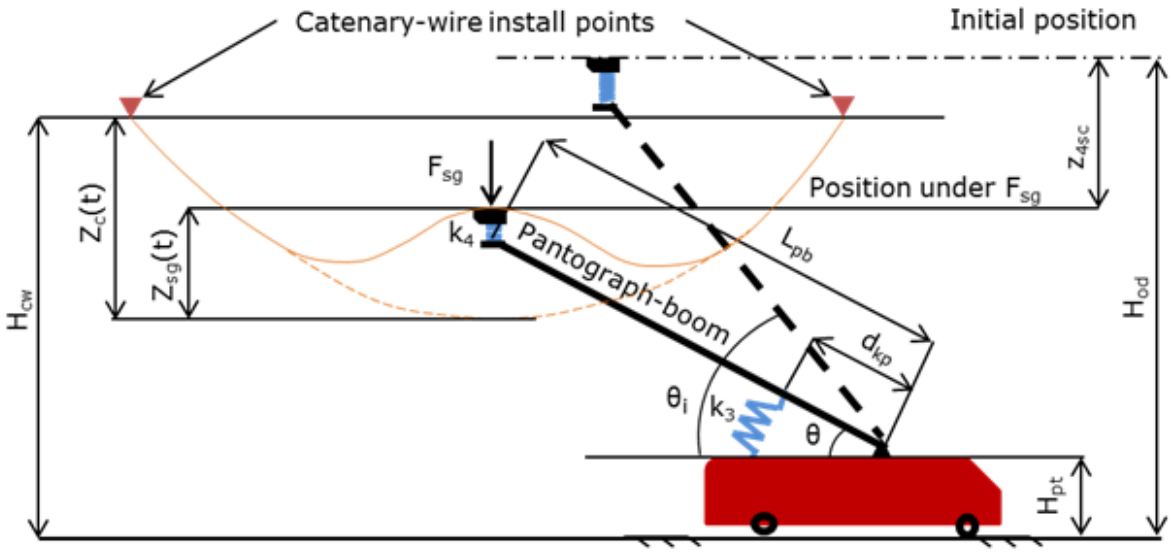

Figure 3.2.5-*Model of self-generation static force (F_{sg})*

Where:

F_{sg}: self-generation static force (N)

H_{od}: initial position of pantograph-head from ground (m)

H_{cw}: installation height of the catenary wire (normally from ground to fixed point on poles). It is determined the BSI British Standards in trolleybus (m) [37]

$Z_c(t)$: original vertical displacement of catenary wire (m)

$Z_{sg}(t)$: vertical displacement of catenary wire under the self-generation static force (m)

z_{4sc}: distance between initial position of pantograph-head from ground (H_{od}) and balance position of pantograph-head under self-generation static force (m).

L_{pb}: length of pantograph-boom (6.0 m)

k_3: pantograph-boom spring stiffness (N/m)

d_{kp}: distance from spring fitting point to pantograph pivot point (m)

k_4: pantograph-head stiffness (N/m)

θ_{max}: pantograph highest rising angle (degrees)

θ_i: pantograph initial rising angle (degrees)

Following Hooke's law and geometrics, the equations of the self-generation static force (F_{sg}) is deduced as shown below:

$$\boldsymbol{F_{sg} = \frac{k_{3eq} \cdot k_4}{k_{3eq} + k_4} \cdot z_{4sc} = Kc(t) \cdot Z_{sg}(t)} \quad \text{E3.2.15}$$

$$\boldsymbol{H_{od} = z_{4sc} + Z_{sg}(t) + H_{cw} - Z_c(t)} \quad \text{E3.2.16}$$

Using both E3.2.15 and E3.2.16, z_{4sc} can be deduced as E3.2.17

$$\boldsymbol{z_{4sc}} = \frac{\boldsymbol{H_{od}-H_{cw}+Z_c(t)}}{\boldsymbol{1+\frac{k_{3eq}\cdot k_4}{K_c(t)\cdot\left(k_{3eq}+k_4\right)}}} \quad \text{E3.2.17}$$

A further derivation can be made to get E3.2.18 for F_{sg}

$$\boldsymbol{F_{sg}} = \frac{\boldsymbol{k_{3eq}\cdot k_4}}{\boldsymbol{k_{3eq}+k_4}} \cdot \frac{\boldsymbol{H_{od}-H_{cw}+Z_c(t)}}{\boldsymbol{1+\frac{k_{3eq}\cdot k_4}{K_c(t)\cdot\left(k_{3eq}+k_4\right)}}} \quad \text{E3.2.18}$$

The dynamic contact force F_{dc} is only generated during the running operation of trolleybus. This force is dynamic and strongly related to the displacement ($Z_c(t)$) and stiffness $K_c(t)$ of the catenary wire as well as the pantograph-head vertical displacement (z_4).

$$\boldsymbol{F_{dc} = K_c(t)\cdot[z_4 - Z_c(t)]} \quad \text{E3.2.19}$$

The integrated contact force (F_{ic}) between the catenary wire and the pantograph-head is therefore the sum of the self-generation static force and the dynamic contact force. This is shown in E3.2.21

$$\boldsymbol{F_{ic} = F_{sg} + F_{dc}}$$

$$\boldsymbol{F_{ic}} = \frac{\boldsymbol{k_{3eq}\cdot k_4}}{\boldsymbol{k_{3eq}+k_4}} \cdot \frac{\boldsymbol{H_{od}-H_{cw}+Z_c(t)}}{\boldsymbol{1+\frac{k_{3eq}\cdot k_4}{K_c(t)\cdot\left(k_{3eq}+k_4\right)}}} + \boldsymbol{K_c(t)\cdot[z_4 - Z_c(t)]} \quad \text{E3.2.20}$$

As the catenary wire gravity force ($g\cdot\rho$) is an element of the pre-vertical displacement of pre-loaded catenary wire $Z_c(t)$ (defined by E3.2.1), the integrated contact force includes a contribution from catenary wire gravity.

From Figure 3.2.4, the equation of sinθ can be deduced as shown in E3.2.21with E3.2.17

$$\boldsymbol{\sin\theta} = \frac{\boldsymbol{H_{od}-H_{pt}-z_{4sc}}}{\boldsymbol{L_{pb}}} \quad \text{E3.2.21}$$

Integrating all these derivations, the final model of the catenary-pantograph of a trolleybus has been shown in E3.2.13, E3.2.9, E3.2.14, E3.2.17, E3.2.20, E3.2.21 and E3.2.22.

3.2.4 Simulation and analysis of trolleybus catenary-pantograph

A Simulink configuration of the trolleybus catenary-pantograph was created covering the models of catenary wire, initial position of pantograph under pre-load and the self-generation

static force of the trolleybus. Figure 3.2.6 shows the configuration of the catenary-pantograph as expressed in equations E3.2.1 and E3.2.2.

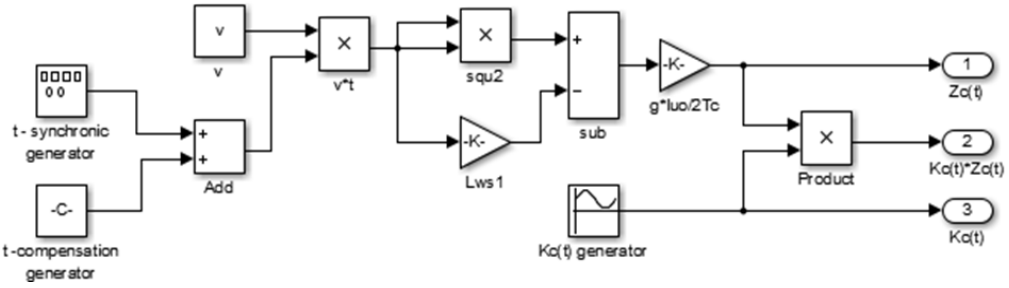

Figure 3.2.6-*Simulink configuration of the catenary*

Figure 3.2.7 shows the configuration of the catenary-pantograph of the trolleybus which covers all the models of catenary wire, initial position of pantograph under the pre-load and integrated vertical catenary-pantograph of the trolleybus as expressed in equations of E3.2.11, E3.2.13, E3.2.14, E3.2.17, E3.2.20 and E3.2.22.

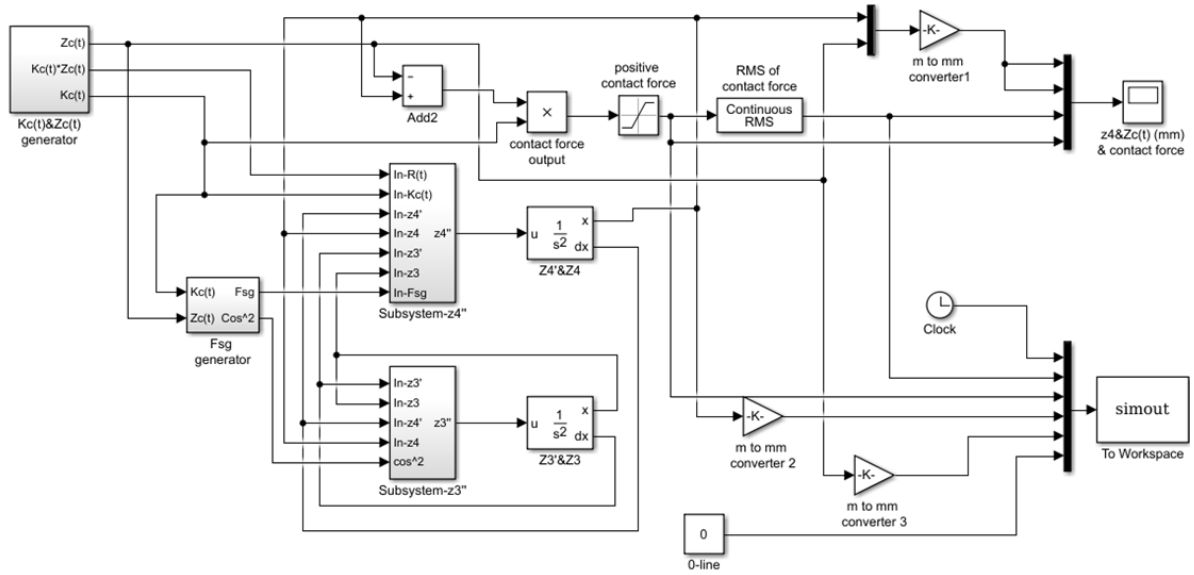

Figure 3.2.7-*Simulink configuration of catenary-pantograph of the trolleybus*

Prior to carrying out the simulation, there were various conditions and parameters that needed to be determined using real-world trolleybus operation. As the trolleybus is for urban public transport, there are three different speed considered in the simulation relating to the specific situations shown in Table 3.2.1. “In depot” models the low speed in depot where the integrated contact force (F_{ic}) approaches the self-generation static force only as the speed of trolleybus is effectively zero. “On street” and “Highest speed” then model the regulation

speed 30 mph (13.3m/s) in British Town [157] and the average maximum speed of trolleybuses which is usually between 60 km/h (16.7m/s) and 80km/h (22.2m/s)) [158]. With this simplification, three different velocities are selected for simulation

Table 3.2.1 Selected trolleybus velocities for simulation

Speed	In depot	On street	Highest speed
V(m/s)	1.0	14.0	20.0

In order to estimate the other parameters, practical measurement had to be carried out in "Crich Tramway Village" [100] and "The Trolleybus Museum at Sandtoft" [101] respectively with the help and supervision of Mr. M. C Carbtree (Crich Tramway Village) and Mr. Francis Whitlehead (The Trolleybus Museum at Sandtoft). In particular, the measurements of an old-style trolleybus, as given by Mr Tim Stubbs [102], were very useful and helpful for modelling and simulations.

In practice, the measured self-generation static force (F_{sg}) varies from 33 to 145N [100,101], the average being simply 89N. The mass of trolleybus pantograph combination (single) including pole and hub etc. was from a practical measurement in Mr Tim Stubbs' garage. The measured mass of the pantograph combination is 76.6kg (single pole and hub) [102]. Taking the additional masses of actuators and relevant mechanism (approximate 20kg), power cables (approximate 17kg, 95mm^2, 600-1000V.) and bolts (approximate 10kg) etc. [103, 104] into account, the mass of pantograph m_3 would be 120 kg in total.

$$\boldsymbol{m_3 \approx 120(kg)}$$

Some specification of trolleybus pantograph and catenary wire cannot be found in the references or not easy getting from real-practice measurement , therefore all data for simulation are gathered from practice measurement in trolleybus and trams stated above as well as the papers involved in light rail (modified referring to [25, 89]) shown in table 3.2.2.

Table 3.2.2 Selected parameters for simulation of trolleybus

Parameters	m_3 (kg)	k_3 (N/m)	b_3 (Ns/m)	m_4 (kg)	k_4 (N/m)	b_4 (Ns/m)	
Value	120	24000 [102]	150	4	7000	30	
Parameters	L_{pb} (m)	d_{kp} (m)	d_{bp} (m)	θ_{max} (degree)		v (m/s)	g ($m/s^{2)}$
Value	6.0	0.1	0.1	72.3		1, 14, 20	9.18
Parameters	L_{ws} (m)	T_c (N)	H_{cw} (m)	H_{pt} (m)	ρ (kg/m)	k_{min} (N/m)	k_{max} (N/m)
Value	30	10^4	5.5	3.5	0.95[75]	1000	3000

Where:

m_3: pantograph-boom mass (kg)

k_3: pantograph-boom spring nominal stiffness (N/m)

b_3: pantograph-boom absorbers damping rate (Ns/m)

m_4: collection head mass (kg)

k_4: collection head spring stiffness (N/m)

b_4: collection head absorbers damping rate (Ns/m)

L_{pb}: length of pantograph-boom (m)

d_{kp}: distance from spring fitting point to pantograph pivot point

d_{bp}: distance from damper fitting point to pantograph pivot point

θ_{max}: pantograph highest rising angle (degrees)

g: gravitation acceleration ($9.8m/s^2$)

L_{ws}: catenary contact wire span between two poles (m)

T_c: tensile force of catenary contact wire (N)

H_{cw}: installation height of the catenary wire (normally from ground to fixed point on poles). It is determined the BSI British Standards in trolleybus (m) [37]

H_{pt}: pivot height of pantograph from ground (3.50 m)

ρ: catenary wire linear mass density (kg/m)

k_{min}: catenary minimum stiffness (N/m)

k_{mean}: catenary average stiffness (N/m)

v: trolleybus speed (m/s)

The simulation was performed at the three speeds, 1m/s (In depot), 14m/s (On street) and 20m/s (Highest speed), defined in Table 3.2.1.

In the following Simulink displays, the following abbreviations are used:

Fic: integrated contact force (N)

Fic (RMS): integrated contact force (RMS) (N)

z4: pantograph-head vertical displacement (m)

Zc(t): original vertical displacement of catenary wire (m)

As the most important values of displacement and integrated contact force (Fic) are between the catenary and pantograph-head, the simulation results at the three different speeds selected are shown in Figure3.2.8, Figure3.2.9 and Figure 3.2.10.

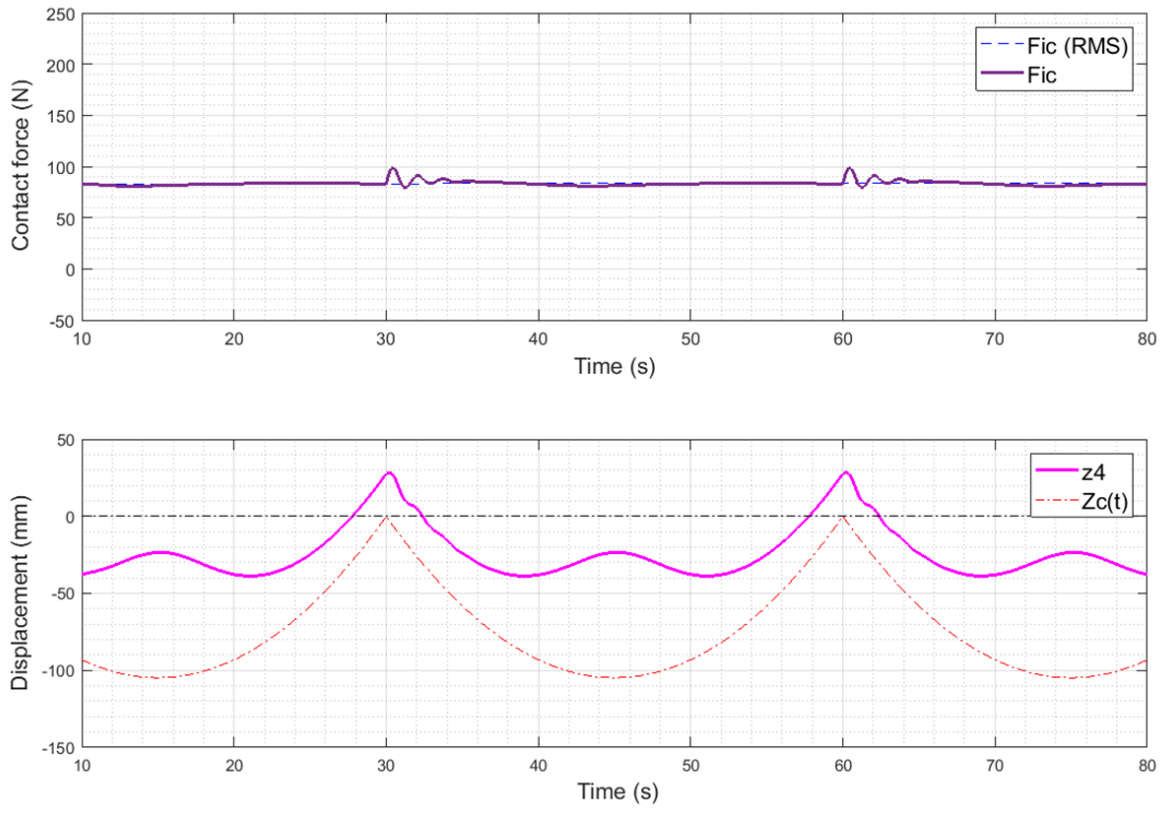

Figure 3.2.8-*Trolleybus' catenary-pantograph simulation result at v=1m/s (In depot speed)*

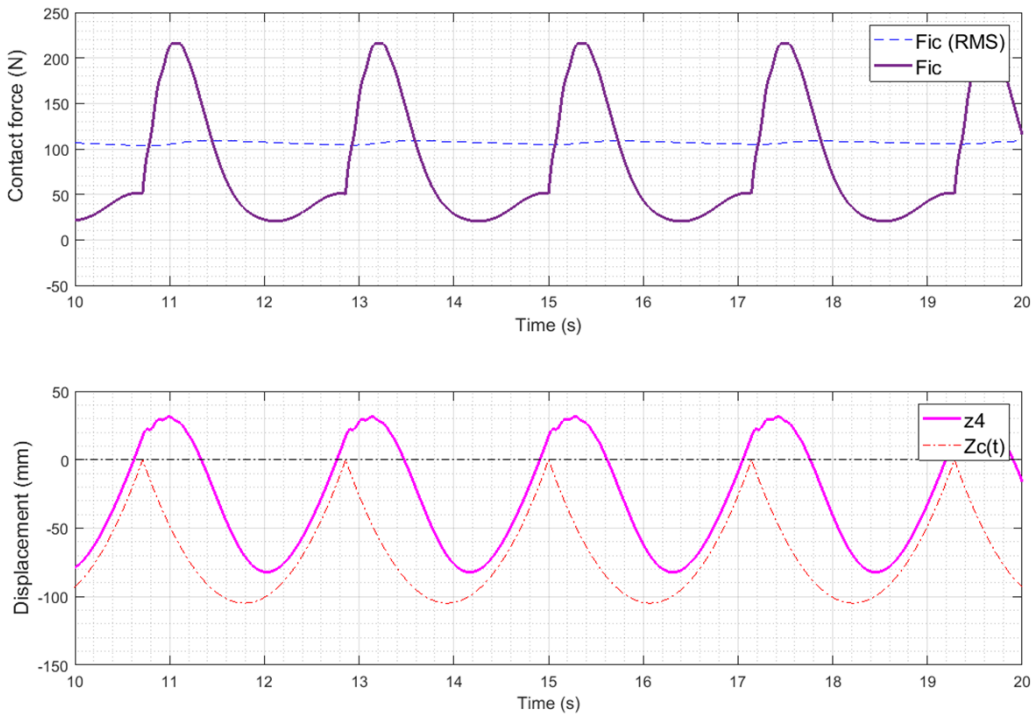

Figure 3.2.9-*Trolleybus' catenary–pantograph simulation result at v=14m/s (On street speed)*

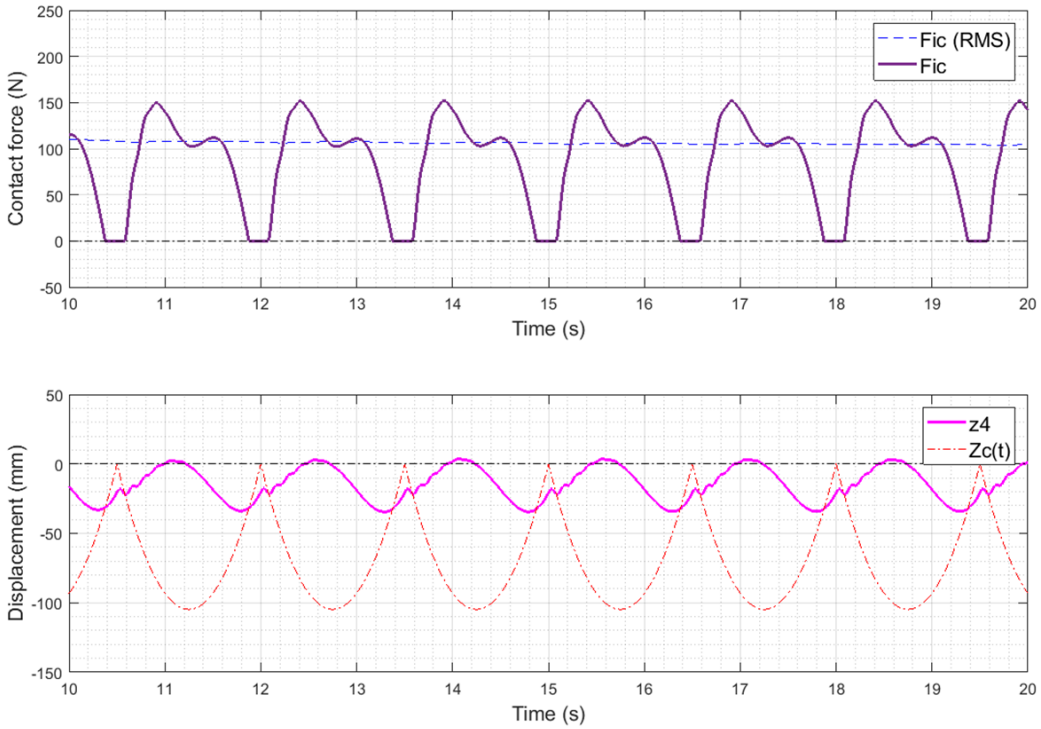

Figure 3.2.10-*Trolleybus' catenary–pantograph simulation result at v=20m/s (Highest speed)*

From Figure 3.2.8 it can be seen that at v=1m/s speed (In depot) the integrated contact force (F_{ic}) value of 89N is close to the average real value of the self-generation static force (84N)

measured at trolleybus museum and the tram at depot in Sheffield [101, 108]. In addition, the value is essentially stable with only a slight vibration at the poles' hang on point (highest stiffness of catenary wire) which is reasonable.

Using Time Scope in the DSP system of Simulink to take a statistical analysis of the integrated contact force (F_{ic}) from Figure 3.2.8, 3.2.9 and 3.2.10 the results listed in Table 3.2.3 were obtained.

Table 3.2.3 Statistical analysis of F_{ic} simulation results

Contact force (N) / Speed (m/s)	F_{ic} (RMS)	F_{ic} (Max)	F_{ic} (Min)	Variation (Max-Min)
1.0 (In depot)	89	98	79	9
14.0 (On street)	105	216	20	196
20.0 (Highest speed)	108	152	0	150

Note: F_{ic} (integrated contact force between catenary wire and pantograph-head)

It is clear from Table 3.2.3 that at trolleybus running speeds of 14.0m/s (On street) and 20.0m/s (Highest speed), the variation of integrated contact force (F_{ic}) is significantly increased to 150N and 196N from the 9N at the 1m/s running speed. This means that the main contribution is from the dynamic contact force. The range of values for the (Fic RMS) of the integrated contact forces is much smaller in comparison to the range in Variation of Fic. This indicates that the main contribution of variability in the integrated contact forces is from self-generation static force.

An interesting point found in Figure 3.2.10, is the fact that contact loss happens around the fixed points of the catenary pole (highest stiffness). This causes the integrated contact forces to be zero (Fic = 0N) at highest speed (20m/s). Additionally, the zones where the pantograph-head is lower than the catenary wire ($z_4 < Z_c(t)$) and the integrated contact force (F_{ic}) is zero are perfectly overlapped, indicating that the catenary wire and pantograph-head are separated without contact.

The results of simulations are explained as follows:

F_{ic} (RMS): The effective value of the positive contact force defines the quality of general contact performance between the pantograph-head and catenary wire.

F_{ic}: The transient contact force (both positive and zero) between the pantograph-head and catenary wire. This is useful to estimate the possible positions of de-wirement, electric arcing and unbalance wearing in different section along the catenary wire between the poles.

Zones of z_4-$Z_c(t)>0$ and positive contact force ($F_{ic}>0$) are perfectly overlapped. It means the catenary wire and pantograph (head) are effectively engaged with effective contact therefore the trolleybus is receiving electrical power from catenary wire.

Zones of z4-$Z_c(t) \leqslant 0$ and zero contact force ($F_{ic}=0$) are perfectly overlapped in Figure3.2.10. This means that the pantograph (head) has separated from the catenary wire. Full quantification of such a loss of contact, with a high probability of arcing and potential de-wirement, might require the development of hybrid models. For example, the catenary wire keeps (or restores to) the original shape (pre-displacement). It could also be assumed that the pantograph (head) is free in inertia-vibration from the separate point (beginning point of Fic=0) with initial position and speed until the re-engaged point (ending point of Fic=0) with catenary. Further discussion of this will be given in Chapter 4.

The catenary wire $Z_c(t)$ shape with 104mm biggest displacement (sag) with 10000(N) tension is reasonable with reality of trolleybus catenary [38]

Variation of F_{ic} increases sharply with increased trolleybus speed. The variation of F_{ic} (RMS) is much smaller than variation of F_{ic}. The discussable points are as follows:

F_{ic} (RMS) meets the requirement of the standard (80-130N) [37] at speeds of 1m/s (In depot), 14.0m/s (On street) and 20.0m/s (Highest speed)

In general, it could be thought that zero contact force (Fic = 0) and the pantograph (head) being separated from catenary wire would be the worst situation in operation of a trolleybus. A more in-depth investigation of this effect will be the key point should be studied and prevented when using an active control system.

3.3 Modelling and simulation of half trolleybus

3.3.1 Model of half passive trolleybus

A trolleybus requires a pantograph which is mounted at a specific position on the trolleybus roof running in contact with the catenary wire. However, this pantograph will have a vertical

displacement and pitch angle that is out of phase with the road disturbances. Therefore, a model of a half passive trolleybus with road disturbance was introduced to investigate this effect. Figure 3.3.1 shows a schematic of the basic half trolleybus vertical passive suspension system model. The suspension has two stages: the tyre stiffness and damping; and the trolleybus' main suspension system after the un-sprung mass.

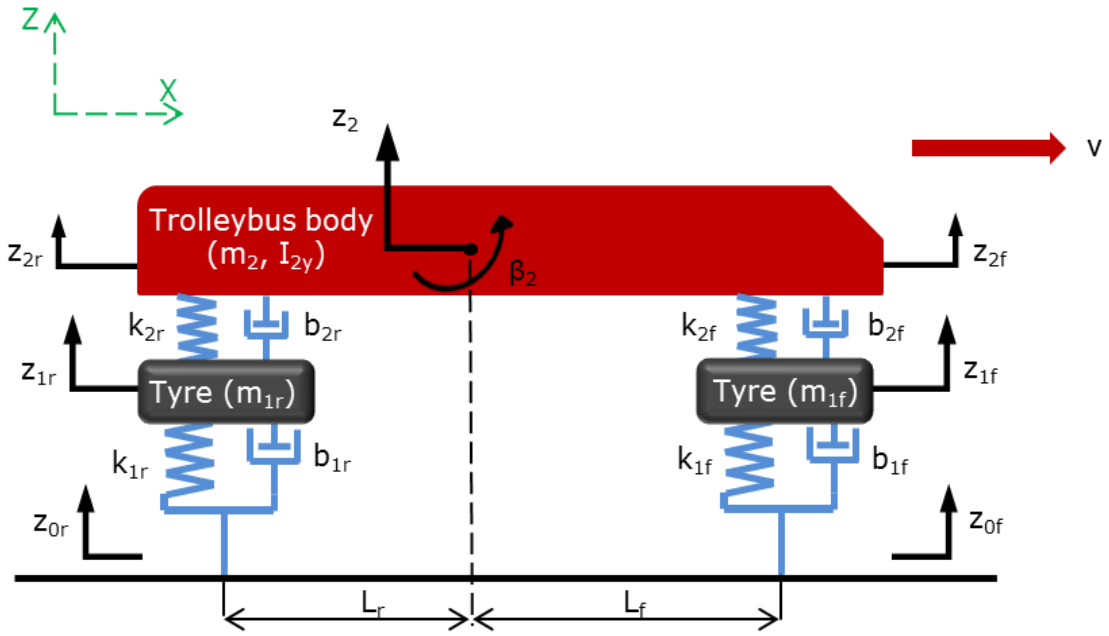

Figure 3.3.1-*Half passive dynamic model of trolleybus*

Where:

z_{0f}: road disturbance (step, random and bump) at the front tyre (m)

z_{1f}: front un-sprung mass vertical displacement (m)

z_{2f}: trolleybus mass vertical displacement at the point of contact with the suspension system (m)

z_{0r}: road disturbance (step, random and bump) at the rear tyre (m)

z_{1r}: rear un-sprung mass vertical displacement (m)

z_{2r}: trolleybus mass vertical displacement at the point of contact with the suspension system (m)

m_{1f}: un-sprung front axle mass (kg)

b_{1f}: front tyre damping (Ns/m)

k_{1f}: front tyre stiffness (N/m)

m_{1r}: un-sprung rear axle mass (kg)

b_{1r}: rear tyre damping (Ns/m)

k_{1r}: rear tyre stiffness (N/m)

L_f: distance between front axle and trolleybus body centre of gravity (m)

Lr: distance between rear axle and trolleybus body centre of gravity (m)

z_2: trolleybus body displacement

m_2: trolleybus body (total sprung) mass (kg)

- m_{2fm}: shared mass on front axle (kg)
- m_{2rm}: shared mass on rear axle (kg)

b_{2f}: front axle damping (Ns/m)

k_{2f}: front axle sprung stiffness (N/m)

b_{2r}: rear axle damping (Ns/m)

k_{2r}: rear axle sprung stiffness (N/m)

β_2: pitch of the trolleybus body around the centre of gravity (assumed to be the y-axis) (Rad)

I_{2y}: moment of inertia of the trolleybus body around the centre of gravity (assumed to be around the y-axis)

v: trolleybus speed (m/s)

Following Newtonian mechanics, the dynamic equations of the half trolleybus model (modified from [95]) are shown in E3.3.1, E3.3.2, E3.3.3 and E3.3.4. The equations of I_2 is written as per [96]

$$\ddot{z}_{1f} = \frac{b_{2f}}{m_{1f}}\left(\dot{z}_{2f} - \dot{z}_{1f}\right) + \frac{k_{2f}}{m_{1f}}\left(z_{2f} - z_{1f}\right) - \frac{b_{1f}}{m_{1f}}\left(\dot{z}_{1f} - \dot{z}_{0f}\right) - \frac{k_{1f}}{m_{1f}}\left(z_{1f} - z_{0f}\right) \quad \text{E3.3.1}$$

$$\ddot{z}_{1r} = \frac{b_{2r}}{m_{1r}}\left(\dot{z}_{2r} - \dot{z}_{1r}\right) + \frac{k_{2r}}{m_{1r}}\left(z_{2r} - z_{1r}\right) - \frac{b_{1r}}{m_{1r}}\left(\dot{z}_{1r} - \dot{z}_{0r}\right) - \frac{k_{1r}}{m_{1r}}\left(z_{1r} - z_{0r}\right) \quad \text{E3.3.2}$$

$$\ddot{z}_2 = -\left[\frac{b_{2f}}{m_2}\left(\dot{z}_{2f} - \dot{z}_{1f}\right) + \frac{k_{2f}}{m_2}\left(z_{2f} - z_{1f}\right)\right] - \left[\frac{b_{2r}}{m_2}\left(\dot{z}_{2r} - \dot{z}_{1r}\right) + \frac{k_{2r}}{m_2}\left(z_{2r} - z_{1r}\right)\right] \quad \text{E3.3.3}$$

$$\ddot{\beta}_2 = -L_f\left[\frac{b_{2f}}{I_2}\left(\dot{z}_{2f} - \dot{z}_{1f}\right) + \frac{k_{2f}}{I_2}\left(z_{2f} - z_{1f}\right)\right] + L_r\left[\frac{b_{2r}}{I_2}\left(\dot{z}_{2r} - \dot{z}_{1r}\right) + \frac{k_{2r}}{I_2}\left(z_{2r} - z_{1r}\right)\right] \quad \text{E3.3.4}$$

$$\textbf{where: } I_2 = \frac{m_2}{3(L_f + L_r)}\left(L_f{}^3 + Lr^3\right)$$

$$z_{2f} = z_2 + L_f \cdot \beta_2$$

$$z_{2r} = z_2 - L_r \cdot \beta_2$$

3.3.2 Modelling of road disturbances

There are three kinds of disturbance that can be applied on the models of integrated vertical catenary-pantograph with half passive trolleybus. These are:

Step disturbance: the step function is one of most useful functions to verify the control design and can be described as a change in the input from zero to a finite value at time t = 0. The response of the system from a step input can be immediately plotted, without need to actually solve for the time response analytically [159]. To model a road disturbance (bump), 0.05m was selected as the value of step.

Random disturbance: Trolleybus vibration input due to road roughness could simulate the normal performance when running on town roads. Longitudinal profiles based on the International Organization for Standardization (ISO 8606) proposed road roughness classification uses power spectral density (PSD) values. For a trolleybus running at speeds of 5-30m/s on paved road, a random road profile of road was generated by a Random Number function associated to trolleybus speed with a gain of 0.45 [160].

Bump disturbance: a road bump was created especially for the trolleybus that combines the two road disturbance models of KTH and SKODA types. The KTH model [47] is shown in Figure 3.3.2. This model was originally assumed for an overhead catenary system providing electric power to a long-distance truck via a Schunk WBL88X2 pantograph that was originally used for the Swedish X2000 high-speed train. However, the assumption used in [47] for a trolley-truck is a10m length bump, may not be suitable for urban trolleybus

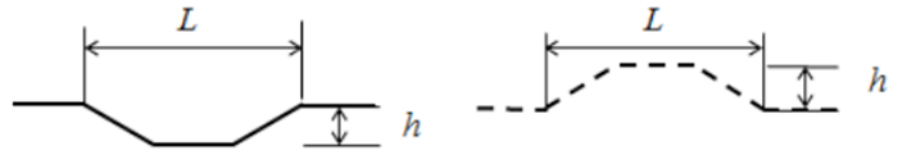

Figure 3.3.2 -*KTH disturbance model* [47]

h=0.04m; L=10m; L is divided into three equally long sections

The SKODA model [48] is shown in Figure 3.3.3. This has an interval between discrete bumps of 20m. It was originally used for modelling of the SKODA 21Tr low-floor trolleybus,

an existing product. The disadvantage of this model is that the crescent shape seems quite dissimilar to real conditions to be expected on the road.

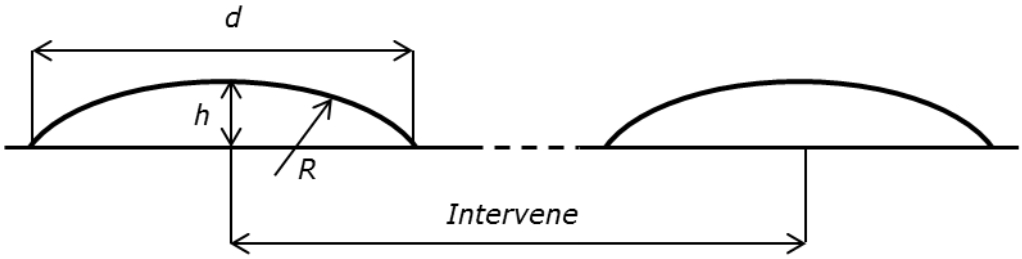

Figure 3.3.3 -*SKODA disturbance model* [48]

h=0.06m; R=0.551m; d=0.5m; Intervene=20m

A new model for the road disturbance is proposed and comply with The Highways (Road Humps) Regulations (HIGHWAYS, ENGLAND AND WALES) [163] in the thesis. In this model, the distance between the bumps is defined as 20m which is same to SKODA model. Meanwhile the shape of the bump is similar to in the KTH model. Detail is shown in Figure 3.3.4.

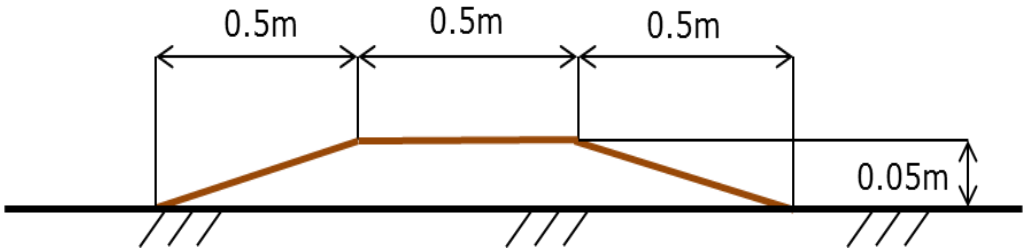

Figure3.3.4-*Proposed shape of ACTCCS road bump (disturbance) model*

3.3.3 Simulation and analysis of half trolleybus

The disturbances simulation equations are defined in section 3.3.2. The "disturbances generator" is shown in Figure 3.3.5. The delay block creates a time delay signal between the front and rear axles which is the distance between the two axles (L_f+L_r) divided by trolleybus speed (v). Therefore, z_{0f} & $k_{1f}\cdot z_{0f}$ and z_{0r} & $k_{1r}\cdot z_{0r}$ are expressed as the disturbances between the front and rear tyres. The three kinds of disturbances mentioned section 3.3.2 are included in this "disturbances generator Simulink configuration". They are Step, Random road and Bump disturbances.

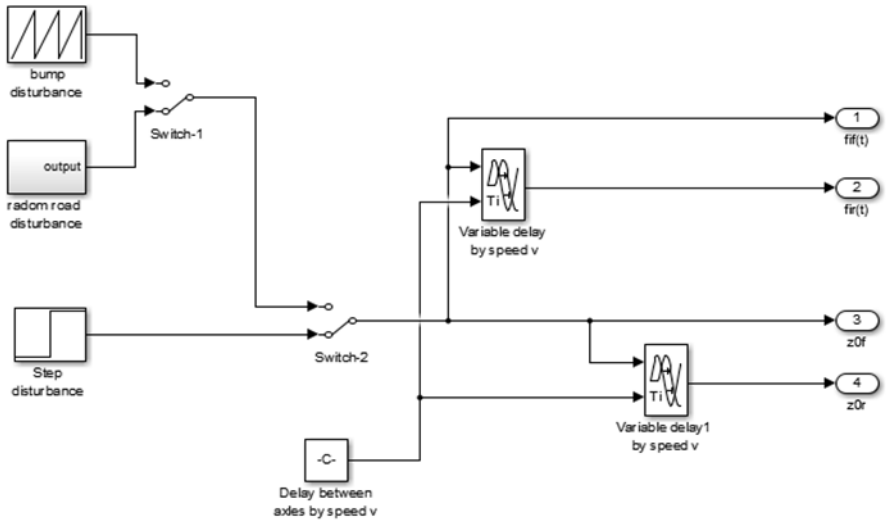

Figure 3.3.5-*Disturbance generator Simulink configuration*

Modelling the dynamic equations E3.3.1, E3.3.2, E3.3.3 and E3.3.4, the Simulink configuration is shown in Figure 3.3.6. The block configuration of 'Bump (disturbances) generator' at the bottom left corner is shown in Figure 3.3.6.

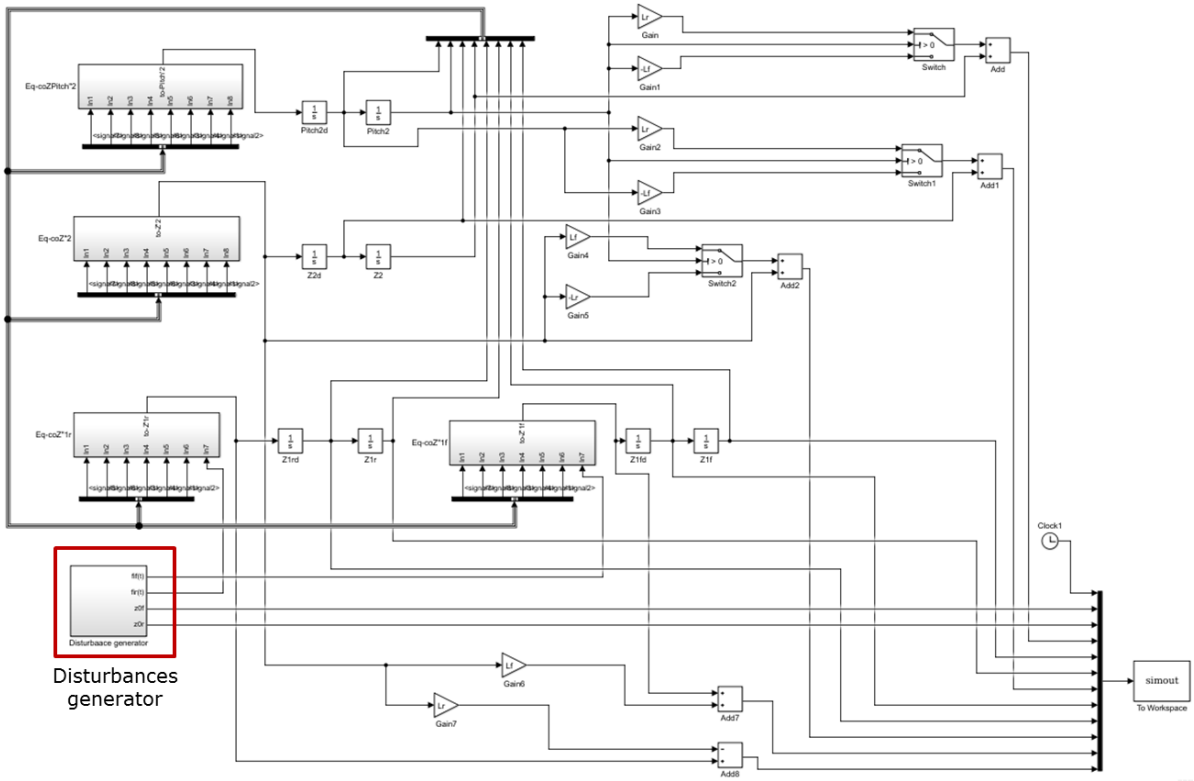

Figure 3.3.6-*Half passive trolleybus dynamic model* (*Trolleybus)*

Simulink configuration (see Scd Fig.3.3.6 in Appendix)

The technical specification of ZF-axles system, VolovB9LA chassis and Continental Tyres [93, 94, 97, 98] which are very popular on urban public transport vehicles are given as the simulation parameters in Table 3.3.1 below.

Table 3.3.1 Half passive trolleybus simulation parameters

Parameters	m_{1f} (kg)	k_{1f} (N/m)	b_{1f} (Ns/m)	m_{1r} (kg)	k_{1r} (N/m)	b_{1r} (Ns/m)
Value	760 [65], [70]	$2x10^6$	1,800	1480 [65], [70]	$2x10^6$	1800
Parameters	m_2 [65] (kg)	k_{2f} (N/m)	b_{2f} (Ns/m)	k_{2r} (N/m)	b_{2r} (Ns/m)	
Value	$1.15x10^4$	$2.4x10^5$	$2x10^4$	$2.4x10^5$	$2x10^4$	
Parameters	L_f (m)	L_r (m)	v (m/s)			
Value	3.8[65]	2.2[71]	1, 14, 20			

Where:

m_{1f}: un-sprung front axle mass (kg)

k_{1f}: front tyre stiffness (N/m)

b_{1f}: front tyre damping (Ns/m)

m_{1r}: un-sprung rear axle mass (kg)

k_{1r}: rear tyre stiffness (N/m)

b_{1r}: rear tyre damping (Ns/m)

m_2: total sprung mass (kg)

k_{2f}: front axle sprung stiffness (N/m)

b_{2f}: front axle damping (Ns/m)

k_{2r}: rear axle sprung stiffness (N/m)

b_{2r}: rear axle damping (Ns/m)

L_f: distance between front axle and trolleybus body centre of gravity (m)

L_r: distance between rear axle and trolleybus body centre of gravity (m)

v: trolleybus speed (m/s)

Simulations of vertical dynamic displacement, velocity and acceleration with the half-passive trolleybus dynamic model with Step, Random and Bump disturbances were carried out at the three different speeds of 1m/s (In Depot), 14m/s (On street) and 20m/s (Highest speed) defined in Table 3.2.1. In fact, the pair of z_{0f} and z_{0r} is disturbances generated by same step (or bump) on front and rear axles respectively with time gap Δt. T_{id} is the duration the trolleybus goes between two bumps' disturbance.

In the following Simulink displays, the following terms are used:

z0f: road disturbance (step) at the front tyre (m)

z0r: road disturbance (step) at the rear tyre (m)

z2: trolleybus body mass vertical displacement (m)

z1f: front un-sprung mass vertical displacement (m)

z1r: rear un-sprung mass vertical displacement (m)

dz2/dt (z2´): trolleybus body mass vertical velocity (m/s)

dz1f/dt (z1f´): front un-sprung mass vertical velocity (m/s)

dz1r/dt (z1r´):: rear un-sprung mass vertical velocity (m/s)

z2¨: trolleybus body mass vertical acceleration (m/s2)

z1f¨: front un-sprung mass vertical acceleration (m/s2)

z1r¨: rear un-sprung mass vertical acceleration (m/s2)

Δt: time gaps between two tyres at certain speed of trolleybus

T_{id}: duration the trolleybus goes between two bumps' disturbance

Lf: distance between front axle and trolleybus body centre of gravity (m)

Lr: distance between rear axle and trolleybus body centre of gravity (m)

v: trolleybus speed (m/s)

The simulation results for the step (value of 0.05m) disturbance at the three speeds of 1m/s (In depot), 14m/s (On street) and 20m/s (Highest speed) are shown in Figure3.3.7, Figure3.3.8 and Figure3.3.9.

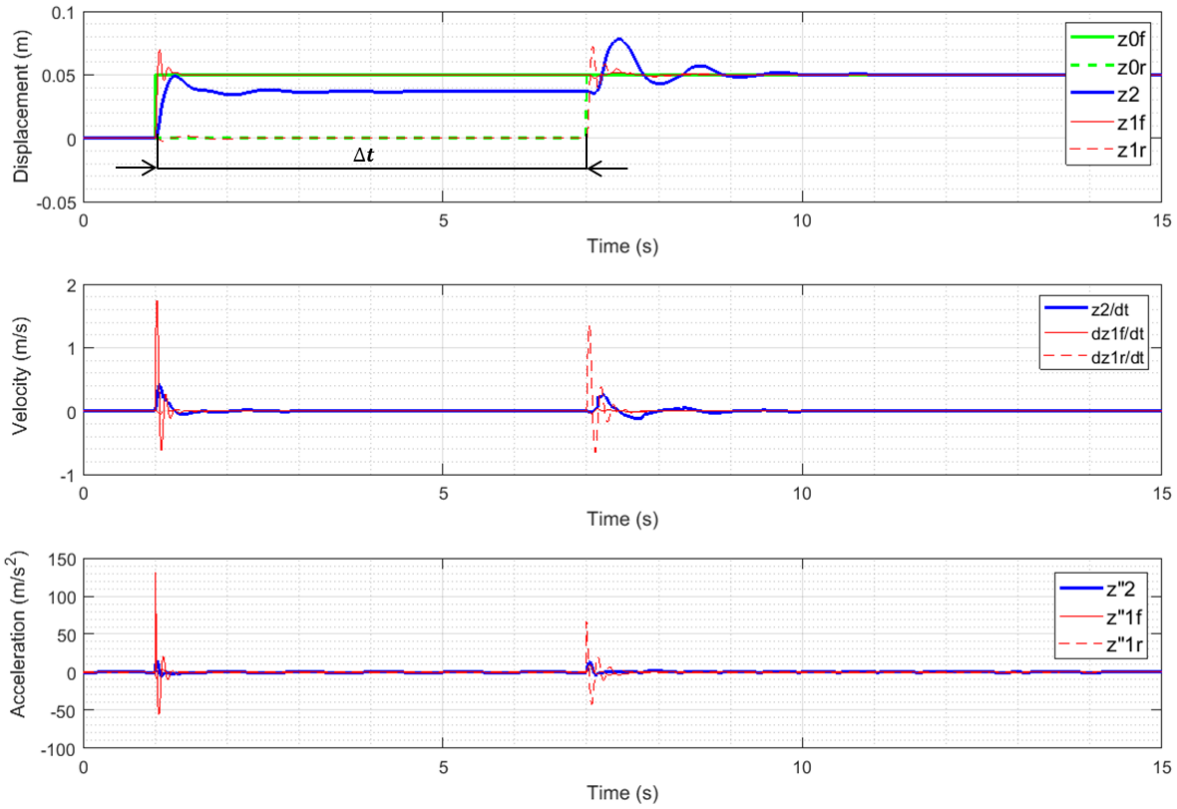

Figure 3.3.7-*Simulation results of half passive trolleybus dynamic model with step disturbance at 1m/s; $\Delta t = (L_f+L_r)/v$*

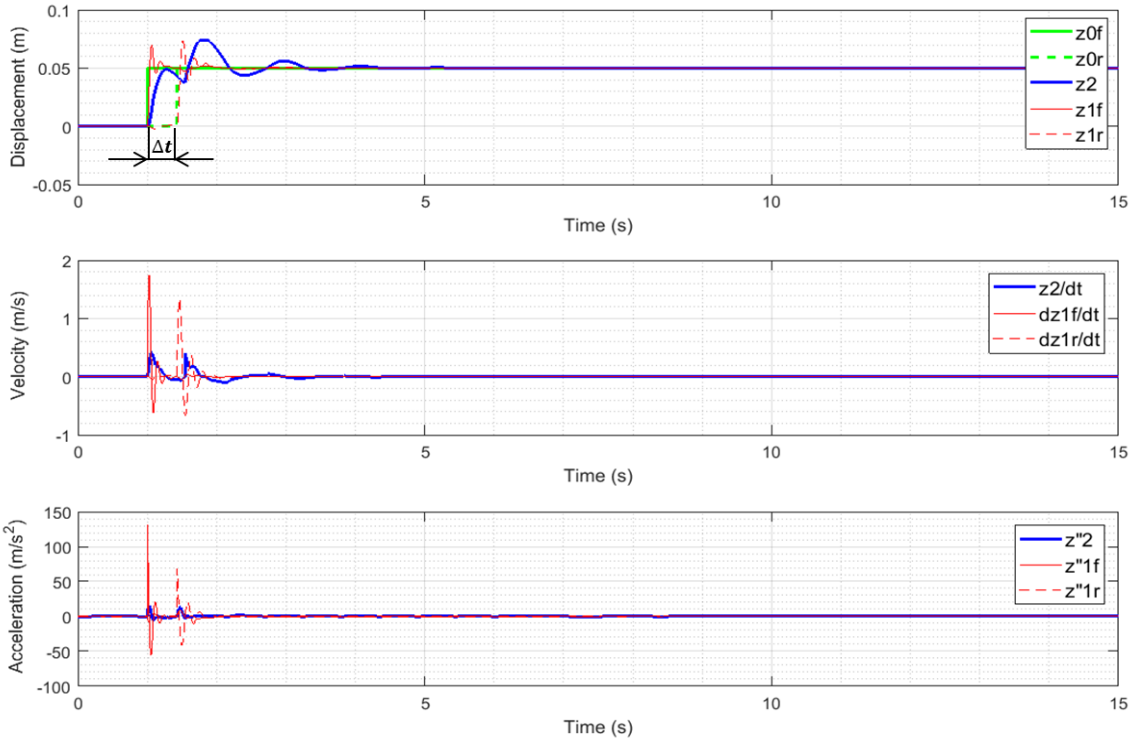

Figure 3.3.8-*Simulation results of half passive trolleybus dynamic model with step disturbance at 14m/s; $\Delta t = (L_f+L_r)/v$*

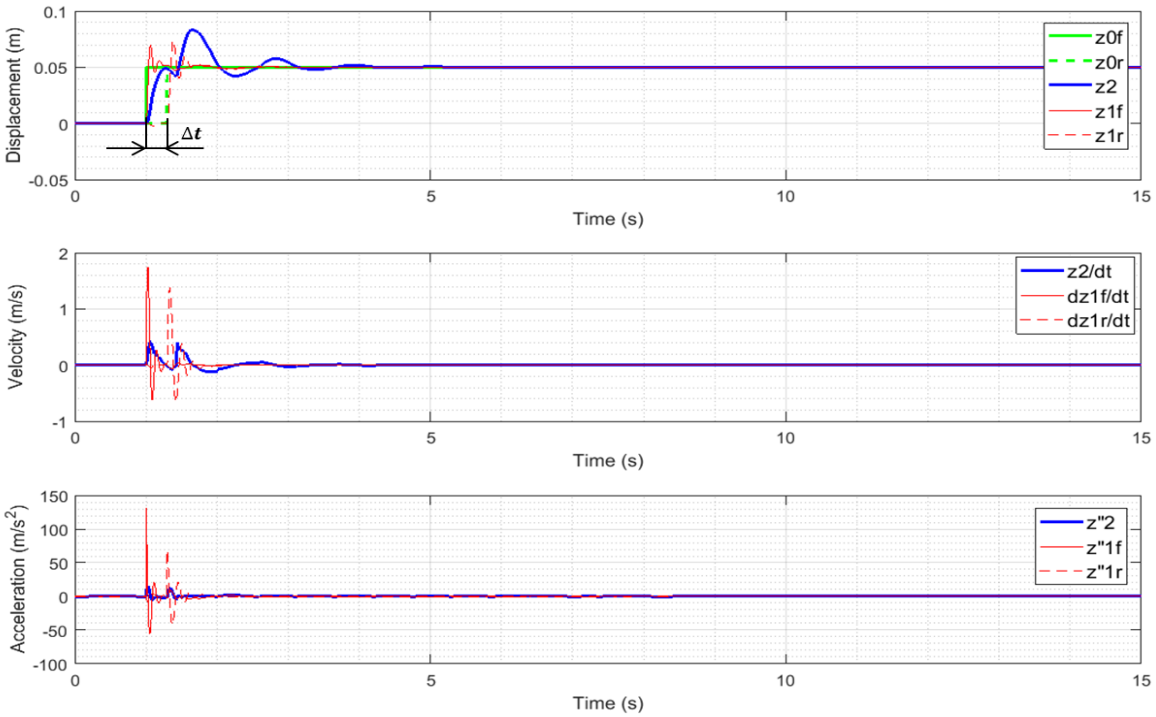

Figure 3.3.9-*Simulation results of half passive trolleybus dynamic model with step disturbance at 20m/s; $\Delta t = (L_f+L_r)/v$*

From Figure 3.3.7, Figure 3.3.8 and Figure 3.3.9, it can be seen that the gap time (Δt: 6, 0.43 and 0.3 seconds with 6m distance between trolleybus axles) qualitatively matches the different speeds (1m/s, 14/s and 20/s). In all three simulations, the displacement gradually attenuates after the step until finally settling at the value of step (0.05m). The most important results are the trolleybus body mass vertical displacement (z_2), velocity (z_2') and (z_2), which are influenced by the two tyres as they go over the step (z_{0f} and z_{0r} show the same step).

At a typical operation status, the half passive trolleybus model, simulation result at 14m/s (On Street) are detailed and analysed in Figure 3.3.10 and Table 3.3.2.

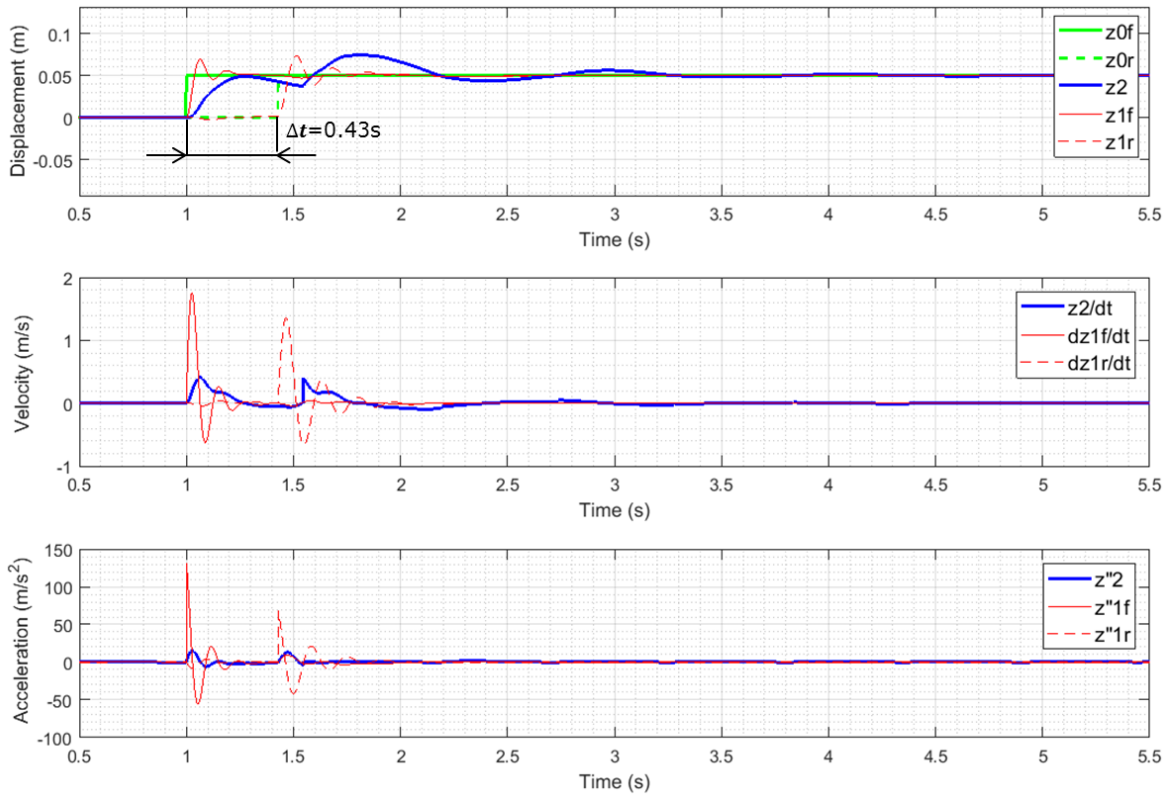

Figure 3.3.10 –***Detailed simulation results of half passive trolleybus dynamic model with step disturbance (0.05m) at 14m/s; $\Delta t = (L_f+L_r)/v$***

The impact effects between front and rear un-sprung mass (tyres) as well as body, the peak displacement, velocity and acceleration (measured directly in Matlab figure) at 14m/s are listed in Table 3.3.2.

Table 3.3.2 Simulation results of vertical displacement, velocity and acceleration of half passive trolleybus system with step disturbance (0.05 m) at speed of 14m/s

Results / Objects	Displacement (m) (z_{1f}, z_{1r}, z_2 peaks)	Velocity (m/s) (z'_{1f}, z'_{1r}, z'_2 peaks)	Acceleration (m/s^2) (z''_{1f}, z''_{1r}, z''_2 peaks)	Vibration lasting time after m1r hitting step (second)
m_{1f}	0.069	1.75	131.6	
(before m_{1r} hitting step)	0	-0.61	-55.57	
m_{1r}	0	0.021	4.14	
(before m_{1r} hitting step)	-0.0026	-0.046	-8.08	
m_2	0.048	0.41	15.73	
(before m_{1r} hitting step)	0	-0.054	-5.89	
m_{1f}	0.052	0.042	9.3	1.2
(after m_{1r} hitting step)	0.047	-0.046	-2.7	
m_{1r}	0.074	1.35	68.06	1.63
(after m_{1r} hitting step)	0.039	-0.67	-41.8	
m_2	0.074	0.40	13.07	3.48
(after m_{1r} hitting step)	0.038	-0.094	-0.44	

From Figure 3.3.10 and Table 3.3.2, it can be seen that at 14m/s, the trajectory of the displacement (z_{1f}) is smoother than step shape after the trolleybus' front tyre (m_{1f}) hits the step. The displacement trajectory (z_{1f}) and highest displacement (0.069m) is also lagged with respect to the step. This phenomenon can be thought of as the tyre being initially compressed as it hits the step; with high full vertical acceleration (131.6 m/s^2). At the same time, the rear tyre (m_{1r}) trajectory (z_{1r}) is slightly influenced with a tiny displacement (-0.0026m). For the trolleybus body trajectory (z2), the displacement goes up but the shape is further smoother than z_{1f} with a longer lag. When the rear tyre (m1r) trajectory (z1r) hits the step, the effect is similar to z_{1f}. The rear tyre trajectory (z1r) is also smoother and lagged with respect to the step. Its highest displacement (0.074m) is again higher than the step and lagged. At the same time, the front tyre is slightly influenced. The trolleybus body trajectory (z_2) also goes up again; reaching its highest displacement (also 0.074m) with further smoother shape and lasting longer than the front and rear tyres displacements.

These results can be explained as the higher stiffness of the tyres (z_{1f} and z_{1r}) apparently causing the un-sprung masses to experience higher velocities and accelerations that are attenuated by the secondary suspension stage. Consequently, the trolleybus body and passengers experience a much lower vertical acceleration and oscillation frequency.

The second phenomenon observed is the slight interference displacement to z_{1r} as the front tyre (m_{1f}) hits the step and the interference to z_{1f} as the rear tyre (m_{1r}) hits the step. This indicates that the front and rear tyres disturb each other as they run through the step. That z_{1f} is bigger in displacement than z_{1r} with higher vibration frequency, but shorter amplitude attenuation, is reasonable as $m_{1r} > m_{1f}$ with both having the same stiffness and damping.

Finally, the trolleybus displacement (z_2) is much smaller than z_{1f} and z_{1r} with lower acceleration. This is also reasonable as the suspension absorbs some of tyre displacement.

A typical example of the Pitch 2 (β_2) of the trolleybus body at 14m/s, is shown in Figure 3.3.11.

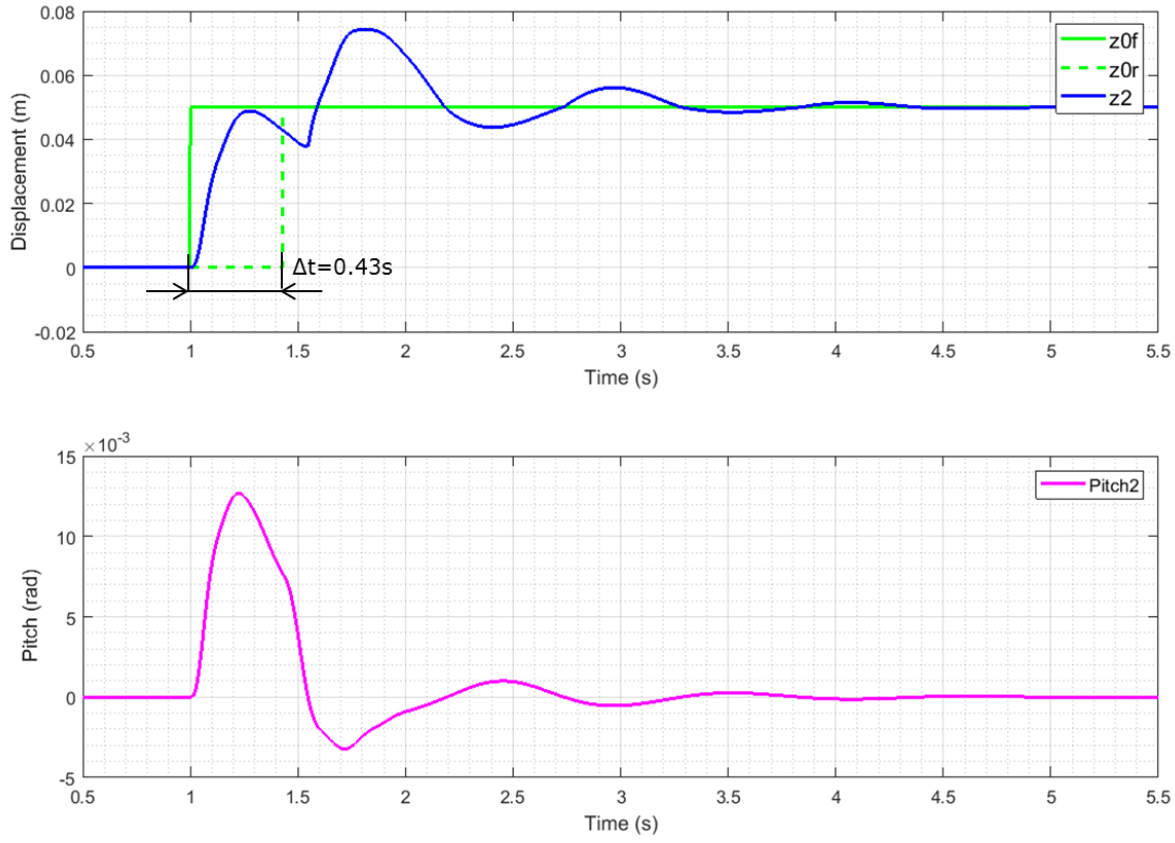

Figure 3.3.11–***Simulation pitch results of half passive trolleybus dynamic model with step disturbance at 14m/s; $\Delta t = (L_f+L_r)/v$***

From Figure 3.3.11, it can be seen that as the distances of the front and rear axles to the gravity centre of trolleybus body are different ($L_{df} > L_{dr}$), the absolute peak values of pitch of the trolleybus body (m2) are asymmetrical. The pitch oscillation is also relatively long; not settling until around 3 seconds after hitting the step.

The Random road disturbance model is only suitable for speeds of 5-30m/s [167]. The road surface roughness' dimension refers the Figure 3.3.12 which the condition is at 70km/s (19.44m/s) and considered to be good [168].

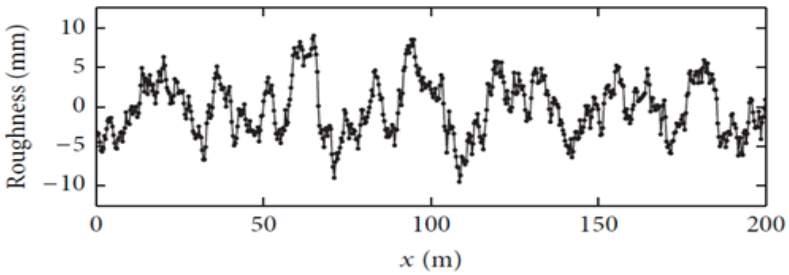

Figure 3.3.12-*The road surface roughness*

Therefore the simulation in thesis only includes the speeds of 14m/s (On street) and 20m/s (Highest speed). These results are shown in Figure 3.3.13 and Figure 3.3.14.

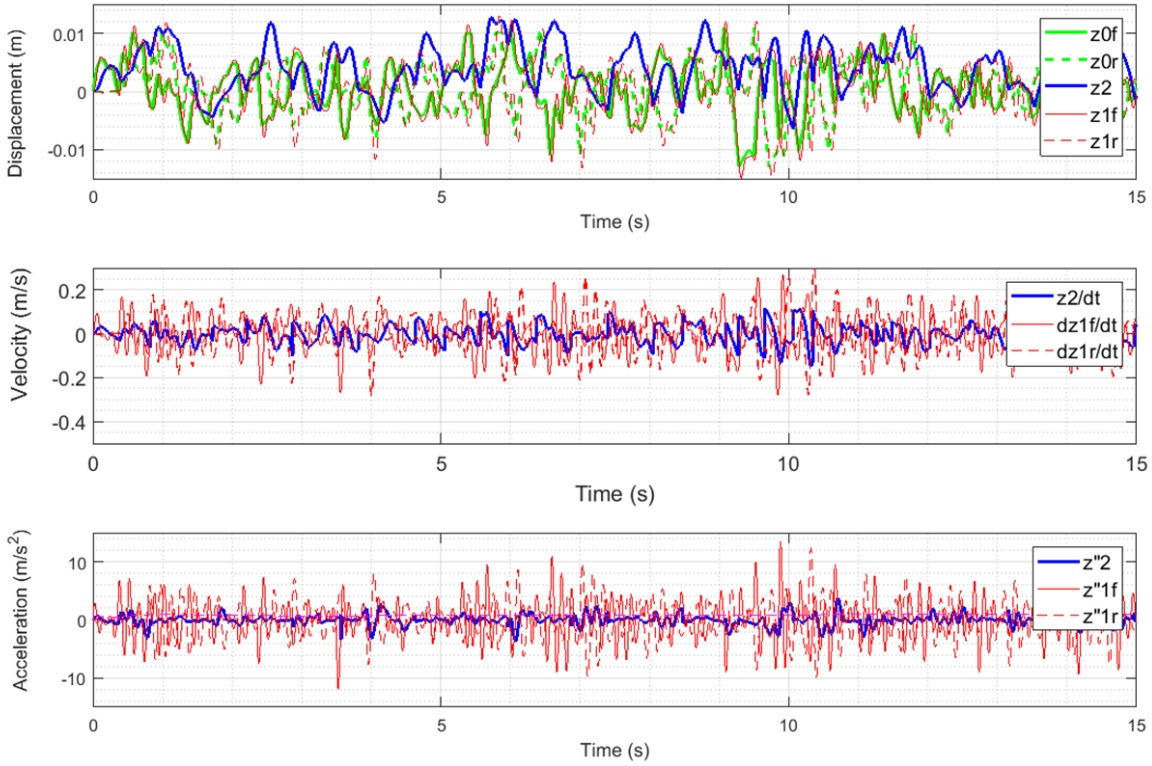

Figure 3.3.13-*Simulation results of half passive trolleybus dynamic model with Random road disturbances at 14m/s*

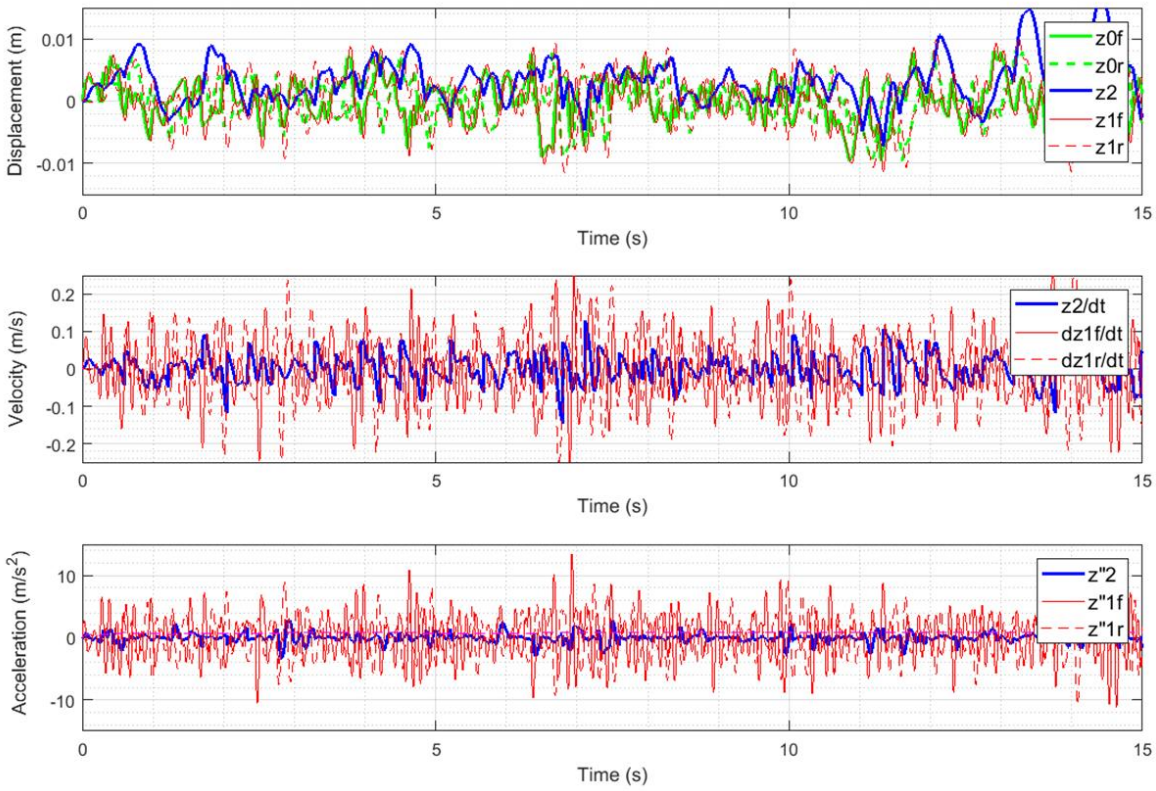

Figure 3.3.14-*Simulation results of half passive trolleybus dynamic model with Random road disturbances at 20m/s*

From Figure3.3.13 and Figure3.3.14, it can be seen that under normal running conditions (i.e. Random road disturbances), the trolleybus body displacement (z_2), velocity (z_2') & acceleration (z_2'') show little difference in displacement from -0.007(-7mm) to 0.015m (15mm) , velocity from -0.15 to 0.12 m/s and acceleration from -3 to 3 m/s^2. The velocity and acceleration of the trolleybus body are smaller than those of the tyres (z_{1f}', z_{1r}', z_{1f}'' & z_{1r}''). However, the displacement of the trolleybus ($z_{2)}$ is currently bigger than tyres with lower vibration frequency. The figures also show that the displacement (z_{1f} and z_{1r}) is nearly parallel to disturbance (z_{0f} and z_{0r}) with a slight lag.

Finally, to simulate a typical operation status, multiple bump disturbances were also simulated at the three different trolleybus speeds. These results are shown in Figure3.3.15, Figure3.3.16 and Figure3.3.17.

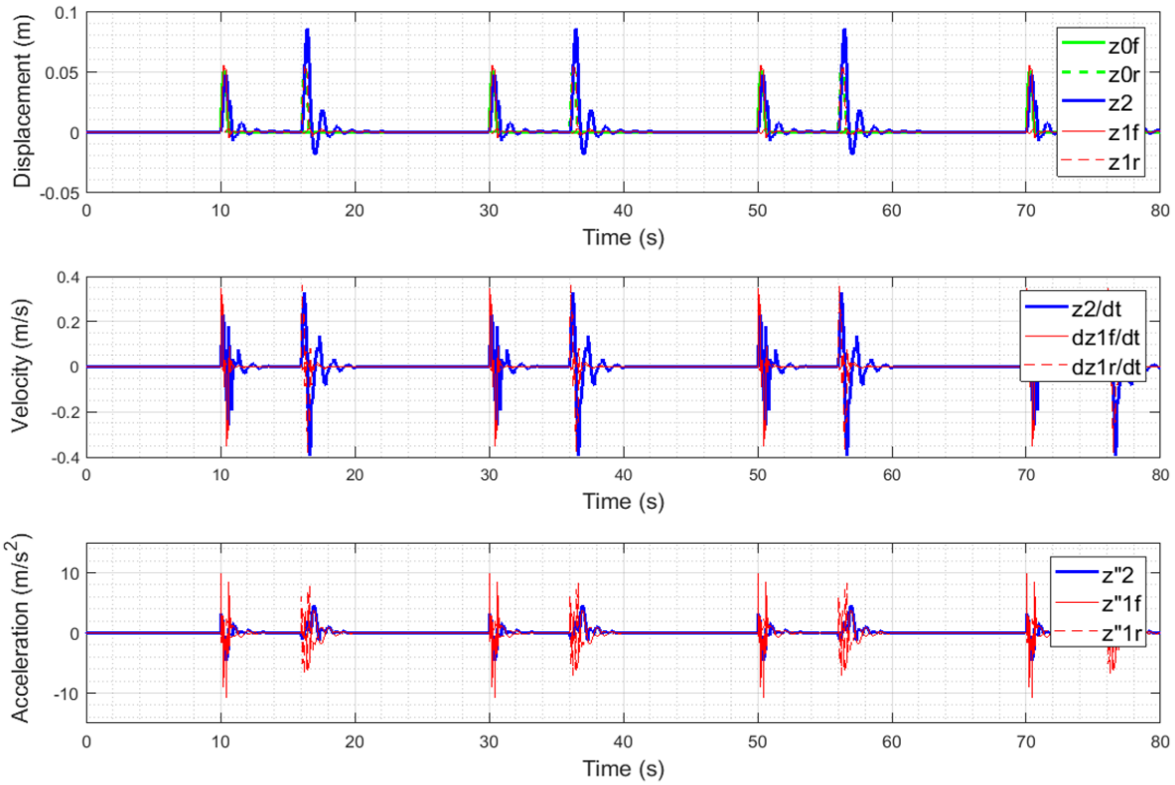

Figure 3.3.15 -*Simulation results of half passive trolleybus dynamic model with multiple bump disturbance at 1m/s; $\Delta t = (L_f+L_r)/v$*

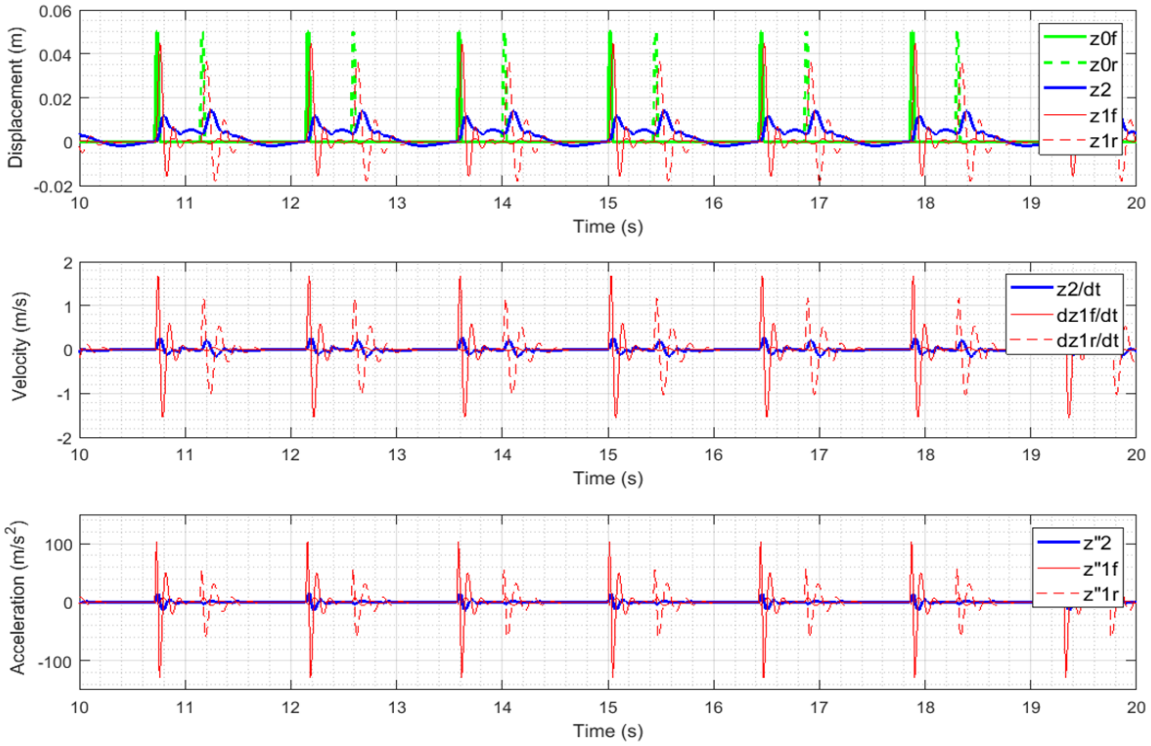

Figure 3.3.16-*Simulation results of half passive trolleybus dynamic model with multiple bump disturbance at 14m/s; $\Delta t=(L_f+L_r)/v$*

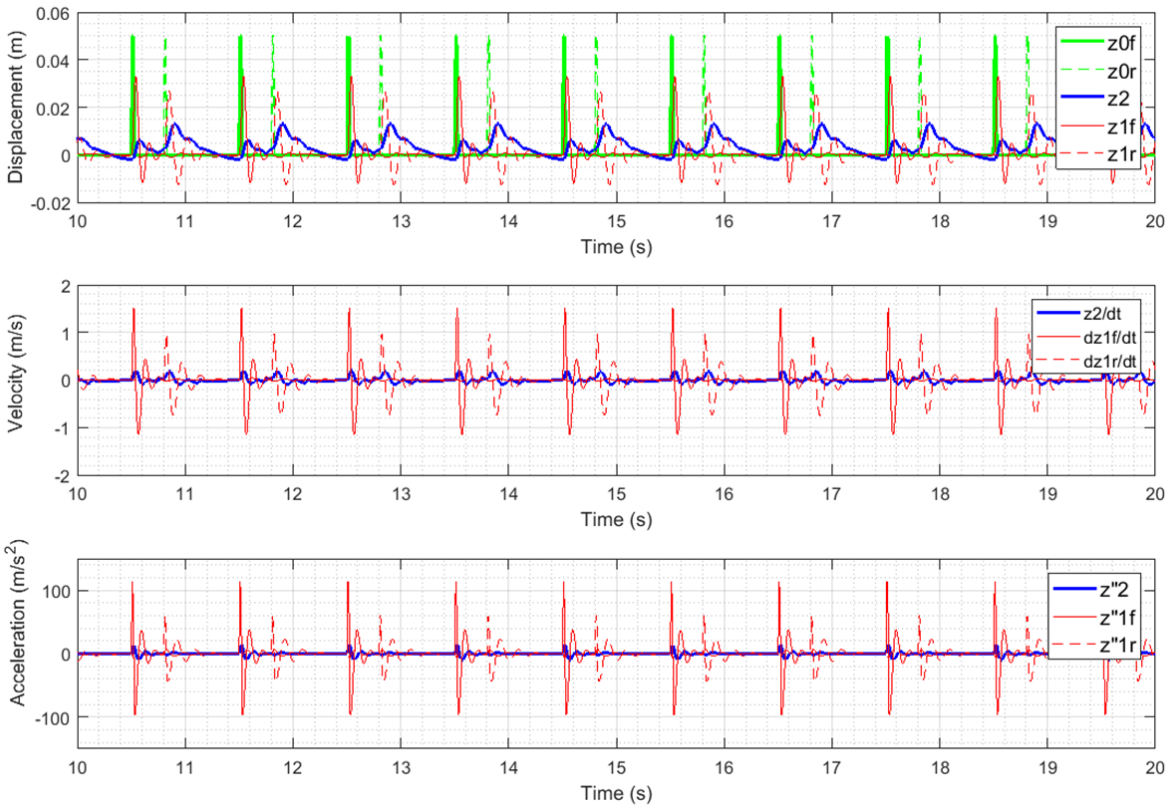

Figure 3.3.17-*Simulation results of half passive trolleybus dynamic model with multiple bump disturbance at 20m/s; $\Delta t=(L_f+L_r)/v$*

From Figure3.3.15, Figure3.3.16 and Figure3.3.17, it can be seen that the gap time (Δt: 6, 0.43 and 0.3 seconds with 6m distance between trolleybus axles) and intervened time (T_{id}: 20, 1.43 and 1 seconds with 20m intervening distance between two bump disturbances) match with the different speeds (1m/s, 14/s and 20/s). The displacements repeatedly cycle with bump length and intervention. In particular, the trolleybus body mass vertical displacement (z_2), velocity (z_2') and (z_2'') are repeatedly influenced by the two tyres as they go over the step disturbance (z_{0f} and z_{0r} they are a same step). At speeds of 14m/s and 20m/s, the tyres are squeezed whilst going through the bumps, the displacements of the tyres (z_{1f} and z_{1r}) are smaller than the bump disturbances (z_{0f} and z_{0r}). This effect is not apparent in the 1m/s simulation.

To quantify the impact effects between front and rear un-sprung masses (tyres) as well as body when going through the bumps, the peak displacement, velocity and acceleration (measured directly in Matlab figures) at 14m/s are listed in Table 3.3.3.

Table 3.3.3 Simulation results of vertical displacement, velocity and acceleration of half passive trolleybus system with bump disturbances at speed of 14m/s

Results / Objects	Displacement (m) (z_{1f}, z_{1r}, z_2 peaks)	Velocity (m/s) (z'_{1f}, z'_{1r}, z'_2 peaks)	Acceleration (m/s^2) (z''_{1f}, z''_{1r}, z''_2 peaks)	Vibration time after m1r hitting step (sec)
m_{1f}	0.045	1.68	103.5	
(before m_{1r} hitting bump)	-0.016	-1.55	-128.7	
m_{1r}	0.0012	0.046	7.5	
(before m_{1r} hitting bump)	-0.0011	-0.028	-7.5	
m_2	0.012	0.27	14.3	
(before m_{1r} hitting bump)	0.003	-0.13	-13.9	
m_{1f}	0.011	0.046	8.3	1.3
(after m_{1r} hitting bump)	-0.013	-0.026	-5.3	
m_{1r}	0.036	1.17	56.11	1.4
(after m_{1r} hitting bump)	-0.018	-1.03	-60.31	
m_2	0.014	14.94	2.15	Still in vibration when m_{1f} hits next bump
(after m_{1r} hitting bump)	-0.0019	-0.15	-2.84	

From Figure 3.3.17 and Table 3.3.3, it can be seen that at 14m/s, when the trolleybus' front tyre (m_{1f}) hits the bump, the tyre trajectory (z_{1f}) is similar to the bump shape and lagged with a highest displacement (0.045m) that is lower than bump. This phenomenon could be thought of as the front tyre being initially compressed with high vertical component acceleration (103.5 m/s^2). Meanwhile, the rear tyre (m_{1r}) trajectory (z_{1r}) is slightly influenced with tiny displacement (-0.0011m). For the body (m2) trajectory (z_2), the highest displacement goes up but lower than z_{1f} and the shape is much smoother with longer lagged and no negative value. When the rear tyre (m_{1r}) trajectory (z_{1r}) hits the bump, it is similar to front tyre, the trajectory (z_{1r}) is smoother than bump shape and lagged with highest displacement (0.036m) which is lower than front tyre (z1f) with lagged. The front tyre (m_{1f}) is slightly influenced. However, the attenuating body (m_2) trajectory (z_2) goes up again until getting highest displacement (also 0.014m) with smoother shape and lasting much longer than the front and rear tyres.

The higher stiffness of the tyres (z_{1f} and z_{1r}), apparently causes the un-sprung masses to experience higher velocities and accelerations (as the only vertical component therefore they are lower than values caused by step) which are attenuated by the secondary suspension stage meaning the trolleybus body and passengers will experience much lower vertical acceleration and frequency.

According to ISO 2631-1:1997 [170] to analysis to driver and passengers riding comfortable performance, the vertical acceleration (RMS) results of trolleybus body (m_2) with bump disturbances at all three selected speeds in simulation are especially shown in Table 3.3.4.

Table 3.3.4 Vertical acceleration (RMS) of trolleybus body (m_2) with bump disturbances at all three selected speeds

Speed (m/s) / Trolleybus body (m_2) Max. acceleration (RMS)	1	14	20
Absolute values (m/s^2)	≈ 0.23	≈ 3.1	≈ 2.7

And the vibration magnitude (RMS) likely reaction in public transport with ISO 2631-1:1997 [170] shown in table and Table 3.3.5

Table 3.3.5 Vertical acceleration magnitude (RMS) likely reaction in public transport [169]

Vibration magnitude (RMS)	Likely reaction in public transport
Less than 0.315 m/s^2	Not uncomfortable
0.315–0.63 m/s^2	A little uncomfortable
0.5–1 m/s^2	Fairly uncomfortable
0.8–1.6 m/s^2	Uncomfortable
1.25–2.5 m/s^2	Very uncomfortable
Greater than 2 m/s^2	Extremely uncomfortable

Comparing to Table 3.3.4 and table 3.3.5, the driver and passengers would be not uncomfortable ($0.23 < 0.315$ m/s^2) when trolleybus going the bump at speed of 1m/s. However, it will make driver and passengers in extremely uncomfortable (3.1 and $2.7>2$ m/s^2 even possible damage the trolleybus suspension mechanism) when trolleybus going the bump at speed of 14 and 20 m/s. That is the key reason the driver has to reduce the speed of `trolleybus.

3.4 Combined model of half trolleybus with catenary-pantograph

3.4.1 Model of half trolleybus with catenary-pantograph

As the location of trolleybus body centre of gravity could not be found either in reference or by measurement, for simplification it was assumed that the pantograph base centre and trolleybus body centre of gravity were at the same level. Integrating the models of the trolleybus catenary-pantograph (in section 3.2.3) and half trolleybus (in section 3.3.1) together, allowed a combined model of a half passive trolleybus with catenary-pantograph to be built. This combined dynamic model is shown in Figure 3.4.1.

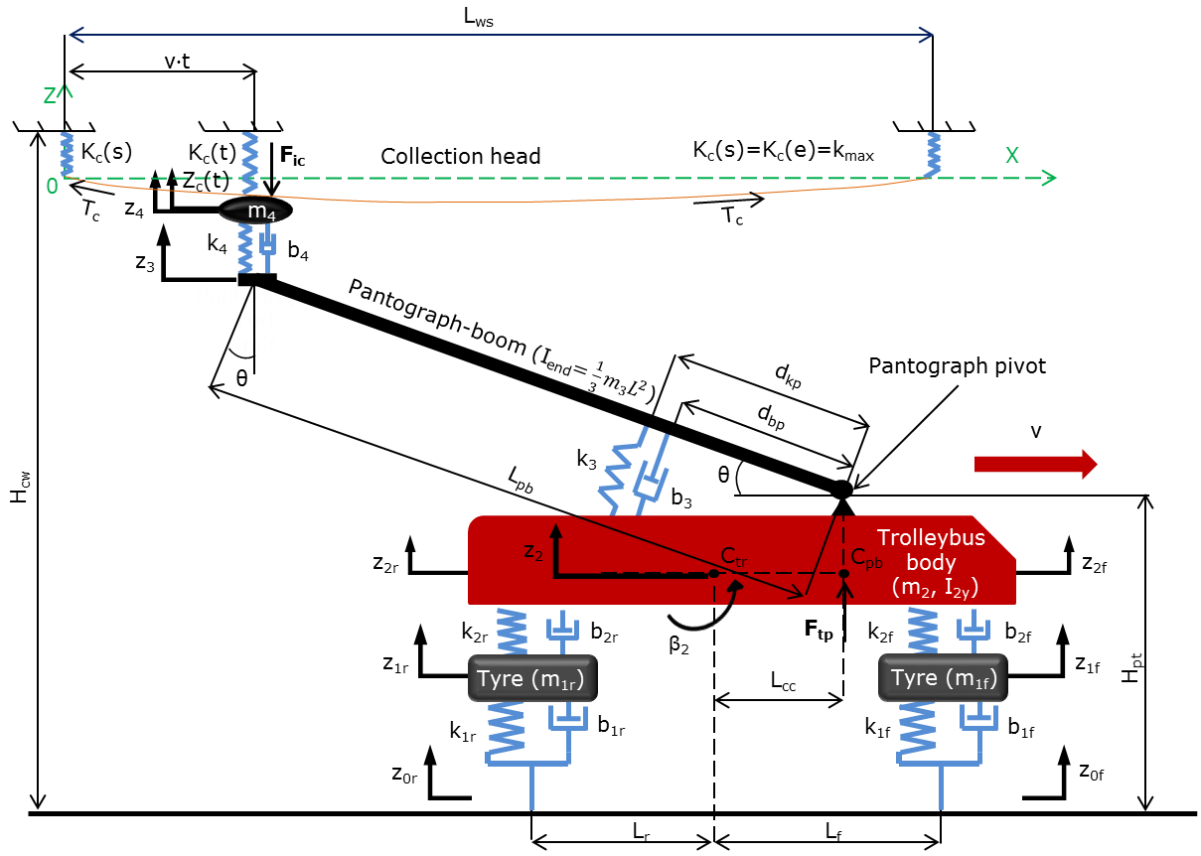

Figure 3.4.1-*Model of catenary-pantograph with half trolleybus*

Where:

Pantograph part:

$K_c(t)$: catenary contact wire nominal stiffness (N/m)

$K_c(s) = K_c(e) = k_{max}$: catenary contact wire maximum stiffness (N/m)

k_{min}: catenary minimum stiffness (N/m) (not showing in Figure 3.2.1)

k_{mean}: catenary average stiffness (N/m)

L_{ws}: catenary contact wire span between two poles (m)

T_c: tensile force of catenary contact wire (N)

$Z_c(t)$: pre-catenary vertical displacement (m)

H_{cw}: installation height of the catenary wire (normally from ground to fixed point on poles). It is determined the BSI British Standards in trolleybus (m) [37]

H_{pt}: pivot height of pantograph from ground (3.50 m)

z_3: pantograph boom vertical displacement (m)

m_3: pantograph-boom mass (kg)

b_3: pantograph-boom absorbers damping rate (Ns/m)

k_3: pantograph-boom spring nominal stiffness (N/m)

d_{bp}: distance from damper fitting point to pantograph pivot point

d_{kp}: distance from spring fitting point to pantograph pivot point

z_4: pantograph-head vertical displacement (trajectory) (m)

m_4: collection head mass (kg)

b_4: collection head absorbers damping rate (Ns/m)

k_4: collection head spring stiffness (N/m)

Fi_c: integrated contact force between catenary and pantograph-head (N)

I_{end}: pantograph-boom moment of inertia to ($kg \cdot m^2$)

θ: pantograph-boom dynamic lifting angle (degrees)

L_{pb}: length of pantograph-boom (m)

Half trolleybus part:

z_{0f}: road disturbance at the front tyre (m)

z_{1f}: front un-sprung mass vertical displacement (m)

z_{2f}: trolleybus mass vertical displacement at the point of contact with the suspension system (m)

z_{0r}: road disturbance at the rear tyre (m)

z_{1r}: rear un-sprung mass vertical displacement (m)

z_{2r}: trolleybus mass vertical displacement at the point of contact with the suspension system (m)

m_{1f}: un-sprung front axle mass (kg)

b_{1f}: front tyre damping (Ns/m)

k_{1f}: front tyre stiffness (N/m)

L_f: level distance between front axle and trolleybus body centre of gravity (m)

m_{1r}: un-sprung rear axle mass (kg)

b_{1r}: rear tyre damping (Ns/m)

k_{1r}: rear tyre stiffness (N/m)

Lr: level distance between rear axle and trolleybus body centre of gravity (m)

m_2: total sprung mass including shared axles (kg)

k_{2f}: front axle sprung stiffness (N/m)

b_{2f}: front axle damping (Ns/m)

k_{2r}: rear axle sprung stiffness (N/m)

β_2: pitch of the trolleybus body around the centre of gravity (assumed to be the y-axis)

I_{2y}: moment of inertia of the trolleybus body around the centre of gravity (assumed to be around the y-axis)

C_{tr}: trolleybus body centre of gravity

C_{pb}: pantograph base centre (assumed at same level of trolleybus body centre of gravity)

L_{cc}: level distance between trolleybus body centre of gravity and pantograph base body centre (m)

F_{tp}: transfer force from trolleybus body to pantograph base

v: trolleybus velocity (m/s)

g: gravitation acceleration (9.8m/s^2)

As the model is very large and complicated, including as it does, E3.2.14, E3.2.11, E3.2.15, E3.2.16, E3.2.21, E3.3.1, E3.3.2, E3.3.3 and E3.3.4, it was assumed that pantograph base is dynamically moving with to the trolleybus body and there is a "Transfer force" between pantograph base and pantograph physically linked by k_{3eq} and b_{3eq} as shown in Figure 3.4.2

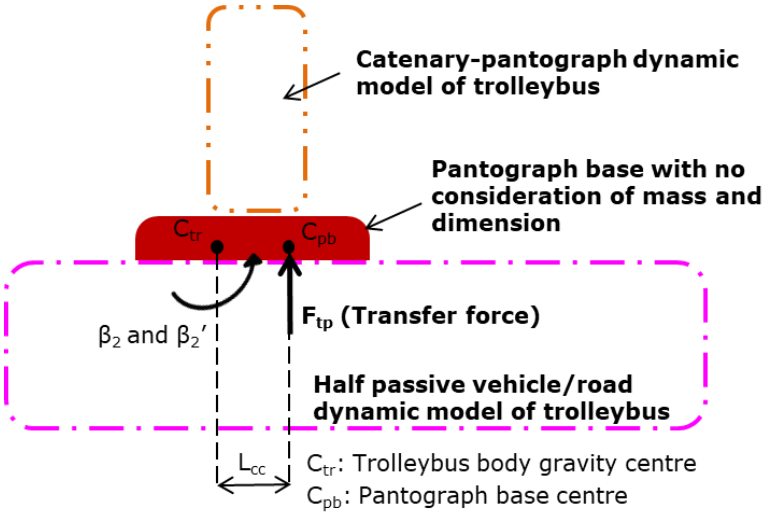

Figure 3.4.2-*Simplified model of half trolleybus with catenary-pantograph including "Transfer force"*

Where:

β_2': pitch angular velocity of the m_2 around gravity centre (assumed y-axle) (rad/s)

The dynamic linkage equations of the "Transfer force" are shown in E3.4.1, in which the $\boldsymbol{b_{3eq}}$ and $\boldsymbol{k_{3eq}}$ are expressed in E3.2.14

$$\boldsymbol{F_{tp} = b_{3eq}(\dot{z}_2 + L_{cc} \cdot \dot{\beta}_2) + k_{3eq}(z_2 + L_{cc} \cdot \beta_2)} \qquad \text{E3.4.1}$$

The data of L_{cc} was hand-measured and calculated from an engineering drawing of SOR TNB12 trolleybus (using VOLVO B9LA chassis [98]) as follows:

$$\mathbf{L_{cc} = 0.027m}$$

Note: the dynamic performance of catenary-pantograph including contact force ($F_{ic)}$ and pantograph head displacement (z_4 with vehicle) are certainly associated to moment of inertial of pantograph and mass of pantograph head. L_{cc} varies depending on different manufacturers; from inspection of photos on websites, most trolleybuses in the world, particularly in Eastern EU countries, have a small L_{cc} which means pantograph base fitted position (on level plane) is normally close to trolleybus's gravity centre. However, the British style was closer to the front axle of the trolleybus.

3.4.2 Simulation and analysis of half trolleybus with catenary-pantograph

The Simulink configuration of the "Transfer force" model, based on equation E3.4.1, is shown in Figure 3.4.3.

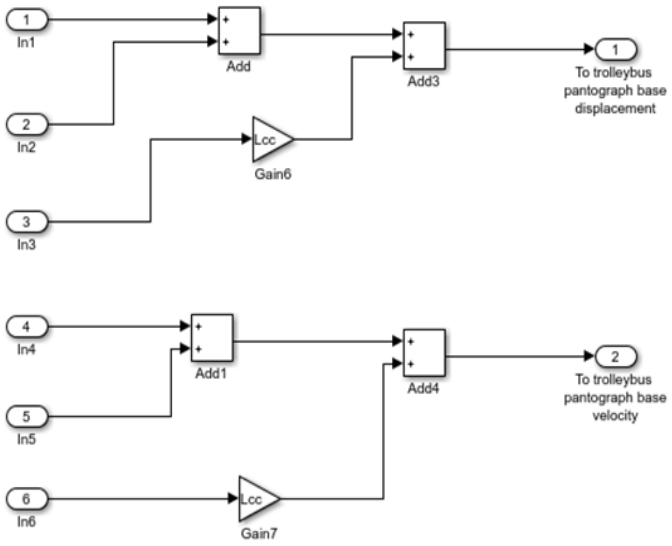

Figure 3.4.3-*Simulink configuration of "Transfer force" module between catenary-pantograph and half trolleybus*

The Simulink configuration of the half passive trolleybus dynamic model with "Transfer force" embedded is shown in Figure 3.4.4.

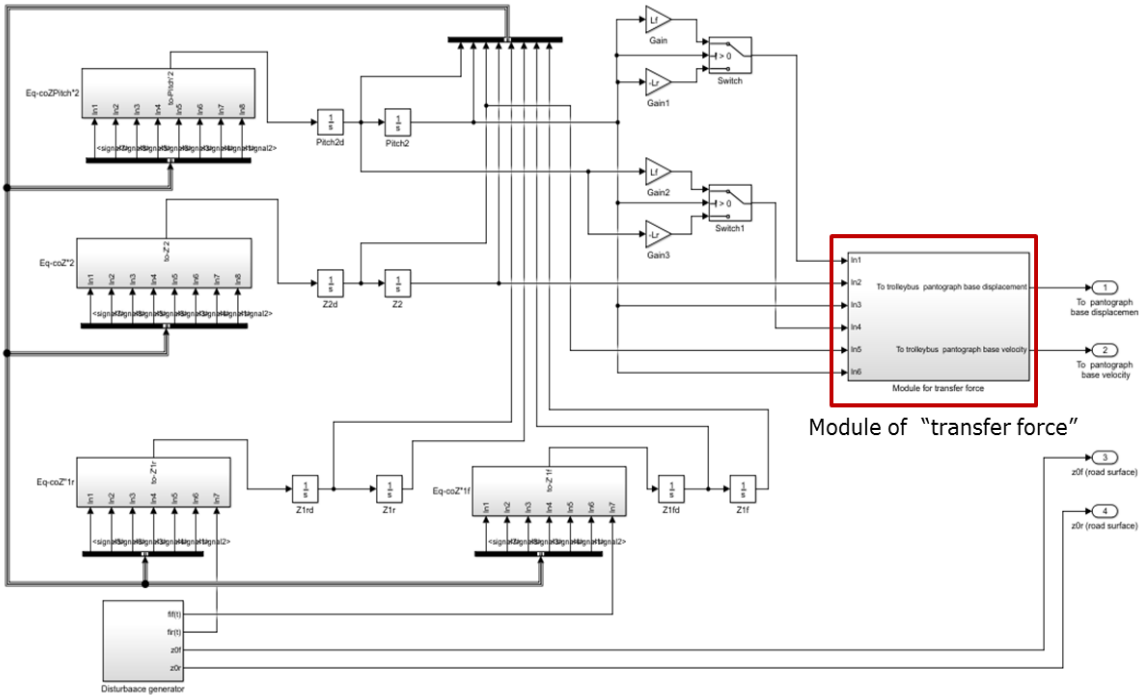

Figure 3.4.4-*Simulink configuration of half trolleybus with "transfer force" module*

Using this Half trolleybus with "transfer force" Simulink configuration module, the full Simulink configuration of the catenary-pantograph with half passive trolleybus is shown in Figure 3.4.5.

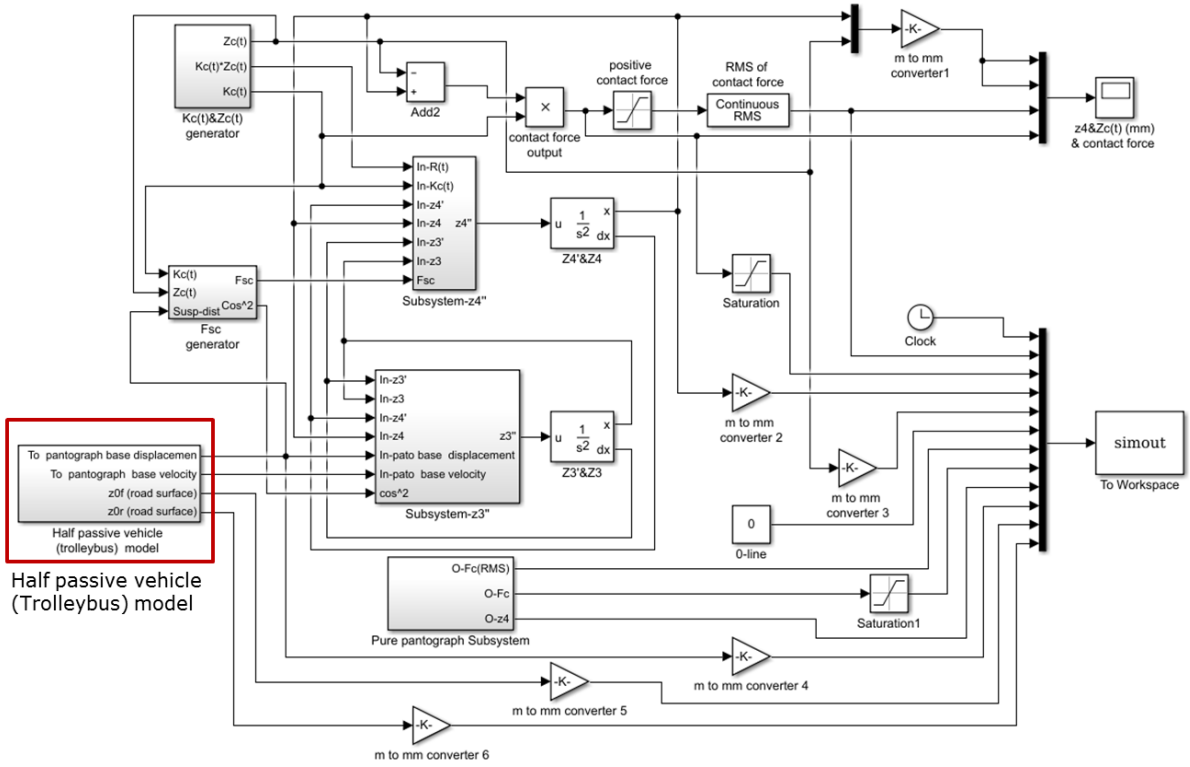

Figure 3.4.5-*Simulink configuration of half passive trolleybus with catenary-pantograph*

The technical specifications of the catenary-pantograph and half trolleybus are the same as those given in Table 3.2.2 (in section 3.2) and Table 3.3.1 (in section 3.3) for all the simulations in this section (section 3.4). The distance between pantograph base centre and trolleybus gravity centre L_{cc} = 0.027m.

Similar to the previous Simulink display functions, the following abbreviations are used in Figure3.4.6 to Figure 3.4.17, Table 3.3.2 and Table 3.3.3:

F_{ic} (RMS) with vehicle: integrated contact force (RMS) with trolleybus (N)

F_{ic} with vehicle: integrated contact force with trolleybus (N)

z_4 with vehicle: pantograph-head vertical displacement with trolleybus (mm)

F_{ic} (RMS): integrated contact force (RMS) without trolleybus (N)

F_{ic}: integrated contact force without trolleybus (N)

z_4: pantograph-head vertical displacement without trolleybus (mm)

$Z_c(t)$: original vertical displacement of catenary wire (mm)

z_2: trolleybus body displacement (mm)

z_{0f}: road disturbance (step, random and bump) at the front tyre (mm)

z_{0r}: road disturbance (step, random and bump) at the rear tyre (mm)

In order to assess the effects of combining the catenary-pantograph model with the half trolleybus model, simulations were carried out, assuming a smooth road surface, at the three different speeds: 1m/s (In depot), 14m/s (On street) and 20m/s (Highest speed). The results are shown in Figure 3.4.6, Figure 3.4.7 and Figure 3.4.8.

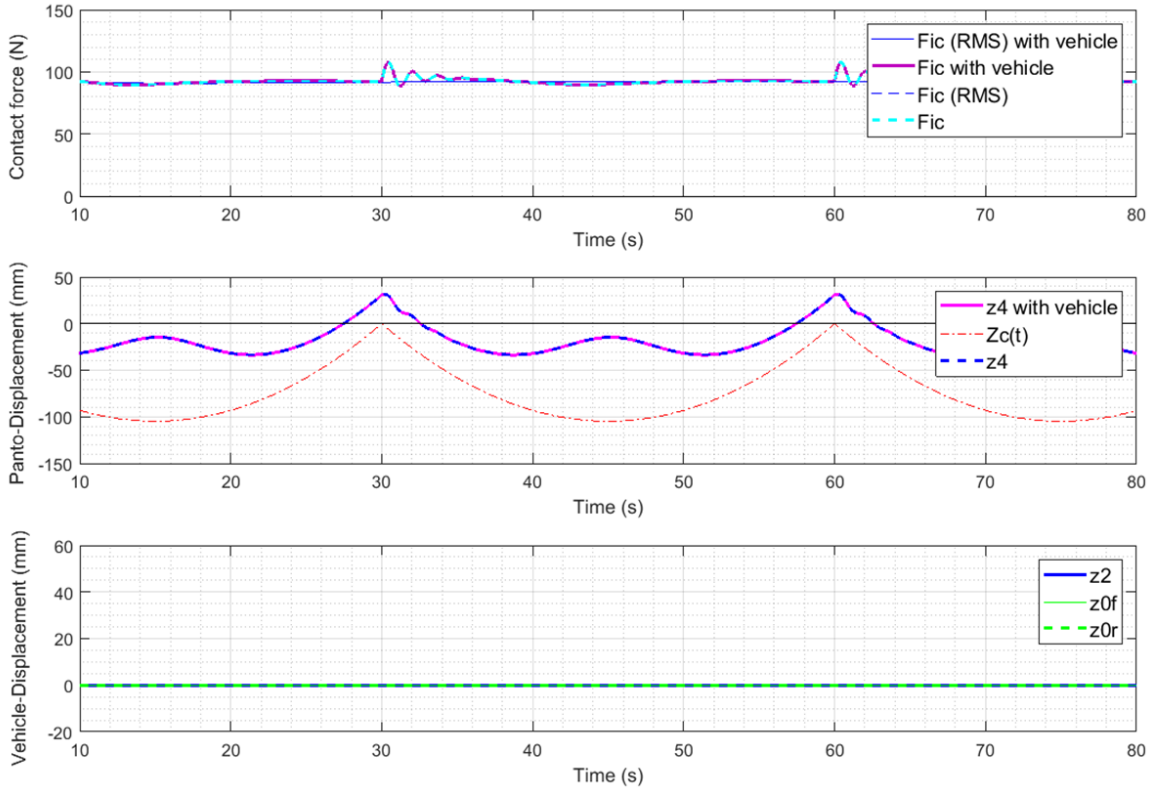

Figure3.4.6-*Simulation result of half trolleybus with catenary-pantograph on smooth surface at v=1m/s*

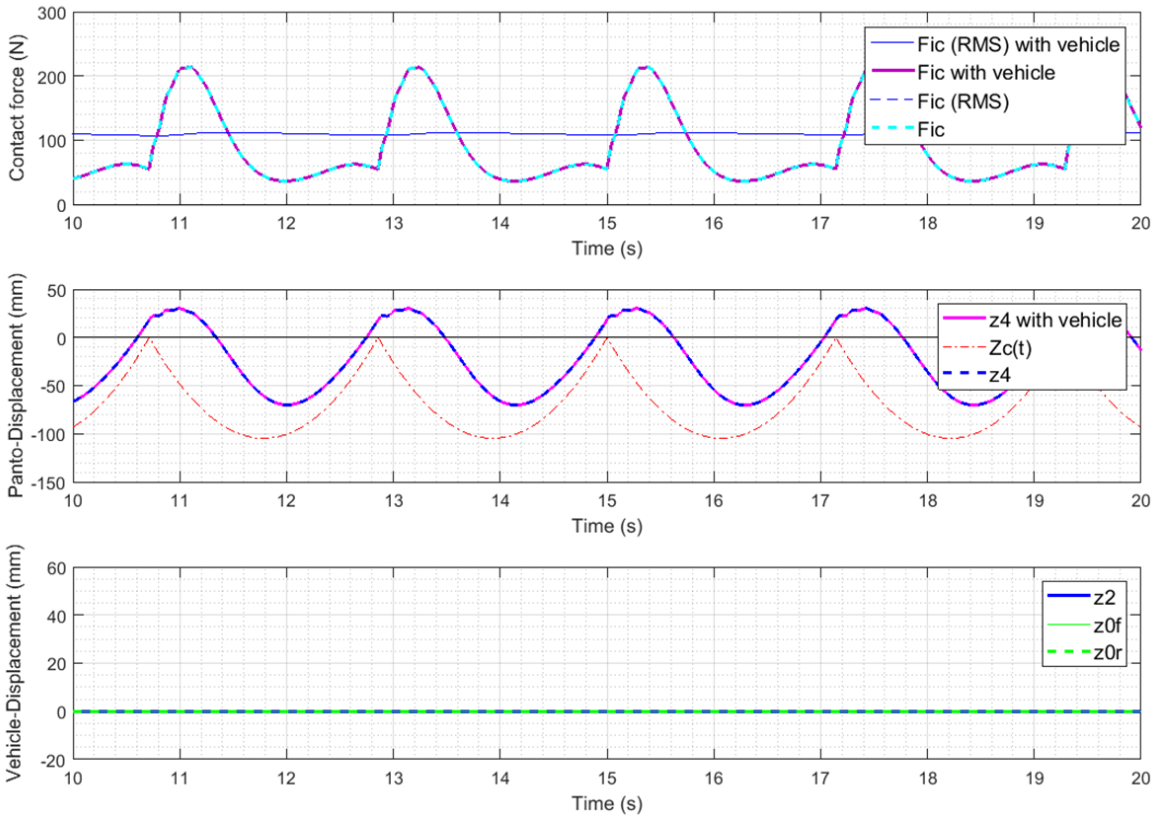

Figure3.4.7-*Simulation result of half trolleybus with catenary-pantograph on smooth surface at v=14m/s*

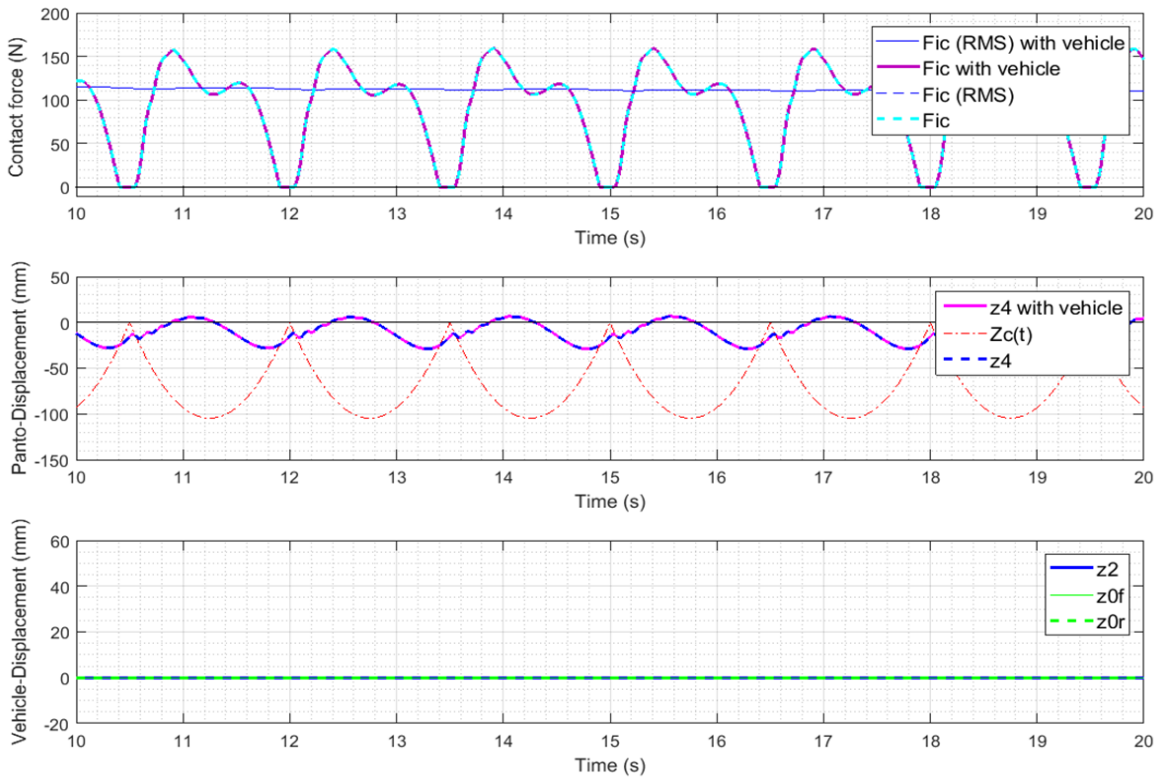

Figure3.4.8-*Simulation result of half trolleybus with catenary-pantograph on smooth surface at v=20m/s*

From Figure3.4.6, Figure3.4.7 and Figure3.4.8, it can be seen that in both the catenary-pantograph with and without half trolleybus models, the contact force F_{ic} (RMS), F_{ic} and displacement (z_4) force effectively overlap at all three different speeds. This can be thought of the consequence of the stiffness of the tyres and body (k_{1f}, k_{1r}, k_{2f} and k_{2r}) of trolleybus being much higher than the stiffness of the pantograph (k_{3eq}).

The simulation results of the combined model with step disturbance (value of 0.05m) disturbance at the three different speeds 1m/s (In depot), 14m/s (On street) and 20m/s (Highest speed) are shown in Figure3.4.9, Figure3.4.10 and Figure3.4.11.

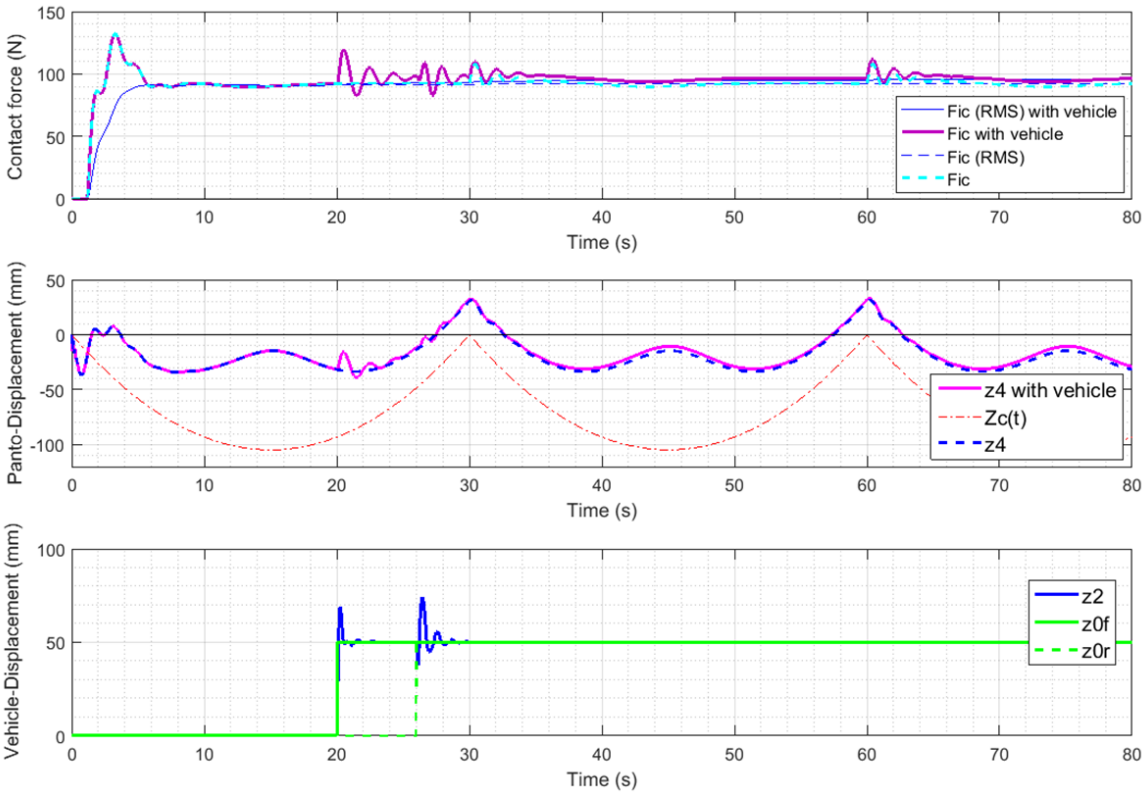

Figure 3.4.9-*Simulation result of catenary-pantograph with half trolleybus with single step disturbance at v=1m/s*

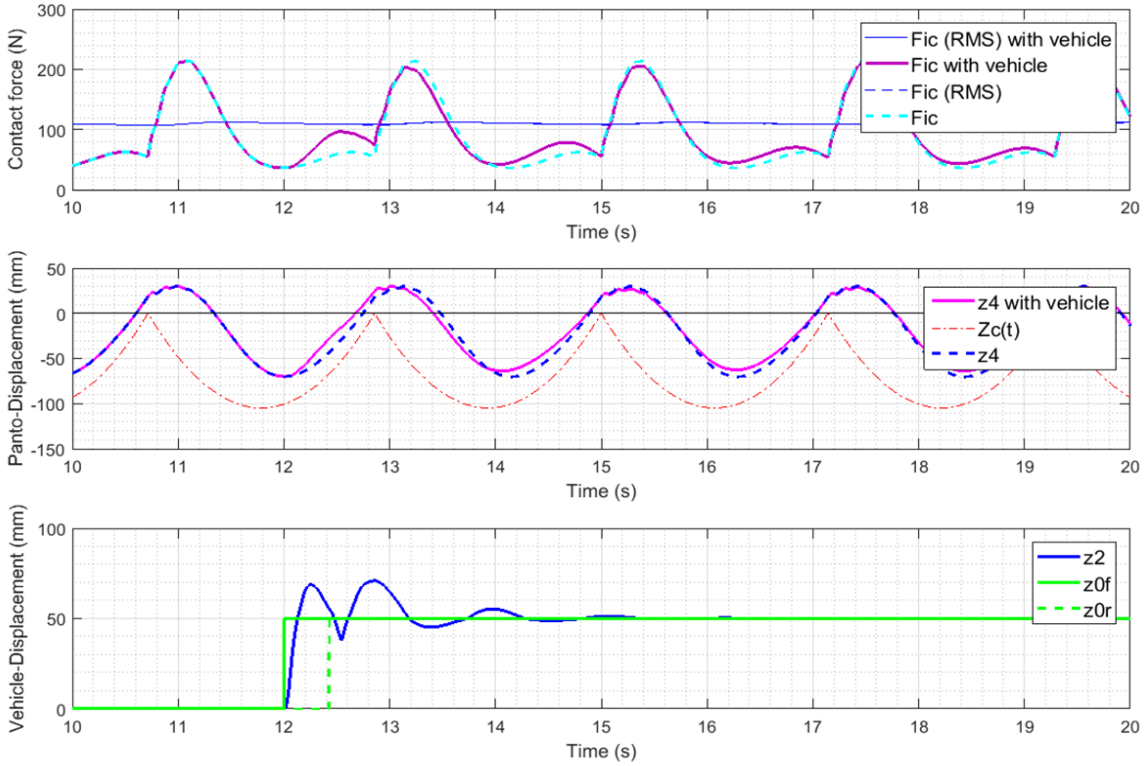

Figure 3.4.10-*Simulation result of catenary-pantograph with half trolleybus with single step disturbance at v=14m/s*

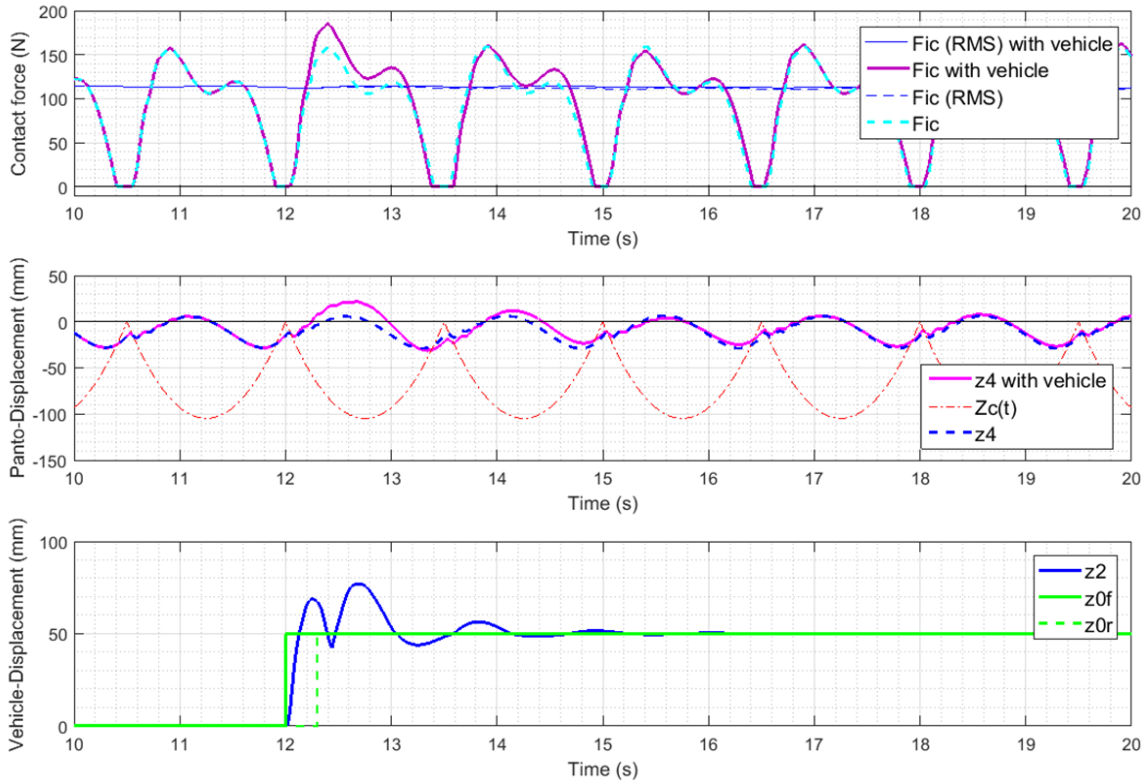

Figure3.4.11- ***Simulation result of catenary-pantograph with half trolleybus with single step disturbance at v=20m/s***

From Figure 3.4.9, Figure 3.4.10 and Figure 3.4.11, it can be seen that there is no significant difference in integrated contact force (F_{ic}) in both the catenary-pantograph with and without the half-trolleybus models. There are small differences in pantograph-displacement (z_4) between the two models, particularly when the tyres hit the step disturbance at 20m/s. At the three selected speeds, the biggest variation in contact force and displacement are from 80 to 120 (N) for the contact force and from -60 to -35 (mm) for the displacement. However, the Fic (RMS) shows almost no difference between the with or without trolleybus models; the values keep around 90N (at 1m/s), 105 (14m/s) and 110N (20m/s). Meanwhile, the integrated contact force (F_{ic} with vehicle) and pantograph-displacement (z4 with vehicle) of the with trolleybus model are slightly higher just after the trolleybus has gone over the step. This is likely to be because the "ground" of trolleybus is higher and the subsequent higher self-generation static force causes the higher contact force (Fic with vehicle).

As the random road disturbance model is only suitable for speeds of 5-30m/s [167], this simulation can only be conducted at speeds of 14m/s (On street) and 20m/s (Highest speed). The results are shown in Figure 3.4.12 and Figure 3.4.13.

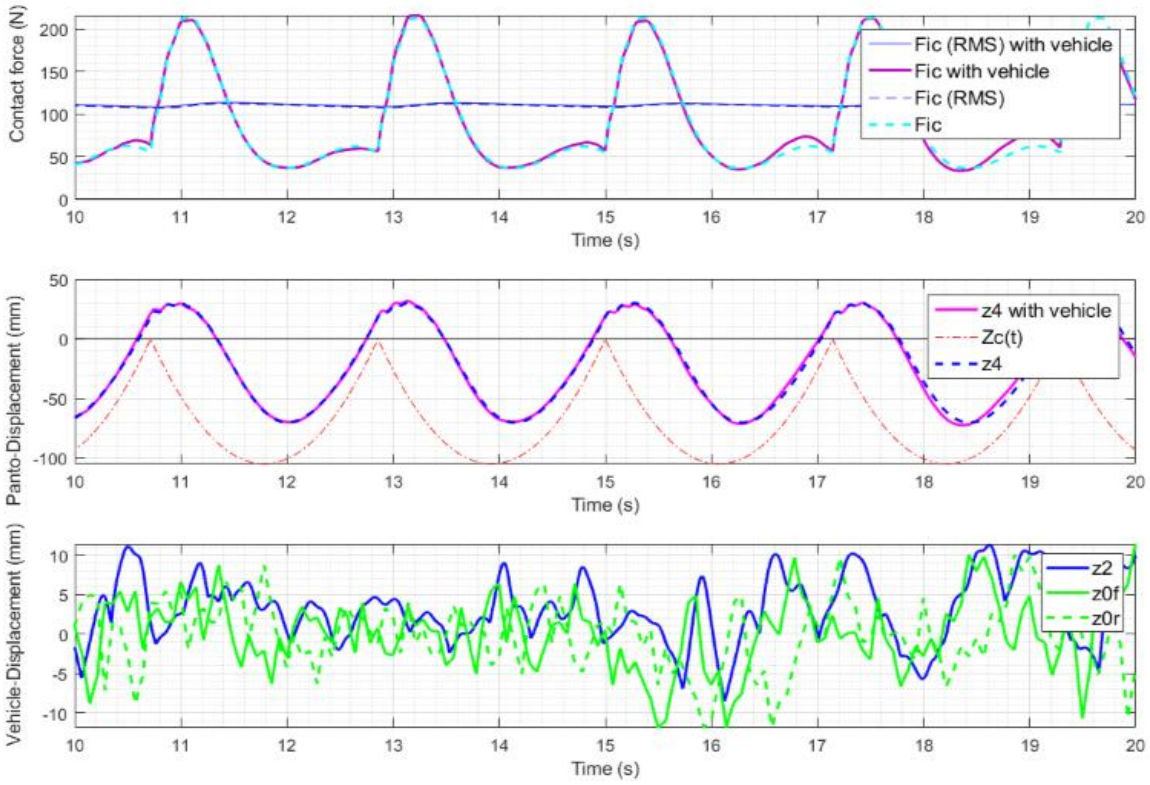

Figure3.4.12-*Simulation result of catenary-pantograph with half trolleybus with random disturbances at v=14m/s*

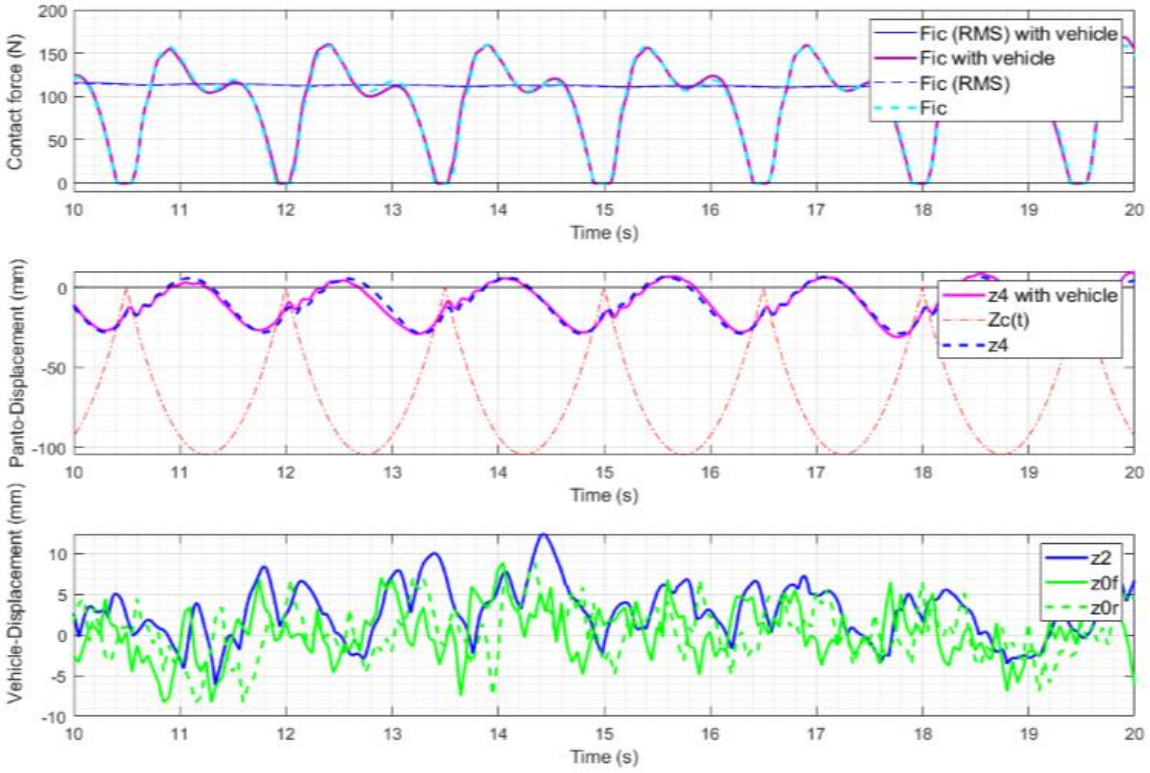

Figure3.4.13-*Simulation result of catenary-pantograph with half trolleybus with random disturbances at v=20m/s*

From Figure3.4.12 and Figure3.4.13 it can be seen that in both the catenary-pantograph with or without half trolleybus models, the contact force F_{ic} (RMS), F_{ic} and displacement (z_4) force effectively overlap at both different speeds. The variation of Fic and displacement (z4) are less than 5N (≤4%) and 2mm (≤2%) respectively. Essentially there is no difference between the two models under normal running conditions.

The simulation of Bump disturbances are carried out in three different speeds 1m/s (In depot), 14m/s (On street) and 20m/s (Highest speed). The results are shown in Figure 3.4.14, Figure 3.4.15 and Figure 3.4.16. In fact, the pair of z_{0f} and z_{0r} is disturbances generated by same step (or bump) on front and rear axles respectively with time gap Δt. Tid is a duration the trolleybus goes between two bumps' disturbance.

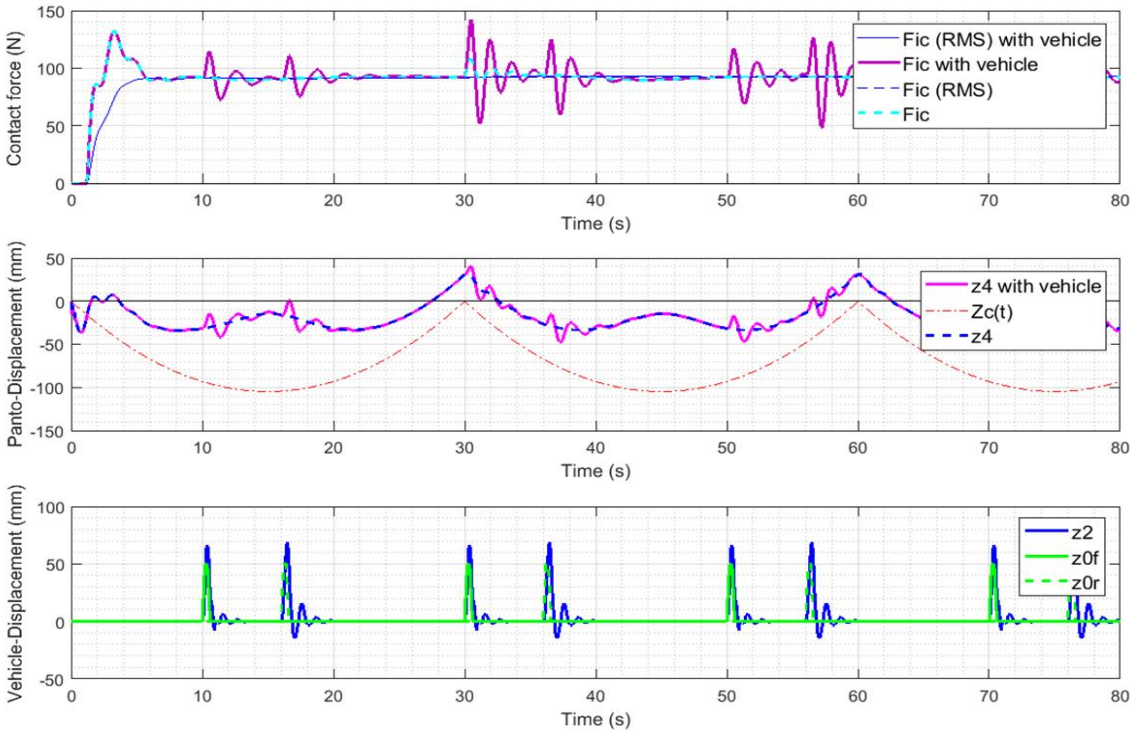

Figure 3.4.14-*Simulation result of catenary-pantograph with half trolleybus with multiple bump disturbances at v=1m/s*

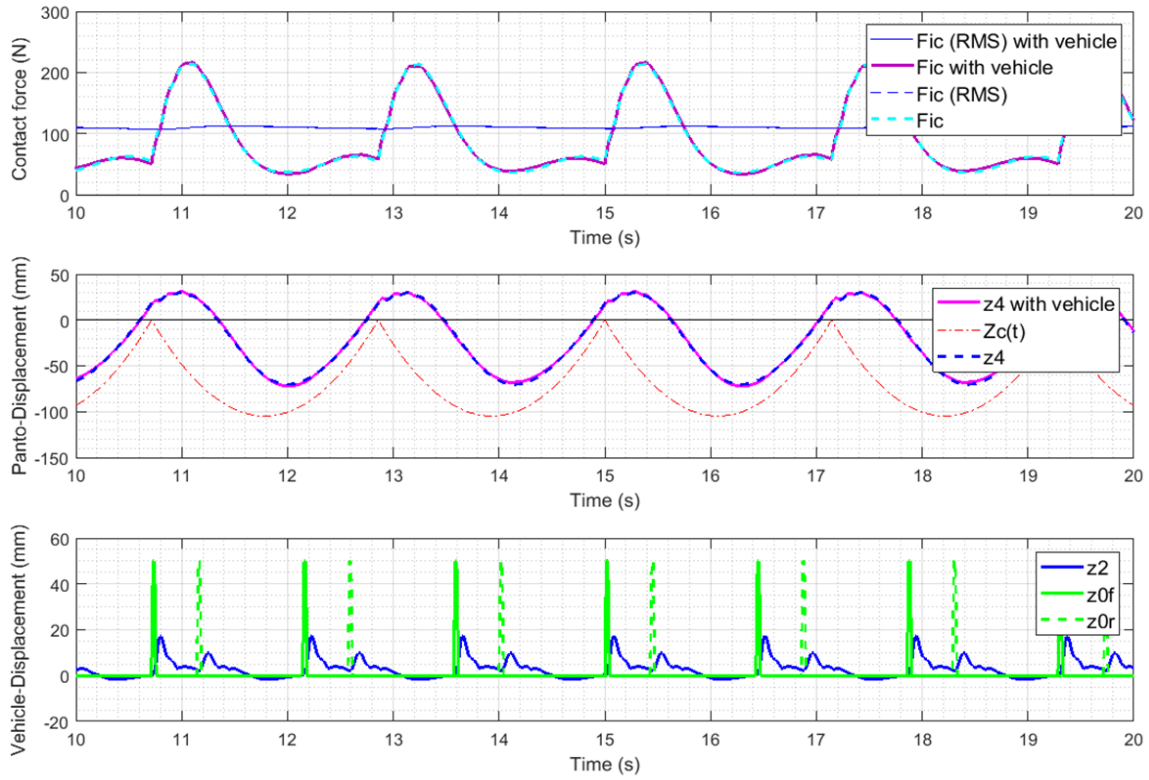

Figure 3.4.15-*Simulation result of catenary-pantograph with half trolleybus with multiple bump disturbances at v=14m/s*

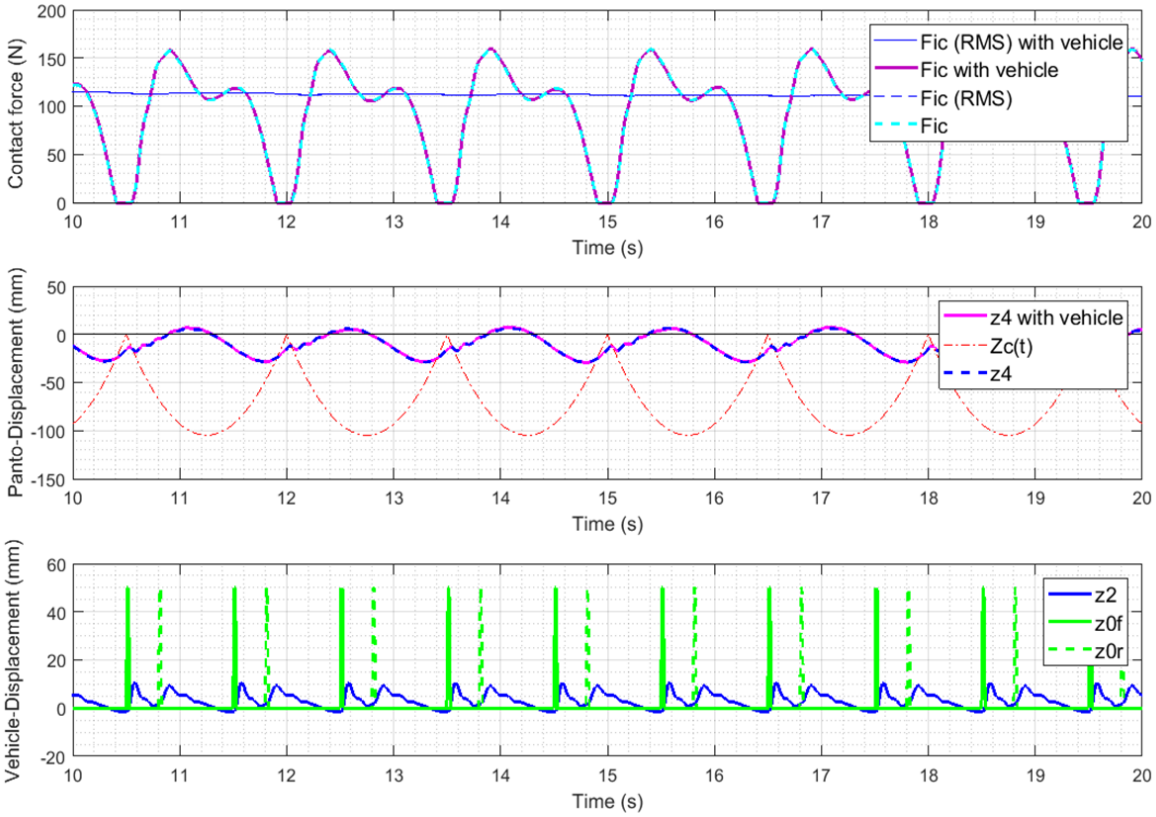

Figure 3.4.16-*Simulation result of catenary-pantograph with half trolleybus*

with multiple bump disturbances at v=20m/s

From Figure3.4.14, it can be seen that the multiple bump disturbances do effect the contact force (F_{ic}) and displacement (z_4) with variation of 100N and 50mm, particularly where the poles of the catenary wire (highest stiffness) are at the same location as the bump disturbances. This phenomenon is likely caused by the higher displacement of the trolleybus (z_2) as it goes over the bumps. The superposition effects of the poles of the catenary wire and bumps cause a higher variation in the contact force and displacement. From Figure 3.4.15 and Figure3.4.16 it can be seen that the contact force (F_{ic} (RMS) and $F_{ic)}$ and displacement (z_4 and z_4 with vehicle) effectively overlap at speeds of 14m/s and 20m/s. This could be due to the lower displacement of trolleybus (the base of pantograph) z_2 (less than 20mm).

Comparing the results in Section 3.2 to those in this Section, it can be seen that there is essentially no significate difference in the results of the catenary-pantograph model only simulations and the catenary-pantograph with half trolleybus model; particular at speeds of 14m/s and 20m/s. As before, the most worrying situation in operation of trolleybus is at the speed of 20m/s when the contact force reaches zero ($F_{ic} = 0$) at the catenary-wire pole positions. This potentially allows the pantograph-head to separate from the catenary wire (unplanned de-wirement).

3.5 Chapter Summary

Evaluating the contact force and displacement of the catenary-pantograph are the fundamental aims and assessment of this ACTCCS research project. Three comprehensive models were built including catenary-pantograph, passive half-trolleybus and catenary-pantograph with passive half-trolleybus including “Transfer force” linkage. Three different speeds for simulation were studied: 1m/s (In depot), 14m/s (On street) and 20m/s (Highest speed). Four kinds of road disturbances were also established and studied: Smooth surface (only applied on the catenary-pantograph with half-trolleybus model), Step disturbance, Random disturbance and Bump disturbance. Twenty-four simulations that have been carried out with the three selected speeds and four kinds of disturbances. In terms of simulation parameters, most of the data came from specification of existing products. In particular, the pantograph (boom) spring nominal stiffness and mass are practical measurement of real

trolleybuses in Trolleybus Museum [101], private collections [102], Tram Museum [100] and Stagecoach Supertram Maintenance [108].

The results from simulations are shown to be reasonable in respect of displacement of the contact force and collection head (trajectory) during trolleybus operation.

In general, the results of simulations between catenary-pantograph model only model and catenary-pantograph with half trolleybus model showed no significate difference, in particular at speeds of 14m/s and 20m/s. As shown in both Section 3.4 and Section 3.2, the worst possible situation in operation of trolleybus occurs when running at speed of 20m/s. The repeated zero contact force (Fic = 0) values at the catenary-wire pole positions can easily allow the pantograph head to become separated from the catenary wire. This is the key point to be studied and prevented by using active control system in forthcoming chapters.

Chapter 4

Hybrid non-linear catenary-pantograph model and analysis

4.1 Introduction of issues

In chapter 3, modelling of a trolleybus catenary-pantograph system was performed. Those simulations indicated that such a system would allow trolleybus (trains and trams) to work successfully at speeds lower than 20m/s (e.g. low speed). However, at speeds equal to or higher than 20m/s (e.g. high speed) the simulations indicated that a loss of contact (i.e. zero contact force) between the catenary wire and pantograph-head occurred repeatedly which was clearly shown in Figure 3.2.10, Figure3.4.8, Figure3.4.11, Figure3.4.13, Figure3.4.16.as well as described in Section 3.2, Section 3.4 and Section3.5. This phenomenon is shown clearly in Figure 4.1.1, which is an expanded version of a section of Figure 3.4.8 from Chapter 3 showing one of the points where the contact force drops to zero (Fic = 0) as the pantograph-head (z_4) separates from the catenary wire ($Z_c(t)$).

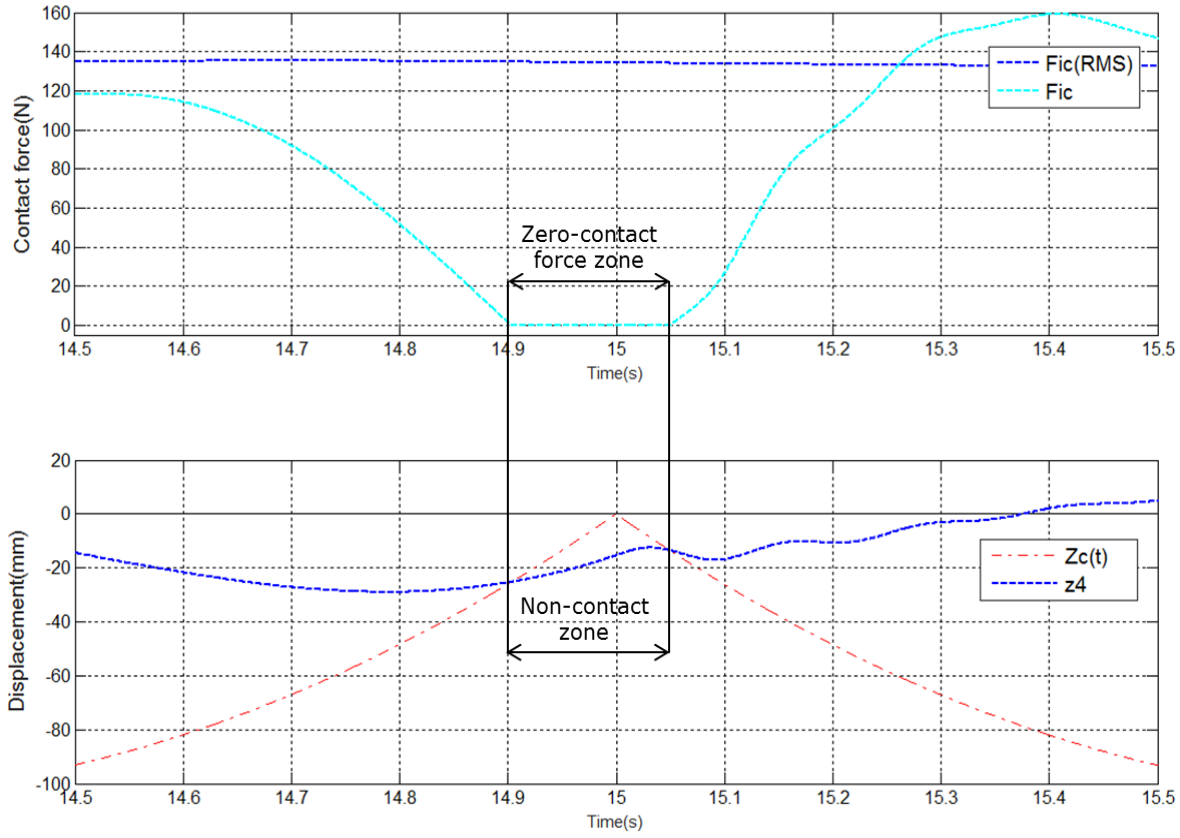

Figure 4.1.1- ***Trolleybus' catenary-pantograph simulation showing non-contact zone with zero-contact force (simulation results at speed of v=20m/s)***

Where:

F_{ic}: contact force (N)

F_{ic} (RMS): integrated contact force (RMS) (N)

z_4: pantograph-head vertical displacement (trajectory with dynamic wire) (mm)

$Z_c(t)$: original vertical displacement of catenary wire (mm)

The identification and further study of the issues occurring during these contact loss periods are important for the active control system design to be described in later chapters. This chapter therefore presents a further modelling study of the trolleybus catenary-pantograph system to better understand this phenomenon.

Two revised trolleybus catenary-pantograph models were developed that examine the dynamic phenomenon of pantograph head oscillation after hitting the catenary spans (non-contact zones). The results from these additional models are presented in sections 4.2 and 4.3. Section 4.4 then discusses the potential consequences of the repeated de-wirement and re-wirement of the pantograph-head during these contact loss periods.

4.2 Trolleybus' catenary-pantograph bouncing model

4.2.1 Introduction

The overhead catenary wire of a trolleybus system is suspended between fixed vertically suspended points and shaped as the catenary wire model previously described in Chapter 3. This catenary wire is essentially horizontal at the mid-point between the two suspension points and gradually rises with increasing steepness towards the outer points, with a corresponding increase in vertical stiffness. The zero-contact force zone occurs at the fixed suspension point between two suspended catenaries, which is where the pantograph–head separates away from catenary wire as the pantograph-head of the trolleybus passes through a fixed suspension point between two suspended catenaries.

In the model presented in Chapter 3, the dynamic wire (z_{4w}) and pantograph-head (z_{4p}) were simulated as always being connected together (including within the zero-contact force zone) while the trolleybus was in operation (shown in diagram of Figure 4.2.1). Whilst this assumption is valid in condition where contact is not lost, it is obviously incorrect for the simulation used to create Figure 4.2.1.

A more realistic assumption would be that the dynamic catenary wire and sliding pantograph-head share a common dynamic displacement (i.e. are in contact) until the two bodies reach a 'separation point' (shown in diagram of Figure 4.2.1). From this 'separation point', the pantograph-head should feely lift up whilst the catenary wire tends to recover its original freely hanging shape ($Z_c(t)$). Subsequently, the pantograph head re-connects with the catenary

wire before bouncing off and then re-connecting a second (or more) times. Eventually the pantograph head and catenary wire stick fully again until reaching the next separation point. To correctly model this phenomenon a new hybrid model of catenary-pantograph had to be developed.

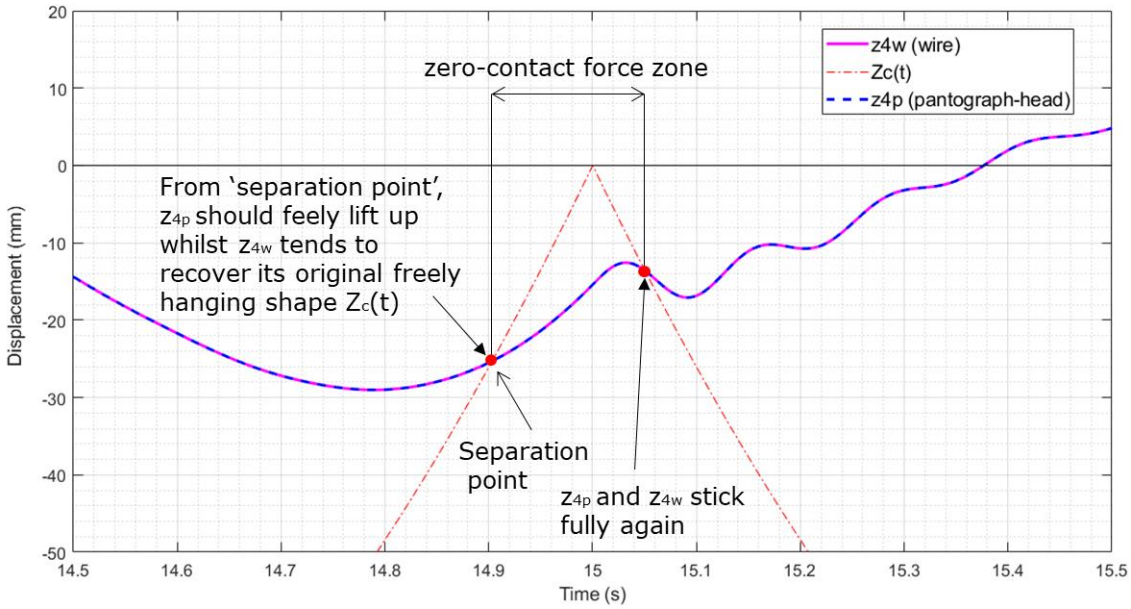

Figure 4.2.1- ***Differences between the simulation result of the normal mode model (in Chapter 3) and the question of what is going on with z_{4w} and z_{4p} during the zero-contact force zone at speed of 20m/s***

Where:

z_{4w}: dynamic wire vertical displacement (trajectory with pantograph-head) (mm)

z_{4p}: pantograph-head vertical displacement (trajectory with dynamic wire) (mm)

$Z_c(t)$: original vertical displacement of catenary wire (mm)

In order to develop and simulate a hybrid model, a two-stage plan was made to create models listed below:

- Bouncing models and simulation of catenary-pantograph system in non-contact zone
- Hybrid model and simulation of trolleys' catenary-pantograph system

Bouncing is a well understood natural phenomenon that can be seen in things such as a dropped ball on the surface or the skimming of spinning stones on the water surface. This principle was even engineered into the famous 'bouncing bomb' used in the Second World War.

Any possible bounce modes between the pantograph and catenary is likely to cause problems such as: electrical arcing (leading to serious damage of the wire and the collector of pantograph [111]) and a high probability of de-wirement (potentially causing wires to be brought down with subsequent danger to material and human life [112]). Thus, modelling the bouncing phenomenon within the catenary-pantograph system is as a key aspect of the hybrid model.

The behaviour of a vertically dropped ball [110,113] can be applied to simulate the impact phenomenon of a catenary-pantograph system with a flexible catenary wire (variable stiffness) and elastic pantograph within the non-contact zone. The majority of the modelling parameters and simulation conditions are inherited from previous work in Chapter 3. Within the basic bouncing assumption of the catenary-pantograph system, the loss of kinetic energy of pantograph head as it lifts up is balanced by the increase in gravity potential energy of the lifted catenary wire when the two re-connect.

No previous work on the bouncing modes of catenary-pantograph interaction has been found in the literature.

4.2.2 Catenary-pantograph system bouncing model

Modelling the impact phenomenon of the catenary-pantograph system with a flexible catenary wire (variable stiffness) and elastic pantograph within the non-contact zone can be modelled as a mass-spring-damper ball model [113] with several important assumptions as follows:

- At the start of contactless point, in general the total energy of pantograph is amount of kinetic energy of velocity and potential of pressed springs. This energy will lift pantograph up and make lasting vibration of both pantograph and catenary when pantograph hitting catenary again.
- Hitting and lasing duration with losing energy is applicable rather than splitting the model into two segments of deformation and restitution which gets lower reflex height than last one
- The natural frequency must be higher than zero [113]
- Impact duration is equal to half the period of natural oscillation

To refer trolleybus catenary-pantograph model presented in Section 3.2.3 in Chapter 3 (shown in Figure 3.2.4), the bouncing model of catenary-pantograph is shown in Figure 4.2.2A. When the pantograph is not in contact with catenary wire neither b_4 and k_4 should not

be taken into account of the equations, only mass m_4 is required. The pantograph is dynamically free lifting up with k_3 and b_3. However, when the pantograph-head hitting with the catenary wire which means it is in re-contact with the catenary wire all three parameters (b_4, k_4 and m_4) need to be included in the dynamic equations. The hybrid system aspect of the catenary bouncing modelling originates from the modelling of a collision of the mass-spring-damper ball model with the ground [110]. If one assumes elastic hitting with catenary wire, then the velocity before the hitting and velocity after the hitting can be related by the coefficient of catenary-pantograph system hitting energy loss [110]. Therefore, the catenary-pantograph bouncing model will display a jump in a continuous state (velocity) at the transition condition under the potential energy charged by k_3 between pantograph (head) initial position and first separate point. In order to simplify the modelling of catenary-pantograph bouncing, the simplified bouncing model of catenary-pantograph is shown in Figure 4.2.2B.

Meanwhile, there is a damped natural frequency (ω_d) of natural oscillation and the minimum nonzero single contact period duration (ΔT) and small [113] between the initial hitting of the between pantograph-head and catenary wire and their eventual separate are given shown in Figure 4.2.2C which bases on simplified bouncing model of catenary-pantograph is shown in Figure 4.2.2B. The natural damped frequency (ω_d) of oscillation is dependent upon the stiffness of catenary wire at the hitting point.

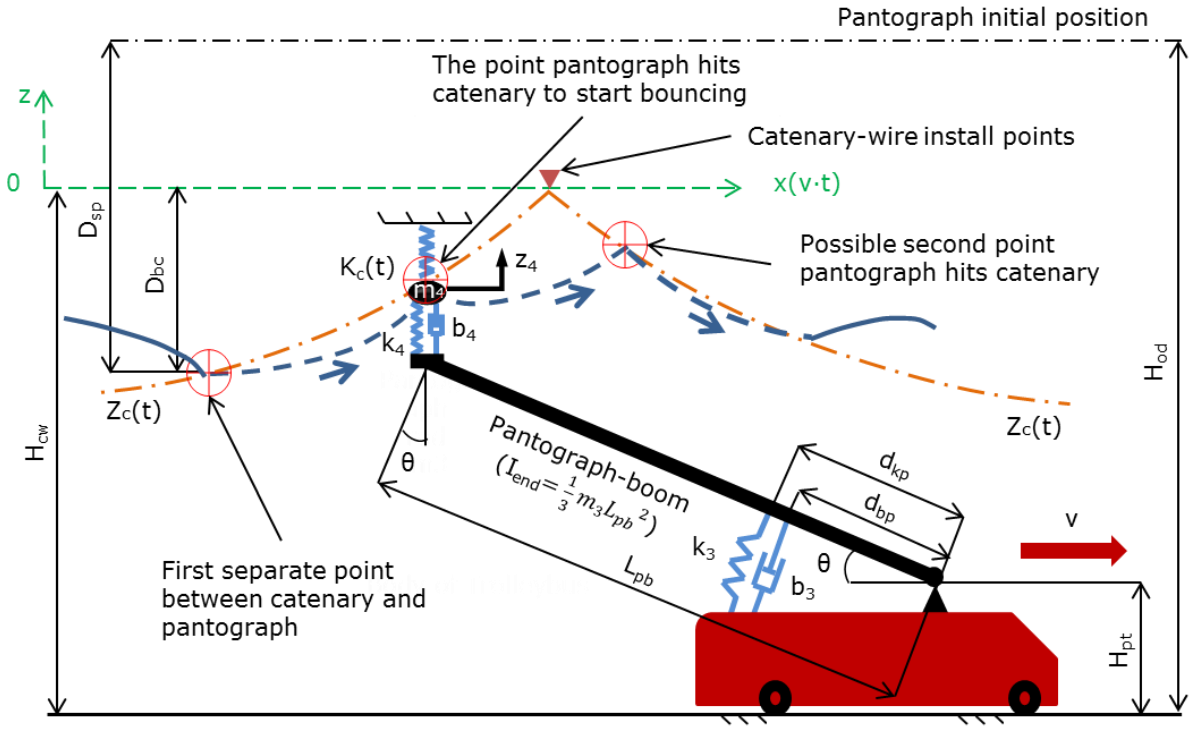

Figure 4.2.2A-*Catenary-pantograph system bouncing model*

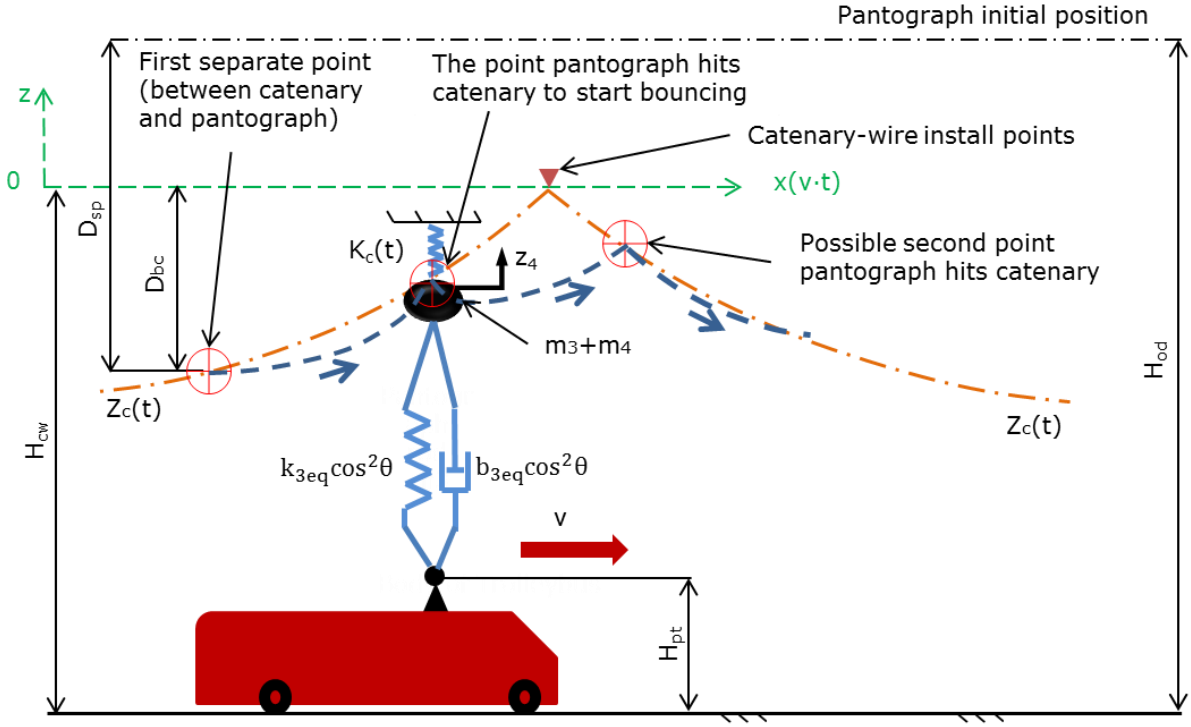

Figure 4.2.2B-*Simplified catenary-pantograph system bouncing model*

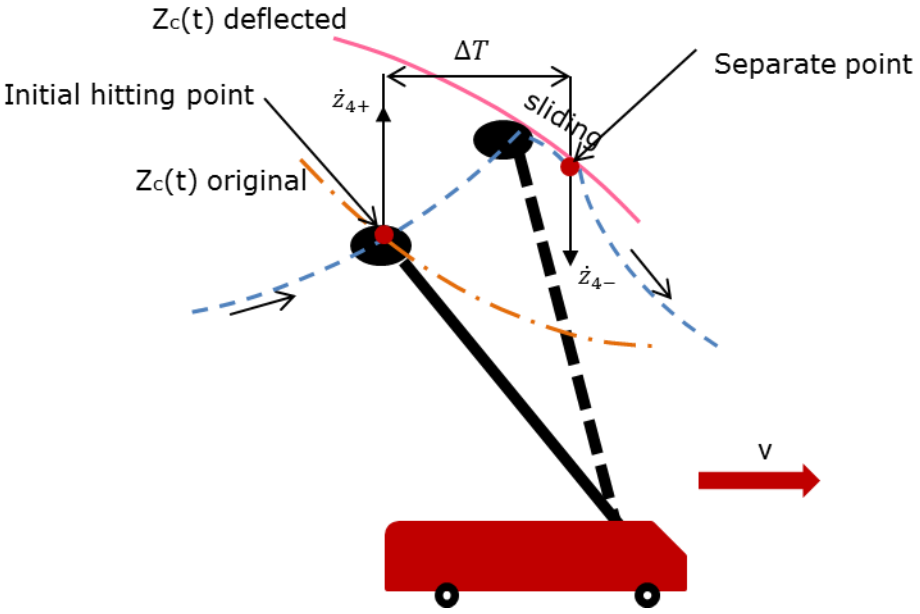

Figure 4.2.2C-*Bouncing deflection definition of original bouncing model*

To refer from E3.2.13, E3.2.21 and basing on simplified catenary-pantograph system bouncing model (shown in Figure 4.2.2) the bouncing linearized dynamic equations (head part) are shown in equations E4.2.1A (during contactless), E4.2.1B (during ΔT) , E3.2.14, E4.2.2, E4.2.3, E4.2.3, E4.2.4 and E4.2.5.

$$(\boldsymbol{m_3 + m_4})\ddot{\boldsymbol{z}}_{\boldsymbol{4}} = -\boldsymbol{b_{3eq}cos^2\theta \cdot \dot{z}_4 \cdot - k_{3eq}\cos^2\theta \cdot z_4 - k_{3eq} \cdot D_{sp}} \qquad \text{E4.2.1A}$$

$$(\boldsymbol{m_3 + m_4})\ddot{\boldsymbol{z}}_{\boldsymbol{4}} = -\boldsymbol{b_{3eq}cos^2\theta \cdot \dot{z}_4 \cdot - k_{3eq}\cos^2\theta \cdot z_4 - \left[k_{3eq} + K_c(t)\right]\left(D_{sp} - D_{bc}\right)} \qquad \text{E4.2.1B}$$

$$\boldsymbol{\cos^2\theta = 1 - sin^2\theta \approx 1 - \left[\frac{H_{od} - H_{pt} - D_{bc}}{L_{pb}}\right]^2} \qquad \text{E4.2.2}$$

$$\boldsymbol{D_{sp} = H_{od} - H_{cw} + D_{bc}}$$

$$\dot{\boldsymbol{z}}_{\boldsymbol{4-}} = -\boldsymbol{e}^{-\frac{\frac{b_{3eq}\cdot b_4}{b_{3eq}+b_4}\pi}{2(m_3+m_4)\omega_d}} \cdot \dot{\boldsymbol{z}}_{\boldsymbol{4+}} \text{ [113]} \qquad \text{E4.2.3}$$

where:

$$\boldsymbol{\omega_d = \frac{1}{2(m_3+m_4)}\sqrt{4\left[\frac{k_{3eq}\cdot k_4}{k_{3eq}+k_4} + K_c(t)\right](m_3+m_4) - \left(\frac{b_{3eq}\cdot b_4}{b_{3eq}+b_4}\right)^2}} \qquad \text{E4.2.4}$$

[113, 114, 121], $\omega_d > 0$ [113]

$$\boldsymbol{\Delta T = \frac{\pi}{\omega_d}} \text{ [113]} \qquad \text{E4.2.5}$$

Where:

D_{sp}: distance between separation point and initial position of pantograph-head (m)

D_{bc}: pantograph-head dynamic displacement (z_4) at separation point (m)

$K_c(t)$: catenary contact wire nominal stiffness (N/m)

$Z_c(t)$: pre-catenary vertical displacement (m)

H_{od}: initial position of pantograph-head from ground (m)

H_{cw}: installation height of the catenary wire (normally from ground to fixed point on poles). It is determined from the BSI British Standards for Trolleybus (m) [37]

H_{pt}: pivot height of pantograph from ground (3.50 m)

m_3: pantograph-boom mass (kg)

b_3: pantograph-boom absorbers damping rate (Ns/m)

k_3: pantograph-boom spring nominal stiffness (N/m)

d_{bp}: distance from damper fitting point to pantograph pivot point

d_{kp}: distance from spring fitting point to pantograph pivot point

z_4: pantograph-head vertical displacement (trajectory) (m)

m_4: pantograph-head mass (kg)

b_4: pantograph-head absorbers damping rate (Ns/m)

k_4: pantograph-head spring stiffness (N/m)

$\dot{z}_{4+}$: at initial hitting point vertical velocity between the pantograph-head and catenary wire (m/s)

$\dot{z}_{4-}$: at separate point vertical velocity between pantograph-head and catenary wire (m/s)

ΔT: minimum nonzero single bouncing period duration

θ: pantograph-boom dynamic lifting angle (degrees)

L_{pb}: length of pantograph-boom (m)

v: pantograph (trolleybus) horizontal move velocity (m/s)

However, as the trolleybus running speed (horizontal velocity) is not included in the basic catenary-pantograph system bouncing model shown in E4.2.3, the dynamic equations were modified as shown in Figure 4.2.3.

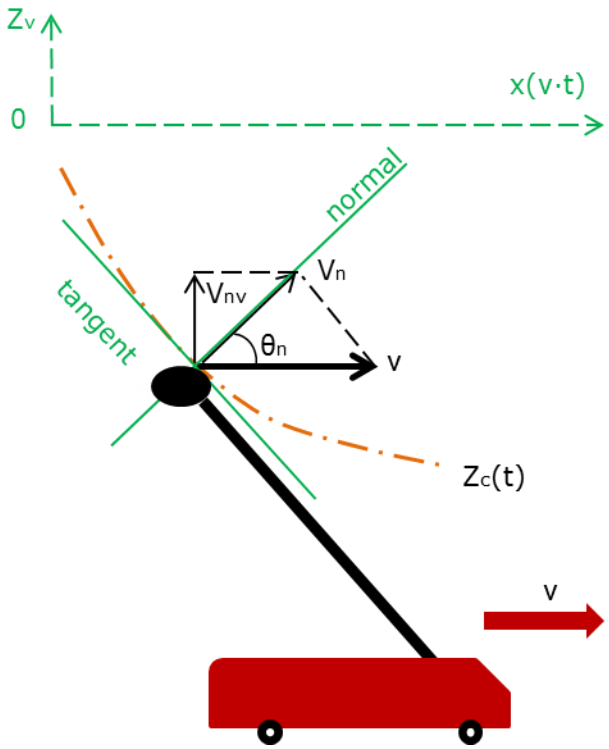

Figure 4.2.3-*Catenary-pantograph system bouncing model with consideration of the horizontal moving velocity 'v' (trolleybus running speed) of the pantograph*

Where:

$Z_c(t)$: catenary displacement with various stiffness (m)

v: pantograph (velocity) horizontal move speed (m/s)

θ_n: angle between normal line and v (x')

V_n: normal component of v (m/s)

V_{nv}: vertical component of Vn (m/s)

Equation and sub-equations:

$$\boldsymbol{V_n = v \cdot \cos \theta_n} \qquad \text{E4.2.6}$$

$$\boldsymbol{V_{nv} = V_n \cdot \sin \theta_n = v \cdot \frac{\tan \theta_n}{\sqrt{1+ \tan^2 \theta_n}} \cdot \frac{1}{\sqrt{1+ \tan^2 \theta_n}} = v \cdot \frac{\tan \theta_n}{1+ \tan^2 \theta_n}} \quad [119] \qquad \text{E4.2.7}$$

As $\boldsymbol{\tan \theta_n}$ can be thought of as the gradient of the normal line [164] to the catenary wire at the re-connection point between catenary and pantograph, it can be derived from E3.2.1 as shown in E4.2.8

$$\boldsymbol{\tan \theta_n = -\frac{1}{\dot{Z}_c(t)} = -\frac{T_c}{g \cdot \rho (v \cdot t - L_{ws})}} \; [164] \qquad \text{E4.2.8}$$

Consequently E4.2.3 can be modified as shown in E4.2.9

$$(\dot{z}_4 + V_{nv})_- = -e^{-\frac{\frac{b_{3eq} \cdot b^4}{b_{3eq}+b_4}\pi}{2(m_3+m_4)\omega_d}} \cdot (\dot{z}_4 + V_{nv})_+ \text{ [113]} \qquad \text{E4.2.9}$$

With the introduction of E4.2.9, the set of dynamic equations for the bouncing pantograph head model (with consideration of v) during the zero contact force periods have been established as shown in E3.2.14, E4.2.1A, E4.2.1B, E4.2.2, E4.2.8 and E4.2.9.

Turning to modelling the catenary wire displacement, the definitions and assumptions of the catenary wire bouncing model are shown in Figure 4.2.4

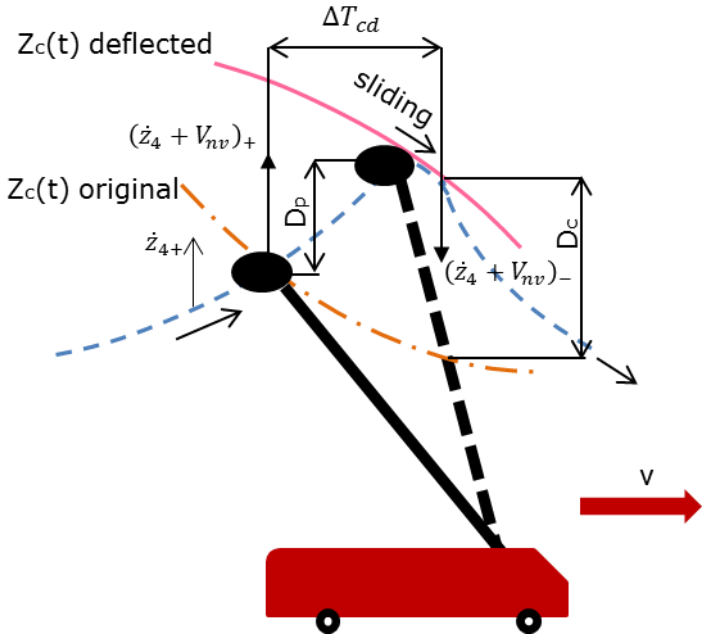

Figure 4.2.4-*Bouncing deflection definition of original bouncing model with considering V_{nv}*

Where:

V_{nv}: vertical component of V_n (m/s)

ΔT_{cd}: pantograph and catenary single bouncing period duration with considering V_{nv}

D_c: catenary bouncing vertical deflection (m)

D_p: pantograph bouncing nominal vertical deflection

z_4: pantograph-head vertical displacement (trajectory) (m)

$(\dot{z}_4 + V_{nv})_+$: at initial hitting point vertical velocity between the pantograph-head and catenary wire with considering V_{nv} (m/s)

$(\dot{z}_4 + V_{nv})_-$: at separate point vertical velocity between pantograph-head and catenary wire with considering V_{nv} (m/s)

It can be assumed that when the pantograph re-connects with the flexible catenary, it deflects away from its original position as the pantograph slides along the catenary for a period $\Delta T_{cd.}$ The pantograph will remain in contact with the catenary until it separates from the catenary wire at the point (position) of starting swing back. In order to simplify the modelling an assumption was made that ΔT_{cd} is small approaching zero and ΔT. The deflection of catenary D_c caused by bouncing deflection of pantograph-head ($D_{p)}$. Hence

$$\boldsymbol{D_c \cong D_p} \qquad \text{E4.2.10}$$

From Figure 4.2.4, D_p can be represented by equation E4.2.10.

$$\boldsymbol{D_c \cong D_p = (\dot{z}_4 + V_{nv}) \cdot \Delta T_{cd} \cong (\dot{z}_4 + V_{nv}) \cdot \Delta T} \qquad \text{E4.2.11}$$

The bouncing model of catenary part from catenary adding (as well as equally) is shown below.

$$\boldsymbol{Z_c(t) \cong \frac{g \cdot \rho}{2T_c}[(v \cdot t)^2 - (v \cdot t) \cdot L_{ws}] + D_c} \qquad \text{E4.2.12}$$

4.3 Trolleybus catenary-pantograph hybrid non-linear model and simulation

4.3.1 Introduction

It was shown in Section 4.1.1 (Figure 4.1.1) that at high running speeds there are two distinct dynamic phases in trolleybus pantograph-catenary operation - with contact and without contact (zero contact force). In this section, a hybrid trolleybus pantograph-catenary model is presented that consists of a normal (tight contact sliding) model between fixing points and a bouncing contact model around the fixing points.

4.3.2 Trolleybus hybrid model

The normal (tight contact sliding) part of the hybrid model of the catenary-pantograph dynamics was described in Section 3.2 of Chapter3: E3.2.1, E3.2.2, E3.2.9, E3.2.11, E3.2.13, E3.2.14, E3.2.17, E3.2.20 and E3.2.21

The bouncing model part of the hybrid model of the catenary-pantograph dynamics is described in section 4.2.

4.3.3 Simulation and analysis

A Simulink configuration of catenary-pantograph was created covering both parts of normal and bouncing models. Figure 4.3.1 shows the Simulink configuration of the catenary-pantograph as expressed in two groups equations (modules) in normal (tight contact sliding) status with equations in section 2 in Chapter 3 and bouncing status with equations in section 2 in Chapter 4. The simulation performs a typical step function between the two sets of equations at the appropriate locations.

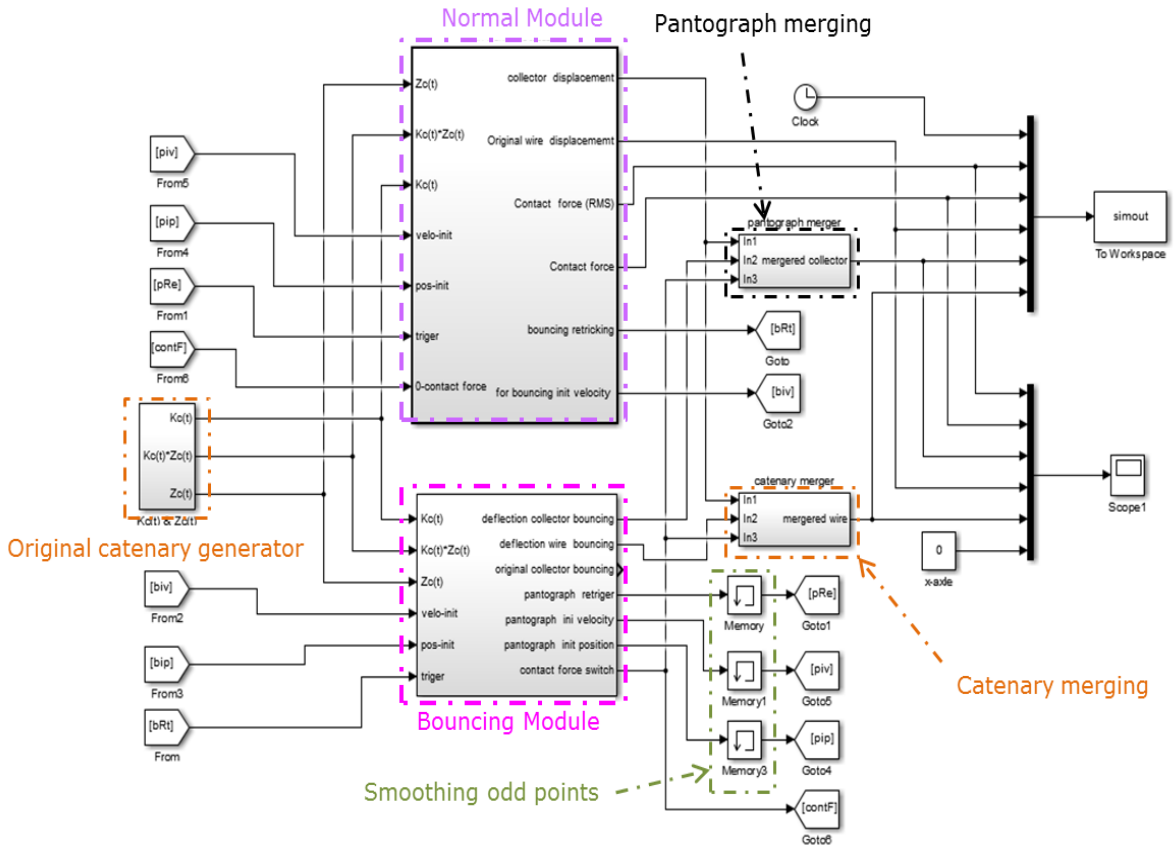

Figure 4.3.1-*Trolleybus' hybrid model dynamic Simulink configuration*

The Simulink specification of trolleybus pantograph and catenary are as given in Table 3.2.2 of Section 3.2.4 in Chapter 3. The simulation was only performed at a running speed of 20m/s; which is where the zero-contact force situation occurs, as explained in section 4.1

In the following Simulink displays, the following abbreviations are used for explaining the results of Trolleybus' hybrid model in normal and bouncing states:

F_{ic}: integrated contact force between catenary wire and pantograph-head; also the impact transient force when the pantograph-head hitting catenary during the bouncing

F_{ic} (RMS): integrated contact force (RMS) (N)

$z4_{ph}$: trajectory of pantograph-head (highest vertical displacement) with bouncing model (m)

$z4_{br}$: trajectory of catenary-wire (highest vertical displacement) with bouncing model (m)

$Z_c(t)$: original vertical displacement of catenary wire (m)

General explanation of simulation results:

The catenary and pantograph displacement and contact force results are shown in Figure 4.3.2. These displacement results clearly show the bouncing phenomenon occurring after each fixing point. The bouncing phenomena can also be observed in the amplitude variation of the contact force (F_{ic}) after each fixing point. Both the displacement and contact force results show the typical characteristic of the catenary-pantograph system repeat period (with equal 30m span of catenary at 20m/s).

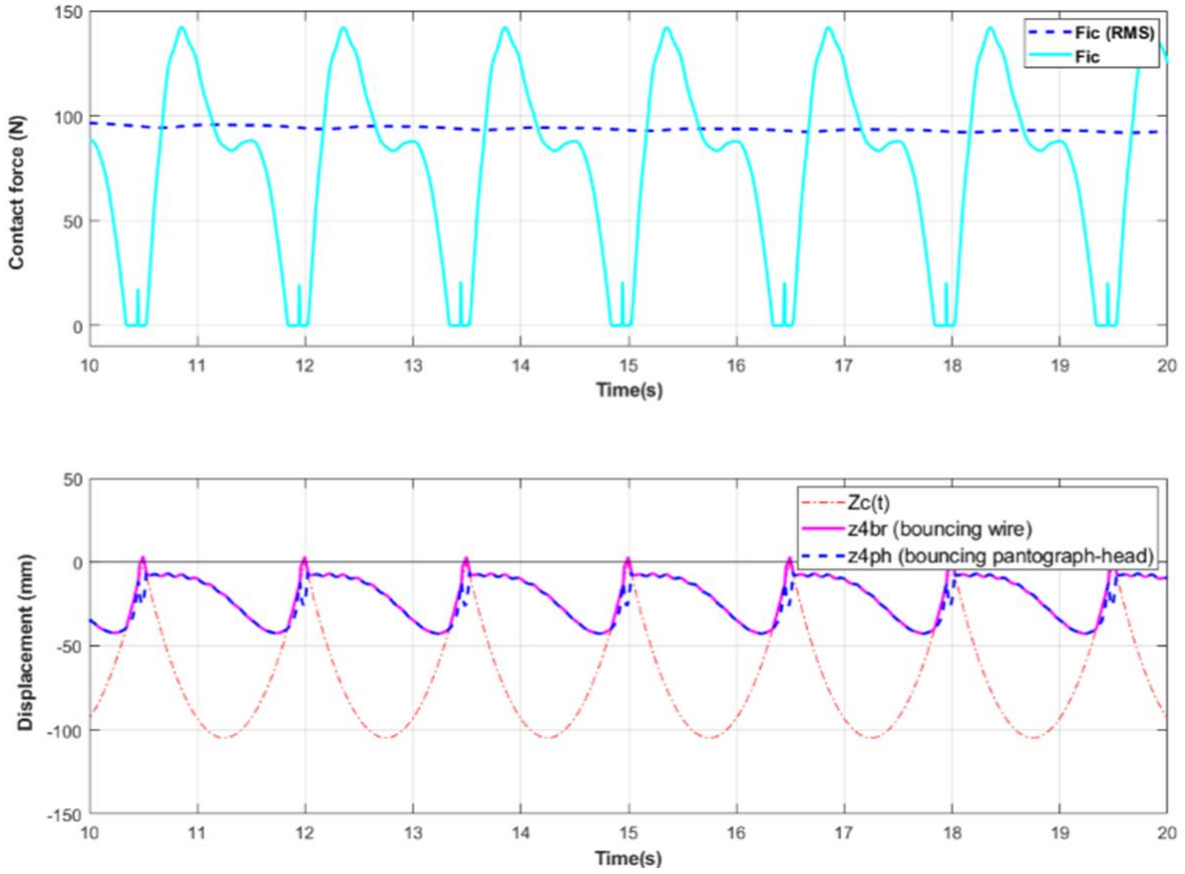

Figure 4.3.2-*Trolleybus' hybrid model dynamic simulation result*

In order to further explain the simulation, an expanded detail of the results between14.5 and 15.5 seconds is shown in Figure 4.3.3

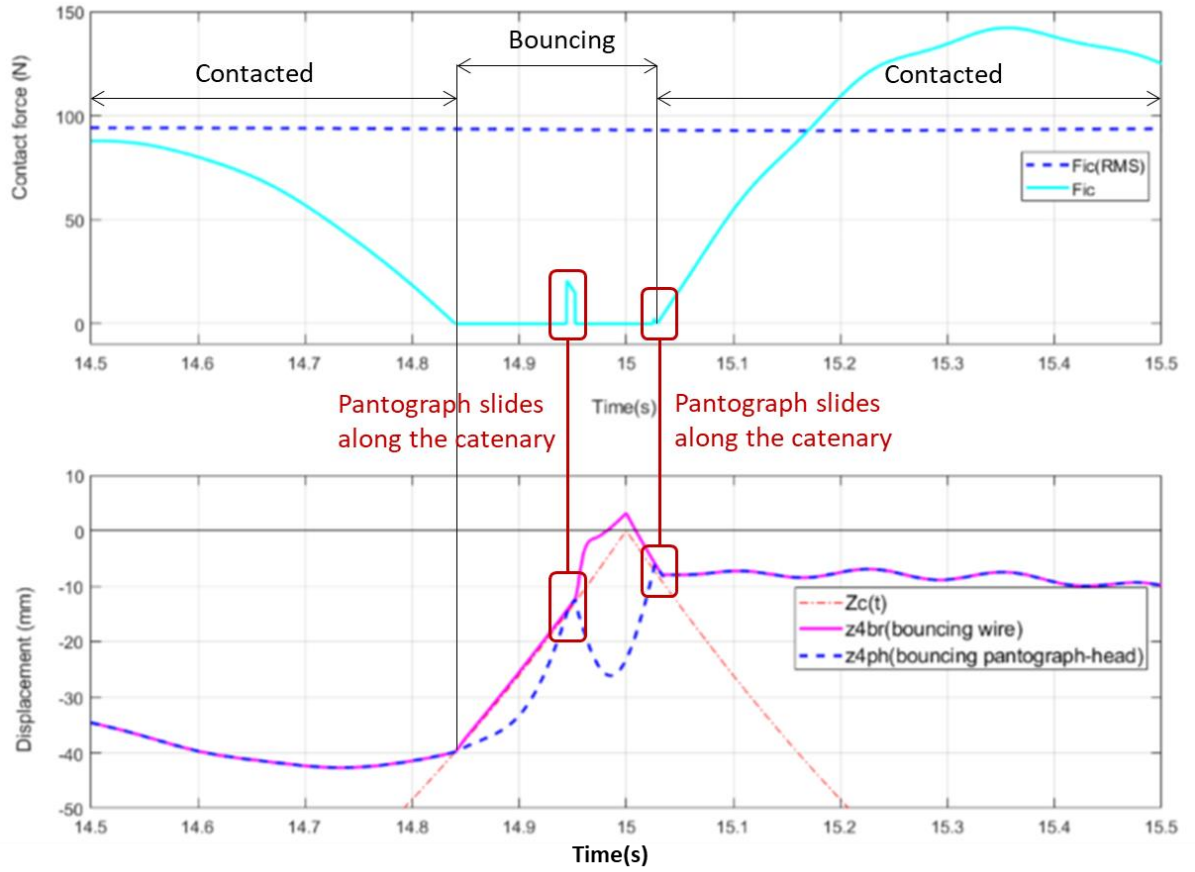

Figure 4.3.3-*Simulation result for Trolleybus' hybrid model*

Explanation of simulation in detail:

A key part of the simulation is the interaction of the catenary and pantograph at the fixed points where separation and bouncing occur. Details of this interaction (also called the bouncing cycle) are formed with two segments of pure bouncing and sliding (descripted in Figure 4.2.4 and relevant paragraph) which are shown in Figure 4.3.3. From the displacement chart there are two observed bouncing cycles. A whole course of bouncing is from the end of normal Contacted mode (14.84 secs), a first bounce (14.84 -14.94 secs) where the pantograph head and catenary are not connected, a very short period where the pantograph re-connects with and slides along the catenary (14.94-14.95 secs), a second bounce (14.95 - 15.025 secs), another very short period where the pantograph re-connects with and slides

along the catenary (15.025-15.035 secs) and then finally back to normal Contacted mode (after15.035 secs).

The contact force results show that there is essentially zero contact force between the pantograph head and catenary wire during the two bouncing segments. There is a very brief contact force pulse period as the pantograph head strikes and then slides along the catenary at the end of the first bounce. However, the peak amplitude of the contact force during this pulse is much lower than the highest dynamic contact force during normal contacted running.

Looking back at Figure 4.3.2, it can also be seen that the bouncing phenomena repeats regularly around each fixing point.

Table 4.3.1 compares the integrated contact force (F_{ic}) results of the normal and hybrid (normal with bouncing) models.

Table 4.3.1 F_{ic} simulation results comparison between normal and hybrid models

Contact force / Model type	F_{ic} (N) (RMS)	F_{ic} (N) (Max)	F_{ic} (N) (Min)
Normal	108	152	0
Hybrid	94.5	142	0

It is clear from Table 4.3.1 that the F_{ic} (RMS) value is reduced by 12.5% from 108N to 94.5N, whilst the contact force F_{ic} (Max) is slightly reduced from 152N to 142N. These reductions indicate that the engaged performance between the catenary and pantograph becomes worse where bouncing occurs. In addition, the risk of de-wirement and arcing increases sharply.

The trajectory of catenary-wire (highest vertical displacement) and profile of dynamic catenary (vertical displacement) are different concepts. In order to better illustrate the interaction between the pantograph and wire that precipitates the bouncing mode a series of ‘snap-shots’ of dynamic catenary(s) with trajectory of pantograph-head displacement (highest vertical displacement) are shown in Figures 4.3.4, to 4.3.10..

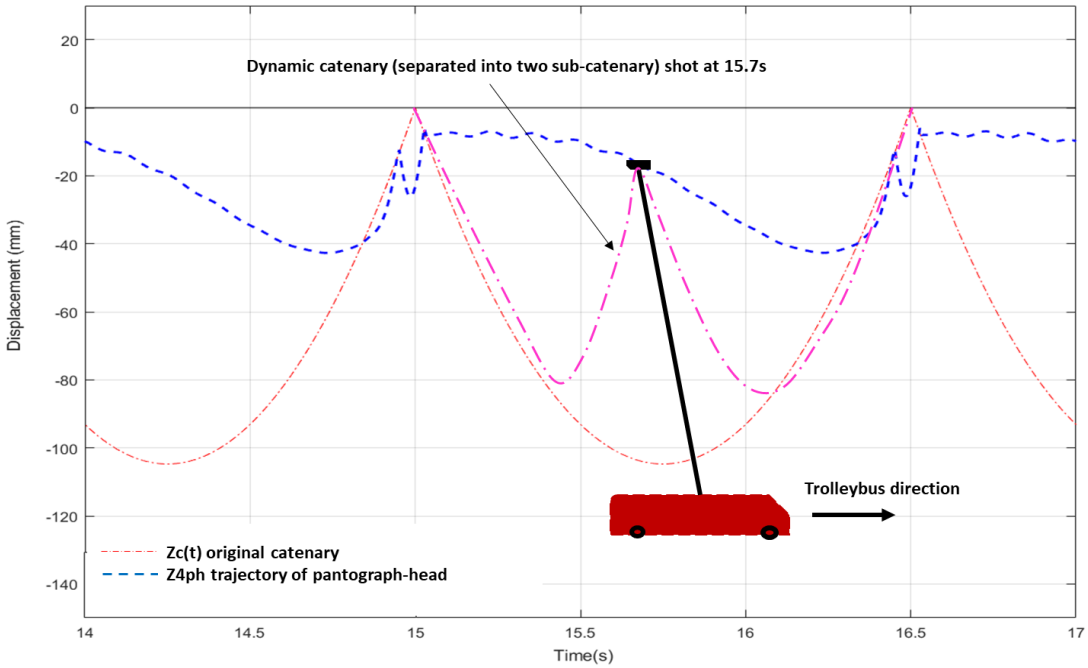

Figure 4.3.4-*shot of dynamic catenary with Trolleybus' hybrid model at 15.7s in normal state*

Figure 4.3.4 shows the pantograph mid-span, with the shape of the wire in front and behind the pantograph evident. This demonstrates a balance of pantograph upward thrust and wire reaction. The pantograph is sitting inside a 'kinematic energy well', meaning that it remains in contact with the wire..

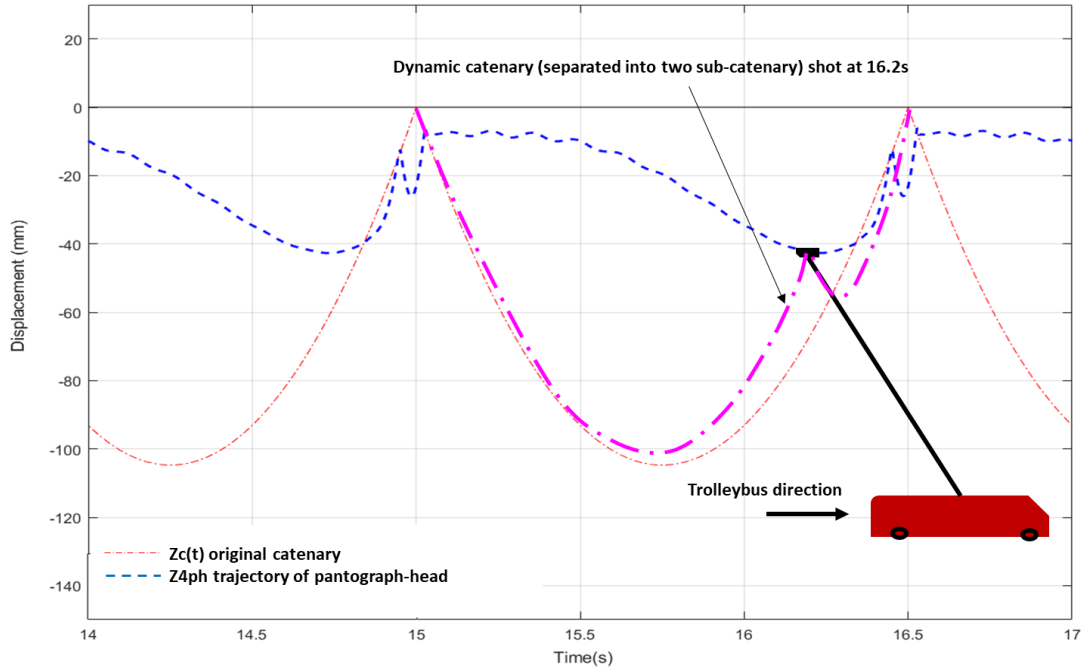

Figure 4.3.5-*shot of dynamic catenary with Trolleybus' hybrid mode at 16.2s in normal state*

Figure 4.3.5 is taken further along the path and demonstrates how the shape of the wire changes as the stantion is approached. The ‘energy-well’ is now much less pronounced as the vertical stiffness of the wire increases relative to the upward force of the pantograph.,

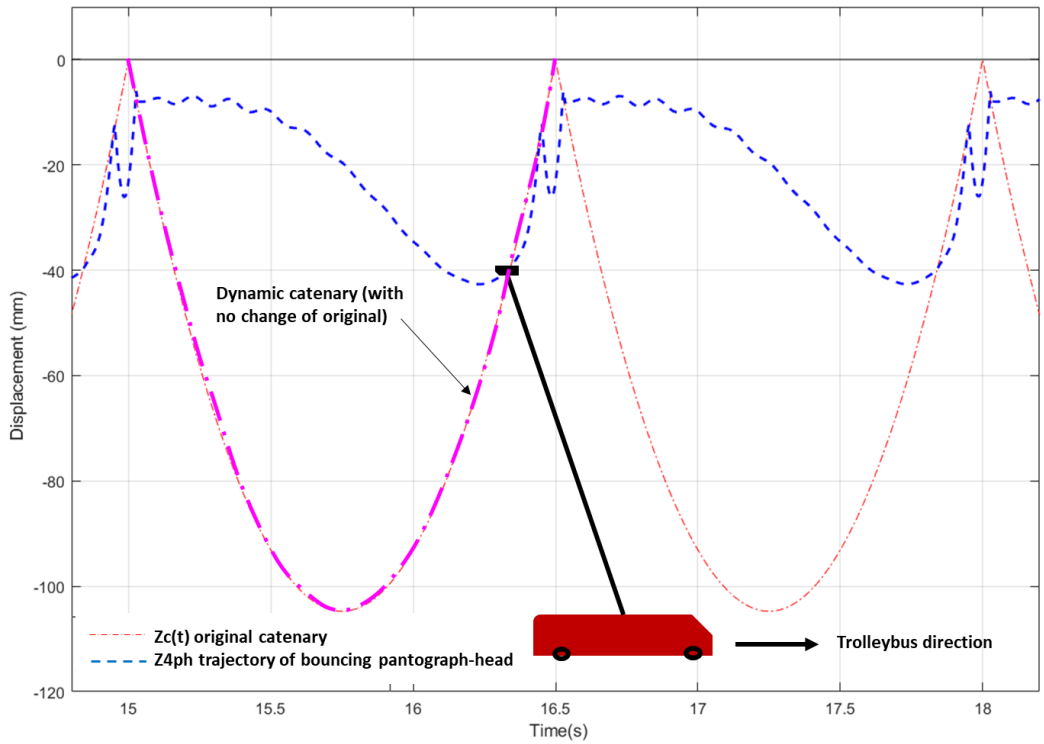

Figure 4.3.6-*shot of dynamic catenary with Trolleybus’ hybrid model at first separating point*

Figure 4.3.6 demonstrates the transition of the force balance, where the pantograph uplift can no longer deform the wire and is therefore no longer in the ‘energy-well’, and is the point where the pantograph begins to separate from the wire due to the forward motion of the vehicle.

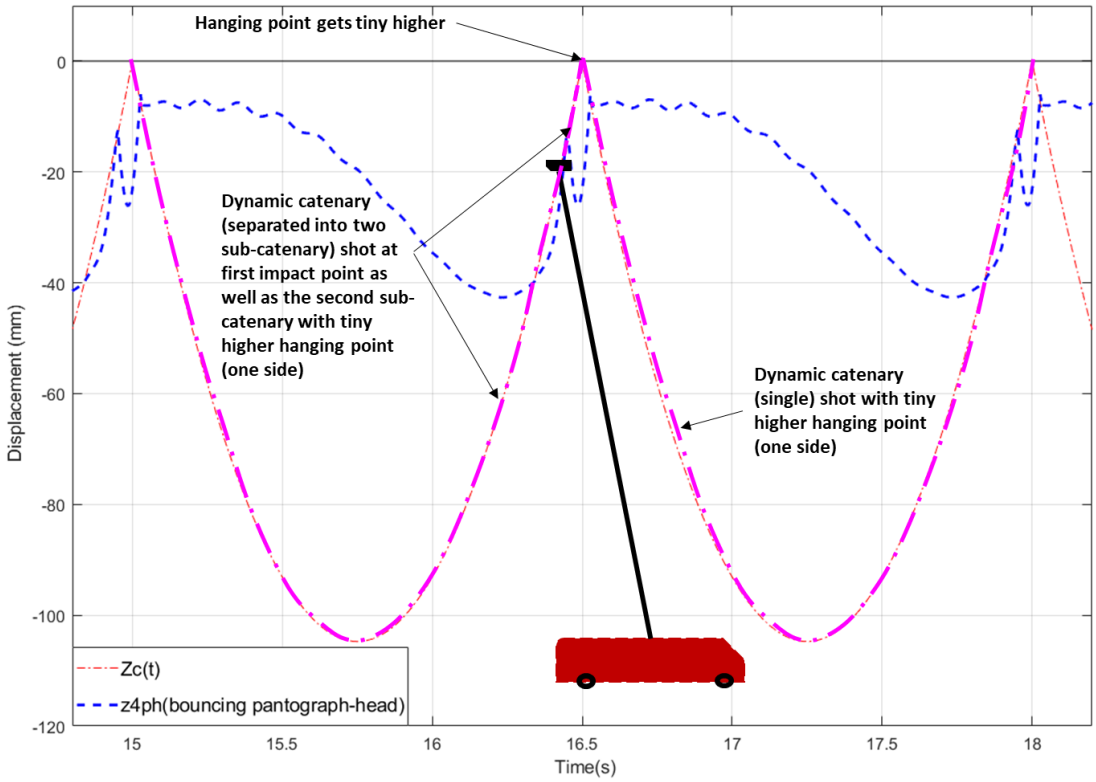

Figure 4.3.7-*shot of dynamic catenary with Trolleybus' hybrid model at first impact point*

Figure 4.3.7 demonstrates how the pantograph detached from the wire, but the unconstrained pantograph then impacts the wire due to the spring de-compressing, beginning the bouncing phase of the motion.

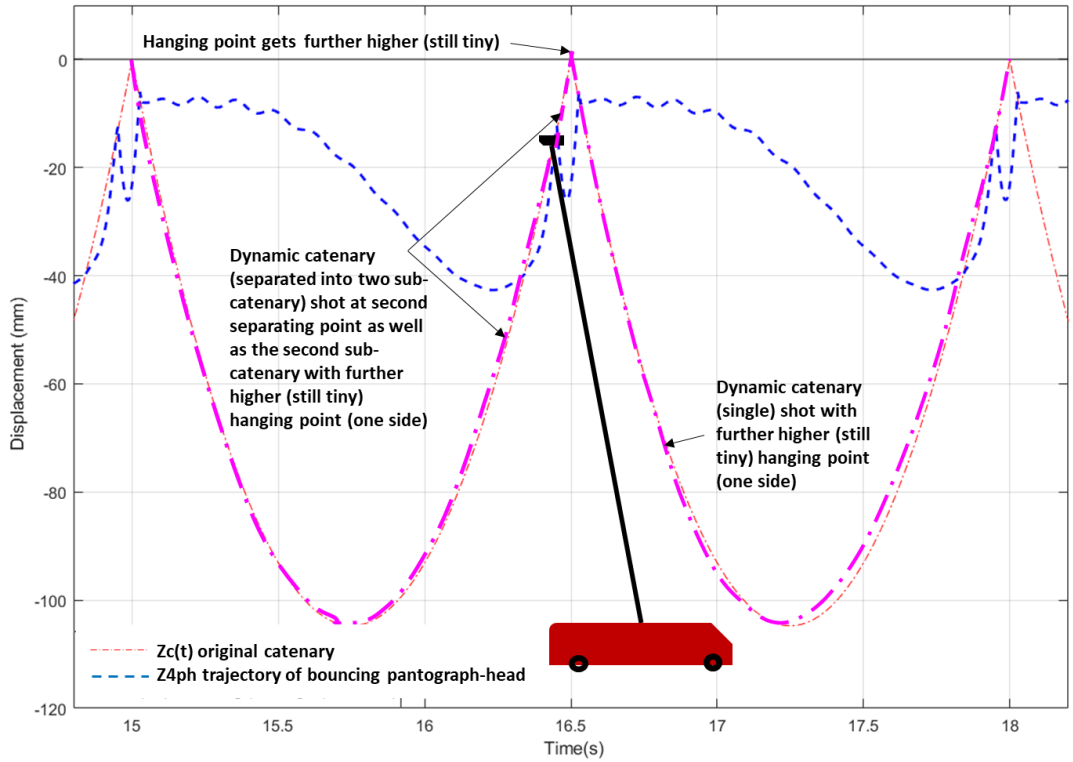

Figure 4.3.8-*shot of dynamic catenary with Trolleybus' hybrid model at second separating point*

Figure 4.3.8 shows the next phase of the bouncing motion as the pantograph 'skips' along a very stiff section of the wire close to the hanging point.

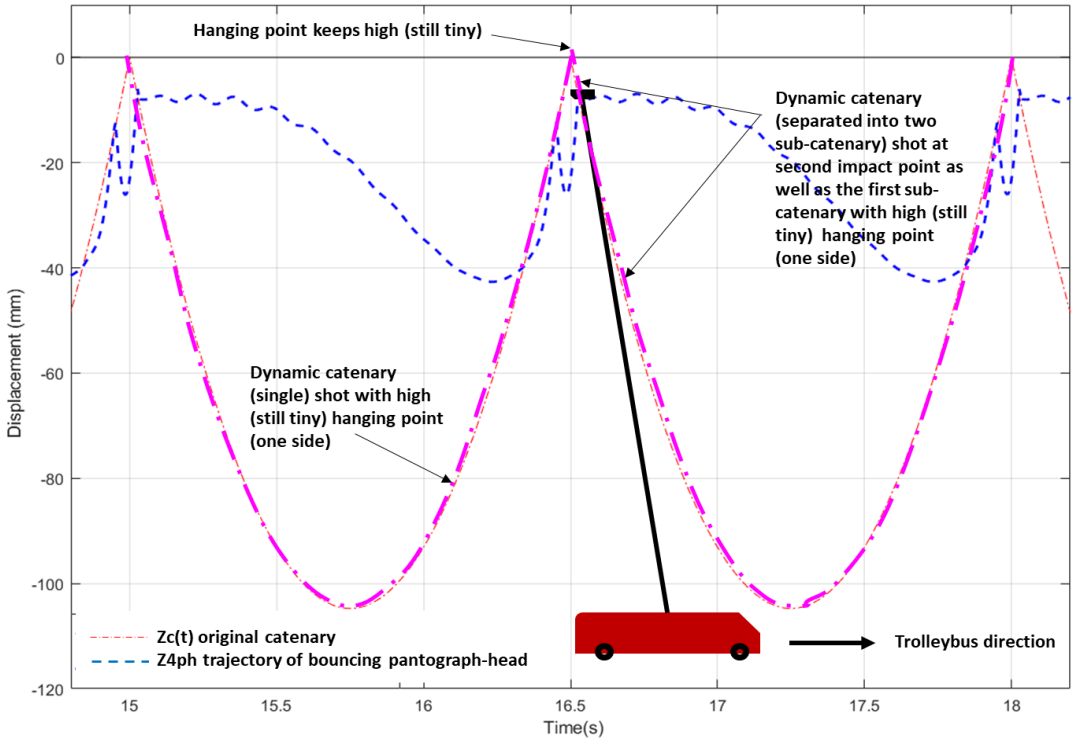

Figure 4.3.9-*shot of dynamic catenary with Trolleybus' hybrid model at second impact point*

Figure 4.3.9 show the pantograph has now traversed the hanger and is coming into first contact with the next section of wire. The wire is very stiff here, so a new smaller bouncing mode is established. This is much smaller due to the geometry of the wire prevent much displacement before re-attachment.

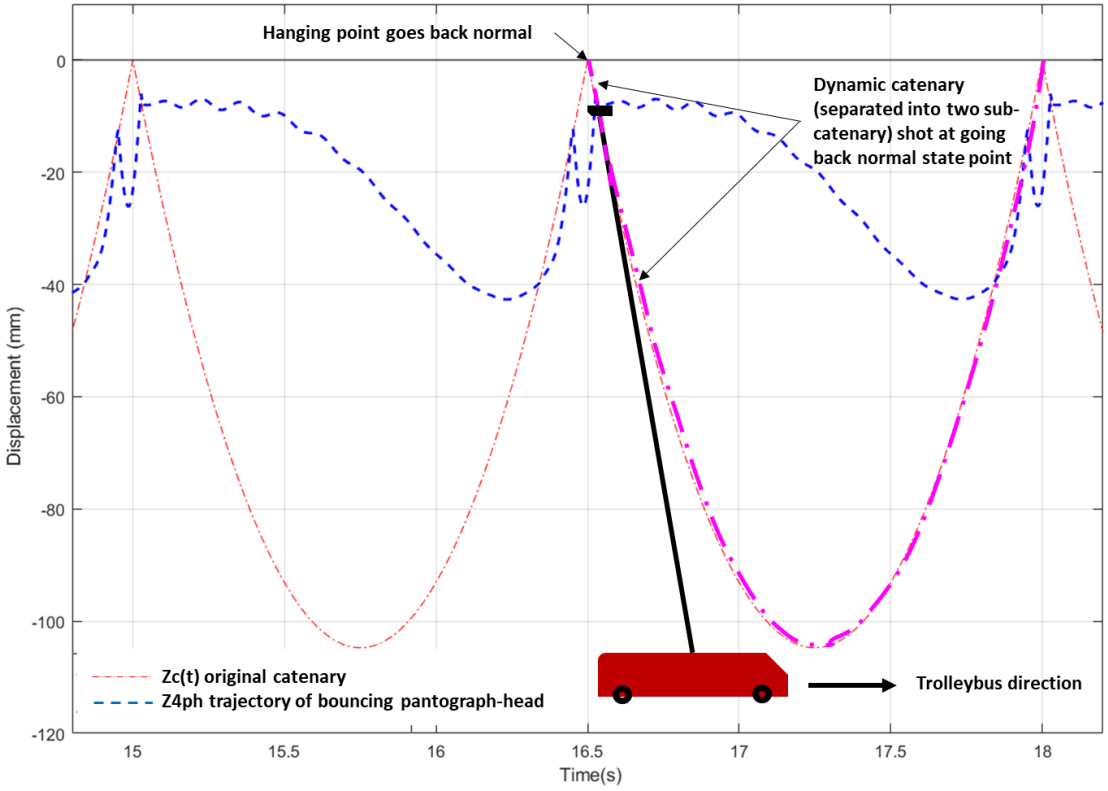

Figure 4.3.10-*shot of dynamic catenary with Trolleybus' hybrid model at going back normal state point (then same to Figure4.3.4 just at different position)*

Figure 4.3.10 shows the pantograph fully re-attached as the balance of stiffness in the pantograph and the wire is restored to the pre-bouncing state.

4.3.4 Summary

A hybrid model has been created that successfully explains the catenary-pantograph dynamics of a trolleybus in all operational aspects. This model consists of two phases of operation: normal (tight contact sliding) and bouncing contact.

As bouncing contact within the catenary-pantograph system can lead to electric arcing or even de-wirement of the trolleybus, the hybrid model should be a useful tool to analysis the risk of arcing and de-wirement under different running and environmental conditions. It could also potentially be used in railway (even high speed) and tram system to investigate

electric arcing phenomena (but not de-wirement as trains and tram use a different definition for de-wirement)

It should be noted that zero contact force would be a necessary and sufficient condition for identifying the potential positions of electric arcing in the catenary-pantograph system of the trolleybuses (as well as trains and trams). Zero contact force is also the necessary condition for identifying the risk of de-wirement of the trolleybus.

The possible extra vertical tremble of catenary phenomenon would be an interesting point for catenary-pantograph system particularly in high speed railway system as it would be beneficial to explore how the potential dynamic stiffness of the catenary and contact force changes with propagation to influence the power supply [130].

In order to further explaining the profile of dynamic catenary (vertical displacement) relation with trajectory of catenary-wire (highest vertical displacement) the further figures of shots are created with trolleybus' hybrid model in both normal and bouncing (at key critical points) states.

4.4 Application of hybrid non-linear catenary-pantograph model in risk analysis of trolleybus' arcing and de-wirement

4.4.1 Introduction

Arcing and de-wirement of trolleybus pantographs is very common during normal everyday operation around world. Figure 4.4.1 provides two photographs showing the moment of a trolleybus arcing event and a de-wirement instance.

Electrical arcing can lead to serious damage at the wire and the collector of the pantograph [111]. De-wirement, in particular on trolleybuses can potentially cause wires to be brought down, with subsequent danger to the residential areas in which they operate [112]. In this section, a study is presented that provides definitions of the conditions necessary for electric arcing and de-wirement of trolleybus to occur and a risk analysis that ranks the most significant factors likely to cause these two problems.

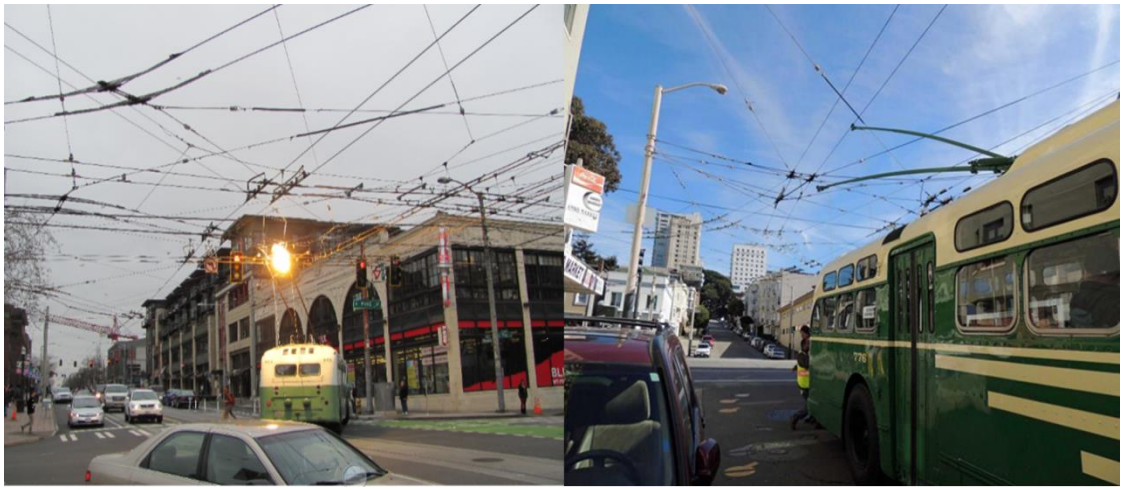

Figure 4.4.1-*Trolleybuses in arcing (left)* [131] ***and de-wirement (right)*** [132]

4.4.2 Arcing and de-wirement definition and models

The arcing principle and phenomenon of trolleybus are the same as for trams and trains, only using different voltages (heavy railway normally uses AC 25kV comparing with DC 600 or 750V. of trolleybuses). However, the de-wirement modes are different, even in the way they are defined.

Fundamentally, arcing is an electric current, often strong, brief, and luminous that jumps across a gap between the electrodes and earth or another electrode. It is usually caused either by a discharge of static electricity [133] or the opening or closing of current carrying contacts. From Paschen's Law, arcing across contacts can occur during the process of opening or closing at voltages above 340 V with a corresponding gap size 7μm in ambient air [165]. As trolleybus power suppler voltages are DC 600 or 750V, electric arcing could occur during catenary-pantograph bouncing. It is possible that when catenary wire and pantograph-head lose contact, as a result of bouncing, with a proper gap greater than 7μm then an electrical spark will be generated by the discharge of supplying electricity. From transition to Paschen's Law for microscale gas breakdown, a modified Paschen Curve for air at atmospheric pressure as long as the voltage is higher than 340V [134]. With original and modified curves, the possible gap between pantograph and catenary with breakdown voltage of various trolleybuses are shown in Figure 4.7.2 [134, 135].

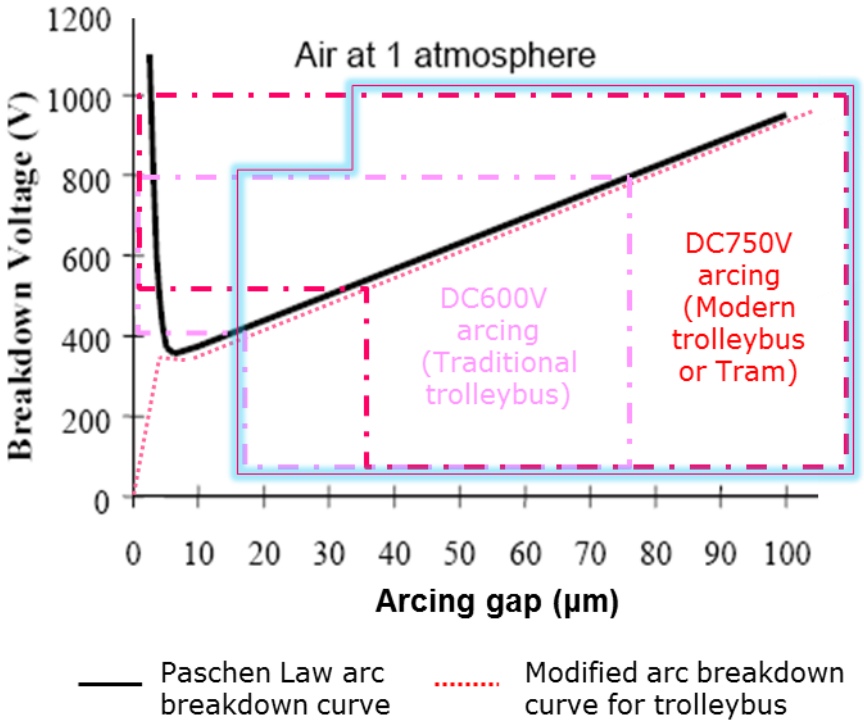

Figure 4.4.2-*Arc breakdown voltage and gap between trolleybus' pantograph-head and catenary*

From Figure4.4.2, in general the trolleybus system operation with DC400-1000V [37, p7], the arcing occurs from separation gap at 35μm (0.035mm) between pantograph and catenary during the operation while apparently the contact force is already at zero.

In respect of de-wirement, it can be assumed that if the gap between the pantograph-head and catenary wire is bigger than trench depth of pantograph-head then even a small external lateral force is likely to result in de-wirement. The gap dimensions between pantograph-head and catenary wire are shown in Figure 4.4.3 [37, p30].

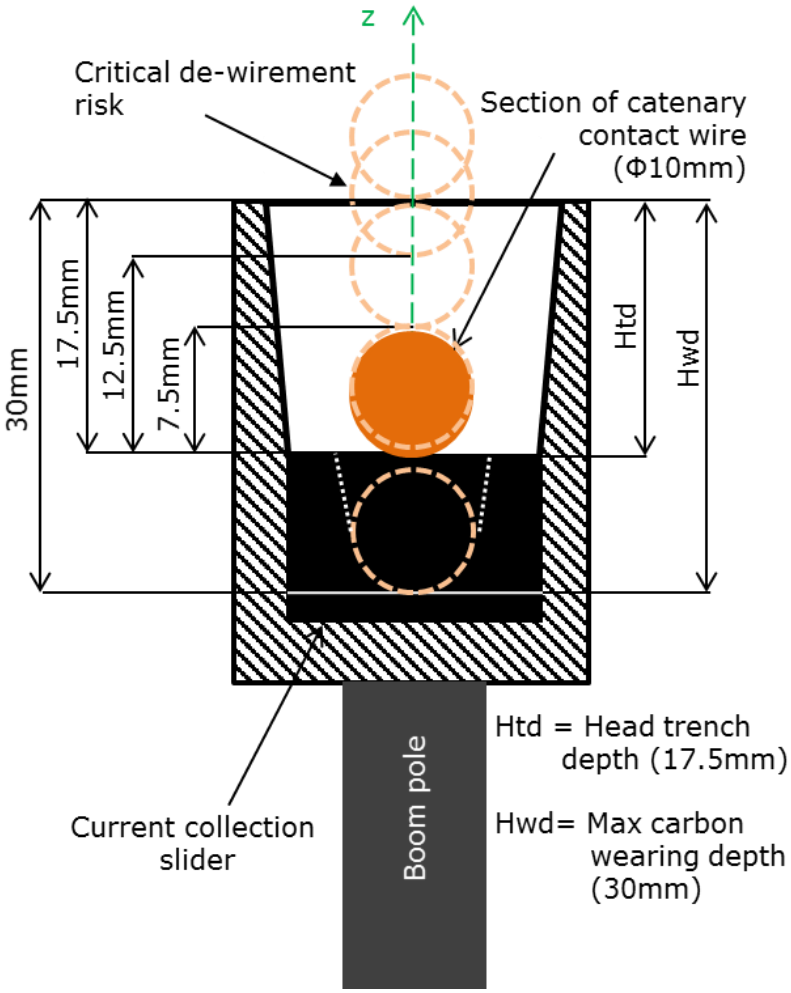

Figure 4.4.3-*Cross-section of pantograph-head and gaps between the catenary wire*

As external lateral force is not a consideration in this study, the gap dimensions between the base of the pantograph-head and catenary wire (in cross-section) were simply used to define the risk of de-wirement. Looking at Figure 4.4.3, it was defined that a critical de-wirement risk exists when half the diameter (5mm) of the catenary wire is above the pantograph-head (12.5mm). An extreme risk of de-wirement was defined as existing if the gap between the pantograph-head and catenary wire is bigger than the trench depth of the pantograph-head (17.5mm); even if the carbon slider is worn to the standard specific limitation [37, p30].

The relation of gap dimension and status ranks is shown in Table 4.4.1

Table 4.4.1 Arcing and de-wirement risk relates to gap dimension and status ranks

Status ranks / Gap Dimension (mm)	Contact force	Electrical arcing	De-wirement
Non-gap	sufficient contact	no	no
From 0 to35μm (0.035mm) during the bouncing	≈0	Arcing when over the critical gap (e.g.7μm)	no
0.035 - 7.5	0	no	no
7.5 - 12.5	0	no	possible risk
12.5 - 17.5	0	no	critical risk
17.5 - 30	0	no	extreme risk

From Table 4.4.1, it can be seen that arcing will occur if the gap between catenary and pantograph-head is near 35μm (0.035mm); assuming a voltage approximately 340 V in ambient air [165]. From hybrid bouncing model simulation results shown in Figure 4.3.3 the arcing between catenary and pantograph-head will occur at any point when contact force is zero. Figure 4.4.4 provides an overlay between these arcing possibilities and the contact force/displacement results produced using the hybrid bouncing model. There is no arcing whilst the pantograph and catenary are in sufficient contact.

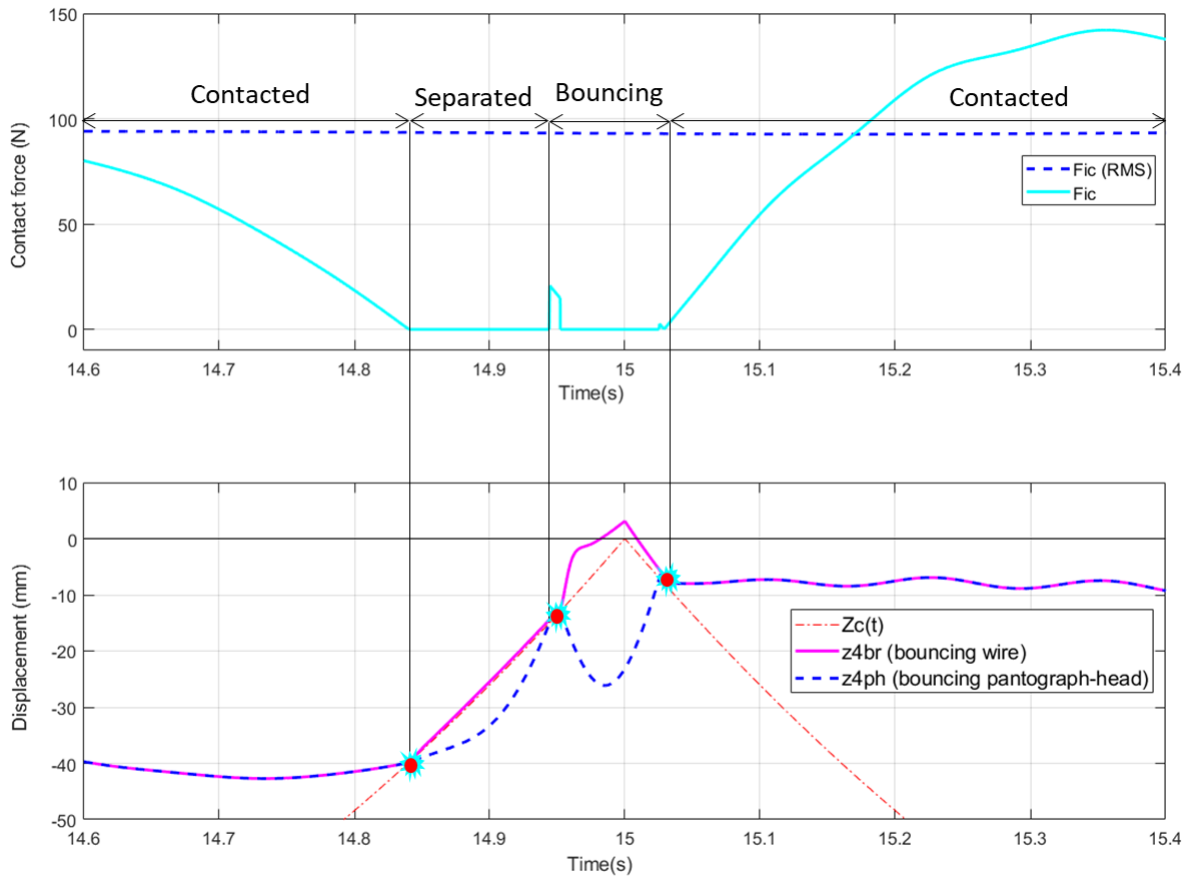

Figure 4.4.4-*Highest possible locations of electrical arcing happens at separating or approaching over critical gap (e.g.35μm) each bouncing hitting point)*

4.4.3 Complex catenary definition and models

The result from both the hybrid non-linear model (presented in Section 4.3) and normal model (presented in chapter 3), show that zero contact force and separation between catenary and pantograph always occurs at segments with high stiffness of catenary. This is normally at fixed point poles, crossroads and sharp bends. These sections increase the risk of electrical arcing and de-wirement.

The highest possibility of arcing and de-wirement are at wire crossroads and switches; where the contact wire webs become more complicated. The webs are braided with rigid catenary and suspension hardware including switches, crossing parts, wire holders, suspension oval tubes and flats etc. as shown in Figure 4.4.6. To reduce the risk of arcing and de-wirement, a modified catenary model (with rigid hardware) could be created and used for analysis of the risk of arcing and de-wirement at such locations.

Figure 4.4.5 and Figure 4.4.6. show the three kind of main elements, pure catenary, crossing and switches.

Figure 4.4.5-*Three main elements of pure catenary (left)* [137]***, crossing (upper right)*** [138] ***and switch (lower right)*** [139] ***form trolleybus' catenary system***

Figure 4.4.6-*Complex catenary at crossroad* [140]

For practically modelling the complex catenary, the crossing or switch could be simplified as rigid hardware of different length as shown in Figure 4.4.7. From the products of

Kummler+Matter Ltd, the actual lengths of the rigid hardware elements are seen to range between 1.2-3.3m [141].

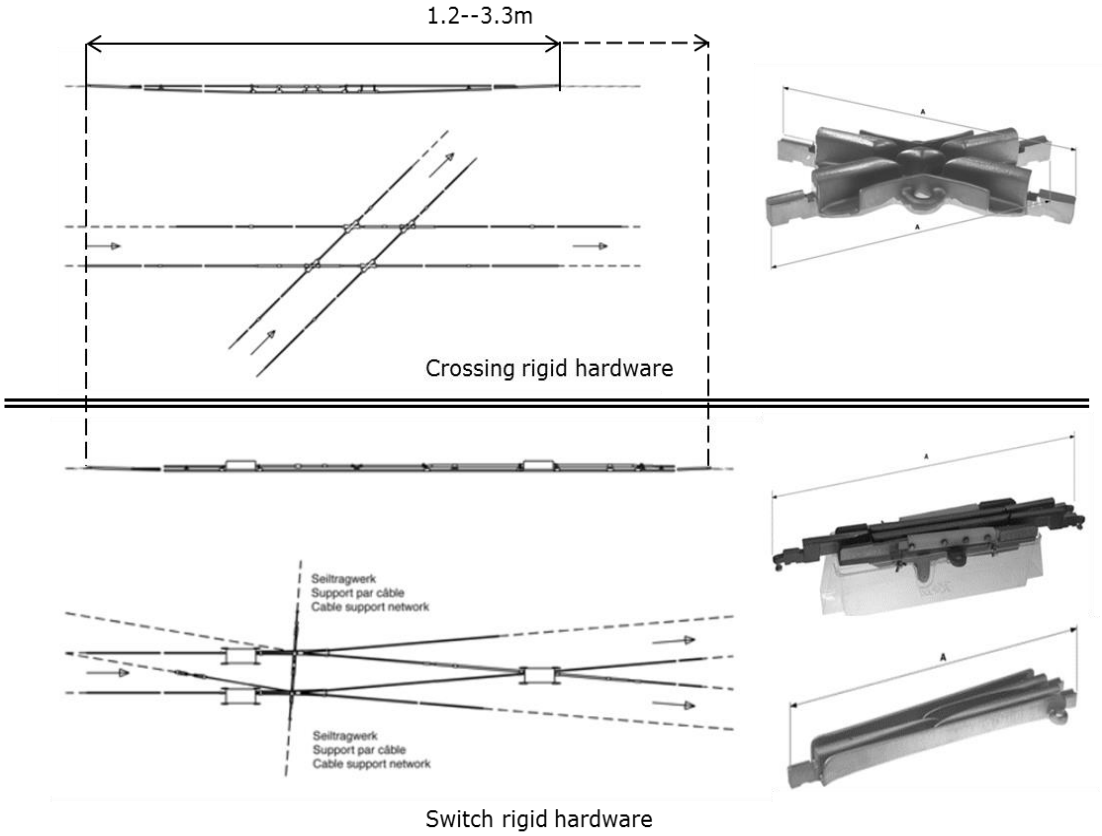

Figure 4.4.7-*Trolleybus crossing (upper) and switch (lower) hardware* [141]

For representing different complication levels of complex catenary at crossroad the various assumed length of the rigid hardware element and combination are given in Table 4.4.2

Table 4.4.2 Assumed rigid hardware equivalent length of complex catenary (including crossovers and switches at crossroads

RHNL (m)	0	1.5	6.5	10	12.5	15 or longer
CCCL	no hardware	single hardware	small comb.	medium comb.	big comb.	very complicated hardware

Where: RHNL: Rigid hardware equivalent length

CCCL: Complex catenary complication level at crossroad

comb.: combination

In practice, the complex catenary model is formed by joining standard catenary models on both sides with a rigid hardware element (or combination) in the middle. Compared to original catenary model the maximum stiffness (k_{max}) remains the same, but the minimum stiffness (k_{min}) depends on the location of connection point of catenary and rigid hardware. Figure 4.4.8 shows the equivalent stiffness curve of the complex catenary model (with example of 10m equivalent length rigid hardware) in relation to the original catenary.

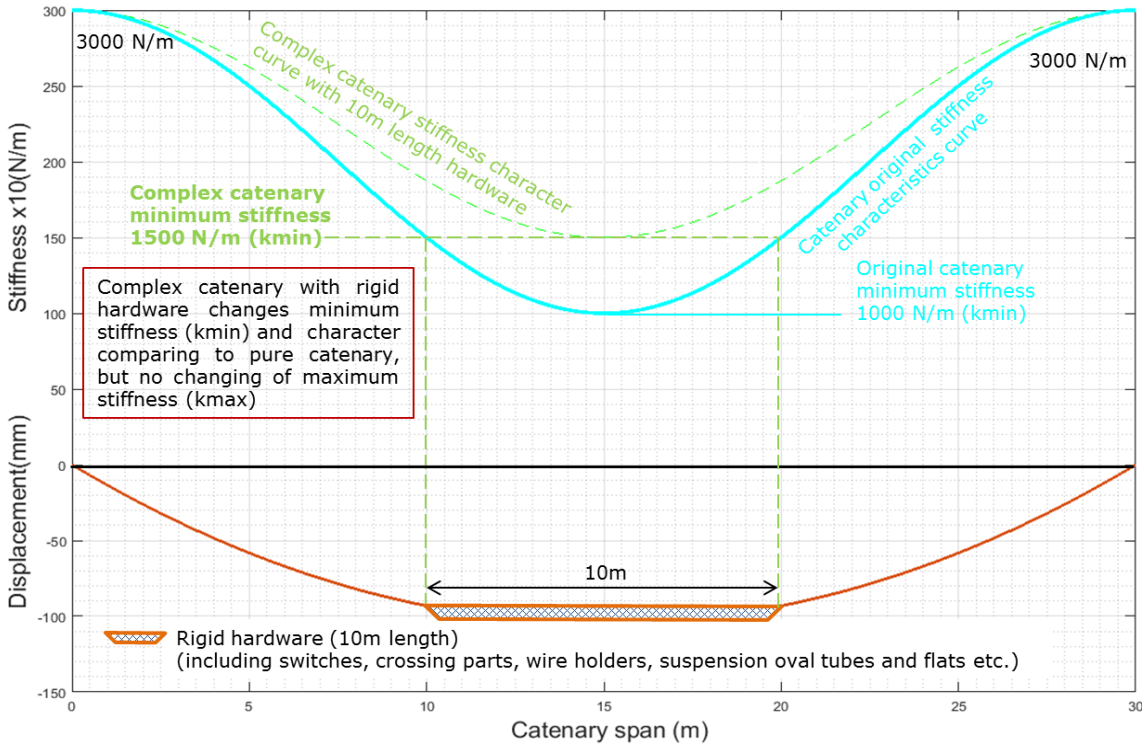

Figure 4.4.8-*Complex catenary model with equivalent stiffness curve of 10m length (for example) rigid hardware*

Table 4.4.2 shows the relevant stiffness values assumed for the various applicable nominal lengths of rigid hardware element and combination.

Table 4.4.3 Rigid hardware equivalent length with relevant stiffness

Rigid hardware length (m) / Equivalent stiffness (N/m)	0	1.5	6.5	10	12.5	15
k_{max}	3000	3000	3000	3000	3000	3000
k_{min}	1000	1050	1250	1500	1750	2000

Figure 4.4.9 shows the various complex catenary models and equivalent stiffness curves with the relevant equivalent length rigid hardware from Table 4.4.3.

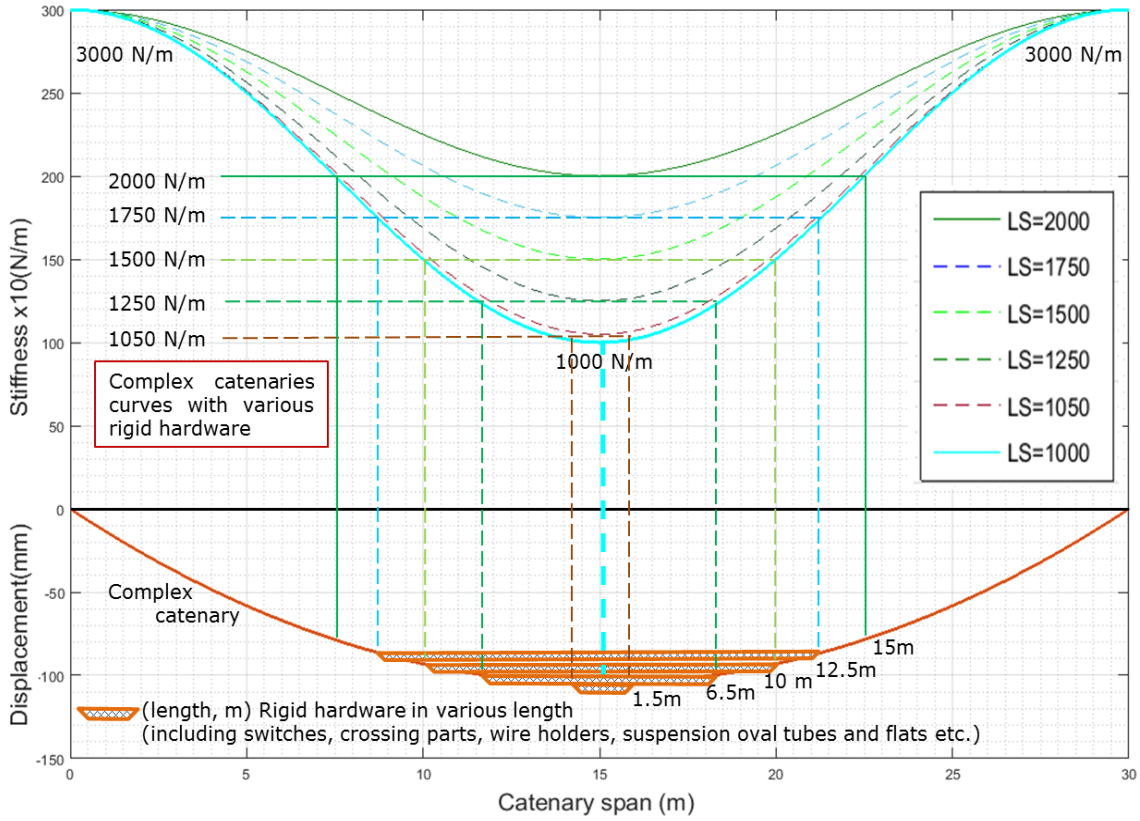

Figure 4.4.9-*Complex catenary models with equivalent stiffness curves of various length rigid hardware. LS: Lowest Stiffness*

For modelling purposes the stiffness equations of E3.2.2 in Section 3.2.1 of Chapter 3 could be used for the complex catenaries with various minimum stiffness (k_{min}) shown in Table 4.4.3.

4.4.4 Risk analysis of trolleybus' arcing and de-wirement with complex catenary model

In reality, a trolleybus is always running with a complex catenary system, therefore using hybrid non-linear catenary-pantograph with complex catenary models to analysis the risk of arcing and de-wirement is a more precise and applicable.

From Sections 4.4.2 and 4.4.3, the risk of arcing and de-wirement was defined to be directly related to the gap dimension between catenary and pantograph (the voltage is constant so can be ignored) which links to the operational speed of the trolleybus and the dynamic stiffness of

complex catenary. The stiffness of the pantograph spring is constant so can also be ignored. Therefore, building a 3D Chart of the gap (between complex catenary and pantograph) in relation to hardware length (complex catenary) and trolleybus operation speeds should make it easier to assess the risk level of arcing and de-wirement.

In section 4.3 it was shown that when the velocity of the trolleybus reached 20m/s the bouncing phenomenon of catenary-pantograph occurred; resulting in an increased risk of arcing or de-wirement. Meanwhile, the results presented in Chapter 3 indicated that the catenary and pantograph would always be in sufficient contact to avoid this risk at speeds of less than 14m/s. Thus, to investigate, the risk of arcing and de-wirement in a complex catenary environment it was only considered necessary to simulate at trolleybus velocities between 14m/s to 22m/s; as shown in Table 4.4.4.

Table 4.4.4 Selected trolleybus vehicle velocities for simulation (Complex catenary model)

v (m/s)	14	15	16	17	18	19	20	21	22

The two sets of equations representing the normal and bouncing phases (section 2 in Chapter 3 and section 2 in Chapter 4) as well as the Simulink configuration of the catenary-pantograph shown in Figure 4.3.1 were combined to create the complex catenary Simulink simulation. As part of this simulation, measurements were of the biggest gap between pantograph-head and complex catenary. The tests were undertaken with various minimum equivalent stiffness of rigid hardware of complex catenary (fixed k_{max} and various k_{min}) and different trolleybus velocities shown in Tables 4.4.3 and 4.4.4. The 3D Chart (graphical representation) of these measurements are presented in Figure 4.4.10.

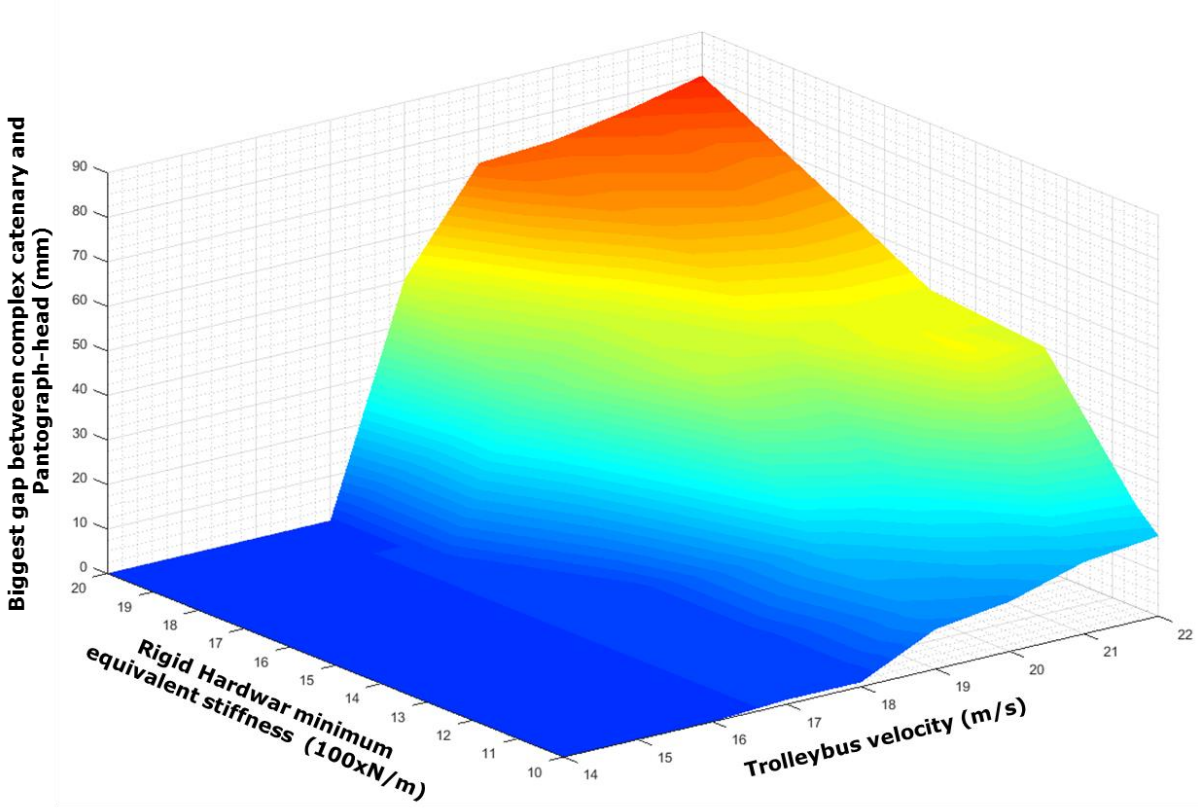

Figure 4.4.10-*Biggest gap between complex catenary (or catenary) and pantograph-head related to rigid hardware minimum equivalent stiffness and trolleybus velocity*

Figure 4.4.10 shows the trend that the gap between the complex catenary (or catenary) and pantograph increases with higher rigid hardware minimum equivalent stiffness (longer rigid hardware) and trolleybus velocity. In order to quantify the risk of arcing or de-wirement, a 2D contour map has been built up using these gap dimension results presented in Figure 4.4.10. The 2D colour contour map shown in Figure 4.4.11 clearly shows the bounds of different risk ranks of arcing and de-wirement.

There are some points to be observed:
The catenary and pantograph are in sufficient contact with no arcing and de-wirement as long as trolleybus running speed is less than 17m/s (61km/h)

Arcing is normally generated at trolleybus velocities between 17 and 19m/s. As well as being longer lasting in lower stiffness of catenary

Large complex catenaries have a higher risk of de-wirement, particular when the rigid hardware is near or longer than 15m (as is quite common at big crossroads in city centres).

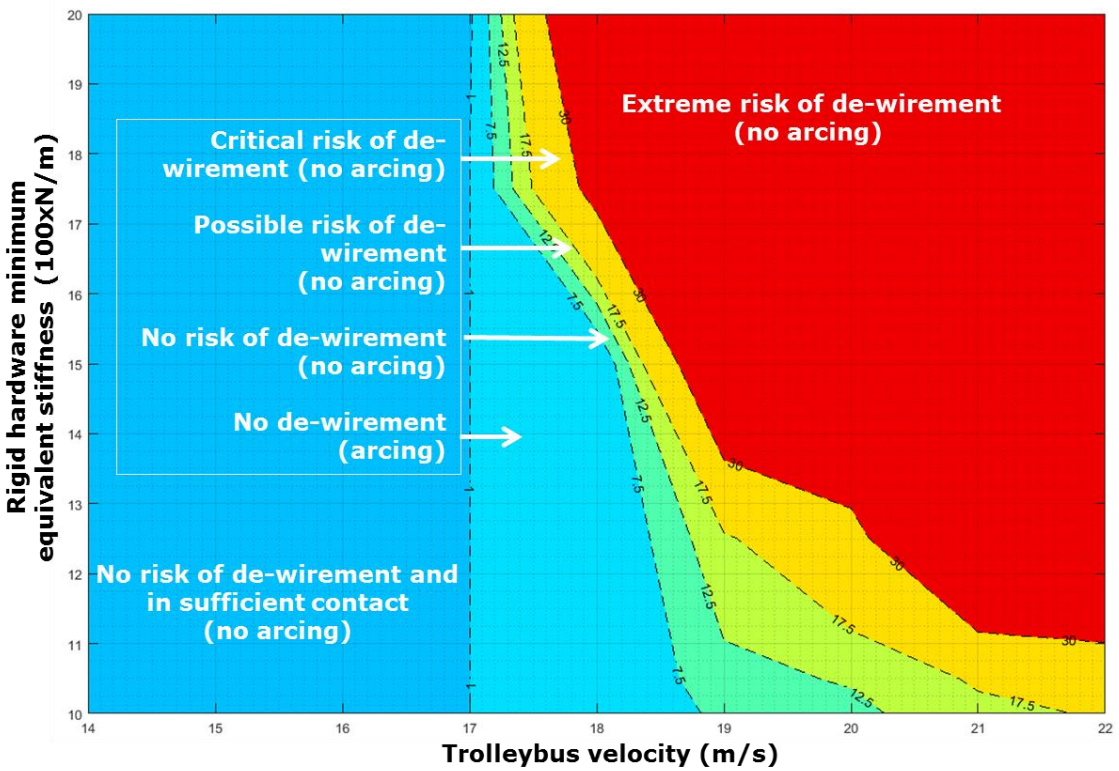

Figure 4.4.11-*Colour contour map of de-wirment risk ranks*

In general, the hybrid non-linear and complex catenary (e.g. crossroad) models could be applied to simulate and analyse the arcing and de-wirement of trolleybuses

Arcing starts from the point of first separation and lasts until bouncing has finished between the pantograph and catenary

De-wirement can occur when the largest gap occurring between the pantograph and catenary is greater than the trench of collection head (normally at first separation point). The highest possibility of de-wirement is when trolleybus pantograph collection head goes through the long rigid hardware switches (normally at big crossroads in the cities)

The method and application presented in this Chapter would be useful for analysing arcing of tram and train catenary-pantograph systems but would not be suitable for analysing de-wirement of the trains' and trams' catenary-pantograph system as their de-wirement definition is different to that of a trolleybus system.

In practice, trolleybus catenary components manufacturers and operators have a different suggestion in their handbook in respect of the recommended operational speed for trolleybus' going through suspension rigid hardware such as switch (e.g. 50-60km/h [142, 143] from

manufacturer; 15-20km/h [142] from operator). The results presented in this chapter indicate that the recommendations of the operators are better suited for preventing the risk of arcing or de-wirement

4.5 Chapter Summary

4.5.1 General

The key point found in Chapter 3 and highlighted in Section 4.1.was the appearance of the zero-contact force zone (non-contact) shown in Figure 4.1.1 and Figure 4.1.2. The issue occurs when the trolleybus experiences specific condition, such as spring stiffness and running speed (e.g. 20m/s). To understand this phenomenon better a novel hybrid non-linear bouncing model trolleybus of catenary-pantograph has been introduced in this chapter.

The starting point was to generate and observe the bouncing motion of the catenary and pantograph system after hitting subsequent catenary spans in the modelling and simulations. The trolleybus hybrid model was formed from two parts consisting of normal and bouncing models. A fundamental assumption for the flexible (changeable stiffness) catenary and elastic pantograph was that the half-period of natural oscillation of the flexible catenary and the impact duration between the catenary and pantograph are equivalent to a bouncing ball with reflexed lingering time and exaggerated [113].

Meanwhile, the further explaining the profile of dynamic catenary (vertical displacement) relation with trajectory of catenary-wire (highest vertical displacement) the further figures of shots are also created with trolleybus' hybrid model in both normal and bouncing (at key critical points) states.

One application of the trolleybus hybrid model was to perform a risk analysis for trolleybus arcing and de-wirement was carried out. Definitions of arcing and de-wirement were established and a sub-model of a "Complex catenary", employing simplified equivalent stiffness values informed by real-world catenary webs and trolleybus operation, were created for simulation and analysis. From the simulation and measurement results, a 2D colour contour map was created that can be used for risk analysis and identification of both arcing and de-wirement in trolleybus systems.

In general, the novel new hybrid model created in this chapter represents the biggest output from the study. It can be used to systematically explain the phenomenon of arcing and de-wirement of trolleybus systems during operation and give more precise dynamic analysis results. The Complex catenary sub-model could also be an effective method to simplify the complicated catenary and network dynamics of trolleybus in for academic and engineering. Meanwhile, hybrid and complex catenary models could be used in catenary-pantograph system of railway system (including train and tram).

4.5.2 Limitations of the hybrid models and possible solutions

As the hybrid model built has only taken vertical dynamics into account and does not include lateral dynamics or propagation, the models' capability for simulating and analysing of trolleybus' catenary-pantograph system in three dimensions is limited. Lateral dynamic models, that can accommodate behaviour such as trolleybus changing lanes and turning at the bends, could be integrated into the models presented in this study as an attachment to the hybrid model.

The arcing risk analysis only takes the electric potential field into account rather than including particles flying off from the materials (carbon slider and cooper wires) by excited electrical thermal energy and longer lasting arcs, as well as operational environment factors such as weather temperature and air humidity which influence the arcing intensity and duration. The Future work could also take into account the power current intensity and effective contact area as well as weather factors to build a new specific comprehensive model for arcing risk analysis.

The models and methods presented in this chapter could not be used to simulate and take risk analysis of de-wirement in railway catenary-pantograph system due to the definition of de-wirement being is different to trolleybus.

Chapter 5

Trolleybus active catenary-pantograph

5.1 Introduction of active catenary-pantograph

The existing design of trolleybus pantograph (current collection) devices is conservative in nature and, due to the passive manner in which the pantograph locates on the overhead wires, there are several operational issues, such as: electrical arcing (damaging the wire and the collector due to variable uplift force); a high probability of de-wiring at junctions (potentially causing wires to be brought down with subsequent danger to human life); the associated difficulty of manual rewiring; inflexible operation; and unsightly overhead webs at road junctions.

Active control pantograph systems are a concept that has been developed for full scale railway with various implementations such as light rail vehicle's pantographs and high-speed railway systems [40, 51]. Although, railway and trolleybus systems differ in their running dynamics, their fundamental similarity suggests that introducing active control algorithms and control design into trolleybus should help address the existing operational issues and facilitate the future uptake of this ‘clean’ technology.

The hybrid model and Complex catenary sub-model developed and analysed in Chapters 3 & 4 can systematically and effectively explain the phenomenon of arcing and de-wirement of conventional trolleybus catenary-pantograph systems under standard operation and when going through crossroads. In this chapter, an advanced ‘Active Control of Trolleybus Current Collection System’ (ACTCCS) concept is explored that it includes uplift control force.

5.2 Basic modelling of active catenary-pantograph

The catenary-pantograph interaction is of key importance to trolleybus and electric railway vehicles. This dynamic interaction is a coupled vibration governed by the contact force which depends both on the running speed and the catenary-pantograph system configuration. There is a hypothesis that catenary-pantograph system will have no contact loss and bouncing phenomenon under active control operation at any speed including highest of 20m/s. The modelling is to base on normal operation speed (14m/s) and the simulation results will compare with bouncing motion of the catenary-pantograph system.

5.2.1 Modelling of the dynamic equations

A schematic of a typical the trolleybus catenary-pantograph system is shown in Fig.5.2.1. As an assumption, the trolleybus catenary-pantograph system has a number of similarities to rail railway overhead current collection systems; with the main difference being the use of a single overhead line rather than an interaction of messenger and contact wires.

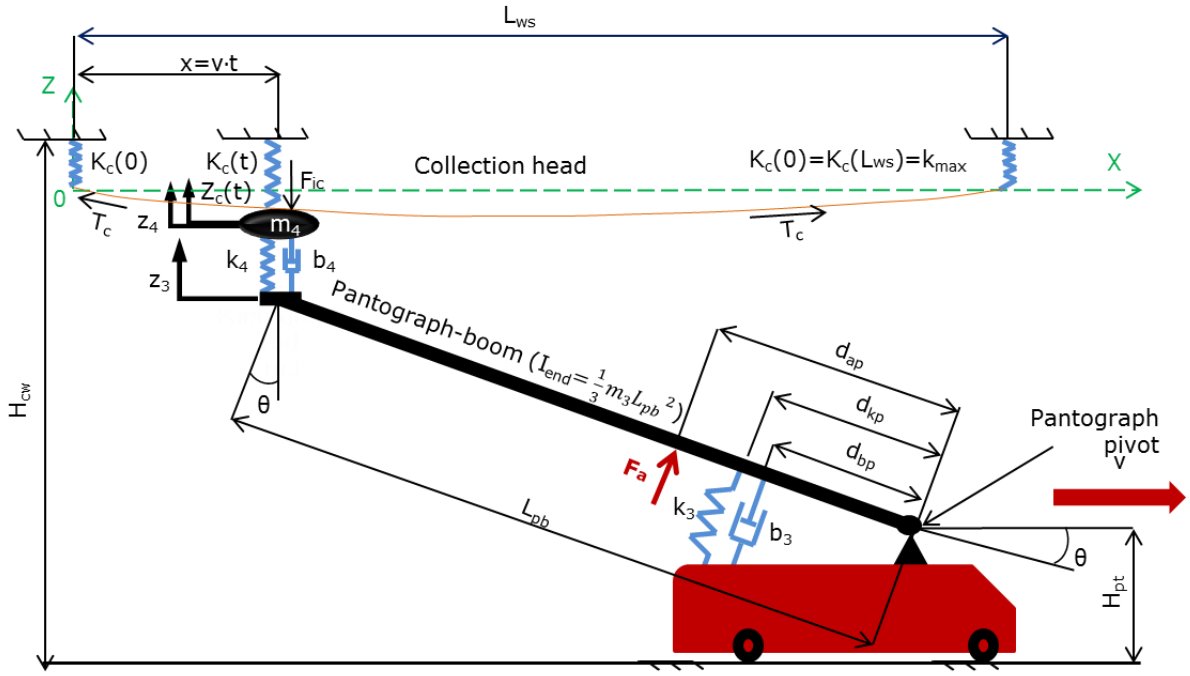

Figure 5.2.1-*Typical model of catenary-pantograph system with force control actuation*

Where:

$K_c(t)$: catenary contact wire nominal stiffness (N/m)

$K_c(0) = K_c(L_{ws}) = k_{max}$: catenary contact wire maximum stiffness (N/m)

k_{min}: catenary minimum stiffness (N/m) (not showing in Figure 3.2.1)

k_{mean}: catenary average stiffness (N/m)

L_{ws}: catenary contact wire span between two poles (m)

T_c: tensile force of catenary contact wire (N)

$Z_c(t)$: pre-catenary vertical displacement (m)

F_{ic}: integrated contact force between catenary and pantograph-head (N) [109]

H_{cw}: installation height of the catenary wire (normally from ground to fixed point on poles). It is determined the BSI British Standards in trolleybus (m) [37]

H_{pt}: pivot height of pantograph from ground (3.50 m)

z_3: pantograph boom vertical displacement (m)

m_3: pantograph-boom mass (kg)

b_3: pantograph-boom absorbers damping rate (Ns/m)

k_3: pantograph-boom spring nominal stiffness (N/m)

d_{bp}: distance from damper fitting point to pantograph pivot point (0.1 m)

d_{kp}: distance from spring fitting point to pantograph pivot point (0.1 m)

d_{ap}: distance from actuator fitting point to pantograph pivot point (0.5 m)

z_4: pantograph-head vertical displacement (trajectory) (m)

m_4: pantograph-head mass (kg)

b_4: collection head absorbers damping rate (Ns/m)

k_4: pantograph-head spring stiffness (N/m)

Fa: actuation force (N)

I_{end}: pantograph-boom moment of inertia to ($kg \cdot m^2$)

θ: pantograph-boom dynamic lifting angle (degrees)

L_{pb}: length of pantograph-boom (m)

g: gravitation acceleration ($9.8 m/s^2$)

ρ: catenary wire linear mass density (kg/m)

x: contact position distance from 0 of x-axis (x=v·t) (m)

v: trolleybus speed (m/s)

Following Newton's law and refer to E3.2.8 E3.2.10 and E3.2.13, the dynamic equation E5.2.1 can be created with E3.2.9 (shown in Chapter 3) that the F_{ic} associate with F_a

$$\boldsymbol{m_3\ddot{z}_3 = -b_{3eq} \cdot \dot{z}_3 \cdot con^2\theta - k_{3eq} \cdot z_3 \cdot cos^2\theta + 3b_4(\dot{z}_4 - \dot{z}_3) \cdot cos^2\theta + 3k_4(z_4 - z_3) \cdot cos^2\theta + 3F_a \cdot \frac{d_{ap}}{L_{pb}} \cdot \cos\theta} \quad \text{E5.2.1}$$

Integrating all the above derivations, the final model for the catenary-pantograph of an ACTCCS trolleybus system will be similar to the equations E3.2.13, E3.2.14, E3.2.17, E3.2.20, E3.2.21 and E3.2.22 (F_{ic}) shown in Chapter. 3

5.2.2 Control design and consideration

A concept diagram of an ACTCCS closed-loop control system is shown in Figure 5.2.2.

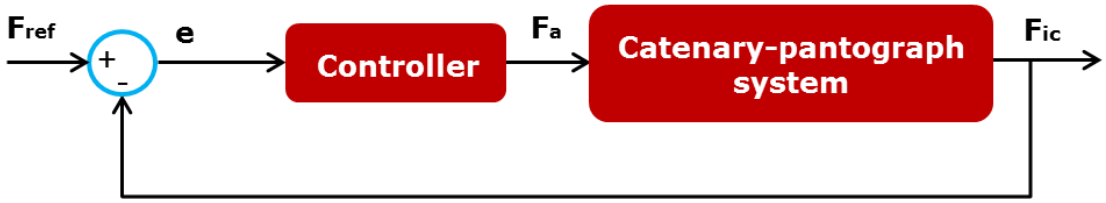

Figure 5.2.2-*Control concept diagram of catenary-pantograph system*

The catenary-pantograph system with force control actuation uses a controller that outputs an Actuation force (Fa) under control of an error signal (e) generated from the actual integrated contact force (Fic) and a reference force (F_{ref}). The actuation force is the input to the catenary-pantograph system which produces sum of contact force over time between the catenary wire and pantograph head. A representation of this Fic is then feedback to the controller to close the feedback loop. The controller is fed the size of the error and determines the amount of control action, "Fa" required to compensate the gap [72, p4] of F_{ref} - F_{ic}

There are three key points that need to be taken into consideration in the control design of such a system [72, p2]:

- Transient response: the system rise time, overshoot (less than 20%) and settling time.
- Steady state response: steady state tracking errors and/or disturbance induced steady state errors. These should be less than 5%.
- Stability: the closed loop must be stable depending on open loop should be with specified gain margins (GM > 6dB) and phase margins (PM > 60◦), [72, p9]. As the phase margin is the number of degrees between the actual phase shift and −180° at the time the loop gain reaches unity, a safety margin of about 45° is recommended [166].

5.3 Proportion (P), Phase advance (PA) and phase advance-integrator (PA-I) control design, simulation and results analysis of catenary-pantograph

5.3.1 Introduction

The well-known proportional-integral-derivative (PID) control system is one of the most widely used feedback control methods. Proportion (P), Phase advance (PA) and Phase Advance-Integrator (PA-I) control systems are three more practically applicable versions of

the basic PID systems that all use feedback control methods. In practice, PA-I can be thought of as being formed as a combination of PI and PA [72].

In this study of an ACTCCS system, the design of the actively controlled pantograph has been carried out to improve the dynamic behaviour of the catenary-pantograph for trolleybus operations.

The P control is simply proportional to the current error value. Using proportional control alone will usually result in an error between the set point and the actual process value, because it requires an error to generate the proportional response. If there is no error, there is no corrective response.

The PA controller can be thought a compensator and is a more practically applicable version of PID [144]. As well as having a lead term followed by a lag term at higher frequencies, phase lead can also be introduced at the required frequencies with no excess of high frequency gain compared to pure differential control schemes [72].

As a combination of PI and PA, PA-I controllers can improve stability and reduce the steady state error in practice.

5.3.2 ACTCCS Control basic design

Figure 5.2.2 shows the simple concept control system configuration of catenary-pantograph system (only vertical dynamic), in which the catenary wire is based on the pure contact wire without messenger cable. The actuation force ideally controls the pantograph boom only as shown in Figure 5.2.1. The three kinds of ACTCCS closed-loop control system are shown in Figure 5.3.1 for comparison.

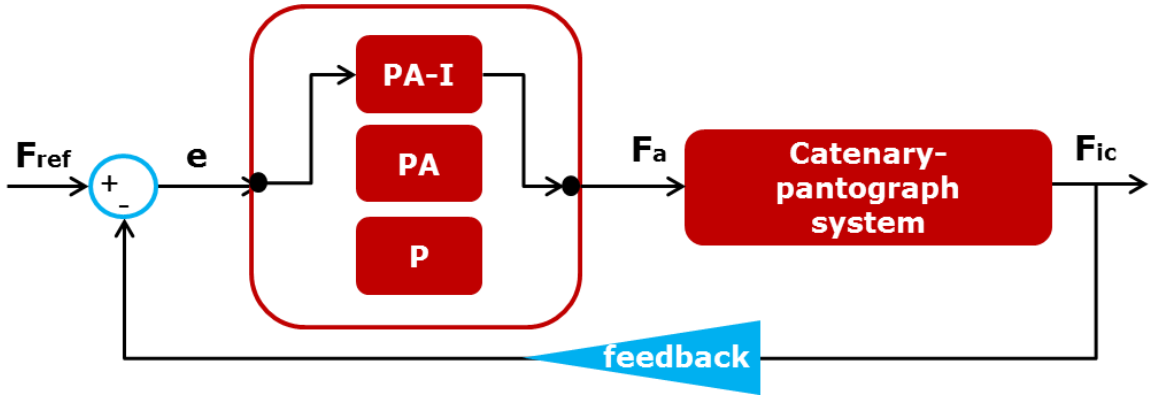

Figure 5.3.1-*Control (P or PA or PA-I) system configuration and comparison*

The basic P, PA and PA-I control equations are shown in E5.3.1, E5.3.2 and E5.3.3

$$\boldsymbol{K(s) = K_p} \quad [72, p6] \qquad \text{E5.3.1}$$

$$\boldsymbol{K_{pa}(s) = K_{pa} * \frac{1 + K_{ratio} * T_l s}{1 + T_l s}} \quad [72, p13] \qquad \text{E5.3.2}$$

$$\boldsymbol{K_{pai}(s) = K_{pai} * \frac{1 + K_{ratio} * T_l s}{1 + T_l s} * \frac{1 + T_i S}{T_i S}} \quad [72, p21] \qquad \text{E5.3.3}$$

Where:

K_p : P proportional gain

K_{pa} : PA proportional gain

K_{pai} : PA-I proportional gain

$K_{ratio:}$ phase advance ratio (Kratio > 1)

T_l: PA lag time constant

T_i: PA-I lag time constant

No specific standard of reference dynamic contact force of trolleybus is currently available, therefore the current railway relevant standard of F_{ref} =110N [145] has been used in this preliminary study. This is a user selected reference and can be varied if required but represents a compromise between wire wear and arcing potential. The simulations shown are carried out with full non-linear model developed in Section 4.3 but only at the highest operating velocity (20.0 m/s, 45mph); as this represent the largest variation in uplift force and displacement in the passive catenary-pantograph case.

5.3.3 Simulink configuration

Using dynamic equations E3.2.1, E3.2.2, E3.2.9, E3.2.11, E3.2.13, E3.2.14, E3.2.17, E3.2.20, E3.2.21, E3.2.14, E3.2.22, E4.2.1, E4.2.2, E4.2.4, E4.2.5, E4.2.9, E4.2.11, E4.2.12, E3.5.1, E3.5.2 and E5.33, a Simulink configuration of P, PA and PA-I control of the trolleybus catenary-pantograph system is shown in Figure 5.3.2. The upper frame represents the passive module, whilst the middle and lower red frame represent the control module respectively.

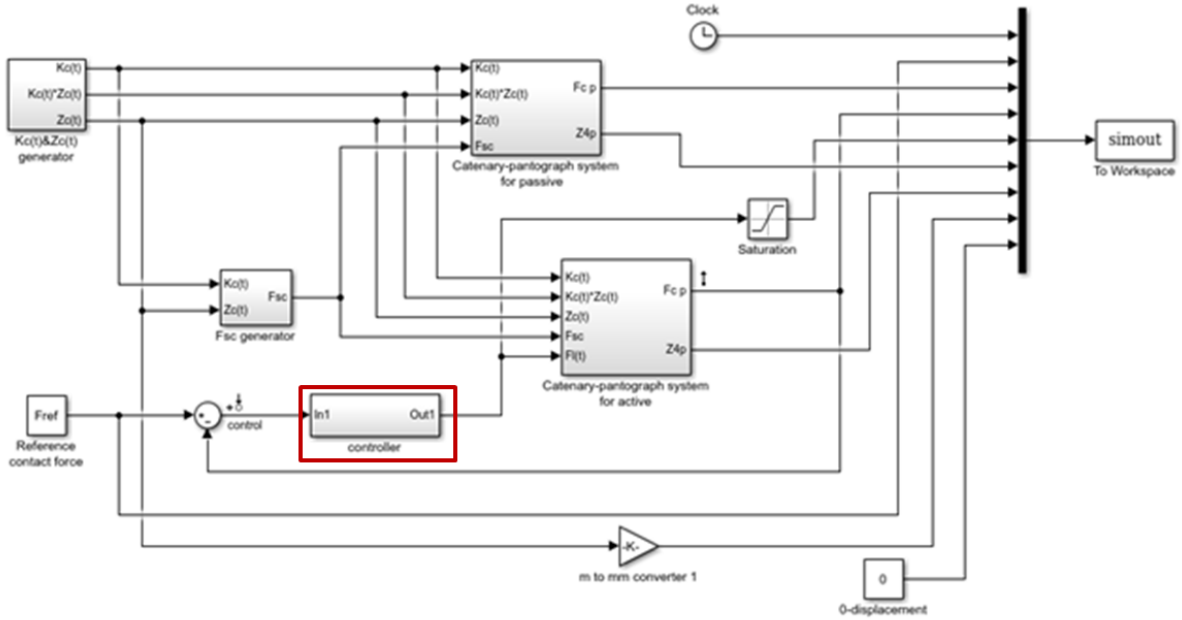

Figure 5.3.2-*Simulink Configuration of P, PA and PA-I control system with catenary-pantograph system*

The detail inside the P, PA and PA-I control module configuration block is shown in Figure 5.3.3.

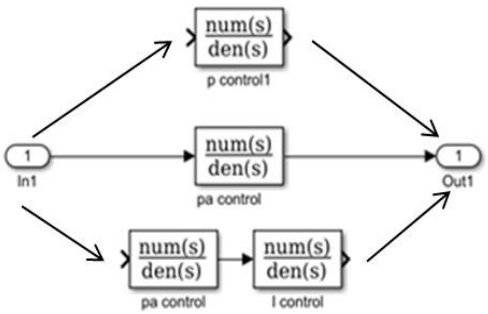

Figure 5.3.3-*Inside Simulink Configuration of control module*

5.3.4 Practical tool for design and analysis

To fulfil the requirements in both frequency response and time response, the following conditions were applied in Table 5.3.1:

Table 5.3.1 Requirements of frequency response and time response in control [72].

Required Condition / Response type	Gain margin (dB)	Phase margin (degrees)	Overshot (%)	Steady-state error (%)
Frequency	≥ 6	≥60°		
Time			≤ 20	≤ 5

The PA and PA-I will be carried practically in this chapter. The first stage in selecting the parameters deals with the catenary-pantograph system (uncondensed) as follows:

- After intimal tests, a phase advance ratio of K_{ratio}= 12 was selected as a compromise practical value - normal is between 4 and 8 [72, p16]
- The Max phase advance was then calculated as $sin^{-1}\frac{K_{ratio}-1}{K_{ratio}+1} \approx 56^{o}$; and Centre point gain as $20 * log_{10}\left(\sqrt{K_{ratio}}\right) \approx 10.4$ dB [72, p18].
- The Nichols diagram of the open-loop uncompensated catenary-pantograph system [146] shown in Figure 5.3.4 was used to identify a phase which can be shifted to -120^{o} (relating to PM of 60^{o}). The point with a phase would be $180^{\circ} - 60^{o}$ (PM) + 56^{o} (Max phase advance) = 176^{o} [72, p19]

From Figure 5.3.4, the closest point of pantograph-catenary system which indicates that there is a gain corresponding gain of 46 dB [72, p9] and frequency of 22.5 rad/s.

- Calculate the proportional gain from $K_{pa} = 10^{\frac{46-10.4}{20}} \approx 59.6$ ([72, p19]
- Calculate the lag time constant T_l using

$$T_l = \frac{1}{\sqrt{(K_{ratio})}(\omega_{lc})} = \frac{1}{\sqrt{(12)}(22.5)} \approx \frac{1}{3.5 * 22.5} \approx 0.0126$$

The three key selected parameters of the PA control system are therefore:

K_{pa}=59.6

K_{ratio}= 12

T_l =0.0126 s

Meanwhile, the from Figure 5.3.4, the PM and GM of P (as a reference), PA and PA-I control system are shown in Table 5.3.2.

Table 5.3.2 PM of P, PA and PA-I control system with catenary-pantograph system

Control system / Results	P	PA	PA-I
PM (degrees)	3.98	61.1	53.3
GM (dB)	3.53	16.3	29.8

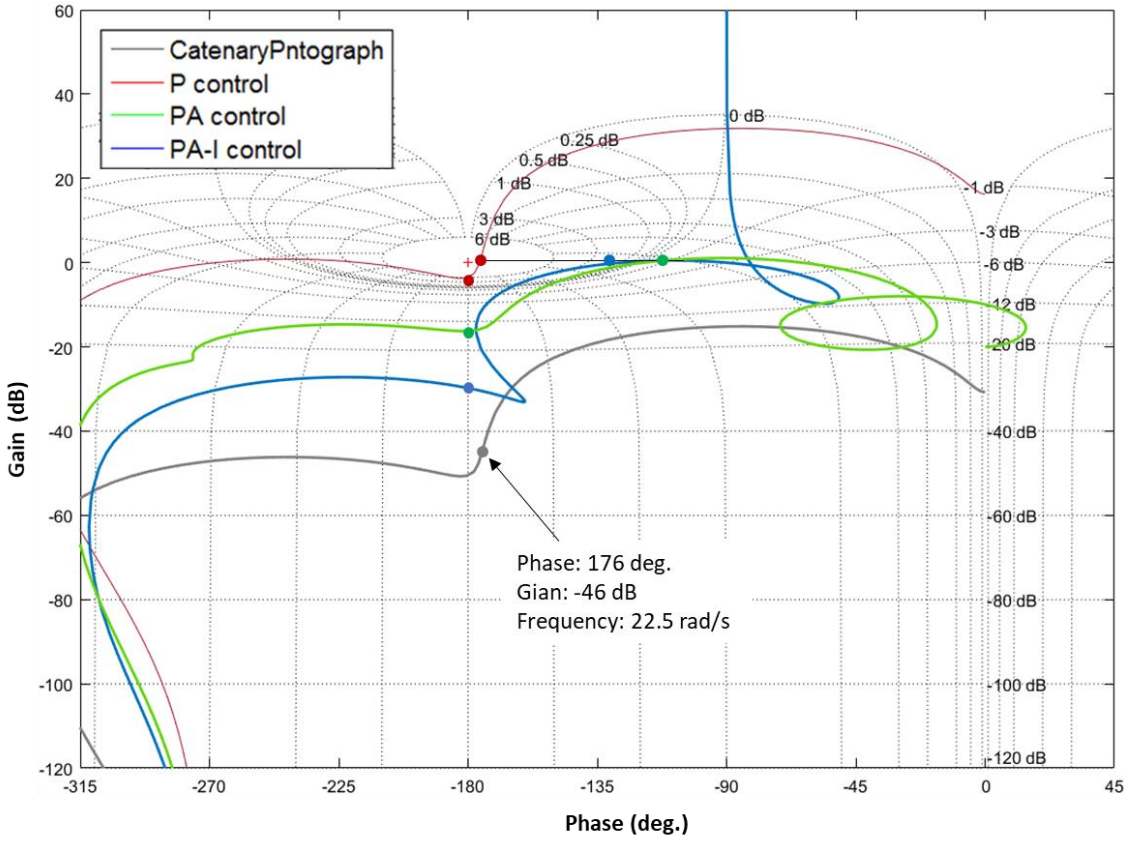

Figure 5.3.4-*Open-loop Nichols diagram of pantograph system and with various control system*

For catenary-pantograph system with P (as a reference), PA and PA-I control systems, closed-loop step diagrams and the steady-state errors are shown in Figure 5.3.5.

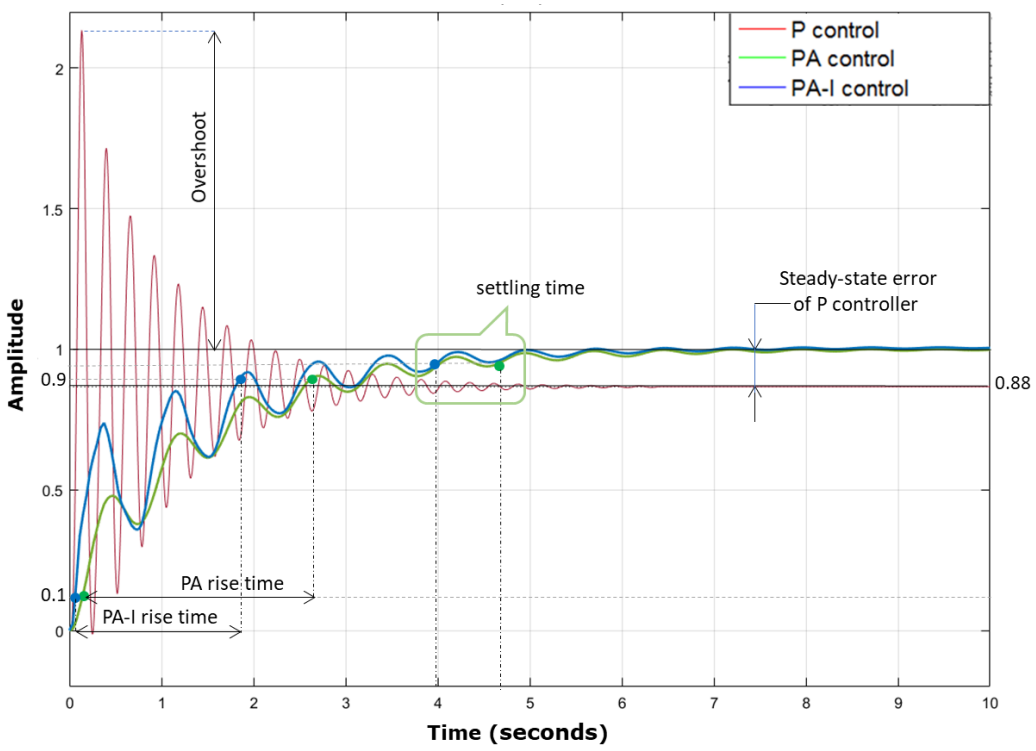

Figure 5.3.5-*Closed-loop step diagram of pantograph system with PA and PA-I control system*

From the step curves shown in Figure 5.3.5, the P control system (as a reference) has a big overshoot which dose obviously not meet the requirement of ≤ 20%. The steady-state error is 12% that is also not meeting the requirement of ≤ 5%. As well as from Table 5.3.2, the GM is 3.53 dB less than requirement of ≥6dB. Comparing the PA and PA-I system, the rise time, setting time and steady-state error control system are shown in Table 5.3.3.

Table 5.3.3 Rise time, setting time, overshoot and steady-state error of P, PA and PA-I control with catenary-pantograph system

Results / Control system	Rise time (s)	Settling time (s)	Overshot (%)	Steady-state error (%)
PA	3.11	4.67	0	Neglectable
PA-I	1.79	3.95	Neglectable	0

From Figure 5.3.5 and Table 5.3.3, both the PA and PA-I control systems both meet the requirements of overshoot and steady-state error, but PA-I has a better performance in rise time and settling time. In general, the PA-I control system is therefore the best control method in respect of requirement. Note. The rise and settling times of the PA-I control system is a bit higher than expectation as well as a quite a few dumping shown with a

harmonic which might be led by non-liner system and other complex factors. Comparing both harmonics of PA and PA-I shows the PA-I gradually falling behind the PA after around 2.5 seconds which it could be thought the cause of integrator adding phase lag into the system (slowing the response) [72, p6], despite it does not affect the response comparison in the thesis. It is not the very ideal control system design and the values are "general good practice" values rather than being specific trolleybus ACTCCS pantograph control design requirements [170]. Consequently, that the PM design requirement has to be compromised (reduce to be 53.3 ^{o}) in order to gain the improved response of rise and settling times (despite there was no strict requirement on these factors, but they still were considered as advisory) as well as steady-state error values (despite is tiny even could be neglectable).

5.3.5 Simulation and results analysis of catenary-pantograph system with finally selected PA-I control system

The simulation results showing details of contact force and displacement with PA-I control at 20m/s are shown in Figure 5.3.6 and Figure 5.3.7.

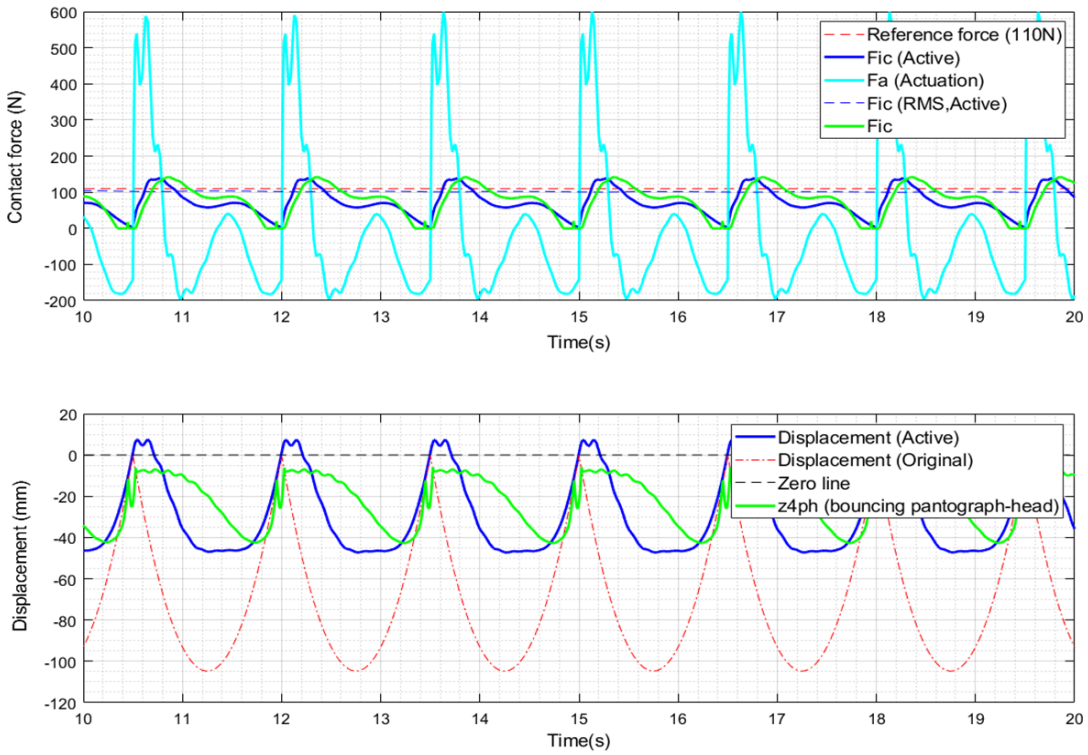

Figure 5.3.6-*Simulation result of catenary-pantograph in contact force and displacement with PA-I control system at 20m/s*

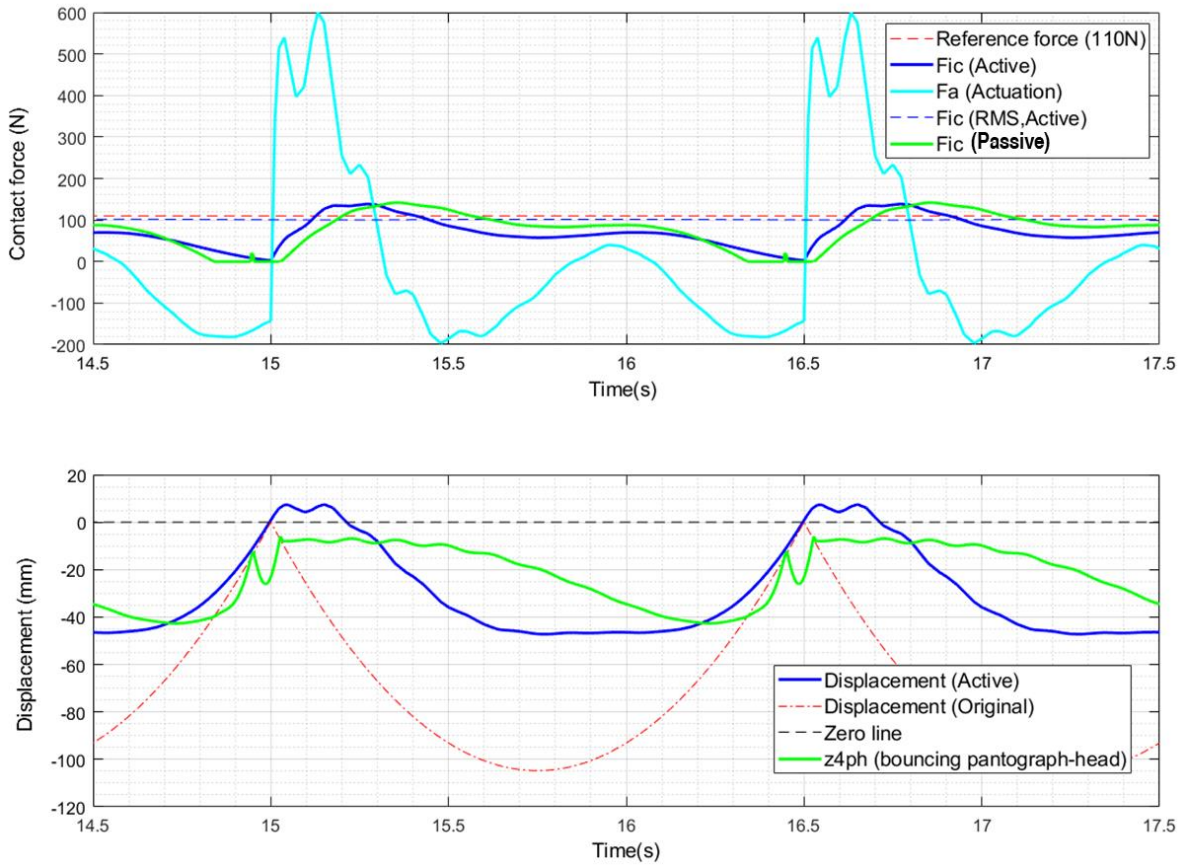

Figure 5.3.7-*Detailed simulation result (14.5-17.5s) of the catenary-pantograph in contact force and displacement with PA-I control system at 20m/s*

From Figure 5.3.6 (upper) and Figure 5.3.7 (upper), it can be seen that there is no contact loss (no contact force less than zero and displacement lower than original catenary wire) at any time. Figure 5.3.7 (upper) also shows that the dynamic variation in the active contact forces is smaller than the passive system contact force. From Figure 5.3.7 (lower) shows that the dynamic variation of active displacement is also reduced and is never lower than original catenary wire displacement. Together, these results indicate that the level of risk associated with the PA-I active control system for both electrical arcing and de-wirement is reduced compared to the passive catenary-pantograph system. A summary of the improvements in contacted force and displacement with PA-I control system are shown in Table 5.3.4.

Table 5.3.4 Comparing detail of the improved contacted force (F_{ic}) and displacement in passive and active (PA-I control)

Comparing parameter / System type	Contact forces max. variation (N)	Contact force variation change (%)	Various actuation force (Fa) (N)	Displace-ment max variation (mm)	Displace-ment variation change (%)
Passive	142			42	
Active (PA-I control)	135	-4.9	-200 to 600	46.7	+1

Table 5.3.4 shows that the PA-I contact force variations is -4.9% lower than the passive system contact force variation. But the PA-I displacement variation however is increased by 1% compared to the passive system displacement variation, however contactless has been eliminated with no zero-contact force as the dynamic displacement is always higher than original displacement of catenary. The actuation force is -200 to 600N.

Turning to a consideration of the possible size of actuator required to cope with the largest actuation force, the basic requirement is that the actuator speed should higher than the biggest vertical velocity of active catenary-pantograph. The further detailed simulation results are shown in Figure 5.3.8.

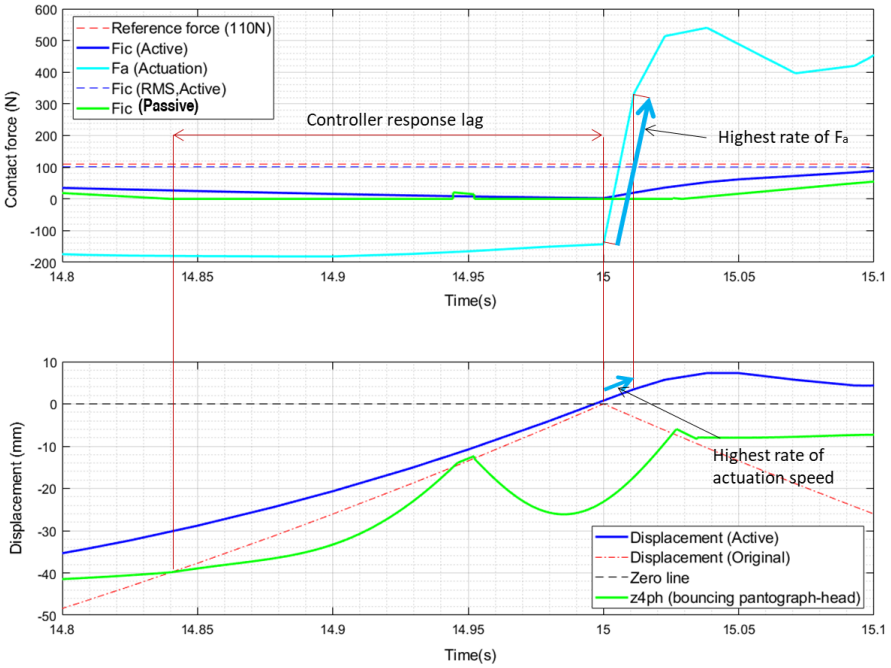

Figure 5.3.8-*Further detailed simulation result (14.8-15.1s) of the catenary-pantograph in contact force and displacement with PA-I control system at 20m/s*

Note: F_{ic} is impact transient force defined in Section 4.3.3 when the pantograph-head hitting catenary during the bouncing

From Figure 5.3.8, it can be seen that the highest rise rate of F_a is 4175 N/s; which equates to a highest vertical actuation speed of 23 mm/s.
As the controller response lag is affected by other factors such as electronic hardware, product provided software and algorithms (has studied in Chapter 3 and 4), this effect was not taken into account in the selection of actuator.

From these results, it can be seen that the actuator size requirement can be initially estimated as being at least higher than 600 N in dynamic loads (from force) and linear speed 23 mm/s (velocity). As the actuator that provides the actuation is shared by the dynamic catenary-pantograph and the planned de-wirement and re-wirement mode. Therefore, the further discussion for final requirement and selection will be made in Chapter 6.

5.4 Chapter Summary

An active catenary-pantograph system has been analysed as a way of solving the issues of de-wirement and arcing in a passive trolleybus catenary-pantograph as the vehicle passes stiff catenary stanchion points. This has been demonstrated through non-linear hybrid modelling. An active solution is proposed by using PA-I (after comparing PA and PA-I systems).

In order to fairly and effectively compare the active solutions against the passive system analysed in chapters 3 & 4, the evaluation considered the contact force and displacement variation, overshoot, steady-state error and largest actuation force. The results presented in this chapter, indicates that the PA-I controller demonstrates better performance in terms of reducing the variation in contact force and displacement. The PA-I controller also eliminates the wire contact loss issues encountered with the passive system at catenary stanchions as well as at crossings and switches etc. With control, a balance can be created between adequate contact, reducing the level of arcing and reducing the level of catenary wear.

Finally, the actuator size requirement was estimated by considering the largest actuation force and highest rate of actuation speed needed to cope with the highest rate of $F_{a;}$ which is equal to the biggest vertical velocity of active pantograph of trolleybus as well as sharing with planned de-wirement and re-wirement mode.

Chapter 6

Trolleybus planned de-wirement and re-wirement for the avoidance of hazards and negotiation of road features

6.1 Introduction

Chapter 5 demonstrated that the inclusion of an active pantograph system onto a Trolleybus can significantly reduce or even eliminate the risk of arcing or de-wirement. The introduction of an active pantograph system does offer other possibilities. For example, it would be possible for a trolleybus to pass through crossroads (or bypass path restrictions due to extra-vehicle emergencies that take the trolleybus out of the kinematic window of the overhead wire) without overhead line if the concept of planned de-wirement and re-wirement could be introduced. The concept is that the active pantograph with function added which can automatically de-wire and re-wire without driver input during standard operation under the full range of operating speeds. Of course, to provide energy for the trolleybus to traverse the 'gaps' in electrical contact an additional power source, such as a super-capacitor or flywheel [148] [169], would be required on the trolleybus that could store energy during wired operation or harvest energy during braking.

In this chapter the assumption is made that planned de-wirement and re-wirement can be achieved in a single operation with adjustable durations for 'down time' that depends on specific circumstances such as crossroad size, traffic situation and driver's behaviour etc. This allows for a novel construction philosophy to be employed at crossings such that the catenary is not a continuous system with the trolleybus traversing using an additional on-board power source. In this way, sections of catenary on either side of a junction are essentially isolated dynamically. A proposed process of desired the planned de-wirement and re-wirement of a trolleybus system is shown in Fig.6.1.1.

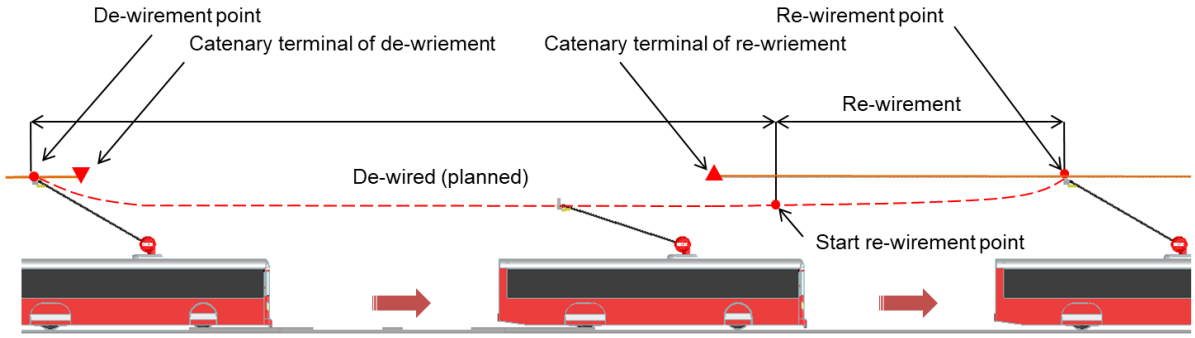

Figure 6.1.1-*Proposed process of planned de-wirement and re-wirement of trolleybus*

From the desired de-wirement point the pantograph is drawn down by the actuator; such that the catenary and pantograph are no longer an interacting dynamic system and behave as individual components. For re-wirement the inverse operation occurs, with the catenary and

pantograph beginning isolated sub-systems and combining to become an interacting system. The desired re-wirement point will determine the duration of the whole process. This chapter focuses on the dynamics of the whole process and control methods for the trolleybus to traverse the ‘gaps’.

6.2 Modelling of the planned de-wirement and re-wirement dynamics

6.2.1 Modelling of the dynamic equations

An integrated model of planned de-wirement and re-wirement can be achieved using a hybrid model formed by two modes: “standard” and “de-wirement & re-wirement”. The standard part of model uses the catenary-pantograph dynamics under normal status using equations E3.4.1, E4.6.1, E4.6.2, E3.4.5 and E3.4.2, as before. This standard mode would be applied before any de-wirement point and after all subsequent re-wirement points; as shown in Figure 6.1.1. This section describes the design, simulation and analysis of the de-wirement and re-wirement modes.

The dynamics of de-wirement and re-wirement are mainly governed by the actuation and pantograph system configuration as well as the running speed. The de-wirement and re-wirement model mainly describe the pantograph dynamics in non-contact mode. Following the assumptions described above a simplified model was built for studying the non-contact catenary phenomenon under actuation. During the planned de-wirement and re-wirement, the catenary and collection head are fully separated, therefore there is no to consider the catenary nominal stiffness Kc(t). The model is shown in Figure 6.2.1.

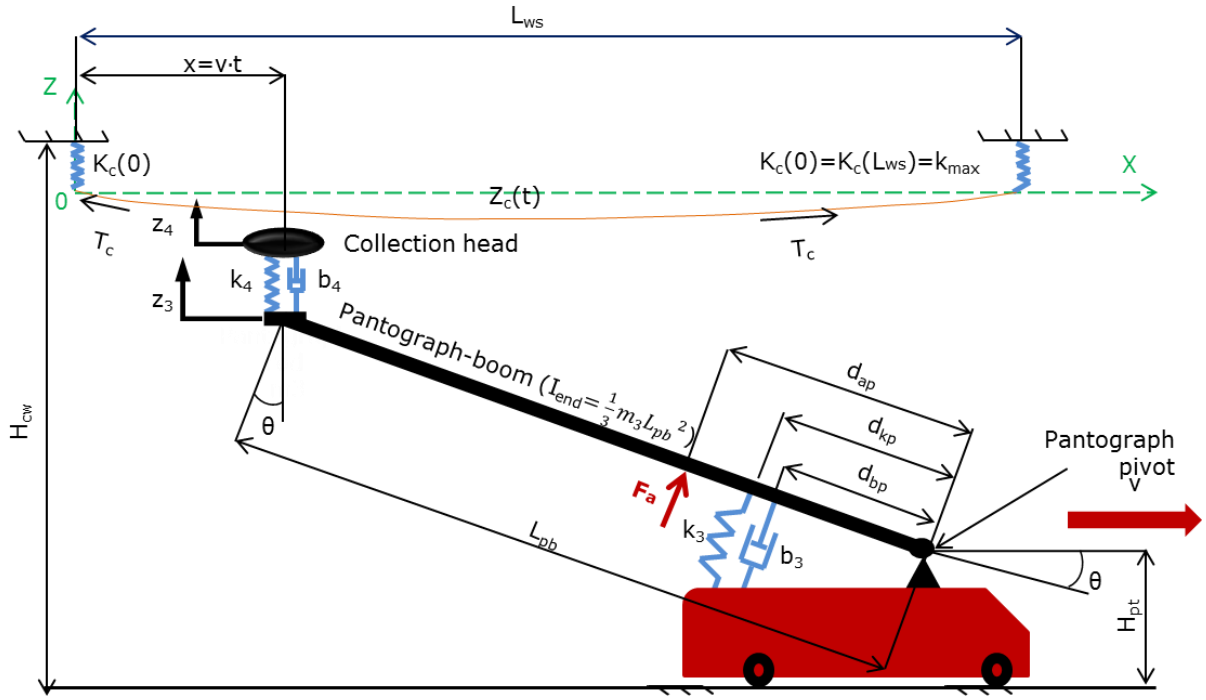

Figure 6.2.1-*Typical model of de-wirement and re-wirement pantograph system (without contact with catenary) with position sensors and force control actuation*

Where:

$K_c(t)$: catenary contact wire nominal stiffness (N/m)

$K_c(0) = K_c(L_{ws}) = k_{max}$: catenary contact wire maximum stiffness (N/m)

k_{min}: catenary minimum stiffness (N/m) (not shown in Figure 3.2.1)

k_{mean}: catenary average stiffness (N/m)

L_{ws}: catenary contact wire span between two poles (m)

T_c: tensile force of catenary contact wire (N)

$Z_c(t)$: pre-catenary vertical displacement (m)

H_{cw}: installation height of the catenary wire (normally from ground to fixed point on poles). It is determined the BSI British Standards in trolleybus (m) [37]

H_{pt}: pivot height of pantograph from ground (3.50 m)

z_3: pantograph boom vertical displacement (m)

m_3: pantograph-boom mass (kg)

b_3: pantograph-boom absorbers damping rate (Ns/m)

k_3: pantograph-boom spring nominal stiffness (N/m)

d_{bp}: distance from damper fitting point to pantograph pivot point (m)

d_{kp}: distance from spring fitting point to pantograph pivot point (m)

d_{ap}: distance from actuator fitting point to pantograph pivot point (m)

z_4: pantograph-head vertical displacement (trajectory) (m)

m_4: pantograph-head mass (kg)

b_4: collection head absorbers damping rate (Ns/m)

k_4: pantograph-head spring stiffness (N/m)

Fa: actuation force (N)

I_{end}: pantograph-boom moment of inertia to ($kg \cdot m^2$)

θ: pantograph-boom dynamic lifting angle (degrees)

L_{pb}: length of pantograph-boom (m)

g: gravitation acceleration ($9.8 m/s^2$)

ρ: catenary wire linear mass density (kg/m)

x: contact position distance from 0 of x-axis ($x=v \cdot t$) (m)

v: trolleybus speed (m/s)

Following the Newton's second laws, dynamic equations (model) can be devised with actuation force (Fa) and refer to E3.2.13, E3.2.9 E3.2.14 the of as shown in E6.2.1 with E3.2.10 and E5.2.1 (shown in Chapter 3 and 5).

$$\boldsymbol{m_4\ddot{z}_4 = -b_4(\dot{z}_4 - \dot{z}_3) - k_4(z_4 - z_3)} \qquad \text{E6.2.1}$$

Integrating all these derivations, the final model of the active catenary-pantograph of a trolleybus can be described by a set of equations similar to E3.2.13, E3.2.14, E3.2.17, E3.2.20, and E3.2.21 as stated in Chapter. 3

6.2.2 Control requirements

Control of de-wirement and re-wirement, with path demand plan, is essentially based on a pantograph position control system. This is different to the catenary-pantograph force and displacement control used in the wired condition. A proposed plan for the profile of de-wirement and re-wirement is shown in Figure 6.2.2. It is like a trapezoidal motion profile [149].

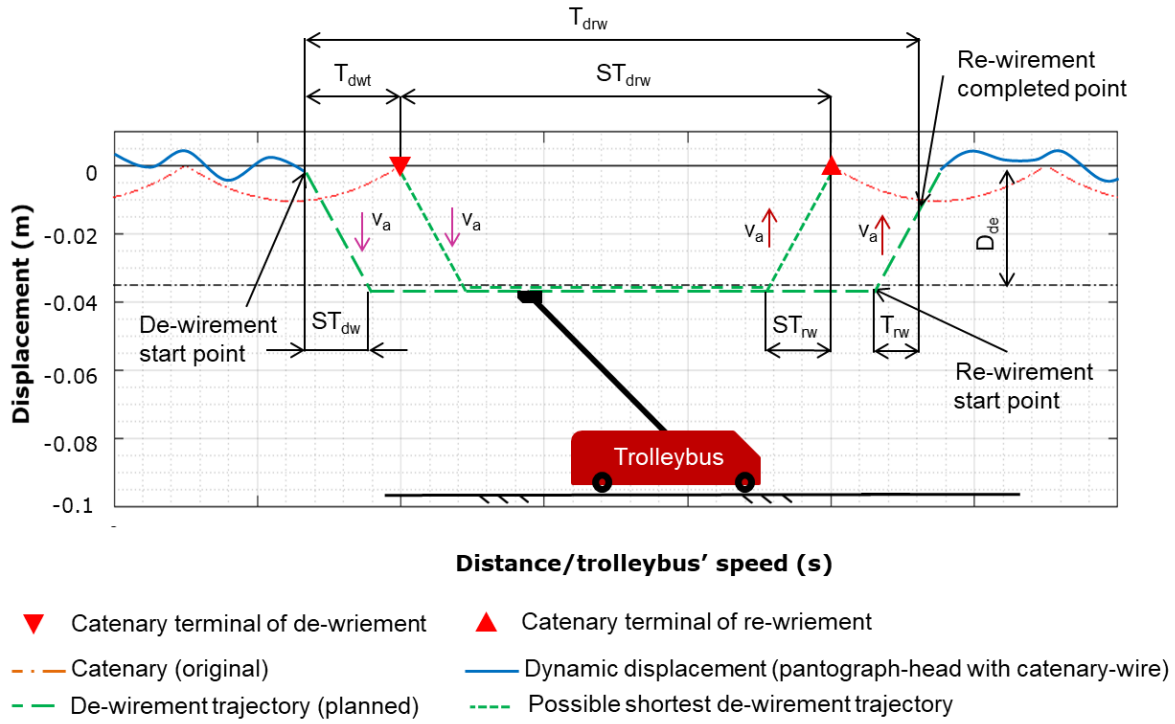

Figure 6.2.2-*Requirement of planned de-wirement and re-wirement pantograph system (exaggerated view at Displacement)*

Where:

D_{de}: desired distance between catenary hang point and pantograph head during de-wirement or re-wirement (m)

T_{drw}: duration between de-wirement start to re-wirement completed point (s)

ST_{dw}: duration between the start points of pantograph de-wirement and complete reached D_{de}

T_{dwt}: duration between de-wirement start point and catenary terminal of de-wirement (s)

T_{rw}: duration between re-wirement start and pantograph up to contact point of catenary and re-wirement completes (s)

ST_{drw}: shortest duration between de-wirement and re-wirement; also called wireless window (s)

ST_{rw} : duration between re-wirement start point and pantograph up to contact point of catenary (s) with lifting up speed v_a

v_a: assumed nominal (average) vertical operation speed of pantograph head in up and down (0.5m/s) by proper actuator [103]

To add a safety margin into the process, the desired distance between the catenary vertical displacement and the pantograph head D_{de} should meet the requirements for insulation distance (electrical clearance in the air) between the catenary and dynamic pantograph head of pantograph. For the avoidance of hazards and negotiation of road features with reference to the standard [37], the safe electrical insulation distance under the catenary, as well as the largest catenary displacement and dynamic displacement values are shown in Figure 6.2.3

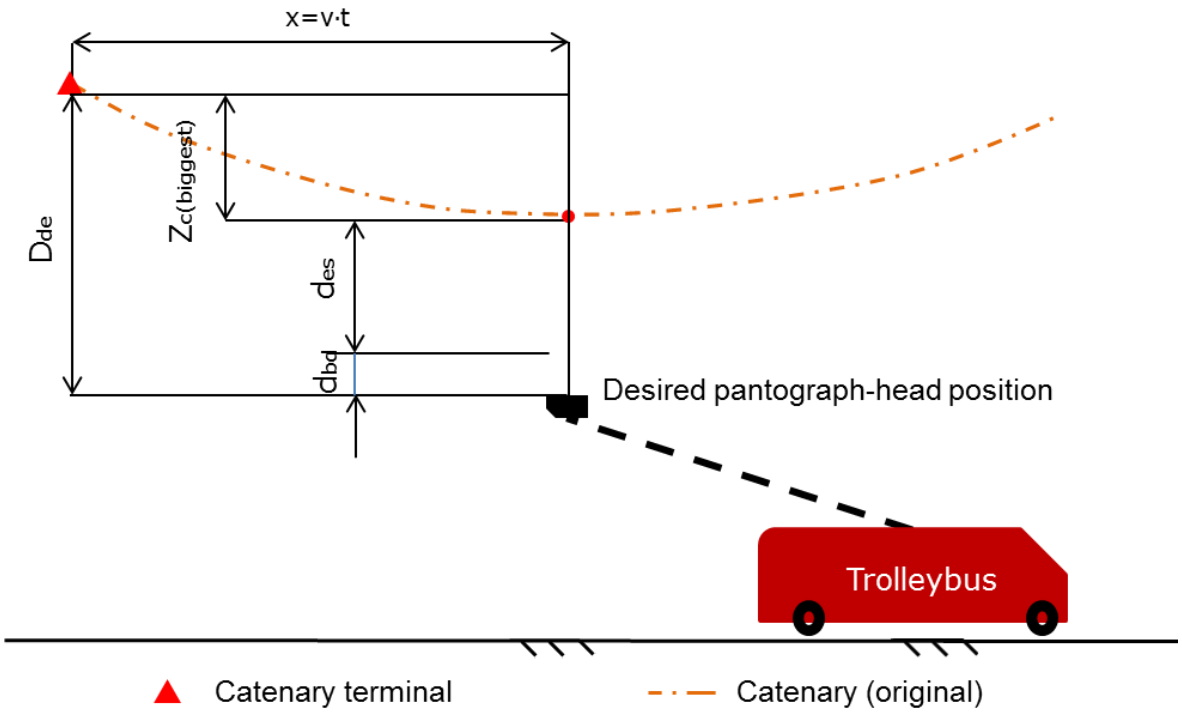

Figure 6.2.3-*Desired distance between catenary hangs point and pantograph-head during de-wirement or re-wirement*

Where:

D_{de}: desired distance between catenary hang point and pantograph head during de-wirement or re-wirement (m)

$Z_{c(biggest)}$: largest catenary displacement 0.105m (refereeing to Figure 3.5.4)

d_{es}: the safe electrical insulation distance under catenary is at least 0.2m [37]

d_{bd}: dynamic displacement approximate 0.04m (refereeing to Figure 5.4.6)

D_{de} can be roughly estimated as follows:

$$\boldsymbol{D_{de} = d_{es} + Z_{c(biggest)} + d_{bd}}$$

Using the values of parameters des, $Z_{c(biggest)}$ and d_{bd} shown in Figure 6.2.3, the value of D_{de} is shown below:

$$D_{de} = 0.2m + 0.105m + 0.04m = 0.345\ m$$

Using the value of D_{de} =0.35m with the assumed nominal (average) vertical operation speed (v_a) of pantograph head, the duration (ST_{dw}) between the re-wirement start point (shown in Figure 6.2.2) and where the pantograph is in contact with the catenary. The vertically down position can be found (with proper actuator) as:

$$ST_{dw} \approx \frac{D_{de}}{v_a} + t_{av} \approx \frac{0.35}{0.5} + 0.0013 \approx 0.7s$$

The shortest duration between de-wirement and re-wirement (assuming a wireless window between two catenary poles of 30m) can be calculated at a trolleybus running speed of 20m/s:

$$ST_{drw} = \frac{L_{ws}}{v} = \frac{30}{20} = 1.5s$$

In order to optimise safety and reliability, it was assumed that the pantograph position is always monitored and positioned by GPS or RTLS (real-time location system) [151, 152]. In addition, a possible image measurement system [153] could be used to detect the distance between the pantograph head and wire as well as the height of the collection head. The process of re-wirement will automatically shift the control mode from de-wirement and re-wirement (by position) to catenary-pantograph dynamic (by contact force) at a certain gap (Gia) below the catenary. The detailed re-wirement start (pantograph begin lifting)and control shifting points are shown in Figure 6.2.4

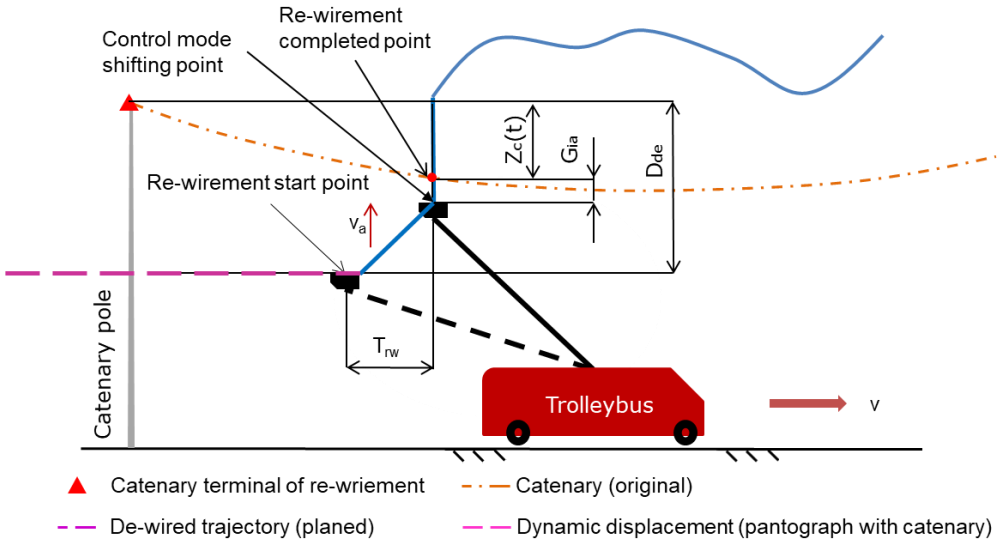

Figure 6.2.4-*Detail of re-wirement start and control modes' shifting points*

Where

G_{ia}: certain gap between catenary and pantograph head at shift the control mode point of re-wirement (m)

Others are same as in Figure 6.2.1 and Figure 6.2.2

The duration between re-wirement commencing and the pantograph contacting the catenary is calculated as

$$\boldsymbol{T_{rw}} \approx \frac{\boldsymbol{D_{de}} - \boldsymbol{Z_c(t)} - \boldsymbol{G_{ia}}}{\boldsymbol{V_a}} + \boldsymbol{t_{dv}} \qquad \text{E6.2.3}$$

The desired start point of de-wirement (switching catenary-pantograph control to de-wirement and re-wirement control) can be at any point within the catenary arc depending on the running operation. Before full separation between pantograph and catenary a contact force remains. The pantograph is drawn down by the actuator with desired up speed v_a until reaching its lowest position (D_{de}). The Pantograph will be in a stationary position until re-wirement is required. The start point of re-wirement is assumed to be anywhere after the de-wirement process has delivered the pantograph to its lowest position (D_{de}). From the start point of re-wirement, the pantograph is lifted up by the actuator with a desired speed v_a until it reaches the gap (G_{ia}) below the catenary wire where the de-wirement and re-wirement control is switched back to catenary-pantograph force control. The assumed nominal (average) vertical operation speed (v_a) of the pantograph head, both up and down, is under control of the actuator [103]). At the shift the control mode point of re-wirement the gap (G_{ia}) is assumed to be 0.05m in this study, the actuation of re-wirement mode is instead of standard control mode. An assumed a high impact force would happen when pantograph head recontact the catenary (re-wirement completed point).

From Figure 6.2.2 and Figure 6.2.4, the whole process period (T_{sc}) of de-wirement and re-wirement with controller and actuator should be longer than the shortest duration of de-wirement and re-wirement (or $T_{sc} \leq ST_{drw}$). The $T_{drw} - T_{rw} \geq ST_{drw} + T_{dwt} - ST_{rw}$. Parameterisation of the requirements is shown in Table 6.2.1

Table 6.2.1 Qualitative satisfactions with essential requirement

Performance / Essential	Requirement
ST_{drw} (s)	≥ 1.5s
T_{dwt} (s)	≥0 (s)
ST_{dw} (s)	≤ 0.7s
T_{sc} (s)	≤ 1.5s

The "window" (ST_{drw}) defines the distance between two catenaries terminals (start de-wirement and completed re-wirement points). The travelling gap is the distance the trolleybus has to traverse the 'gap' without contact, under control of the additional power source. The 'window' can be applied at crossroads, junctions, depots and emergent by-passing etc. A schematic of the trolleybus re-wirement system is shown in Figure 6.2.2.

6.2.3 Control concept

It can be assumed that the control system for planned de-wirement and re-wirement would be a single closed loop with the demand being the planned de-wirement point and pantograph position. The planned de-wirement and re-wirement pantograph system uses a force input demand to the actuator (that could be implemented as current control in an electromagnetic actuator). In general, the closed-loop control system is shown in Figure 6.2.5.

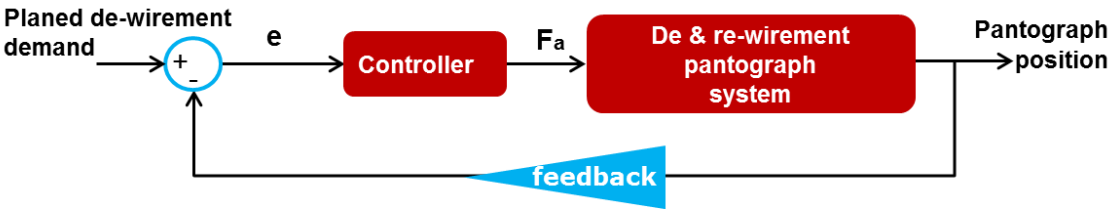

Figure 6.2.5-*Control system concept diagram of pantograph system planned de-wirement & re-wirement (with position sense and force actuation)*

As mentioned in chapter 5, there are three key points that should be considered in the design of the control system [72]:

- Transient response: the system rise time, overshoot (e.g. less than 20%) and settling time etc.

- Steady state response: steady state tracking errors or disturbance induced steady state errors should be less than 5% error
- Stability: the closed loop must be stable depending on open loop with specified gain margins (GM > 6dB) and phase margins (PM > 60°), [72, p9].

6.3 Phase advance (PA) and phase advance-integrator (PA-I) control design, simulation and results analysis of planned de-wirement and re- wirement

6.3.1 Introduction

Phase advance (PA) can be thought as a more practically applicable version of a PD control system [72]. The PA has a lead term followed by a lag term that can be applied at the required frequencies without getting the excessive high frequency gain of the PD control system [72]. The model of planned de-wirement and re-wirement (without the catenary after planned de-wirement and before re-wirement) is a catenary-pantograph system with position control.

In addition, the phase advance (PA) control can decrease the torque ripple of the electric motor Brush-less DC (BLDC) motor [154] of actuator which is beneficial to improve stability of the planned de-wirement and re-wirement. It is also a reason the phase advance control is applied for planned de-wirement and re-wirement.

6.3.2 PA and PA-I Control basic design

Figure 6.3.1 shows the simple PA (or PA-I) system concept control diagrams of the de-wirement and re-wirement system.

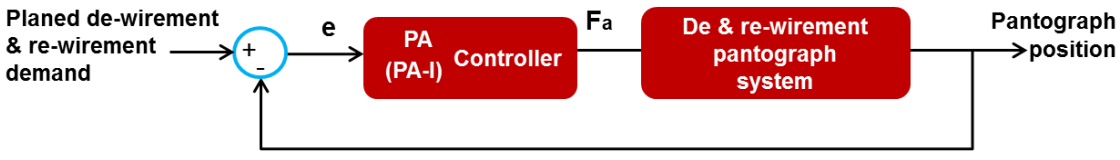

Figure 6.3.1-*PA (PA-I) concept control system diagram of planned de-wirement and re-wirement system*

Where:

F_a: actuation force (N)

e: control error which is based on the pantograph position planned de-wirement and re-wirement demand and (m)

The essential planned de-wirement and re-wirement pantograph system equation E6.2.2 is shown in section 6.2.1.

The applicable equations of E5.3.2 and E5.3.3 for PA and PA-I control have been given in Chapter 5

6.3.3 Simulation configuration

The simulation of planned de-wirement and re-wirement is based on an active catenary-pantograph with lifting and down actuation under dynamic PA or PA-I control. The control feedback is switched from contact force to position between the de-wirement and planned re-wirement points. With clearly showing the whole process, the simulation includes a hybrid model formed by two parts: “standard” (discussed in Chapter 5) and planned “de-wirement & re-wirement” and re-wirement start and control modes’ shifting points. The de-wirement start and control modes’ shifting point has two different in standard (automatically) and emergency (manually).

The simulation configuration (including all parts described above paragraph) of planned de-wirement and re-wirement is shown in Figure 6.3.2.

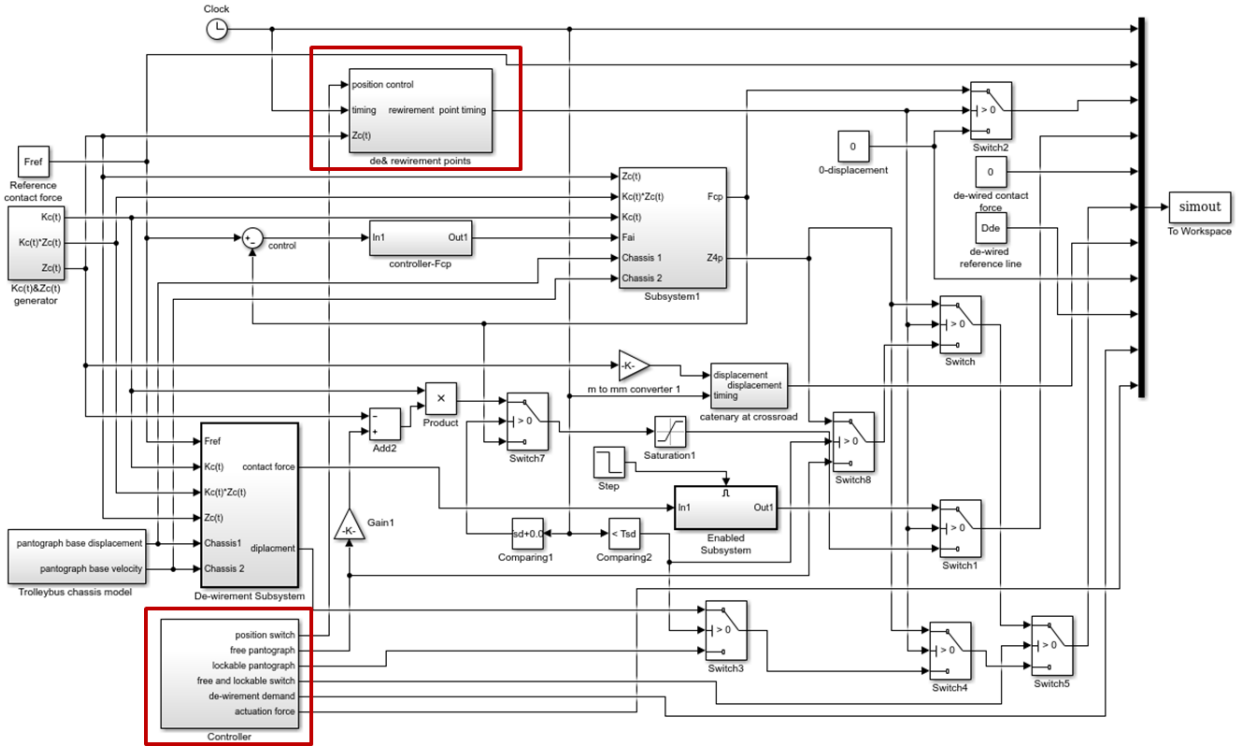

Figure 6.3.2-*Simulink configuration of trolleybus' planned de-wirement and re-wirement*

The upper red frame is the planned re-wirement Simulink configuration block which is with E6.2.3 and table 6.2.1 and shown in detail including start and modes shifting point in Figure 6.3.3.

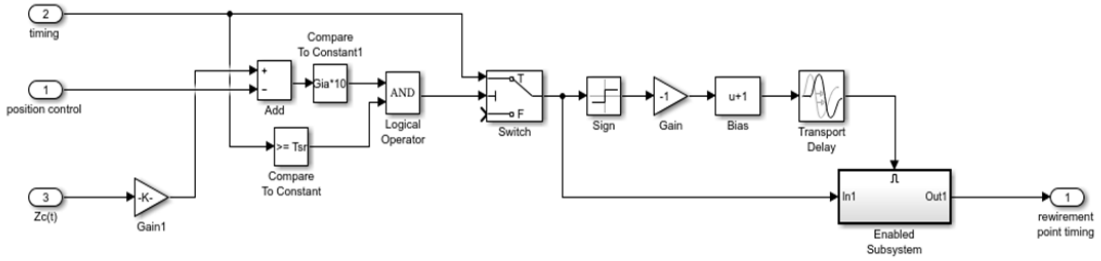

Figure 6.3.3-*Simulink configuration detail of planned re-wirement*

The lower frame is the control system block of planned de-wirement and re-wirement which is shown in detail in Figure 6.3.4.

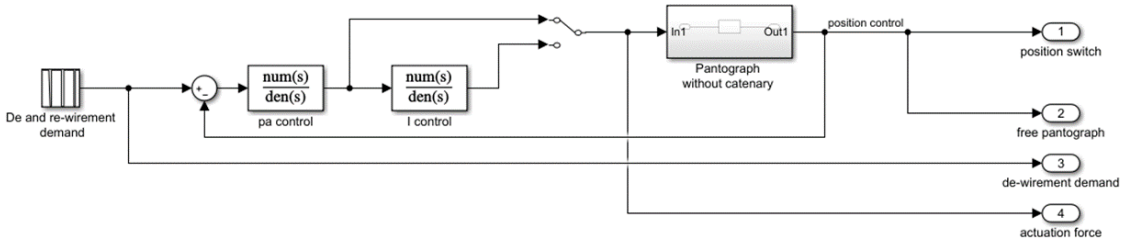

Figure 6.3.4-*Simulink configuration of planned de-wirement & re-wirement control systems*

6.3.4 Parameter selection of planned de-wirement & re-wirement control system

To maintain agreement with the system requirements used on the ACTCCS system described in Chapter 5, the frequency response and time response requirements for the planned de-wirement & re-wirement system are defined on Table 5.3.1 in Chapter 5

The first stage of selecting the parameters deals with de-wirement & re-wirement pantograph system (uncondensed) as follows:

- A Phase advance ratio of K_{ratio}= 8 was chosen as compromise value for this study - normally between 4 and 8 [72, p16].
- The Max phase advance was calculated by $sin^{-1}\frac{K_{ratio}-1}{K_{ratio}+1}$ ≈51° and the Centre point gain by $20 * log_{10}\left(\sqrt{K_{ratio}}\right) = 9\text{dB}$ [72, p18]
- Using Nichols diagram of de-wirement & re-wirement pantograph system [153] to identify a phase which can be shifted to −120°(relating to 60° of PM) by 180° − 60° (PM) + 51°(Max phase advance) = 171° [72]

The corresponding gain of -76.5 dB (cross 0 dB) and a frequency (ω_{lc}) of 7.31 rad/s was obtained from the Nichols diagram shown in Figure 6.3.6

The second stage of selecting the parameters is for the PA control of the de-wirement & re-wirement pantograph system as follows:

- The proportional gain value was calculated as $K_{pa} = 10^{\frac{76.5-9}{20}} \approx 2371$ [172, p19]
- The lag time constant T_l was obtained by

$$T_l = \frac{1}{\sqrt{(K_{ratio})}(\omega_{lc})} = \frac{1}{2.8 * 7.31} \approx 0.048s$$

The three key selected parameters of the PA control system are: K_{pa}=2731; Kratio= 8; T_l=0.048s. The Nichols diagram curve of the pantograph with PA control is shown Figure 6.3.6.

From Nichols diagram curve of pantograph curve in Figure 6.3.5, the GM and PM are far away to meet the requirement. The curves of pantograph with PA and PA-I controls, it can be found that the GM (PA: 4.84; PA-I:4.87) and PM (PA: 60°; PA-I:56°) are closed at a crossover frequency of 7.31 rad/s. However both systems obviously do not satisfy the requirement of GM(> 6dB) and PM(> 60◦) [72] at same time. Therefore, a compromise might be necessary in the zero steady state error or other factors.

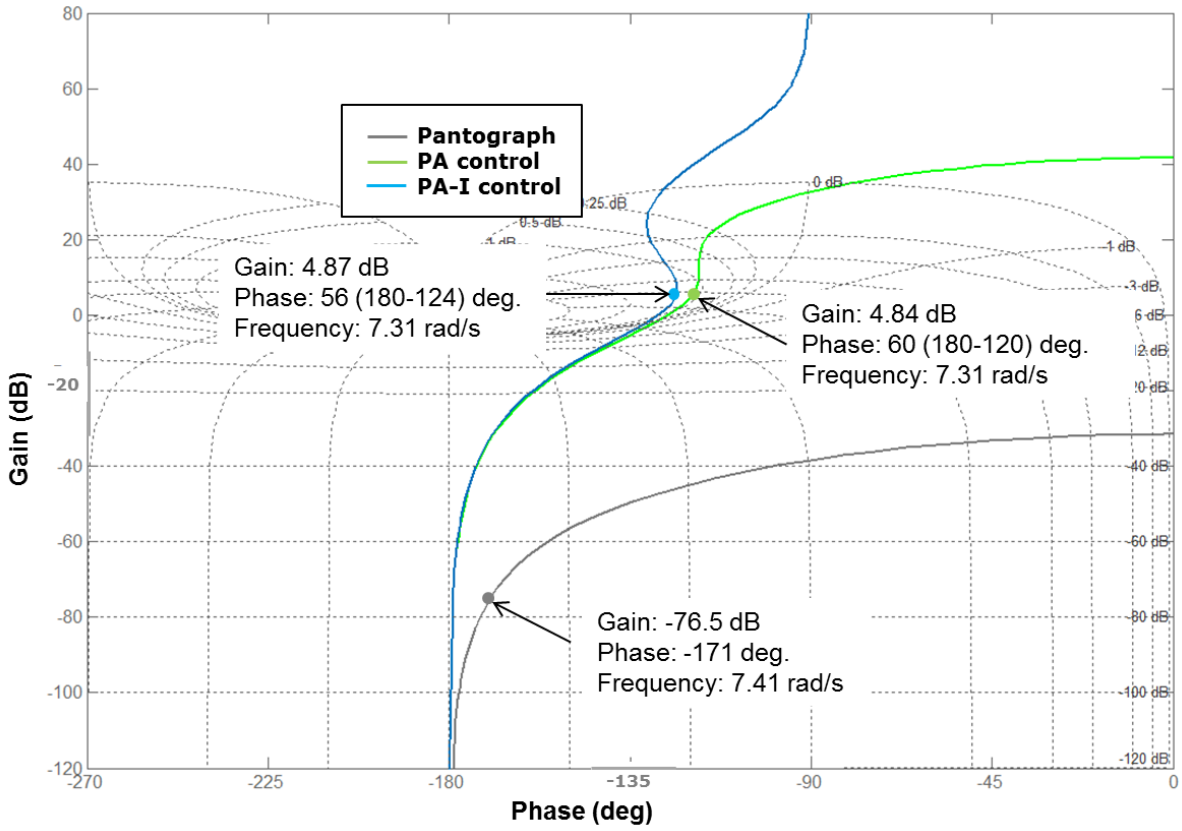

Figure 6.3.5-*Open-loop Nichols diagram of pantograph and with various control systems*

From Figure 6.3.5, it can be seen that the GM is infinite due to the locus never crossing the −180◦ line of the y-axis. Therefore, the value of proportional gain could be increased for better output performance of the planned de-wirement and re-wirement system [72, p9]. This is simpler and more certain than the dynamic catenary-pantograph system simulated in Chapter 5.

The simulation closed-loop step diagrams and the steady-state error are shown in Figure 6.3.6 and Figure 6.3.7 respectively, for the planned de-wirement and re-wirement system with PA and PA-I control.

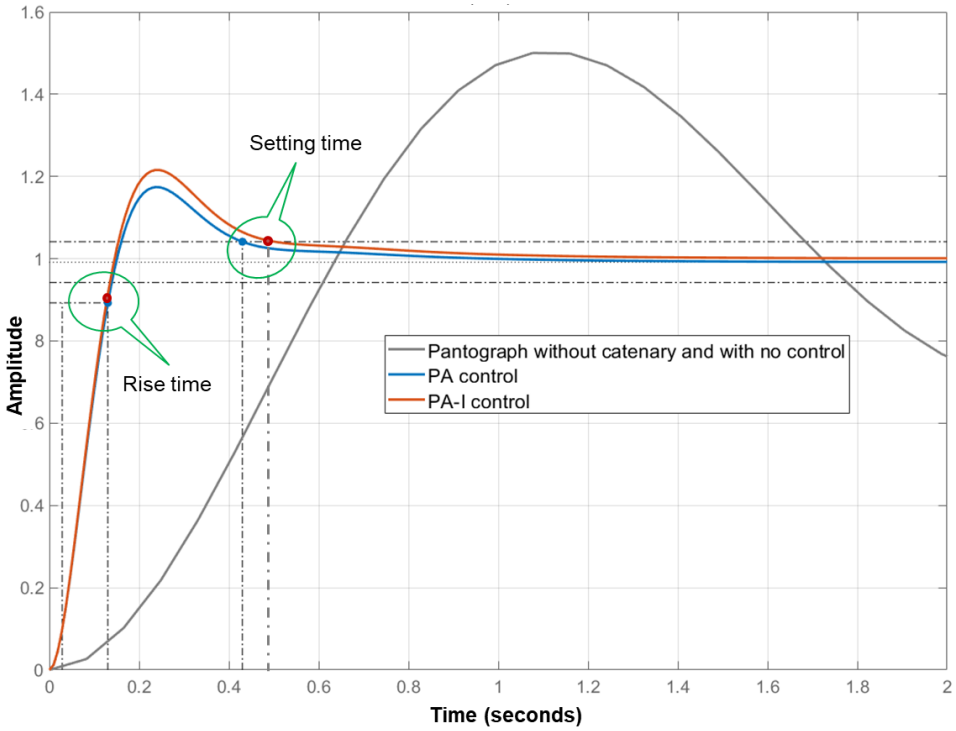

Figure 6.3.6-*Closed-loop step diagram of pantograph with PA and PA-I control systems*

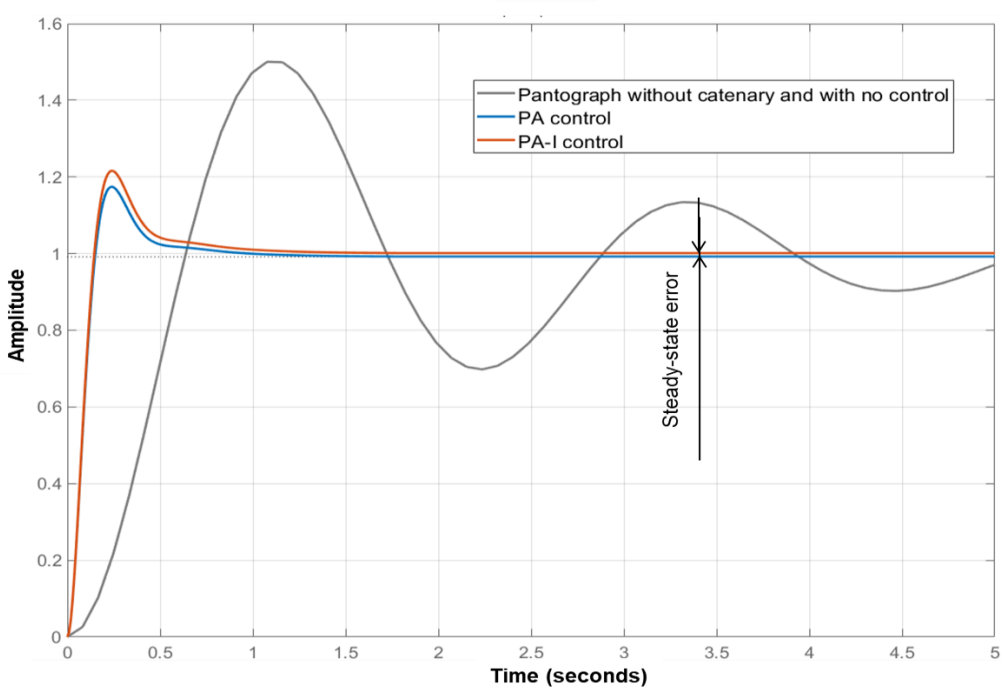

Figure 6.3.7-*Closed-loop step steady-state error diagram of pantograph with PA and PA-I control system for*

From Figure 6.3.6 and Figure 6.3.7, behaviour of pantograph with no control during de-wired dose not meet the requirement. With PA and PA-I control the curves showing overshoot are

both less than 20%. The rise time, setting time and steady-state error are shown in Table 6.3.1.

Table 6.3.1 Rise time and setting time and with steady-state error of PA and PA-I control system with de-wirement and re-wirement pantograph system

Results / Control system	Rise time (s)	Settling time (s)	steady-state error (%)
PA	0.129	0.43	0.05
PA-I	0.129	0.50	0

Comparing Table 6.2.1 and Table 6.3.1, it can be seen that both PA and PA-I satisfy the essential requirement of planned de-wirement and re-wirement. However, from the three factors shown in Table 6.3.1, it is obvious that the PA-I control system has better performance than PA control when working with the planned de-wirement and re-wirement pantograph system.

6.3.5 Simulation and results analysis of de-wirement and re-wirement system with PA-I control system

In order to simplify the simulation, the simulation is based on an optimised PA-I control and assumes that the trolleybus go through the crossroad with smooth road surface at 14m/s (normal operation speed). The complete de-wirement and re-wirement simulation results in respect of contact force and displacement is shown in Figure 6.3.8.

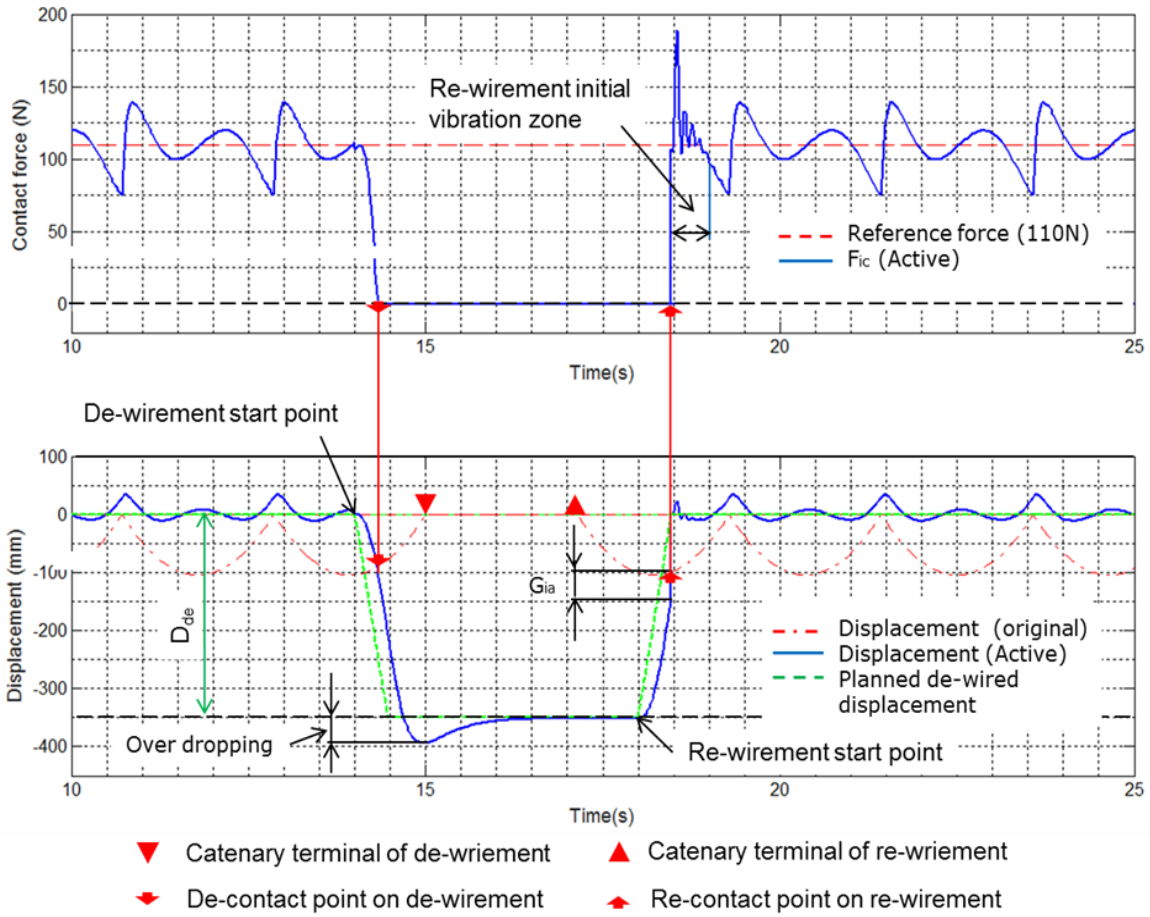

Figure 6.3.8-*Whole process of de-wirement and re-wirement simulation in contact force and displacement with PA-I control system at 14m/s*

Note: F_{ic} is the impact transient force when the pantograph-head hitting catenary at the re-contact point of the re-wirement., It is acceptable with over dropping of 44mm as the gap between the pantograph head and trolleybus top is still much smaller than safety requirements of British Standards [37]

In Figure 6.3.8, the trajectory of de-wirement and re-wirement (displacement) with PA-I control is close to the planned demand. The lower displacement segment below Dde (in demand) after de-wirement is caused by a combination of physical overshoot of the pantograph and the control dynamic.

It would be assumed that the de-wirement are either automatically start from selected point somewhere within last catenary before crossroad or manually selected by driver at the emergency. From the de-wirement start point the pantograph is drawn down by electric actuator (or pneumatic actuators) under the PA-I control and the catenary-pantograph control mode is switched from contact force to de-wirement and re-wirement position. The contact

force initially drops slowly, probably due to the controller and actuator response lag, and then drops quickly to zero, when the trolleybus loses electric energy from catenary. The trolleybus then continues under operation with additional power source. Meanwhile, the pantograph actuator continues to move the pantograph-head down until it passes below the actual demand position Dde. This over-dropping is led by the inertia of the pantograph and controller and actuator response lag.

At the re-wirement start point the pantograph is lifted up by actuator with speed v_a until at the planned gap (G_{ia}) the de-wirement and re-wirement where the control mode is switched back to the catenary-pantograph control mode. After re-contacting with the catenary, the trolleybus regains electric energy from catenary. At the re-contact point, the pantograph-head impacts the catenary causing the impact transient force (F_{ic}) sharply increases up to 180N.

The detailed results of the actuation force and speed in de-wirement and re-wirement are shown in Figure 6.3.9 and Figure 6.3.10.

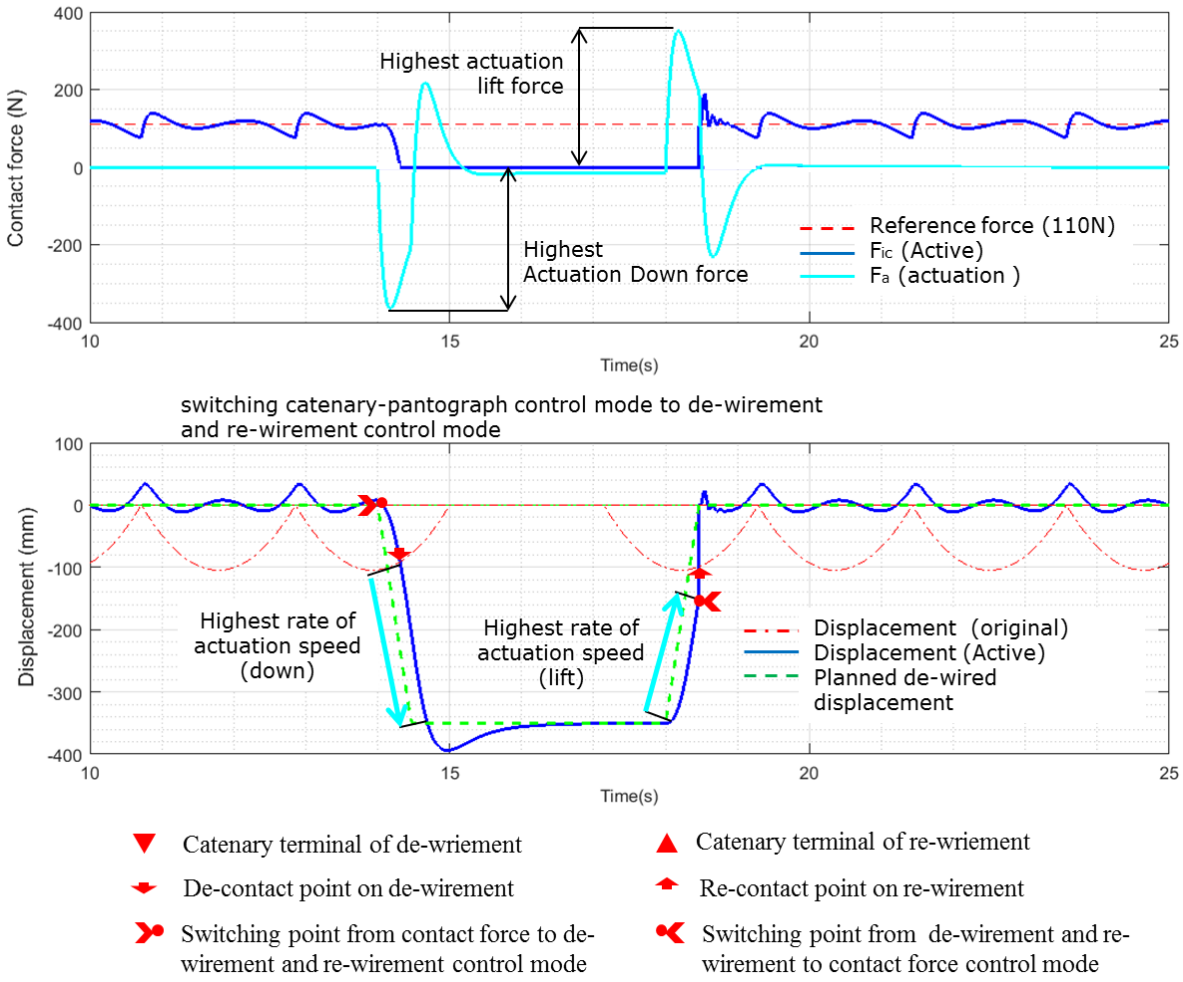

Figure 6.3.9-*Simulation result* of *contact and actuation force and speed in de-wirement and re-wirement with PA-I control system at 14m/s*

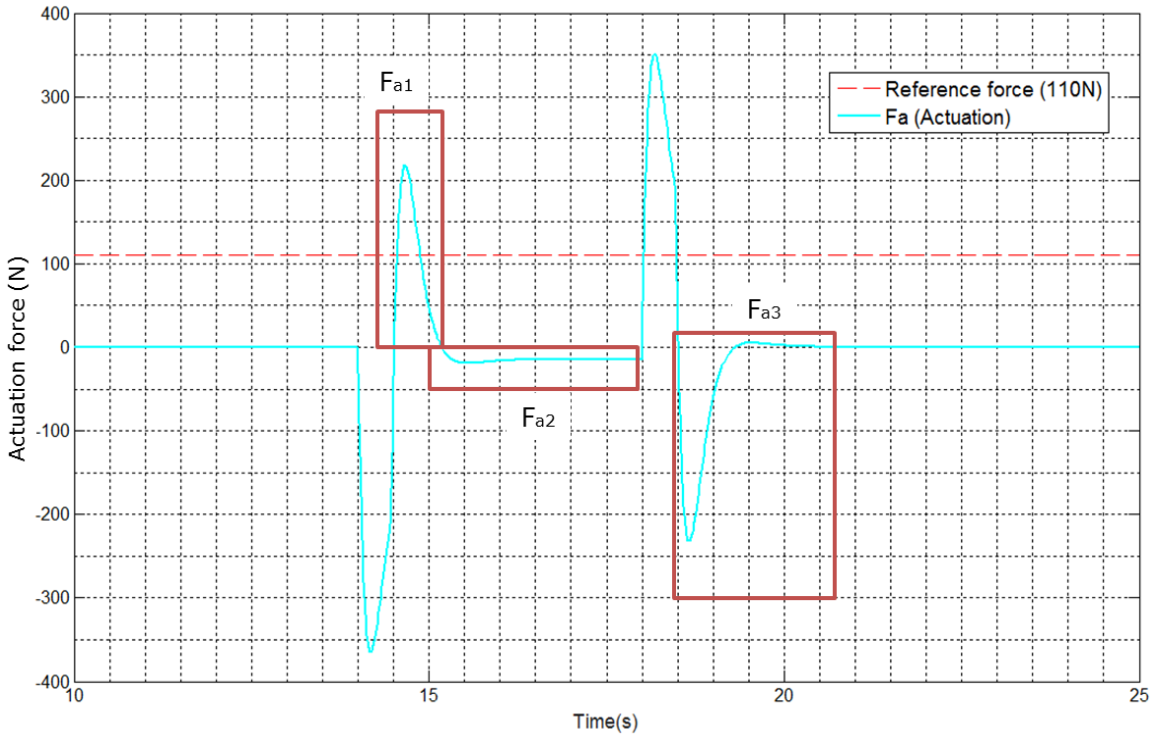

Figure 6.3.10-*Detailed actuation force in de-wirement and re-wirement with PA-I control system at 14m/s*

Figure 6.3.9 shows that the highest absolute drawn down (negative) and lift up (positive) forces are both about 380N. The highest the highest absolute drawn down (negative) and lift up (positive) speeds are 440mm/s and 484mm/s respectively. The three framed segments highlight the actuation forces F_{a1}, F_{a2} and F_{a3} deliver the compensative function of actuation. By referring to Figure 6.3.9, it can be seen that the very high positive F_{a1} value results from the lower displacement segment below D_{de}; caused by combination overshoot of pantograph (physical) and control dynamic. The value of F_{a2} can be thought of a result of a combination of the physical overshoot of the pantograph, as well as charged main spring of pantograph during de-wirment and before re-wirement start point. The very high negative F_{a3} value is due to the high impact and contact force of re-wirement.

6.4 Selection of Actuator

The planned actuator that provides the actuation is shared by the dynamic catenary-pantograph and the planned de-wirement and re-wirement process. In ACTCCS, electro-mechanical actuation is selected to meet the main requirement for the active control to stabilize the kinematic modes and curving performance [161]. Consequently, the speed and dynamic loads selected for the actuator should cover both applications with the highest values

estimated for both dynamic catenary-pantograph and planned de-wirement and re-wirement. The highest values of actuation are obtained from section 5.3.5 in Chapter 5 and section 6.3.5 in this chapter and shown in Table 6.4.1.

Table 6.4.1 Highest actuation force and speed of pantograph [103] **in both catenary-pantograph and de and re-wirement control modes with PA-I control**

Parameters	Catenary-pantograph control mode actuation force (N)	De and Re-wirement control mode actuation force (N)	Catenary-pantograph control mode actuation speed (mm/s)	De and Re-wirement control mode actuation speed (mm/s)
Highest Value	600	380	23	445

The basic selection requirements for the actuator should at least cover the dynamic loads of 380N and linear speed of 445 mm/s. The proposed actuator might approach 100% duty cycle or at least operate for multiple cycles [150] in safety factor in actuation force; therefore the maximum dynamic loads of actuator would be chosen as 400N in dynamic load with a choice of higher linear speed than 445 mm/s. With sharing both static (including pantograph mounting plane on the top dose not in duty) and dynamic dis placement to refer the Figure 3.2.2, Figure 5.2.1 and Figure 6.3.8 the stroke of actuator selected would be ±400 mm (actuator fitted position was taken into account of modelling in Chapter 5 and Chapter 6). The actuator parameters approximately selected for the planned de-wirement and re-wirement Trolleybus pantograph are shown in Table 6.4.2

Table 6.4.2 Selected standard actuator parameters selected for pantograph [103]

Parameters	Dynamic loads (N)	Max. linear speed (v_a)	Accepted longest Stroke
Value	575	500 (mm/s)	800 (mm)

The pantograph mounting plane on the top dose not in duty has been in consideration of actuator stroke.

6.5 Chapter Summary

In this chapter, a study of planned de-wirement and re-wirement was undertaken to explore the behaviour of an ACTCCS operation when drawing down and lifting up the trolleybus pantograph head when passing through non-wired gaps at crossroads and junctions etc. During these non-wired operations, the trolleybus would need to be powered from additional power source such as a super-capacitor or flywheel that could store energy during wired operation or through braking without power from catenary.

The “window” between two catenaries terminals (de-wirement and re-wirement points) effectively determines the requirements for the control system. The most importance is to introduce phase advance (PA) and phase advance plus integral (PA-I) control actuation (motor) [150] during contact loss with the catenary wire. After using a Nichols diagram to analyse and compare the PA and PA-I control systems, PA-I was found to be the preferred control system and this system was applied in a simulation of de-wirement and re-wirement.

After the de-wirement point, the catenary and pantograph are no longer connected, so the pantograph control feedback switches to depending on position rather than contact force. Once re-wirement has been achieved, the catenary and pantograph can be considered a combined system again and control switches back to depending on contact force.

With PA-I control, the de-wirement and re-wirement displacement was close to planned demand and the value of actuation force and speed was also found to be acceptable. The other system requirements were selected so as to also cover the requirement of the active catenary-pantograph control studied in Chapter 5. Consequently, an example actuator was selected that could be shared with the ACTCCS catenary-pantograph control system. The simulation indicated that the various values of contact force and displacement of de-wirement were much smaller than re-wirement and is always less than the acceptable standard value of 300N.

The actuator size is 575N in dynamic with 500mm/s max linear speed and 800 mm longest stroke.

Chapter 7

Conclusion and Recommendations for future research

7.1 General and main contribution

In this thesis, a novel concept of Active Control of Trolleybus Current Collection System (ACTCCS) consisting of an actuator-controlled trolleybus' catenary-pantograph (solo pantograph-rod with single overhead line) system has been simulated and analysed.

As the key contribution in this thesis, the self-generation static force and bouncing phenomenon of catenary-pantograph are identified and studied with models which impact, and influence would be the comprehensive and profound in science and engineering of catenary-pantograph system. As well as the proposed process of planned de-wirement and re-wirement in this thesis are also the big contribution which provides the more effective and much better methods (with concept of solo pantograph-rod with single overhead line) and solution dealing with the unwell solved problems of de-wirement and re-wirement (e.g. ehighway project [9] and much likely potential application in state-of-art In-Motion-Charging trolleybus system [169]). From literature view, no same researches have been found in the world so far in the world. In addition, the passive, hybrid and active (with PA-I control methods) trolleybus catenary-pantograph system models have been developed and analysed in the study. Keeping all advantages of conventional trolleybus systems, it can automatically de-wire and re-wire to facilitate selected wireless operation (with back-up energy) for much more flexible operation which could possibly lead to new generation trolleybus system. The main research objectives achieved are as follows:

- Dynamic model of half passive trolleybus with a passive catenary-pantograph system
- Self-generation static force is introduced for modelling of catenary-pantograph system
- Dynamic model identified the worst situation of a trolleybus with a passive catenary-pantograph system (at 20m/s) over different road disturbances
- Dynamic bouncing and hybrid models of passive catenary-pantograph system
- Profile of dynamic catenary (vertical displacement) relation with trajectory of catenary-wire (highest vertical displacement) in both normal and bouncing states.
- Complex catenary definition and models - such as at crossroad and switches
- Use dynamic bouncing and complex trolleybus webs models to build risk rank of unexpected de-wirement and electrical arcing
- PA-I Control model of an ACTCCS active pantograph system for a trolleybus system under standard operation using contact force feedback
- PA-I Control model of active pantograph of trolleybus for planned de-wirement and re-wirement operation using pantograph-head position

The main goals for this study were to fully understand the vertical dynamics and modelling (including of self-generation static force, bouncing and hybrid model) the trolleybus'

catenary-pantograph system. Introducing self-load and dynamic bouncing into the catenary-pantograph system dynamics is an exploration in engineering and science. The results both explain arcing and unplanned de-wirement phenomenon in standard operation and provide a risk evaluation of the possibility of arcing and unplanned de-wirement. Simulation of an active pantograph system also shows that arcing and unplanned de-wirement can be significantly reduced using an active pantograph system controlled by feedback of the contact force between the pantograph and catenary wire. Finally, modelling a novel planned de-wirement and re-wirement trolleybus pantograph system, with the trolleybus running on back-up energy without power from catenary, is novel extensions that may help facilitate the uptake of this 'clean' technology.

Taken together, this research should help support the development trend of more environmentally friendly trolleybus systems (greener, lower noise and better sight in cities etc.); quicker cities' transports without a kind of congestions caused by unexpected de-wirement of traditional trolleybuses.

A potential application of the ACTCCS research for E-motorway is under active investigation by Siemens for their eHighway project. The research outputs of ACTCCS would be an option for creating next generation trolleybus system and demand of the potential market. The results from this work can also be applied in railway and tram systems.

7.2 Limitation of the research

This thesis only investigated the vertical dynamics of trolleybus catenary-pantograph systems. The operation of trolleybus is not only moving straight, but with considerable lateral motion which it leads to lateral force and displacement as well as increasing the risk probability of unplanned de-wirement and arcing.

The dynamic model of half passive trolleybus is trick to explain the realistic feeling when vehicle going through the bump disturbance despite tried quite a few similar models from different references.

As the phase margin of the PA-I control is smaller than the original PM design requirement with over dumping and harmonic. It is not very ideal mothed, therefore the different methods of control that do meet this requirement could be considered for research in the future.

7.3 Recommendation of future research

The reality is that the catenary-pantograph of a trolleybus is highly related with lateral force and displacement during making manoeuvre and turning, but the speed is low (compared to main line rail vehicles), therefore it is different to train and light rail (trams). The lateral manoeuvre which it leads to lateral force and displacement as well as high likely increasing the risk probability of unplanned de-wirement and arcing. Therefore, the lateral dynamics of catenary-pantograph of trolleybus must be taken into account in future research. Regarding the human factor, how the drivers' behaviours to affect the performance and control design of ACTCCS such as selecting positon of pantograph base and control methods with parameters for minimising the working load of drivers during re-wiremnt.

The except lateral dynamics of catenary-pantograph, some further possible subjects getting involved in trolleybus might be in consideration as follows:

- The different methods of control could be considered for research in the future.
- New combination controls in consideration of lateral dynamics of catenary-pantograph of trolleybus
- Catenary with messenger cables for longer span in application [40]
- Extra tensions of catenary caused by lateral force reshaped catenary as two straight rigid lines during rotating around the axis of two hang points (centre line of the catenary) with certain moment inertial under the lateral force while the trolleybus running along a elliptic trajectory apart from centre line of the catenary

Meanwhile the alterative control methods should be introduced in catenary-pantograph as well as de-wirement (planned) and re-wirement for comparison and choice of application.

In addition, the difference between the realistic feeling and dynamic model when vehicle going through the obstruction (such as bumps etc.) an exploration of varied static stiffness of spring under the pre-load might could be made despite it get involved in fundamental in science. A very initial exploration has been done as a separate topic, but the idea was inspired by ACTCCS study.

Reference

[1] Jean-Paul Rodrigue , Chapter 8, The Environmental Impacts of Transportation The Geography of Transport Systems, New York: Routledge, ISBN 978-11386695742013

[2] Sellick, Rebeka, Market Research Summary Report, Innovations, Engineering and Business Consultancy, 2016, [Cited 2016 September]. Available from: rsellick@trl.co.uk, Sat 24/09/2016 07:06

[3] Slaven Tica, Snežana Filipović, Predrag Živanović, Stanko Bajčetić; Development of Trolleybus Passenger Transport Subsystems in Terms of Sustainable Development and Quality of Life in Cities; International Journal for Traffic and Transport Engineering, 2011, 1(4): 196–205

[4] Trolleybus UK, 2012, [Cited 2014 January]. Available from: http://www.tbus.org.uk/article.htm

[5] NGT, 2014, [Cited 2014 February], Available from: http://www.ngtmetro.com/about/

[6] Trolley roadmap 2013, [Cited 2014January]. Available from: http://www.trolley-project.eu/index.php?id=117

[7] Gunter Mackinger; Trolley Roadmap-Operator Perspective on Ebus Future; Workshop "The Future of Electric Public Transport"; Brussels, 12 March 2013

[8] Hutnyak Consulting, Trolley History, Oct. 2014, [Cited 2016 October]. Available from: http://hutnyak.com/Trolley/trolleyhistory.html

[9] Siemens, eHighway, Innovative electric road freight transport, [Cited 2016 October]. Available from: http://w3.siemens.com/topics/global/de/elektromobilitaet/PublishingImages/ehighway/siemens-ehighway-en.pdf

[10] 2013 News; Trolleybus UK, 2012, [Cited 2013 November]. Available from: http://www.tbus.org.uk/news2013.html

[11] Conclusion; Trolleybuses, [Cited 2013 November]. Available from: http://trolleybuses.org/conclusion/

[12] Andrew Robb, The New Bus for London–Diesel/electric hybrid, September 2014, [Cited 2016 April]. Available from: http://www.clean-fleets.eu/fileadmin/New_Bus_for_London_Case_Study_for_Clean_Fleets_final.pdf

[13] Dave Wilsher; Trolleybus Overhead; Trolleybus UK 2012, [Cited 2014 August]. Available from: http://www.tbus.org.uk/liketosee.htm

[14] eHighway, Electric road hybrid truck, Scania G 360 4x2 (Hybrid Truck with Siemens pantograph on the roof) Gävle, Sweden, [Cited 2016 October]. Available from: https://www.scania.com/group/en/images-ehighway/

[15] Stefan Björklund, Christoffer Soop, Kaj Rosenqvist, Anders Ydstedt; New Concepts for Trolley Buses in Sweden; KFB-Rapport 2000:70

[16] Škoda in Plzeň 14Tr Trolleybus no.409 Linka 12.Feb 1994; [Cited 2013 July]. Available from: https://www.flickr.com/photos/sludgeulper/3606907647/

[17] Chris Hebbron; Old Bus Photos; 27/06/12, [Cited 2013 November]. Available from: http://www.old-bus-photos.co.uk/?cat=346

[18] D. J. Hartland; Hartland, D.J “Good Looking Overhead Wires”, IMechE conference, 27th April 1999 -Inner City Urban Railways

[19] Analysis and Design of Tbus Overhead, [Cited 2013 June]. Available from: http://www.tbus.org.uk/analysis.pdf

[20] Messerschmidt Jan, US20130245876, United States Patent and Trademark Office (USPTO) 2013

[21] Christman, US20130018766, United States Patent and Trademark Office (USPTO) 2013

[22] CLERC, EP0026147, European Patent Office (EPO) 1983

[23] Brignon, EP0030906, European Patent Office (EPO) 1981

[24] Paul Ridden; Siemens tests “eHighway of the Future vision” with tram-like overhead cables; May 23, 2012, [Cited 2013 July]. Available from: http://www.gizmag.com/siemens-ehighway-of-the-future-concept/22648/

[25] Yu-Chen Lin, Chun-Liang Lin and Chih-Chieh Yang; Robust Active Vibration Control for Rail Vehicle Pantograph; IEEE Transactions on Vehicular Technology, Vol. 56, No. 4, July 2007

[26] C. Sanchez-Rebolloa, J.R. Jimenez-Octaviob* and A. Carnicerob; Active control strategy on a catenary–pantograph validated model; Vehicle System Dynamics, 2013 Vol. 51, No. 4, 554–569

[27] A. Collina, A. Facchinetti,F. Fossati, F. Resta ; An Application of Active Control to the Collector of an High-Speed Pantograph: Simulation and Laboratory Tests; 44th IEEE Conference on Decision and Control, and the European Control Conference 2005 Seville, Spain, December 12-15, 2005

[28] G. Hass-Klau, G. Grampton, C. Biereth, V. Deutsch; Bus or Light Rail: Making the Right Choice; Environmental and transport planning, 2003

[29] KFB; New Concepts for Trolley Buses in Sweden, Introduction, KFB-report 2000:70, KBFs dnr 1999-46, p3.

[30] NGT, 2010, [Cited 2014 January]. Available from: http://www.ngtmetro.com/news/positive-trolleybus-meeting-with-minister/

[31] The electric trolleybus system of Quito, Ecuador, 2003, [Cited 2014 April], Available from: http://pub.iges.or.jp/contents/APEIS/RISPO/inventory/db/pdf/0044.pdf

[32] New wave of interest in trolleybus in turkey and worldwide, UITP Trolleybus Workshop 2015, 01-02 Oct.2015, [Cited 2016 January]. Available from: http://www.uitp.org/events/uitp-trolleybus-workshop-2015

[33] Arnaud Devie, Pascal Venett, Serge Pelissier and Rochdi Trigui; Battery duty profile of a heavy-duty trolleybus; 2012 IEEE Vehicle Power and Propulsion Conference, Oct. 9-12,2012, Seoul, Korea

[34] Andrés Emiro Diez, Armando Bohórquez, Edder Velandia, Luis Fernando Roa; Modern Trolleybuses on Bus Rapid Transit: key for electrification of public transportation; 978-1-4244-6742-6/10, 2010 IEEE

[35] P. Polacha, M. Hajzmana; Multibody Simulations of Trolleybus Vertical Dynamics and Influences of Spring-damper Structural Elements; Applied and Computational Mechanics 2 (2008) 101–112

[36] IEEE; Draft Guidelines for the Design of Direct Current Overhead
Contact Systems for Transit Systems; 2010

[37] BSI British Standards; Railway applications—Rolling stock—Electric equipment in trolleybuses—Safety requirements and connection systems; DD CLC/TS 50502:2008

[38] Analysis and Design of Tbus Overhead, [Cited 2013 June]. Available from: http://www.tbus.org.uk/analysis.pdf

[39] Liam Stoker, Tension and strain on overheated trains; 2011, [Cited 2014 March]. Available from: https://www.railway-technology.com/features/featuretension-and-strain-on-overheated-trains/

[40] D. J. Hartland; Trolleybus Overhead; Trolleybus UK 2012, [Cited 2014 April]. Available from: http://www.tbus.org.uk/overhead.htm

[41] Dr. Jan Messerschmidt; DIaLOGIKa-LibroDuct: Oberleitungsbusse freigelassen (Trolleybus automatically reconnecting with overhead), 2013, [Cited 2013 October]. Available from: http://www.dialogika.de/wp content/themes/dialogika/lib/docs/uploads/Flyer_ LibroDuct_A4.pdf

[42] Hartland, D.J.; Senior Projects Engineer. Brecknell. Willis and Company, [Cited 2013 November]. Available from: http://www.tbus.org.uk/overhead.htm

[43] DIaLOGIKa - Trolleybus automatically reconnecting with overhead; Published on 8 Aug 2013, [Cited 2013 October]. Available from: https://www.youtube.com/watch?v=uPejgdyiXZ4

[44] Patent Seekers Ltd, Patentability Search Report, Case 10391, Ref: L124.008.00, April 2016

[45] Gene F. Franklin, J. David Powell, Abbas Emami-Naeini; Chapter7. State-Space Design, Feedback Control of Dynamic Systems, Sixth Edition; Pearson Education, Inc., Upper Saddle River, New Jersey, 07458 2010; Page 431-439

[46] R.S. Prabakar, C. Sujatha, S. Narayanan; Optimal semi-active preview control response of a half car vehicle model with magnetorheological damper; Journal of Sound and Vibration 326 (2009) 400–420

[47] Jenny JERRELIND, Lars DRUGGE, Annika STENSSON TRIGELL and Mikael NYBACKA; Simulation of Vehicle-Overhead Power System Interaction on Electric Roads; KTH Royal Institute of Technology SE-100 44 Stockholm, Sweden 2012

[48] P. Polacha, M. Hajzmana; Multibody Simulations of Trolleybus Vertical Dynamics and Influences of Spring-damper Structural Elements; Applied and Computational Mechanics 2 (2008) 101–112

[49] Technical Description Ar-163P Technical symbol – EN Pneumatic Current Collector; GTKB, [Cited 2014 March]. Available from: http://www.gtkb.hu/download/PTB74068D-EN.pdf

[50] A. E. Díez, I.C. Diez, J.A Lopera; Trolleybuses in Smart Grids as effective strategy to reduce greenhouse emissions; Electric Vehicle Conference (IEVC), 2012 IEEE International, Issue Date: 4-8 March 2012

[51] A. Collina, A. Facchinetti,F. Fossati, F. Resta ; An Application of Active Control to the Collector of an High-Speed Pantograph: Simulation and Laboratory Tests; 44th IEEE Conference on Decision and Control, and the European Control Conference 2005 Seville, Spain, December 12-15, 2005

[52] Ken Shores; Catenary on Japanese Railroads; Sumida Crossing, An N-Scale, Japanese-Themed, Urban Railroad 2014, [Cited 2014 March]. Available from: http://sumidacrossing.org/Prototype/PrototypeCatenary

[53] Guido P. A. Koch; Chapter2: Vehicle Suspension Systems, Adaptive Control of Mechatronic Vehicle Suspension Systems; Technische Universitat Munchen 2011; Page 10-39

[54] Trolley Buses - Straight Lines & Curves; Atlas Rail Components ltd. [Cited 2014 September]. Available from: http://www.atlasrail.co.uk/tr_lines.php

[55] Trolley Buses; Atlas Rail Components ltd. [Cited 2014 September]. Available from: http://www.atlasrail.co.uk/trolley-buses.php

[56] Shahin Hedayati Kia, Fabio Bartolini, Augustin Mpanda-Mabwe, Roger Ceschi; Pantograph-Catenary Interaction Model Comparison; IECON 2010 - 36th Annual Conference on IEEE Industrial Electronics Society

[57] Aldo Balestrino, Ottorino Bruno, Alberto Landi & Luca Sani (2000); Innovative Solutions for Overhead Catenary-Pantograph System: Wire Actuated Control an Observed

Contact Force, Vehicle System Dynamics: International Journal of Vehicle Mechanics and Mobility, 33:2, 69-89 2010

[58] M. Tsunemoto, et al; The Effect of Resistance at Supporting Point on Tension and Current Collection Performance of Overhead Contact Line; Railway Technical Research Institute, Tokyo Japan 2008

[59] R.D. Poshusta; Classical Vibrating String; 08/03/99, [Cited 2014 June]. Available from: http://www.idea.wsu.edu/Quantum/Vibr_string.htm

[60] Jose Santos; Wave reflection for fixed end rope; January 8, 2009, [Cited 2014 June]. Available from: http://www.digital-brain.info/documents/field_theory/boundary_cond.html

[61] Tong-Jin Park, et al; A Catenary System Analysis for Studying the Dynamic Characteristics of a High Speed Rail Pantograph; KSME International Journal, VoL 16 No.4, 2002; pp. 436-447

[62] C. Sanchez-Rebollo, J. R. Jimenez-Octavio & A. Carnicero (2013): Active Control Strategy on a Catenary–pantograph Validated Model, Vehicle System Dynamics: International Journal of Vehicle Mechanics and Mobility, 51:4, 554-569 2013

[63] Gator Trax; Suspension Bridges Module; College of Engineering, University of Florida 2004

[64] MathWork, Model a Bouncing Ball in Continuous Tim, R2015a, [Cited 2015 January]. Available from: http://uk.mathworks.com/help/stateflow/ug/modeling-a-bouncing-ball-in-continuous-time.html

[64] Tomasz Kapitaniak, 8.7 Impact oscillators, Chaotic oscillations in mechanical systems, Manchester University Press Oxford Road, Manchester M13 9PL, 1991, p166-160

[65] Kuldeep Singh, Charpter4 Trigonometry and Waveforms, Engineering Mathematics Through Applications, Palgrave MacMillan, Houndmills, Basingstoke, Hampshire RG21 6XS, 2003, p206-207

[66] Mark Nagurka and Shuguang Huang, A Mass-Spring-Damper Model of a Bouncing Ball, Proceeding of the 2004 American Control Conference Boston, Massachusetts June 30 - July 2, 2004

[67] Allan Bower, Jen Franck, K-S. Kim; 5.3 Free vibration of a damped, single degree of freedom, linear spring mass system, EN40 Dynamics and Vibrations, School of Engineering, Brown University, Spring 2015

[68] Dr Nidal M. Ershaidat, Springs - Two Springs and a Mass, Phys. 207 Waves and Light, Physics Department, Yarmouk University, Irbid Jordan, 2007

[69] Gary L. Henderson , Appendix G. Introduction to Mechanics of Inclined Cables, Wind-Induced Vibration of Stay Cables (Report), Publication No. FHWA-HRT-05-083 August 2007, p213

[70] Kuldeep Singh, Section A Graphs, Engineering Mathematics Through Applications, Published by PALGRAVE MACMILLA Houndmills, Basingstoke, Hampshire RG21 6XS, 2003,p100-103

[71] A. Chapanis, Notes On An Approximation Method for Fitting Parabolic Equations To Experimental Data, The Johns Hopkins University, Psychometrika Vol. 18, NO. 4, December, 1953

[72] C.P. Ward, R. Dixon, ELB004: Control System Design, Handout Part D: Introduction to controller design, School of Electronic, Electrical and Systems Engineering Control Systems Group, Loughborough University, 2010

[73] PID Theory Explained, National Instruments, Mar 29, 2011, [Cited 2017 October]. Available from: http://www.ni.com/en-gb.html

[74] C. Sanchez-Rebollo, J. R. Jimenez-Octavio & A. Carnicero (2013): Active Control Strategy on a Catenary–pantograph Validated Model, Vehicle System Dynamics: International Journal of Vehicle Mechanics and Mobility, 51:4, 554-569 2013

[75] M S Mohd, M N Karsiti and M S Mohd, Effect Of Phase Advance on The Brushless DC Motor Torque Speed Respond, 3rd International Conference of Mechanical Engineering Research (ICMER 2015), IOP Conf. Series: Materials Science and Engineering 100 (2015) 012004 doi:10.1088/1757-899X/100/1/012004

[76] Dr P. D. Hubbard & Dr C. P. Ward, Handout Part A: Advanced Control Methods Section 4: Controller Design Using Pole Placement, ELC041: Advanced Topics in Control, Loughborough University,

[77] Dr Peter Hubbard, Prof Roger Dixon & Dr Chris Ward, ELD527/ELP027, Systems Modelling for Control, School of Electronic, Electrical and Systems Engineering Control Systems Group

[78] Mathworks, Linear-Quadratic-Integral control, [Cited 2016 March]. Available from: https://uk.mathworks.com/help/control/ref/lqi.html

[79] Dr P. D. Hubbard & Dr C. P. WardELC041: Advanced Topics in Control, School of Electronic, Electrical and Systems Engineering Control Systems Group

[80] Tong-Jin Park, et al; A Catenary System Analysis for Studying the Dynamic Characteristics of a High Speed Rail Pantograph; KSME International Journal, VoL 16 No.4, 2002; pp. 436-447

[81] Kiyotaka Yamamura and Mitsuru Tonokura; Formulating hybrid equations and state equations for nonlinear circuits using SPICE; International Journal of Circuit Theory and Applications Int. J. Circ. Theor. Appl. 2013; 41:101–110

[82] HSE, Introducing the key topics, [Cited 2016 October]. Available from: http://www.hse.gov.uk/humanfactors/top-ten.htm

[83] Balensiefen, Tobias; email to Min Chen, [27 2014 March]. Available from: mailto:T.Balensiefen@vkd.vossloh.com

[84] M. Weigel, P. Lugener and M. Plochl; A Driver Model for a Truck-semitrailer Combination; The Dynamics of Vehicles on Roads and on Tracks; Vehicle System Dynamics Supplement 41 (2004), p.321-331

[85] Autonomous Vehicles: Self-Driving Vehicles, Autonomous Parking, and Other Advanced Driver Assistance Systems: Global Market Analysis and Forecasts; 2012, [Cited 2013 November]. Available from: http://www.navigantresearch.com/research/autonomous-vehicles

[86] Jisc infoNet, The Transition Curve, Jisc infoNet, Newcastle upon Tyne UK 2012, [Cited 2014 March]. Available from: http://www.jiscinfonet.ac.uk/infokits/change-management/transition-management/ transition-curve/

[87] Lauren A. Leotti and Tor D. Wager; Motivational Influences on Response Inhibition Measures; Journal of Experimental Psychology: Human Perception and Performance 2009

[88] Donald G. Reinertsen; Chapter4 It's All About Information, Managing The Design Factory; The Free Press and colophon are trademarks of Simon & Schuster Inc. TS170.R45 1997; p68-83

[89] Product catalogue–Overhead contact lines, Kummler+Matter Ltd; 2012, p12073-12304/6487

[90] Suspension: System Modelling; Control Tutorials for Matlab & Simulink, [Cited 2013 November]. Available from: http://ctms.engin.umich.edu/CTMS/index.php?example=Suspension&section=SystemModeling

[91] Gene F. Franklin, J. David Powell, Abbas Emami-Naeini; Chapter2. Dynamic Models, Feedback Control of Dynamic Systems, Sixth Edition; Pearson Education, Inc., Upper Saddle River, New Jersey, 07458 2010; Page 25-26

[92] Gene F. Franklin, J. David Powell, Abbas Emami-Naeini; Chapter7. State-Space Design, Feedback Control of Dynamic Systems, Sixth Edition; Pearson Education, Inc., Upper Saddle River, New Jersey, 07458 2010; Page 431-439

[93] ZF Industries, Inc; The open road with ZF technology, [Cited 2013 December]. Available from: http://www.zf.com/media/media/document/corporate_2/downloads_1/flyer_and_brochures/bus_driveline_technology_flyer/ZF_AxleSystems_Coaches_US_EN11.pdf

[94] Lloyd Davis, Dr Jonathan Bunker; Development of a Software Model of a Heavy Vehicle Suspension for Research; Queensland University of Technology, 2008

[95] R.S. Prabakar, C. Sujatha, S. Narayanan; Optimal semi-active preview control response of a half car vehicle model with magnetorheological damper; Journal of Sound and Vibration 326 (2009) 400–420

[96] Sunil Kumar Singh; Moments of inertia of rigid bodies (application); Connexions module: m14365, [Cited 2014 April]. Available from: http://cnx.org/content/m14365/1.5/

[97] 2014 Tire Data Guide Commercial Vehicle Tires; Continental Tire the Americas, LLC, [Cited 2014 September]. Available from: http://www.continental-truck.com/www/download/transport_us_en/continental_dataguide.pdf

[98] VOLVO B9LA; Volvo Bus Corporation, [Cited 2013 November]. Available from: http://www.volvobuses.com/sitecollectiondocuments/vbc/united_kingdom_and_ireland/downloads/b9la_rfs_rhd10.pdf

[99] 5.24 Wave propagation velocity, BSI Standards; Railway applications — Fixed installations — Electric traction overhead contact lines; EN 50119:2009+A1:2013

[100] Crich Tramway Village, [Cited 2014 February]. Available from:
http://www.tramway.co.uk/

[101] The Trolleybus Museum at Sandtoft, [Cited 2014 July]. Available from:
http://www.sandtoft.org.uk/

[102] Mr Tim Stubbs' garage, 1 Highfield Drive, Burton upon Trent. The pantograph measured was from the trolleybus having last been used in service in 1950 in the UK,
[Cited 2017 November]. Available from: tim.stubbs@highfieldengineering.co.uk, 21/11/2017 5:23pm, 12/09/2018 2:17pm and 14/09/2018 11:50]

[103] SA 3 (BS3), SA Series Servoactuators, Linear Servoactuators, Linearmech S.r.l.Via Caduti di Sabbiuno, 3 - 40011 Anzola dell'Emilia (Bologna), ITALY

[104] Single Core XLPE/PVC/AWA/PVC Power Cable
http://objects.eanixter.com/PD313675.PDF
[Cited 2017 October]

[105] Virtual work, [Cited 2017 September]. Available from:
https://en.wikipedia.org/wiki/Virtual_work

[106] Martin Houde, Chapter 4. Lagrangian Dynamics, Classical Mechanics I, Courses Physics 350/Applied Math 353, University of Western Ontario Canada, Page 80-84

[107] Collina, A., Fossati, F., Resta, F.; An innovative OHL diagnosis procedure based on the pantograph dynamics measurements; WCRR'01, 2001, Koln, Germany

[108] Chris Jackson, Stagecoach Supertram Maintenance Ltd, Nunnery Depot, Woodbourn Road, SHEFFIELD, S9 3LS. The pantograph measured was from LR33D made by Brecknell Willis

[109] Sung Pil Jung,Young Guk Kim, Jin Sung Paik and Tae Won Park, Estimation of Dynamic Contact Force Between a Pantograph and Catenary Using the Finite Element Method, Journal of Computational and Nonlinear Dynamics October 2012, Vol. 7 / 041006-1

[110] MathWork, Model a Bouncing Ball in Continuous Tim, R2015a, [Cited 2016 April]. Available from: http://uk.mathworks.com/help/stateflow/ug/modeling-a-bouncing-ball-in-continuous-time.html

[111] Paul White, Improvement of Rail and Trolley Bus Overhead Contact Systems Operation with Diode Section Insulators, 2012 Rail Conference, 2012

[112] PF White, MA Chelmsford, AJ Gillespie, Operational and Safety Improvements to OCS with Non-conducting Span Wire, 2010 Rail Conference, 2010

[113] Mark Nagurka and Shuguang Huang, A Mass-Spring-Damper Model of a Bouncing Ball, Proceeding of the 2004 American Control Conference Boston, Massachusetts June 30 - July 2, 2004

[114] Allan Bower, Jen Franck, K-S. Kim; 5.3 Free vibration of a damped, single degree of freedom, linear spring mass system, EN40 Dynamics and Vibrations, School of Engineering, Brown University, Spring 2015

[115] Rhett Allain, Modelling a Bouncing Ball, 2011, [Cited 2015 January]. Available from: http://www.wired.com/2011/04/modeling-a-bouncing-ball/

[116] Tomasz Kapitaniak, 8.7 Impact oscillators, Chaotic oscillations in mechanical systems, Manchester University Press Oxford Road, Manchester M13 9PL, 1991, p166-160

[117] MathWork, Simulation of a Bouncing Ball, R2015a, [Cited 2015 January]. Available from: http://uk.mathworks.com/help/simulink/examples/simulation-of-a-bouncing-ball.html

[118] Paul M. Fishbane et al, Chapter 6.1, Physics For Scientists And Engineers, Extended Version, Prentice-Hall, Inc., A Division of Simon & Schuster Englewood Cliffs, New Jersey, 1993, p162

[119] Kuldeep Singh, Charpter4 Trigonometry and Waveforms, Engineering Mathematics Through Applications, Palgrave MacMillan, Houndmills, Basingstoke, Hampshire RG21 6XS, 2003, p206-207

[120] CDR E. J. Tucholski , Doppler Effect, Underwater Acoustics and Sonar , SP411 Handouts and Notes Fall 2006, USNA Physics, The United States Naval Academy (USNA), p290 (19-3), 2006

[121] Dr Nidal M. Ershaidat, Springs - Two Springs and a Mass, Phys. 207 Waves and Light, Physics Department, Yarmouk University, Irbid Jordan, 2007

[122] Gary L. Henderson , Appendix G. Introduction to Mechanics of Inclined Cables, Wind-Induced Vibration of Stay Cables (Report), Publication No. FHWA-HRT-05-083 August 2007, p213

[123] Kuldeep Singh, Section A Graphs, Engineering Mathematics Through Applications, Published by PALGRAVE MACMILLA Houndmills, Basingstoke, Hampshire RG21 6XS, 2003,p100-103

[124] Suppose that the cable profile of a small suspension bridge carrying a uniformly distributed load, Chegg.com, [Cited 2015 March]. Available from: https://www.chegg.com/homework-help/questions-and-answers/suppose-cable-profile-small-suspension-bridge-carrying-uniformly-distributed-load-correspo-q1308567

[125] Paul M. Fishbane et al, Chapter 7.2, Physics For Scientists And Engineers, Extended Version, Prentice-Hall, Inc., A Division of Simon & Schuster Englewood Cliffs, New Jersey, 1993, p195

[126] A. Chapanis, Notes On An Approximation Method for Fitting Parabolic Equations To Experimental Data, The Johns Hopkins University, Psychometrika Vol. 18, NO. 4, December, 1953

[127] Chapter 7 Approximation Theory, [Cited 2015 October]. Available from: http://www4.ncsu.edu/~mtchu/Teaching/Lectures/MA530/chapter7.pdf

[128] Five Colleges Amherst, Hampshire, Mount Holyoke, and Smith Colleges, and the University of Massachusetts, Chapter 2. Successive Approximations, Handbook, Five Colleges, Inc. 2008, p32

[129] Problem 10-9, Design of machinery, solution manual 10-9-1, [Cited 2015 May]. Available from:
http://facstaff.cbu.edu/pshiue/Courses/ME318/Homework/HW1Sol.pdf

[130] Andriy Zynovchenko et al, Resonance phenomena and propagation of frequency converter harmonics in the catenary of railways with single-phase A.C. Power Electronics and Applications, 2005 European Conference, 11-14 Sept. 2005

[131] Photo of Arcing through special work; IEEE OCS Subcommittee for Rail Transit Meeting; January 27th & 28th 2014; King County Metro Seattle, Washington, USA, [Cited 2015 June]. Available from:
http://grouper.ieee.org/groups/railtransit/ocs/OCSarchive2014/1-29-14_094.JPG

[132] Xerces Fobe2, 776's Trolley Poles de-wired and came down on a turning, October 2012, [Cited 2015 June]. Available from:
http://www.rmweb.co.uk/community/index.php?/topic/86041-trolleybuses/

[133] Electric arc. (n.d.); The American Heritage® Science Dictionary, [Cited 2015 September]. Available from: http://dictionary.reference.com/browse/electric+arc

[134] Fabian W. Strong , Jack L. Skinner , Paul M. Dentinger , Norman C. Tien; Electrical Breakdown across Micron Scale Gaps in MEMS Structures; Reliability, Packaging, Testing, and Characterization of MEMS/MOEMS V, 611103 (6 January 2006); University of California, Davis, Department of Electrical and Computer Engineering 2 Sandia National Laboratories, Livermore, CA; SPIE 6111

[135] High Voltage Arc Gap Calculator; Cirris Systems Corp., 1991 Parkway Blvd, Salt Lake City, UT 84119 U.S.A. [Cited 2015 September]. Available from:
http://www.cirris.com/learning-center/calculators/50-high-voltage-arc-gap-calculator

[136] R. Cumeras, E. Figueras, C. E. Davis, J. I. Baumbachc and I. Gràciaa; Review on Ion Mobility Spectrometry. Part 2: hyphenated methods and effects of experimental parameters; Analyst, 2015,140, 1391-1410

[137] Alefilobus 2010, [Cited 2015 September]. Available from: https://farm3.staticflickr.com/2692/4315072150_52330cba64_b.jpg

[138] Fedor Sidorov, Trolley bus lines crossing, isolated, [Cited 2015 June]. Available from: http://www.123rf.com/photo_597795_trolley-bus-lines-crossing-isolated.html

[139] David Nemeth, Trolley wire "Trailer", Flickriver December 2009, [Cited 2015 June]. Available from: http://www.flickriver.com/photos/tags/electrictrolleybus/interesting/

[140] Yomgaille, Trolleybus' wires, San Francisco, July 2014, [Cited 2015 June]. Available from: https://www.flickr.com/photos/yomgaille/15939618573/

[141] Crossing ETB-ETB, Product catalog – Overhead contact lines Kummler+Matter Ltd 2012, 12078, 12178, 12155/6487

[142] Report of The Electric Trolleybus Town Eberswalde, Switches, 2.3 Direct current supply and trolleybus overhead, August 2015

[143] Elektroline Inc., TBUS –Overhead Contact Line (OCL) and Speed limit in curve, 2009-06-15, [Cited 2015 September]. Available from: http://www.elektroline.cz/download_area.php

[144] Sreeraj P V, Design and Implementation of PID Controller with Lead Compensator for Thermal Process, International Journal of Computer Applications (0975 – 8887) Volume 67– No.1, April 2013, [Cited 2017 September]. Available from: https://pdfs.semanticscholar.org/98d4/2a82962cf2f297428b379f794044f80ab9f0.pdf

[145] BS EN 50318. Railway applications. Current collection systems. Validation of simulation of the dynamic interaction between pantograph and overhead contact line, 2002

[146] Christopher Ward, controller_design_for_Min_V2, 2018 (code), teaching course, [Cited 2018 March]. Available from: C.P.Ward@lboro.ac.uk, 23/3/2018

[147] Motion Engineering, Understanding / Reading Bode Plots, Bode tools, [Cited 2015 July]. Available from: http://support.motioneng.com/utilities/bode/bode_16.html

[148] A J Deakin, High performance and low CO2 from a Flybrid® mechanical kinetic energy recovery system, 2015

[149] Electric Cylinder Sizing and Selection, Parker Hannifin Corporation, Automation Actuator Division, Wadsworth, Ohio USA, [Cited 2018March]. Available from: http://www.parker.com/parkerimages/automation/cat/English/1894a005.pdf

[150] The Maintenance Engineer's Guide to Industrial Actuators, Thomson Industries, Inc., [Cited 2019 May]. Available from: https://www.thomsonlinear.com/en/support/2018-02-20-link-na

[151] Chenyang Lu Brian M. Blum, RAP: A Real-Time Communication Architecture for Large-Scale Wireless Sensor Networks, Eighth IEEE Real-Time and Embedded Technology and Applications Symposium (RTAS'02), 2002 IEEE

[152] Thomas Bucher, Measurement of Distance and Height in Images based on easy attainable Calibration Parameters, IEEE Intelligent Vehicles Symposium 2000, Dearborn (MI), USA October 3-5, 2000

[153] Tae-Yong Lee*, Jun-Young Song*, Jaehong Kim**, Yong-Jae Kim**, Sang-Yong Jung*and Jung-Moon Je†, Phase Advance Control to Reduce Torque Ripple of Brush-less DC Motor According to Winding Connection, Wye and Delta, J Electr Eng Technol Vol. 9, No. 6: 2201-2208, 2014

[154] Christopher Ward, Controller_design_for_Min_V1 (code), 2018, teaching course, [Cited 2018 March]. Available from: C.P.Ward@lboro.ac.uk, 19/3/2018

[155] Design of clearance and creepage distances in electrical equipment, Measurement of clearance and creepage distances according to VDE / IEC, 2014/2015

[156] Charles H. Holbrow, 2.4 Angles and angular measure, Modern Introductory Physics, Second edition, 2010, p32

[157] Bus speeds reports, Buses performance data, 2017/2018, [Cited 2018 September] Available from: http://content.tfl.gov.uk/borough-am-bus-speeds-to-p10-2018.xlsx

[158] J. Zavada, J. Blašković Zavada, K. Miloš: Conditions for Implementing Trolleybuses in Public Urban Transport, Oct 2010

[159] Speed Bumps, Available from: [Cited 2019 March] https://www.theramppeople.co.uk/road-ramps/speed-bumps

[160] Feng Tyan and Yu-Fen Hong, Generation of Random Road Profiles, ITRI Project: 5353C46000, November 2007

[161] Mohammad Mirzapour, T. X. Mei, Detection and isolation of actuator failure for actively controlled railway wheelsets, 2014 UKACC International Conference on Control (CONTROL), July 2014

[163] The Highways (Road Humps) Regulations 1999, HIGHWAYS, ENGLAND AND WALES, 1999 No. 1025, March 1999

[162] Stefano Bruni, The results of the pantograph–catenary interaction benchmark, Vehicle System Dynamics, Vol. 53, No. 3, 412–435, 2015

[162] Lyde´ ric Bocquet, The physics of stone skipping, 2003 American Association of Physics Teachers.

[164] Email Webmaster, Tangents and Normals, Academic Skills Kit, Newcastle University, Last updated 12 March 2018

[165] Vytenis Babrauskas, Arc Breakdown in Air over Very Small Gap Distances, Conference: Interflam 2013, Volume: 2; pp. 1489-1498, January 2013

[166] Sang-Hoon Kim, Chapter 2 - Control of direct current motors, Electric Motor Control, DC, AC, and BLDC Motors, 2017, Pages 39-93

[167] Feng Tyan and Yu-Fen Hong, Generation of Random Road Profiles, ITRI Project: 5353C46000, November 2007

[168] Qingxia Zhang, Aukasz Jankowski and Zhongdong Duan, Simultaneous Identification of Moving Vehicles and Bridge Damages Considering Road Rough Surface, Mathematical Problems in Engineering Volume 2013, p12, November 2013

[169] Iveco Bus, In-Motion-Charging Another Idea of Electric Bus, Oct 2018, [Cited 2019 July] https://www.iveco.com/ivecobus/en us/ Documents /IvecoBUS_Products /Leaflet_TrolleyBus_EN%2007-18.pdf

[169] Fabian Leo´ n-Vargas , Fabricio Garelli and Mauricio Zapateiro, Limiting vertical acceleration for ride comfort in active suspension systems, Systems and Control Engineering 232(3), 2017

[170] Roger Dixon, TX Mei, Main Report from Degree of Doctor of Philosophy, 19 September 2019

Appendix

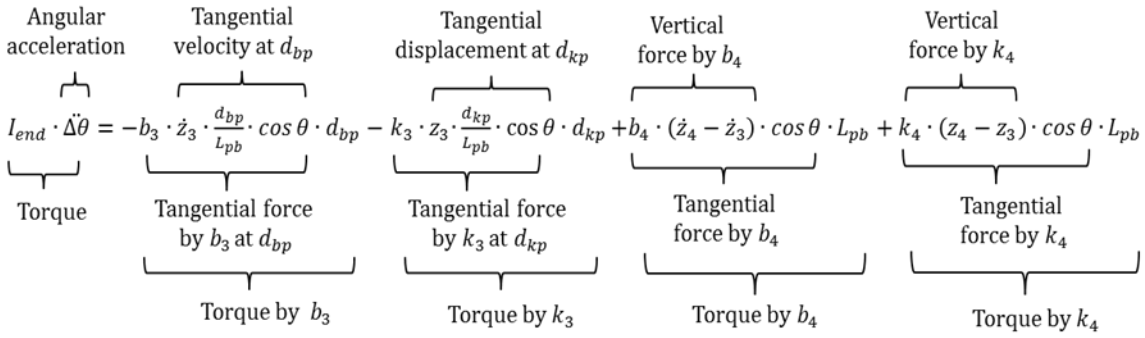

Scd 3.2.8-Derivation of equation E3.2.8

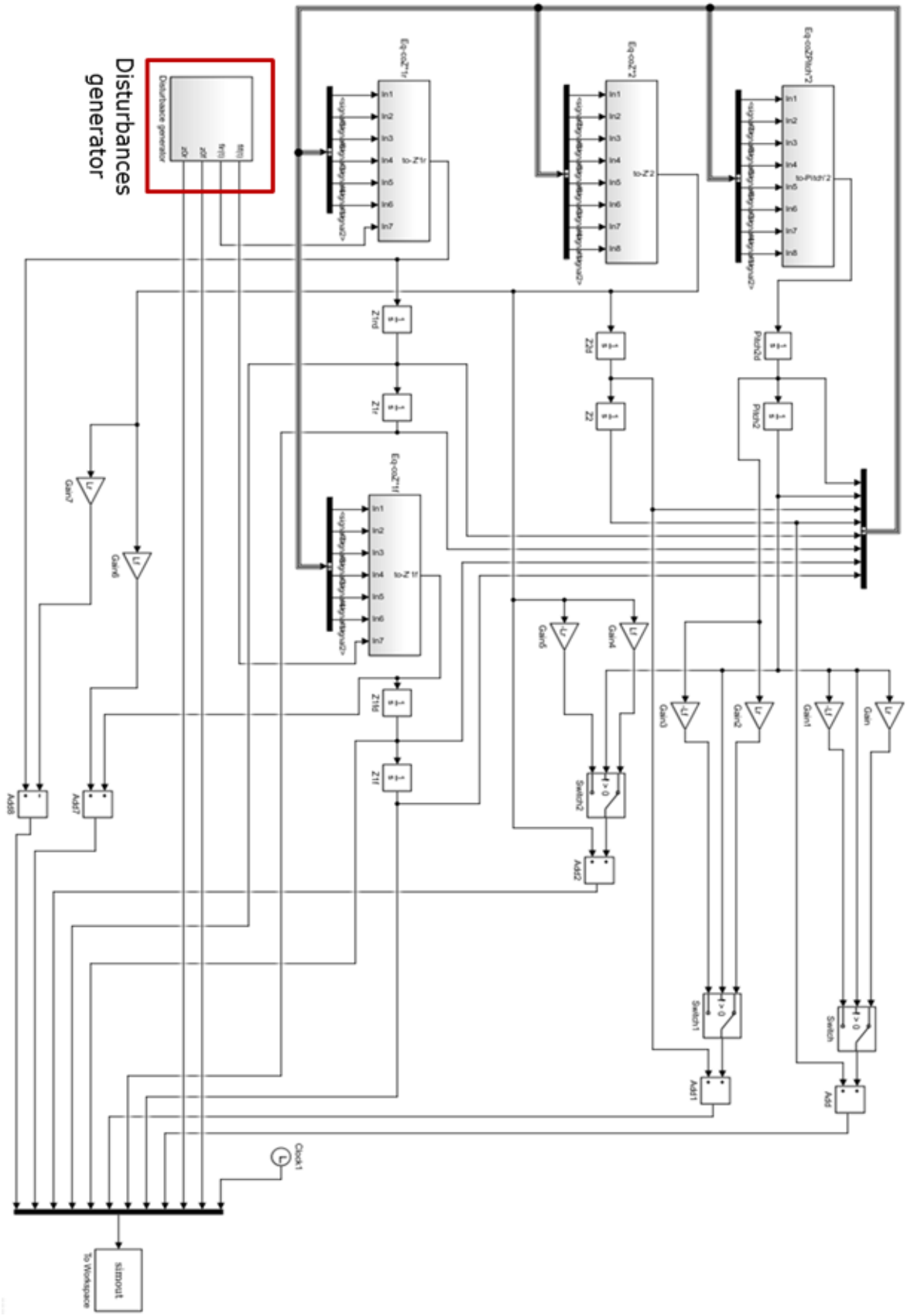

Scd 3.3.6-*Half passive vehicle/road dynamic model* (*Trolleybus) Simulink configuration*

(Same to Figure 3.3.6)

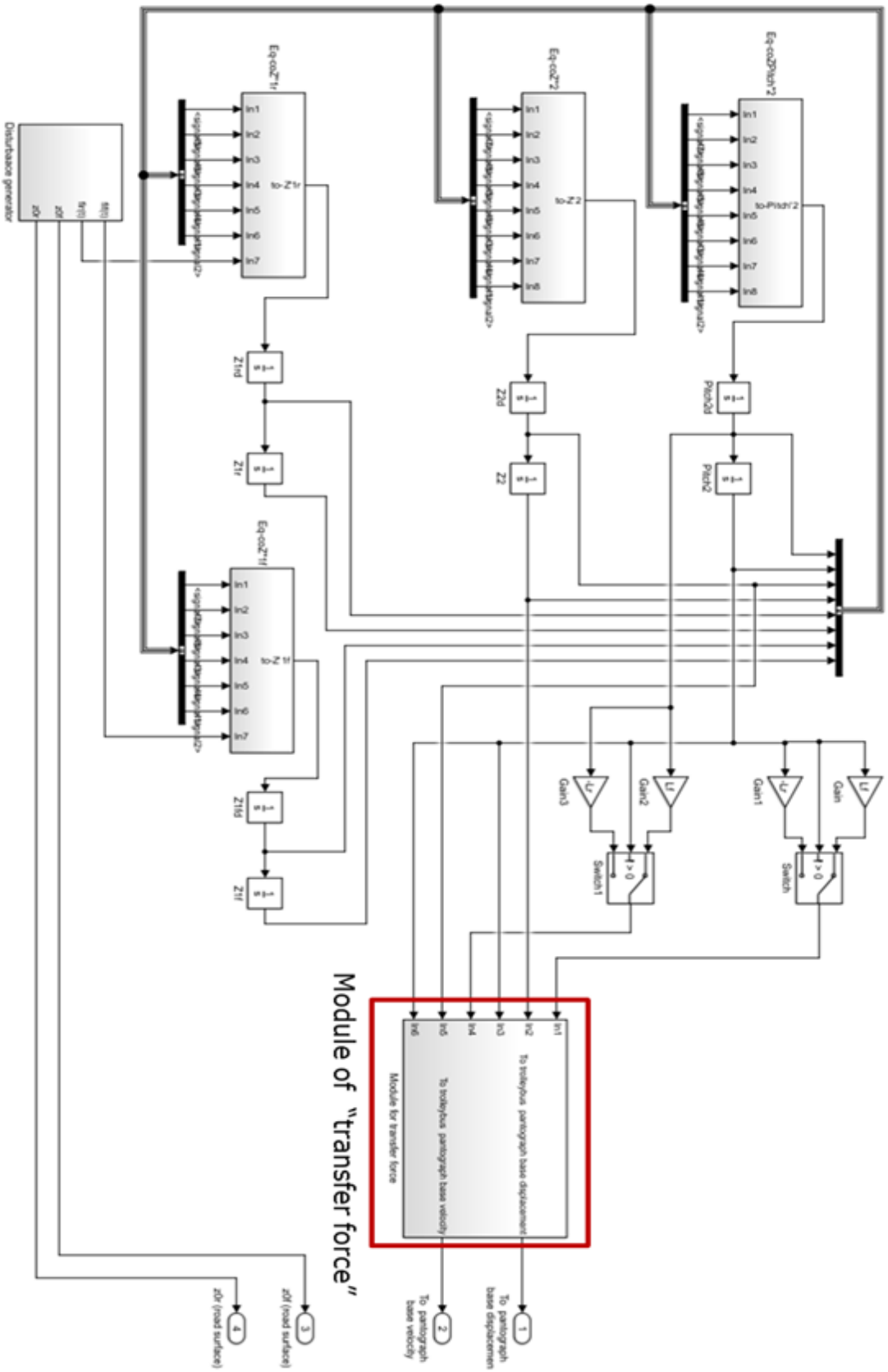

Scd 3.4.4-*Simulink configuration of half trolleybus with "transfer force" module (Same to Figure 3.4.4)*

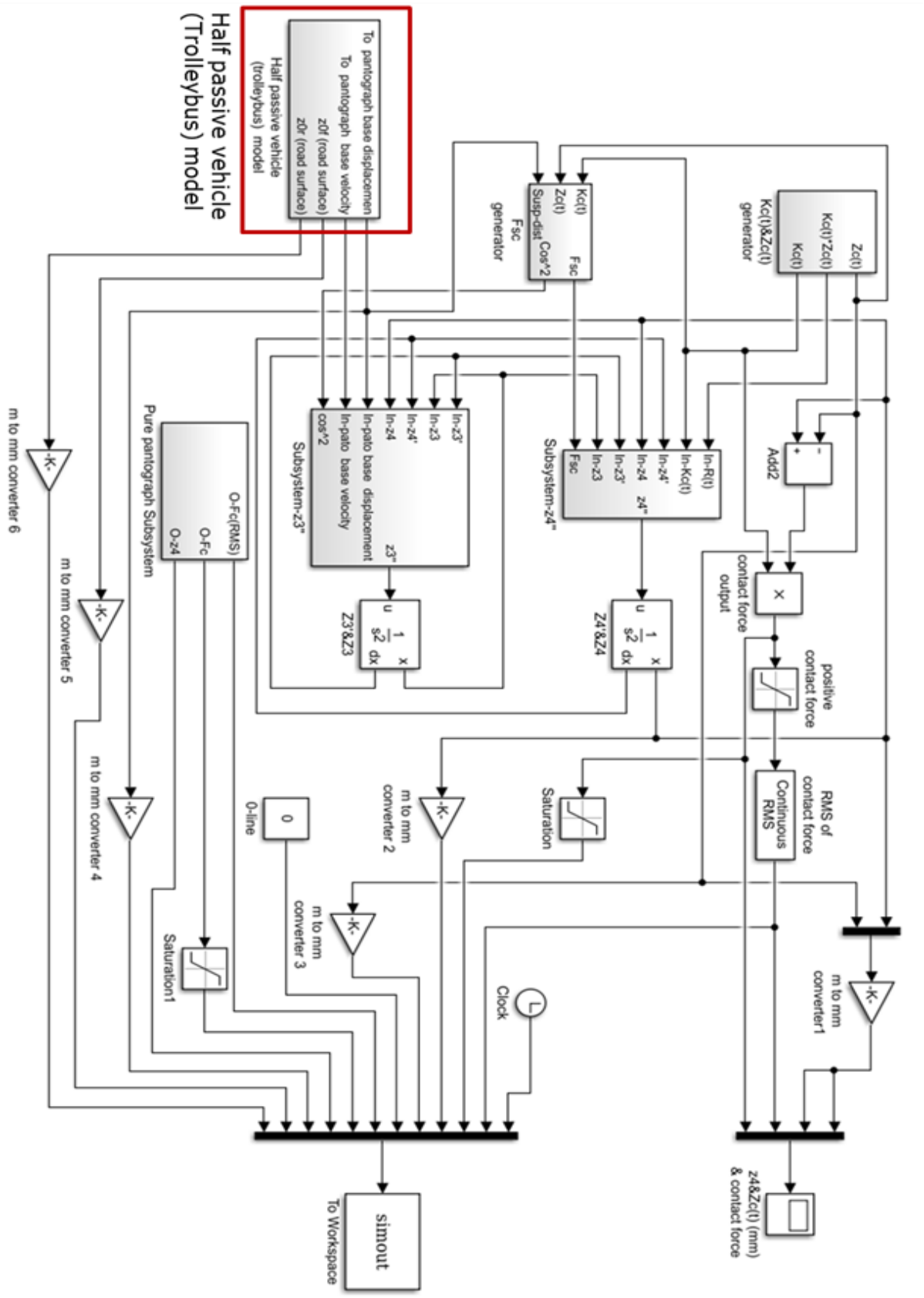

Scd 3.4.5-*Simulink configuration of half passive trolleybus with catenary-pantograph*
(Same to Figure 3.4.5)

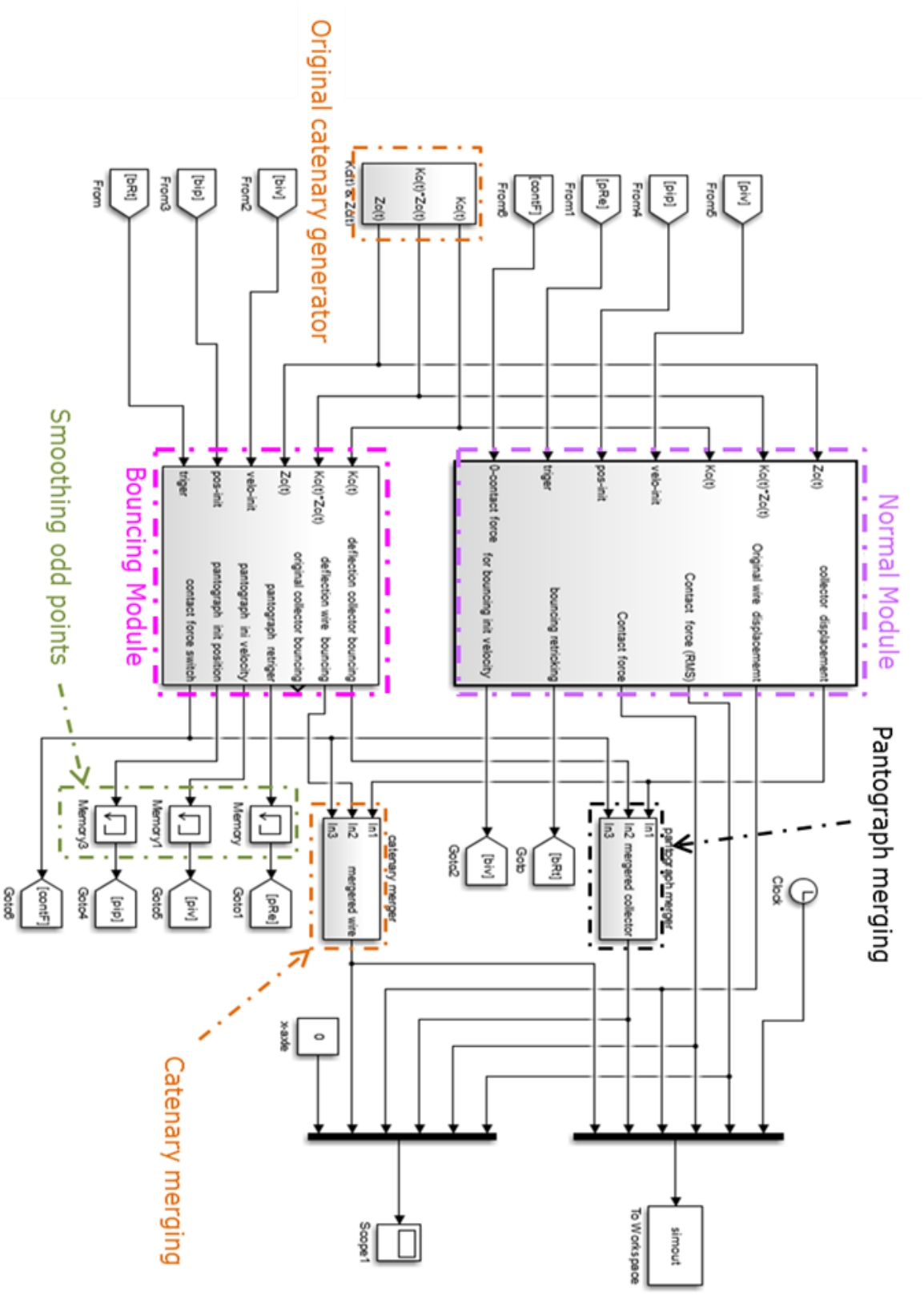

Scd 4.3.1-*Trolleybus' hybrid model dynamic Simulink configuration*

(Same to Figure 4.3.1)

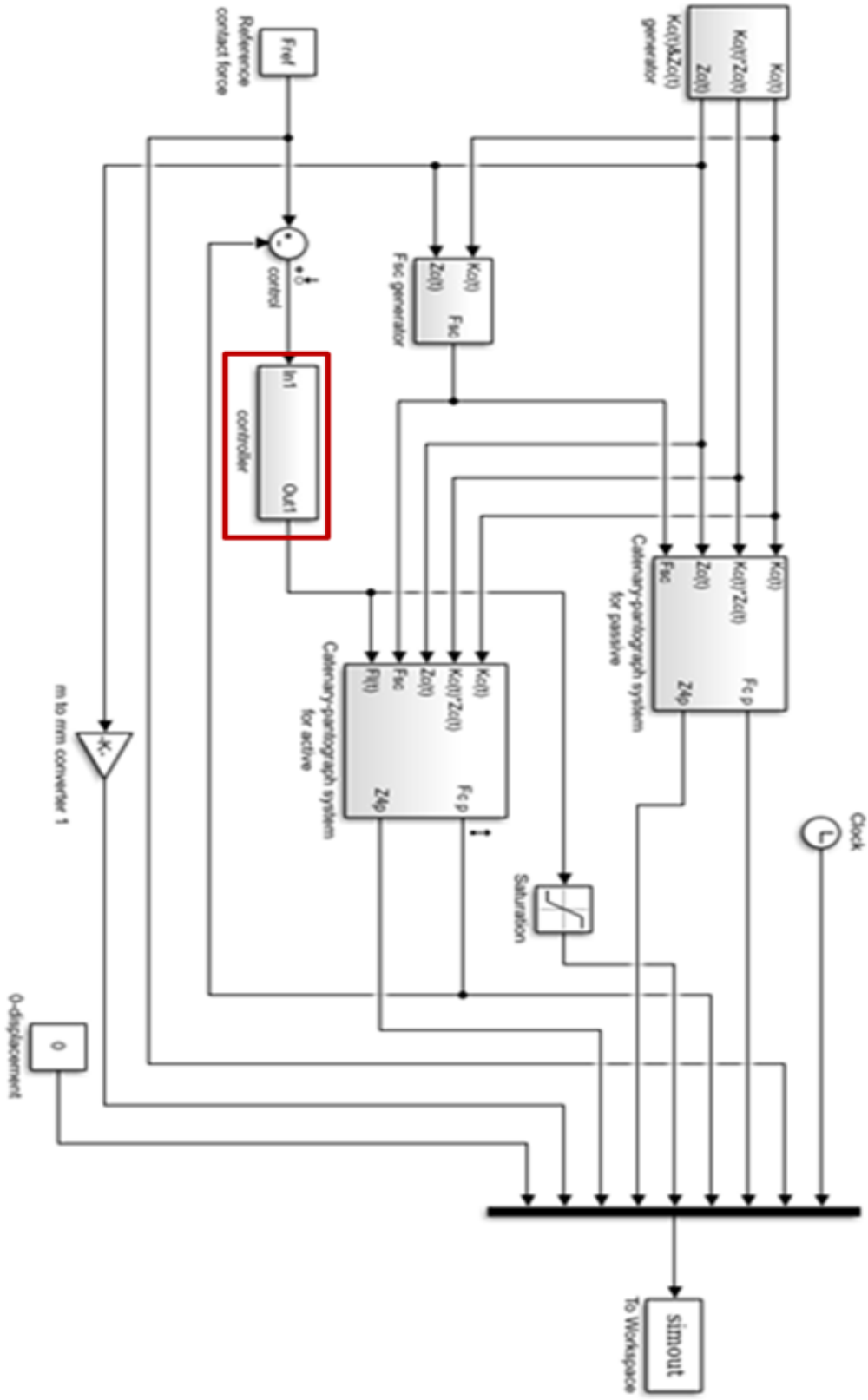

Scd 5.3.2-*Simulink Configuration of P, PA and PA-I control system with catenary-pantograph system*

(Same to Figure 5.3.2)

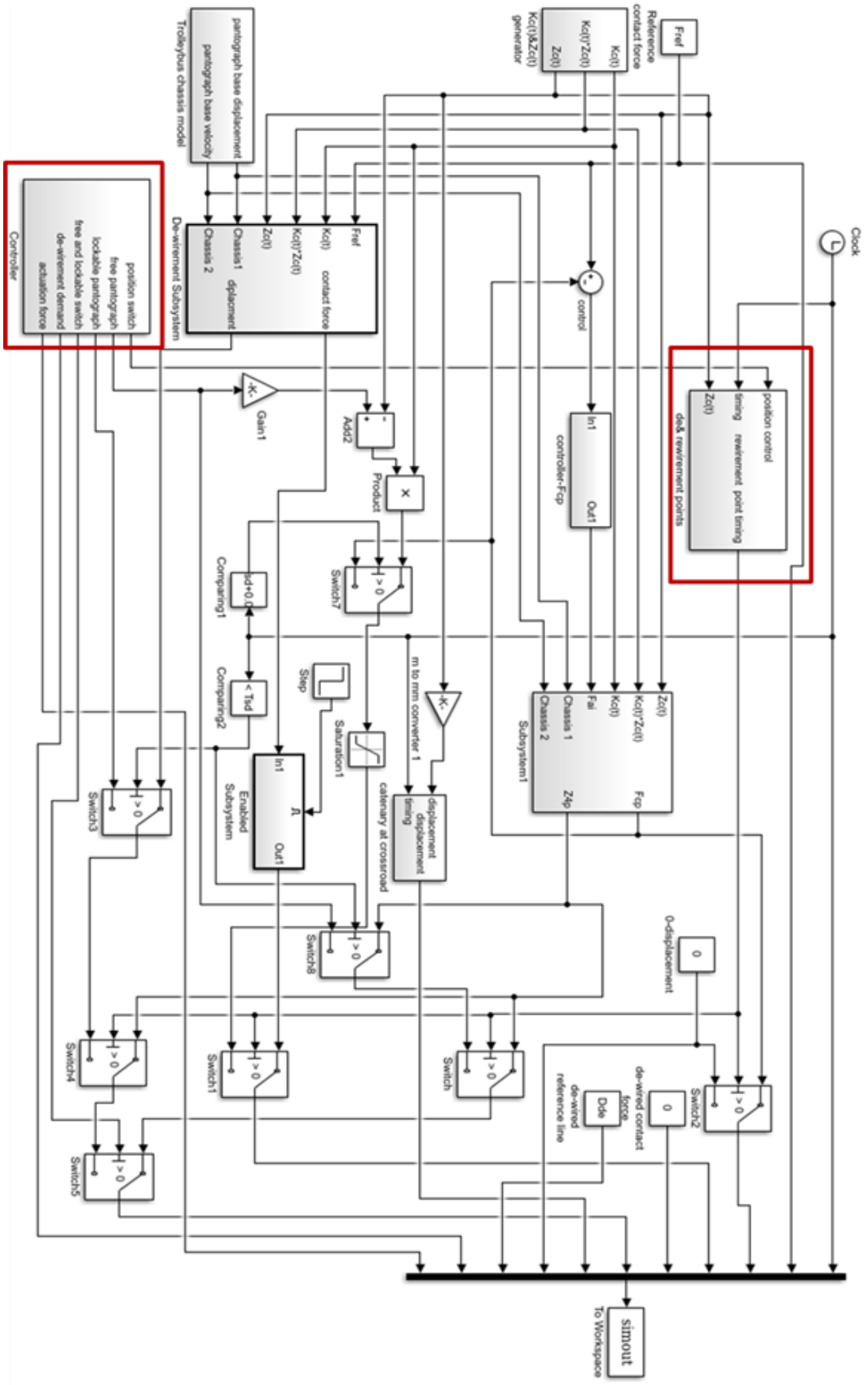

Scd 6.3.2-*Simulink configuration of trolleybus' planned de-wirement and re-wirement*

(Same to Figure 6.3.2)